Selective Separation of Metallic Phases from Chalcopyrite

Nicola Payne

Submitted in accordance with the requirements for the degree of Ph.D.

Department of Materials
University of Leeds

July 2000

The candidate confirms that the work submitted is her own and that appropriate credit has been given where reference has been made to the work of others.

ACKNOWLEDGEMENTS

I would like to thank the Department of Materials for their continued support and provision of facilities throughout my period of study. I also wish to express my gratitude to the helpful and resourceful technical staff of the Department.

Special thanks are due to my friends and fellow researchers within the department. In particular, to Rosa, Sam and Arline for their encouragement, inspiration and simple ability to keep my spirits up.

I would like to take this opportunity to thank my family for their love and support during all of my academic studies. Finally I would like to say a special thank you to Robert, whom along with my family I would like to dedicate this thesis to.

ABSTRACT

Owing to the environmental problems associated with copper extraction alternative processes are sought. The carbothermic reduction of natural chalcopyrite concentrates, from Ghatsila mines in Bihar, India, in the presence of lime, was studied across the temperature range 850-1250°C. Studies have been completed previously in synthetic chalcopyrite. This study stresses the need to investigate the reduction of natural chalcopyrite.

The reduction of chalcopyrite proceeds in two steps, initially with the direct reduction by carbon. This is followed by indirect reduction by the carbon monoxide evolved from the first stage of reduction. Both stages of the reduction were investigated to determine the reaction mechanism. Metallic copper and iron are produced from the reduction of chalcopyrite. The oxysulphide phase, C_{111}, also produced from the reduction of chalcopyrite, was not previously categorised. X-ray diffraction analysis and scanning electron microscopy were utilised to evaluate the structure of C_{111}.

Silver is an important by-product of copper extraction therefore it was necessary to study its path during the reduction of chalcopyrite. This was achieved by additions of Ag and Ag_2S prior to reduction. Silver will preferentially segregate out with the copper phase hence providing a valuable metallic product from the reduction reaction. The addition of Ag to the reduction mixtures facilitates metallic phase separation of copper and iron.

Arsenic and antimony are deleterious elements present in naturally occurring chalcopyrite. The addition of calcium sulphate and silica to chalcopyrite, heat treated under partially reducing conditions, will produce a calcium silicate slag phase that will entrain impurities such as arsenic and antimony, thus providing a method of control of those elements. An initial investigation into the possible control and elimination of impurities during extraction of copper has been conducted with favourable results.

CONTENTS

LIST OF FIGURES

Chapter Seven

Appendix 2

LIST OF TABLES

LIST OF SYMBOLS AND ABBREVIATIONS

J	Joule
T	Temperature (K)
°C	Degree Celsius
G	Gibbs free energy
ΔG	Free energy of formation
ΔG_M	Free energy of mixing
H	Enthalpy
AH	Heat of formation
ΔH_M	Enthalpy of mixing
S	Entropy
ΔS_M	Entropy of mixing
X_A	Concentration of A
γ_A	Activity coefficient of A
a_A	Activity of A
L_A	Distribution coefficient of A
R	Gas constant
K	Equilibrium constant
In	Natural log
log	$\log_{10}$
atm	Atmosphere
Ω	Interaction energy
P_A	Partial pressure of A
EMF	Electromotive force
E	EMF (mV)
mV	Milli-volts
z	Electrochemical valency
d_{hkl}	Interplanar d-spacing
2θ	Diffraction angle
Å	Angstrom
a and c	Lattice parameters
λ	Wavelength

XRD	X-ray diffraction
SEM	Scanning electron microscope
SEI	Secondary electron image
BSE	Back scattered electron
EDX	Energy dispersive X-ray
EPMA	Electron probe microanalyser
TGA	Thermograviametric analysis
Muf.	Muffle furnace
mins	Minutes
W_a	Actual weight
W_s	Stochiometric weight
g	Gram

CHAPTER ONE

Introduction

Chalcopyrite is one of the most common minerals used today for the extraction of copper. The current copper making process is based on the employment of flash furnace smelters for making Cu_2S-FeS matte and then conversion of matte to blister copper in oxidative conditions which is then refined to >99.99% pure copper.

Although this method is very efficient in the production of copper, there are some major disadvantages. One of these factors is that the production of sulphur dioxide, in the copper extraction process route, is particularly detrimental to the environment. Although the gas is further processed, leaks to the environment are still possible. Another disadvantage of the extraction process occurs during smelting, the iron component of the matte is oxidised and irretrievably lost in the silicate slag phase and is fluxed out. This means that there is an overall loss of 50% of metal into the slag phase. The iron silicate slag is usually dumped into a landfill site without further treatment.

The alternative to the current processing routes is to facilitate copper production via reduction methods. Iron has been produced from the reduction of iron oxide by carbon for several centuries. Many authors have discussed this technology with respect to processing metal sulphides such as NiS, ZnS and FeS to produce the metals directly. Iron oxide can be reduced to metallic iron directly from the addition of carbon, however this is thermodynamically unfeasible for the reduction of a metal sulphide. The addition of a basic oxide to the metal makes the reaction more favourable. Due to the addition of CaO, the reaction proceeds in two steps, namely exchange and reduction. Initially the metal sulphide reacts with the lime resulting in an exchange between the sulphide and oxide ions:

$$MS_{(s)} + CaO_{(s)} = MO_{(s)} + CaS_{(s)} \qquad (1.1)$$

This metal oxide is subsequently reduced by carbon:

$$MO_{(s)} + C_{(s)} = M_{(s)} + CO_{(g)} \quad (1.2)$$

The overall reaction is:

$$MS_{(s)} + CaO_{(s)} + C_{(s)} = M_{(s)} + CaS_{(s)} + CO_{(g)} \quad (1.3)$$

The result, therefore, is the production of pure metal with the sulphur combined as a solid product and not as a gas harmful to the atmosphere.

This project aims to demonstrate that via reduction processing both the copper and iron can be recovered from the natural chalcopyrite mineral concentrate as in equation 1.4. The mineral concentrate used in this study originates from the Ghatsila Mines in Bihar, India.

$$CuFeS_{2(s)} + 2CaO_{(s)} + 2C_{(s)} = Cu_{(s)} + Fe_{(s)} + 2CaS_{(s)} + 2CO_{(g)} \quad (1.4)$$

The process will mean a SO_2 free copper making route that is environmentally friendly and that also avoids disposal of the iron slag phase. Previously the technology has been applied to the reduction of synthesised chalcopyrite by Jha and Grieveson (1992b) with favourable results. However, the process needs to be conducted on natural chalcopyrite to validate these results for copper extraction. The aim of this research is to charaterise the reduction of chalcopyrite by investigating the exchange and reduction reactions and the possible mechanism for selective separation of the metallic phases.

Silver is an important by-product of the copper extraction process and is recovered from the anode slimes collected during eletrorefining of fire refined copper. This research aims to investigate the path of silver during the reduction process in order to ascertain the recoverability of this metal during reduction of chalcopyrite.

For copper extraction from a naturally occurring chalcopyrite mineral there are three important considerations. Firstly, to distinguish the phase equilibria of Cu, Fe and S during the extraction of copper. Secondly, to investigate the recovery of precious metals such as silver and gold as by-products of copper extraction and finally, to consider the

control and elimination of impurities such as arsenic and antimony which are harmful to the environment.

These impurities are usually volatilised during smelting and converting or stay in copper to be removed during electrorefining. Another approach to processing chalcopyrite is considered with the aim to establish a possible reaction mechanism to control this detrimental content of chalcopyrite by encapsulation in a basic calcium iron silicate slag.

1.2 Thesis Outline

Chapter two details briefly the geology of chalcopyrite minerals and their location around the world. A background of the extractive metallurgy of copper from the mineral concentrate is given including precious metal recovery and processing of impurities.

The reduction of metal sulphides by both hydrogen and carbothermic reduction is discussed in chapter three leading onto, specifically, reduction of chalcopyrite. Included in this chapter is the separation of precious metals from the copper extraction process as well as the control and elimination of impurities from copper. The phase equilbria pertaining to the reduction reaction and silver analysis are also discussed. In chapter four the theoretical considerations relevant to the reduction reaction and the path of silver during reduction are given.

Chapter five outlines the experimental methods undertaken for the research of this thesis with the relevant reaction conditions and analytical procedures employed. The results from the experiments detailed in chapter five are presented in chapter six. A discussion of these results is provided in chapter seven. The research for this thesis is concluded in chapter eight including suggestions for further work.

CHAPTER TWO

The Geology of Chalcopyrite and Extractive Metallurgy of Copper

2.1 Introduction

Chalcopyrite is the most abundant copper-bearing mineral, of the formula $CuFeS_2$, in which copper, iron and sulphur are in nearly equal concentrations. The name is derived from the Greek word for copper, *chalkos*, and was once known as copper pyrites. Pyrite comes from the Greek word, *pyros*, meaning fire as pyrite ignites when heated in air. The mineral is tetragonal in structure with a brass yellow appearance and is closely related to bornite (Cu_5FeS_4), idaite (Cu_5FeS_6) and cubanite ($CuFe_2S_3$) (Habashi 1978).

A generalised discussion of the geology of the mineral ore deposits of chalcopyrite and their location around the world is offered in this chapter. The geology is of particular interest because the mineral concentrate used in this study is from a natural source. The chalcopyrite mineral concentrate was obtained from the Ghatsila mines in India. Chalcopyrite is the major mineral utilised in the copper extraction industry. The process used for copper extraction is referred to in section 2.4 of this chapter in which the extraction of precious metals as by-products and the control for elimination of impurities is also detailed.

2.2 Geology of the Chalcopyrite Mineral

Chalcopyrite mineralisation can occur from different sources usually with other copper bearing minerals, such as bornite and chalcocite along with other associated sulphide minerals including pyrite. Most chalcopyrite ores are found as hydrothermal vein deposits. Other types of deposit include magmatic, contact-metasomatic and sedimentary sulphides (Deer et al. 1977).

2.2.1 Hydrothermal Vein Deposits

There are two types of hydrothermal vein deposits, replacement and cavity filling with replacement being dominant over cavity filling. Replacement deposits form by the process of dissolving one mineral and the simultaneous deposition of another in its place, see figure 2.1. In this process not only the minerals of the country rock are affected but also the ore and gangue minerals. Chalcopyrite is found in all three types of replacement deposits, which are massive, lode and disseminated. However, the most widespread occurrence is as disseminated hydrothermal deposits known as porphyry copper deposits (Skinner 1969). The associated minerals are chalcocite, enargite, bornite, tennanite, tetrahedrite and covellite. The term 'porphyry copper' deposit is given to a group of very large low-grade ore bodies from which most of the world's copper is extracted (Pennebaker 1954).

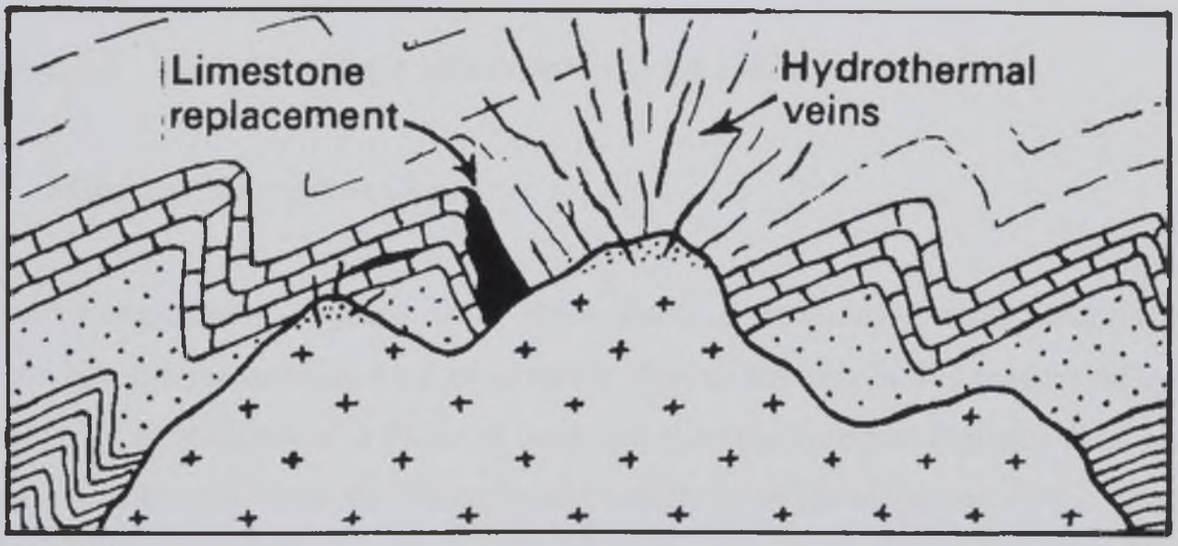

Figure 2.1 Replacement of limestone by veins filling fractures near a granite intrusion (+++++) (Blythe and de Freitas 1979).

The second type of hydrothermal deposit is cavity filling, where minerals are deposited from solution in rock openings. There are several different types of cavity filling; fissure veins, shear-zone, stockworks, saddle reefs, ladder veins, pitches and cracks, breccia filling, solution cavity fillings, pore-space fillings and vesicular fillings. Of particular importance to chalcopyrite mineralisation are fissure, stockworks, breccia,

pore-space and vesicular fillings (Jensen and Bateman 1979). Figure 2.2 is an example of a fissure vein occupying a normal fault.

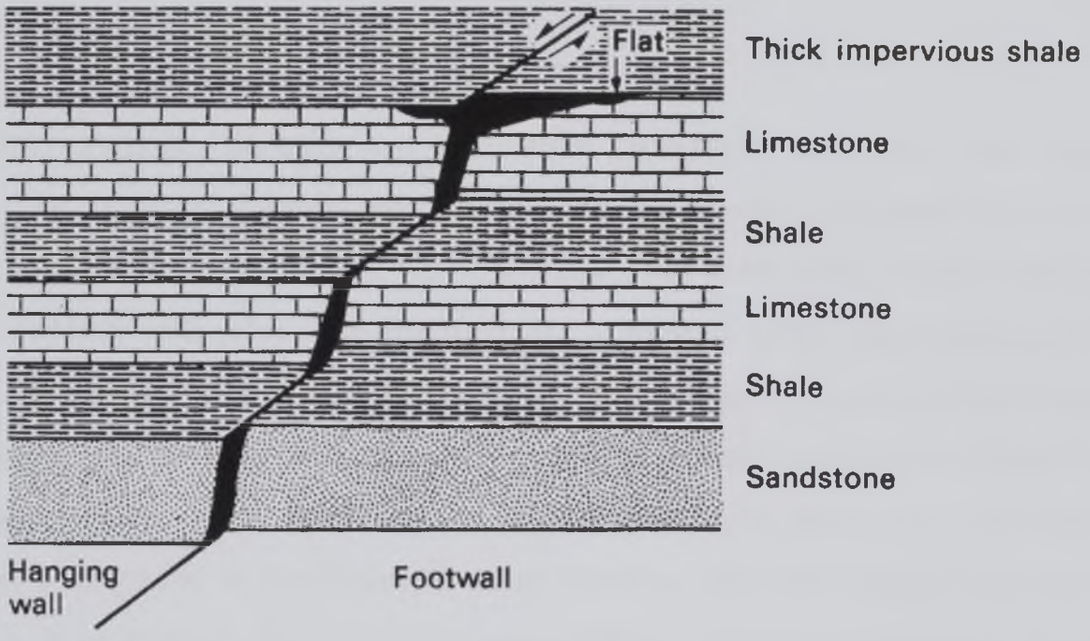

Figure 2.2 Vein occupying a normal fault (Evans 1983).

2.2.2 Magmatic Segregation Deposits

Magmatic segregation deposits form from direct crystallisation from magma and injected into the surrounding rock as intrusive igneous masses. In this process different ore minerals crystallise out at different rates, for example chromite deposits form early during crystallisation whereas chalcopyrite crystallises towards the end of the process (Read and Watson 1973). The chalcophile elements in the magma combine with sulphur and some residual amounts of arsenic, antimony, bismuth, selenium and tellurium to form sulphides and related compounds. The liquid fraction containing sulphide minerals is injected out into the surrounding rock depositing the sulphides (Berry and Mason 1959).

2.2.3 Contact-Metasomatic Deposits

From volcanic outbursts, fluids are released which stay in solution with magma. Most magma flows do not reach the surface but become enclosed within the Earth's crust.

These high temperature 'outburst fluids' can escape into the surrounding rock carrying with them other elements from the magma. The metasomatic reaction of these fluids and the contact rock form new minerals (Jensen and Bateman 1979).

2.2.4 Sedimentary Sulphide Deposits

Sedimentary sulphide deposits can form from two types, stratiform and volcanic massive. The stratiform deposits are affiliated with sedimentary rocks and occur in non-volcanic and deltaic environments, which are stratiform in structure and are concordant with the bedding with more than one layer of ore formed. Other than chalcopyrite the minerals present are bornite, chalcocite, galena and sphalerite all mineralising in rocks of sandstone, limestone and dolomite (Evans 1983). Mineralisation occurs from filling pore spaces, replacement orebodies or synergenetic ores from the exhalation of mineralising solutions at the sediment-water interface. Red-bed formation, shown in figure 2.3, is an example of this type of deposit where copper minerals form in porous sandstone (Gablina 1984).

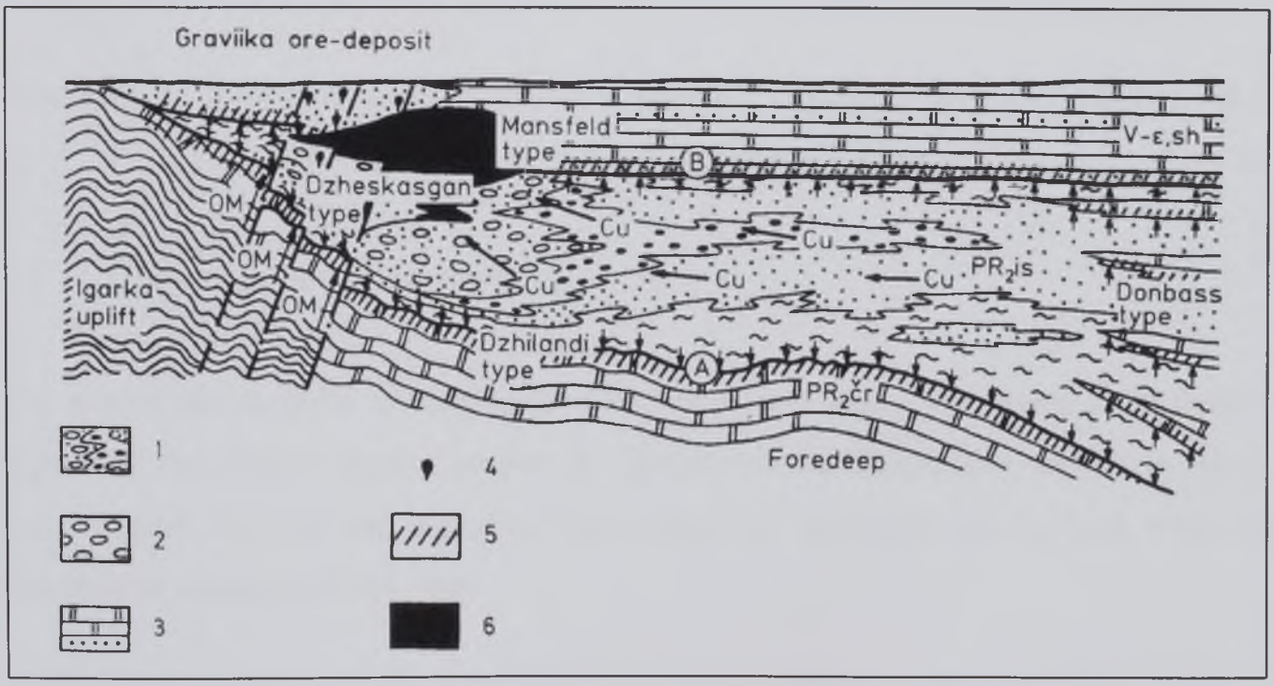

Figure 2.3 A model of the types of copper mineralisation in the Igarka area; 1 – red-bed formation; 2 – bleached conglomerates; 3 – grey marine and lagoonal deposits; epigenetic organic matter; 5 – lean stratified mineralisation; 6 – rich sulphide ores (Gablina 1984).

Massive sulphides are located near borders of submarine volcanic extrusive centres. Mineralisation occurs from the inflow of sulphide mud and/or detrical sulphide material into topographical depressions around submarine volcanoes (Strauss and Gray 1984). Figure 2.4 is a diagram showing an example of mineralisation in these massive sulphides.

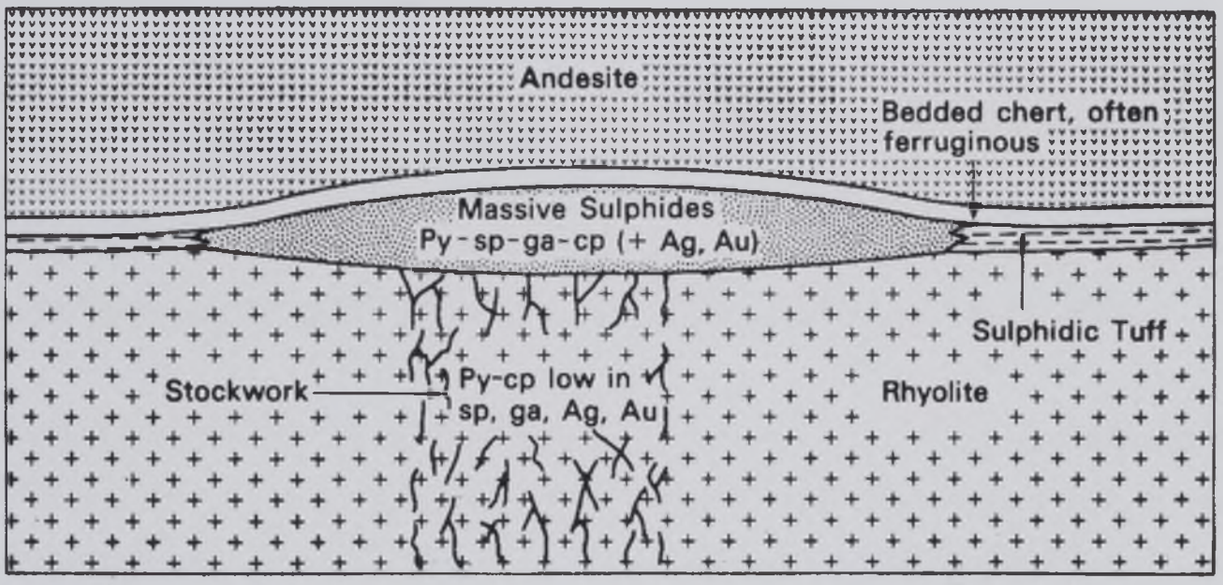

Figure 2.4 Idealised volcanic massive sulphide deposit where Py – pyrite, sp – sphalerite, ga – galena and cp – chalcopyrite (Evans 1983).

2.3 Occurrence of Chalcopyrite Ores

The natural chalcopyrite mineral studied in this project was concentrated from the ore deposit of the India Copper Complex at Ghatsila of the Singhbhum district in Bihar, India. Figure 2.5 is a map depicting the occurrences of copper ore in India with the Singhbhum copper-belt indicated.

In an early discussion of economic geology in India, Wadia (1953) mentions the only deposits worked with some degree of success were those of the Singhbhum district. The most important deposits of copper ore are found in this district which is a shear zone extending over 160km (G.S. of I, 1974). A geological map of the Singhbhum copper belt is given in figure 2.6, showing all the copper occurrences. The mineralisation of the

copper ore at Singhbhum is composed of chalcopyrite, pyrrhotite, pentlandite, violarite-cubanite and vallerite (Rao 1971). Chalcopyrite predominates over all the other sulphides in the copper belt and is found occurring in the finer grains of braided ores, the most important ore type economically. These ores formed as a result of filling fractures in the host rock (Sengupta and Das 1968). Chalcopyrite is also located in xenomorphic grains, 0.09mm to 0.6mm in diameter, in massive ores. These ores are zones of intense shearing which have become thoroughly impregnated by hydrothermal ore solutions.

The mine at Ghatsila is one of two main copper production sites in India. The other is at the Kethri Copper Complex in Rajasthan (Radhakrishna 1979). At Kethri Copper Complex the Madhan-Kuhan and Koilhan chalcopyrite deposits form as a result of mineralisation of hydrothermal solutions in the Kheti copper belt (Jaireth 1986).

Although India is not one of the recognised major producers of copper, Radhakrishna (1979) suggests that self-sufficiency can be attained. In fact the mining industry in India has seen rapid growth in the post-independence era after 1947 (Mining 1997).

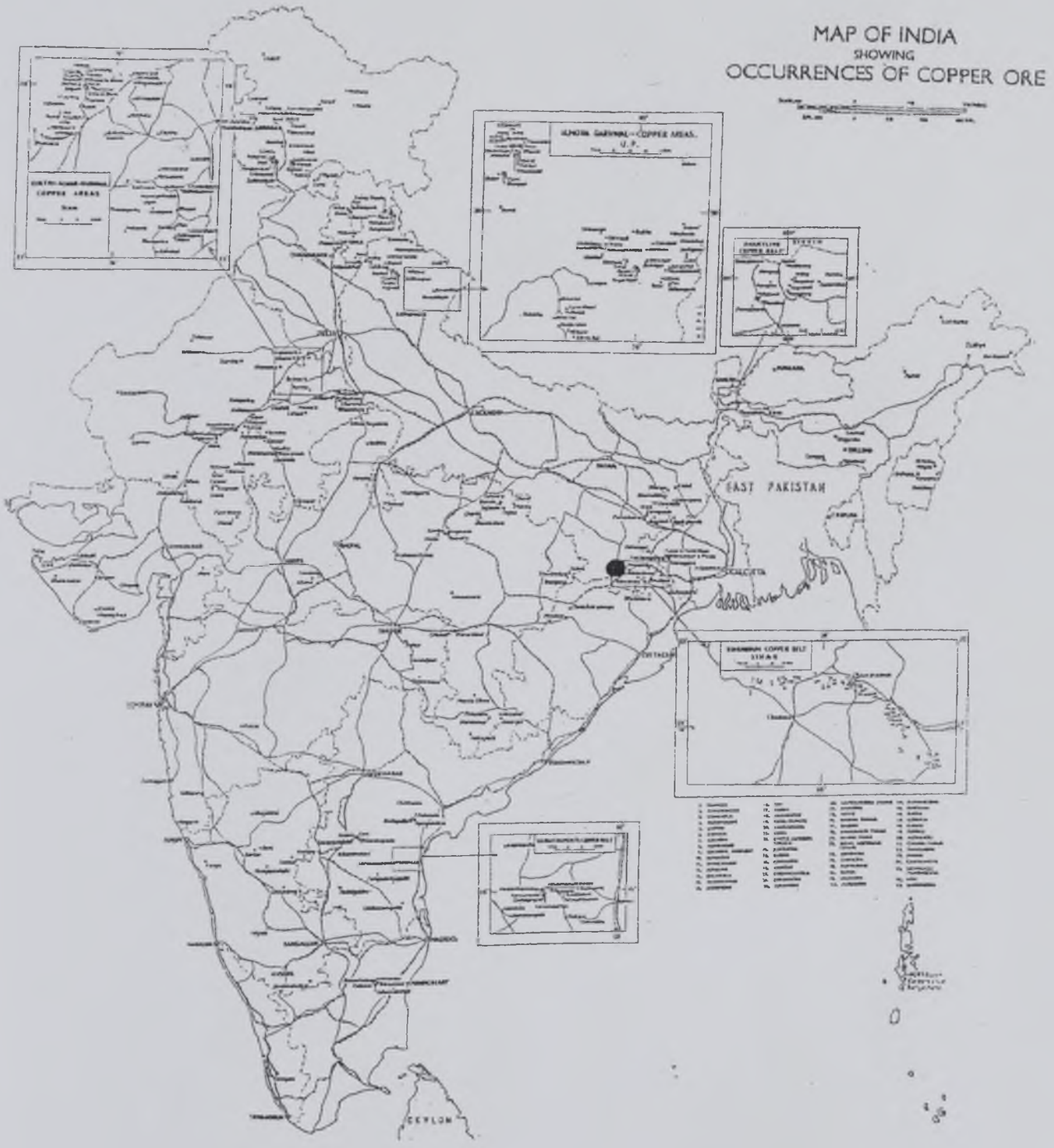

Figure 2.5 Map of India indicating occurrences of copper ore (Dunn 1964).

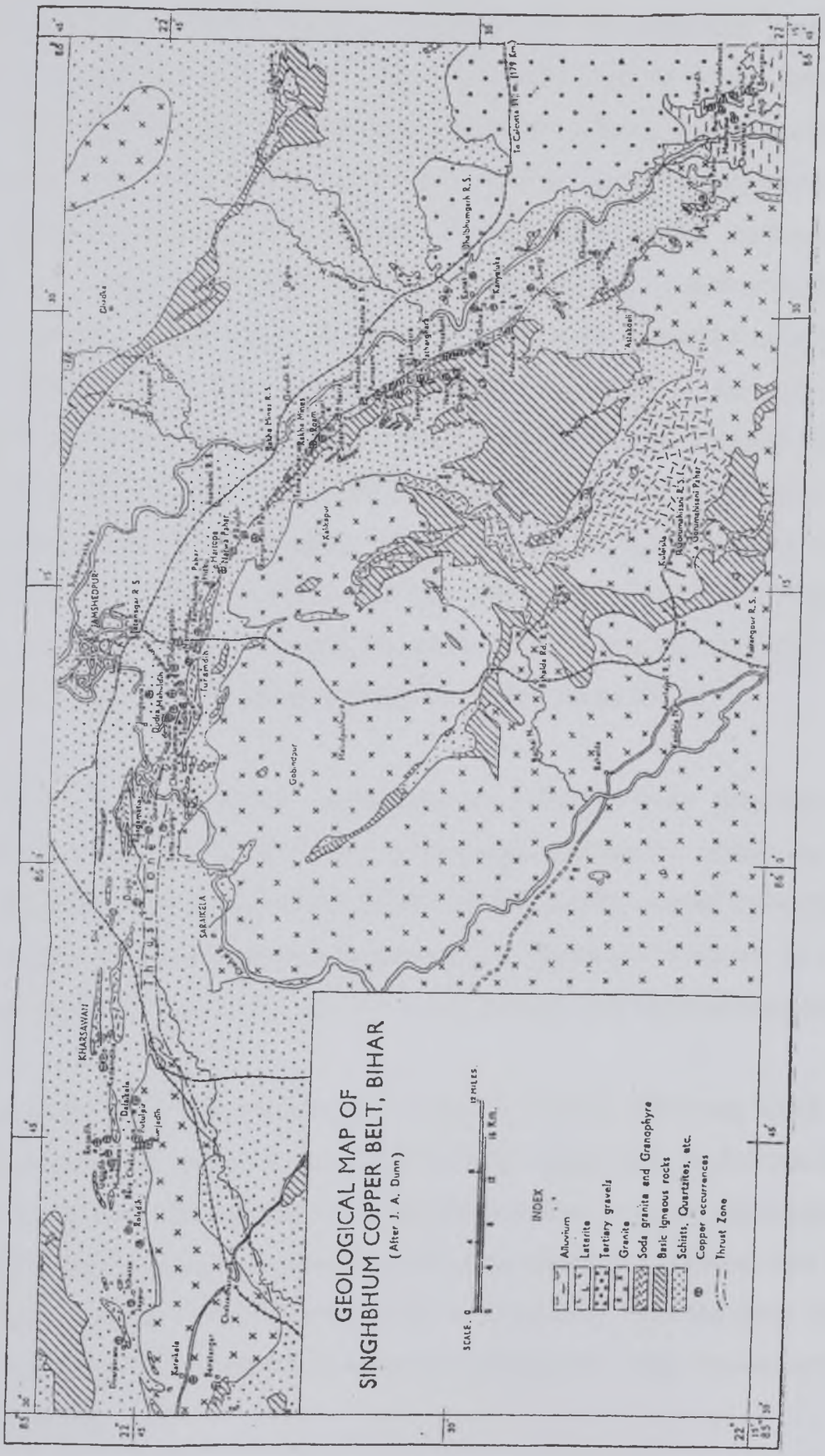

Figure 2.6 Geological map of the Singhbhum copper belt in Bihir, India (Dunn 1964).

Copper production is widespread around the rest of the world, the major producers being the Americas, Zaire, Zambia and Russia. In the Americas porphyry copper deposits are exploited from Alaska, Canada, eastern United States through Central America to Peru and Chile. The ore deposits of North America are predominantly of the porphyritic copper type. Stratabound copper deposits are located in east south central Alaska where the mineralisation includes chalcopyrite, digenite, chalcocite, djurleite, covellite and bornite (Sood at al. 1984). In the Wilcox ore located at Parry Sound, on the Georgian Bay, Lake Huron, chalcopyrite is the most important mineral (Schwartz 1923). Chalcopyrite is one of the predominant sulphides occurring in the South Kawishiwi Intrusion, Duluth Complex, Minnesota (Foose and Weiblen 1984). One of the world's most famous mining districts is found at Butte, Montana, named the 'richest hill on earth'. Here mineralisation of chalcopyrite took place from hydrothermal solutions passed upwards and outwards over a long period of time through a steadily evolving fracture system. At Island Mountain in California the deposit is found as a volcanogenic massive base metal sulphide ore (Hutchinson 1973).

In northern Haiti at Meme, mineralisation resulted from extensive magmatic assimilation of magma. In Chile the main copper production routes use porphyritic copper deposits. Chile produces around 20% of the world's copper (Minerals Yearbook 1993). The largest copper reserve in the world is found at Collahuasi in Chile, where two major porphyry copper deposits are found, Rosario and Ujina (Chadwick 1999).

In Africa, principal copper production is found in Zambia, Zaire and South Africa. The Zambian copper belt is part of the central African copper-belt. In Zambia the Murfilira deposit occurs as a vein orebody in the arenaceous host. In Zaire, chalcopyrite deposits are found as zoned primary sulphides in dolomitic shales at Kambove, also a part of the central African copper-belt (Cailteux 1984). At Kipushi in Zaire the main mineralisation of the hydrothermal polymetallic vein is chalcopyrite with bornite and sphalerite (Clifford 1997b).

In Europe the Kupferschiefer deposit lies on a belt from Germany through Poland, Holland and to England. The deposit, a copper rich shale, is an example of stratiform sulphide deposit of sedimentary affiliation and is mined in Germany and Poland. Poland is the principal copper producer in Europe (Clifford 1997a). Chalcopyrite is found at

Rio Tinto in Spain, the most important ore field in the Iberian Pyrite Belt as sedimentary massive sulphides (Strauss and Gray 1984). Current operations in Rio Tinto are carried out on chalcopyrite stockworks of the Cerro Colarado open pit (Chadwick 1998). The ore deposits Skouriotissa, Mavrovuni, Limni and Mavrida in Cyprus are examples of volcanogenic massive base metal sulphide ores (Hutchinson 1973).

East of Europe the Udokan ores in the Urals are dominated by chalcopyrite and bornite mineralisation which is also true of the Dzhezkazgan deposit in Central Kazakhstan (Bogdanov 1984). Chalcopyrite has been identified in cupriferous sandstones and shales on the Siberian platform (Krendelev 1984). West of the Siberian platform chalcopyrite deposits are associated with the Venedian red-bed formation in the Igarka area (Gablina 1984). Disseminated chalcopyrite is one of the predominant sulphides mined at the Sar-Chesmeh porphyry copper mine situated near the centre of the Zagros mountain range in Kerman province, Iran (Abdollahy 1996).

At Hixbar in the Philippines, chalcopyrite deposits form as volcanogenic massive base metal sulphide ores (Hutchinson 1973). Many copper deposits in Australia are sediment hosted, which are formed from hydrothermal fluids. These deposits include the Olympic Dam in South Australia, and Mount Isa in Queensland (Lambert et al. 1984).

2.4 Extractive Metallurgy of Copper

Copper occurs predominantly as sulphide ores, chalcopyrite ($CuFeS_2$), bornite (Cu_5FeS_4) and chalcocite (Cu_2S) being examples of such ores. Within the ore body containing these minerals, the copper concentration is very lean at around 0.5-2 wt. %. Copper also forms as oxide minerals although these are not as common as the sulphide minerals. Copper extraction from the sulphide minerals occurs as a result of mineral beneficiation to a rich concentrate followed by smelting and refining whereas hydrometallurgical methods are employed for the oxide minerals. Pyrometallurgical methods are used to produce about 80% of the world's production, the rest being produced via hydrometallurgical routes and from the recycling of scrap copper (Gilchrist 1989).

The most comprehensive work on the extraction of copper from its sulphide is by the authors Biswas and Davenport (1980). The extraction of copper occurs in different steps, detailed later in this section. Figure 2.7 is a flow sheet generalising these different routes for copper extraction. The first stage to any extraction process of copper by pyrometallurgical methods is the concentration of the chalcopyrite ore. In early extraction processing the concentrate was sintered prior to being heat treated in a blast furnace although this was replaced by the use of reverberatory and electric smelters; both methods are now on the decline with current process technology revolving around flash smelting and continuous processes.

2.4.1 Concentration of Sulphide Ores

All sulphide ores are concentrated via physical methods because the sulphide ores are too lean to be smelted directly (Bosqui et al. 1954). Concentration means the isolation of the copper mineral, first by crushing and grinding down to a size sufficiently fine to liberate the copper mineral grains from the non-copper mineral particles and then by froth flotation. The resultant copper mineral concentrate normally contains around 25-30 wt. % copper. The concentrate is roasted prior to smelting in reverberatory or electric furnaces, or dried before being smelted in flash furnaces. In continuous converting the concentrate is sent straight to the furnace for a single step process

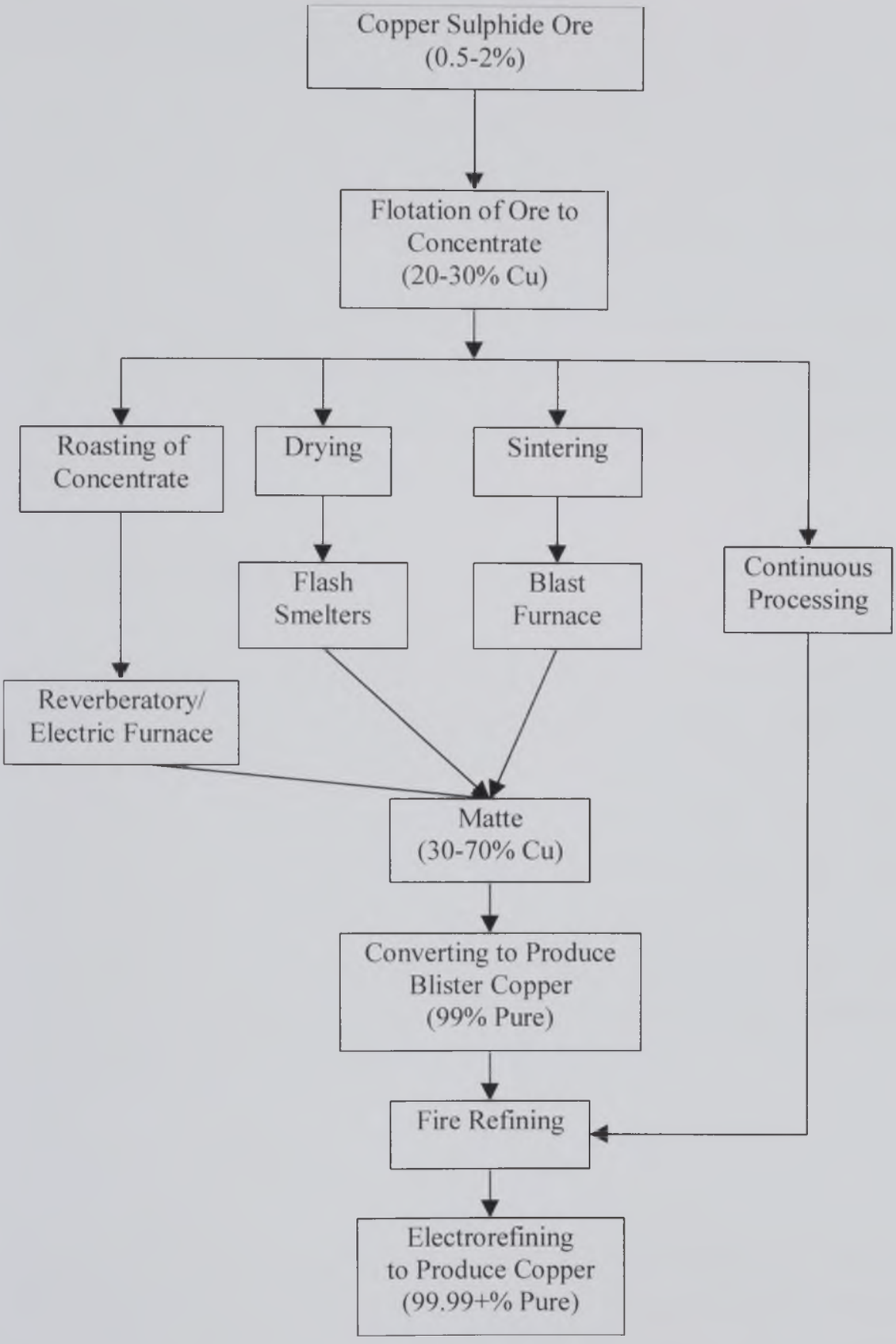

Figure 2.7 Generalised flow sheet for the extraction of copper from copper sulphide mineral ores via different processes.

2.4.2 Roasting of the Concentrate

Roasting is a process used to partially oxidise the Cu-Fe-S concentrate with air in a temperature range of 700 to 750°C (Boggs 1954). Roasting is carried out in fluidised beds, which operate on the principle of blowing air through a mass of particles. These particles are suspended in the air stream and so are oxidised from the process. A hot, dry calcine is produced which is then smelted in reverberatory and electric furnaces. Roasting of the concentrate is in decline; this process is now only used prior to smelting in reverberatory and electric smelters. In modern processes the roasting is carried out in flash smelters.

2.4.3 Reverberatory Furnace

Reverberatory furnaces replaced the old blast furnaces in copper extraction routes. The reverberatory furnace is a fossil-fuelled furnace that smelts a copper iron sulphide calcine with concentrate, ore, slag and fluxes, which are fed into the top of the furnace. Reactions occur at the interfaces to form a molten copper matte, which is then transferred to Pierce-Smith converters to produce blister copper. Also produced is a molten iron silicate slag, which is discarded, the evolved SO_2 gas is sent for further processing. In 1970 Milliken foresaw the phasing out of these furnaces in preference to flash smelters. Indeed the number of these furnaces has reduced around the world, their being replaced by flash smelters.

2.4.4 Electric Smelting

The electric smelter smelts a dried or moist roasted concentrate to produce a matte containing 50-60 wt. % copper which is sent to the converters, a molten slag and an off-gas containing SO_2. The energy for the smelting of the concentrate comes from the passage of an electric current through the melt between two carbon electrodes (Robiette 1973). The use of electricity makes the process more expensive than the flash smelters which require external heat sources only for control. The electric smelter has not been widely adopted since its introduction.

2.4.5 Flash Smelting of the Concentrate

Smelting involves the melting of the mineral concentrate in a large flash furnace, at a temperature of 1220°C. Two types of flash furnaces are the Outokumpu and the INCO. The aim of smelting is to oxidise the mineral concentrate to produce a matte containing a high copper concentration between 35-70 wt. %. The matte phase is seen as a mixture of Cu_2S and FeS (Rosenqvist 1975). An oxidised phase known as the slag is also produced containing as little copper as possible. The fayalite slag ($FeO.SiO_2$) is discarded, and the sulphur dioxide containing gas generated is processed further to sulphuric acid. The overall equation for the smelting process is given as:

$$2CuFeS_{2(conc)} + {}^{5}/_{2}O_2 + SiO_{2(flux)} = Cu_2S.FeS_{(matte)} + FeO.SiO_{2(slag)} + 2SO_{2(g)} \qquad (2.1)$$

The molten matte and slag are tapped off separately as they build up. The matte is sent to the converters in its molten state to be turned into blister copper. The slag is treated for reclamation of any residual entrained copper. Iron silicate slag is finally dumped in a landfill site.

Copper smelting, in terms of the Cu-Fe-S-O-SiO_2 system at 1300°C, has been described in terms of sulphur-oxygen potential diagrams, two of which are given here. The first one is given in figure 2.8 on which the conventional oxidation process in matte smelting occurs between A and B (Yazawa 1974). In this method of illustration of copper smelting the stability regions of the condensed phases are given as a function of the sulphur and oxygen potentials. In the region denoted by pqrst, two liquid phases are present, a matte phase and a slag phase. These two phases are in equilibrium with a gas phase. The line tp represents the upper limit at which both matte and slag coexist with a gas phase under atmospheric conditions. The line st corresponds to an iron silicate slag saturated with both silica and magnetite. Above this line the slag is no longer stable due to separation of magnetite. The stability region of matte exists between those for Cu_2S and FeS. The line pq represents a silica saturated slag in equilibrium with a FeS-FeO matte. The co-existence of liquid copper and Cu_2S in equilibrium with an iron silicate slag is represented by the line rs.

Sridhar et al. (1997a) produced a second sulphur-oxygen copper smelting diagram for copper smelting which is given in figure 2.9. This smelting diagram was constructed from available data in the Cu-Fe-O-S-SiO_2 system and from the operating data of commercial smelting furnaces. On this diagram levels for oxygen partial pressure, sulphur partial pressure, slag copper levels and slag magnetite levels up to about70% grade are shown. Copper smelting takes place in the shaded region with some plant operations plotted in terms of their matte copper content. This diagram is seen by Sridhar et al as an useful diagnostic tool for providing details for copper losses to slag, magnetite level and expected sulphur level for any specified matte grade.

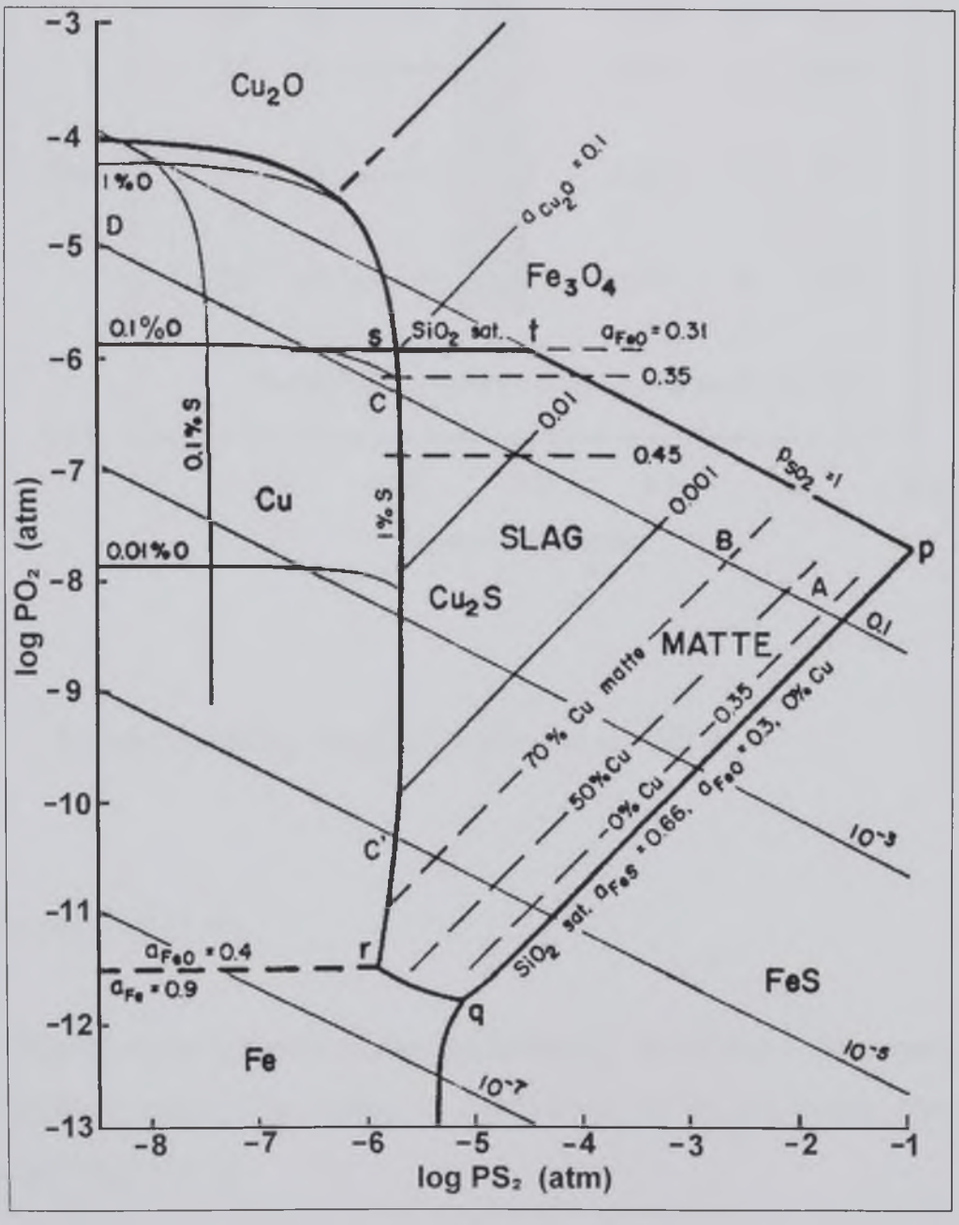

Figure 2.8 Sulphur-oxygen potential diagram for the Cu-Fe-S-O-SiO_2 system at 1300°C (Yazawa 1974).

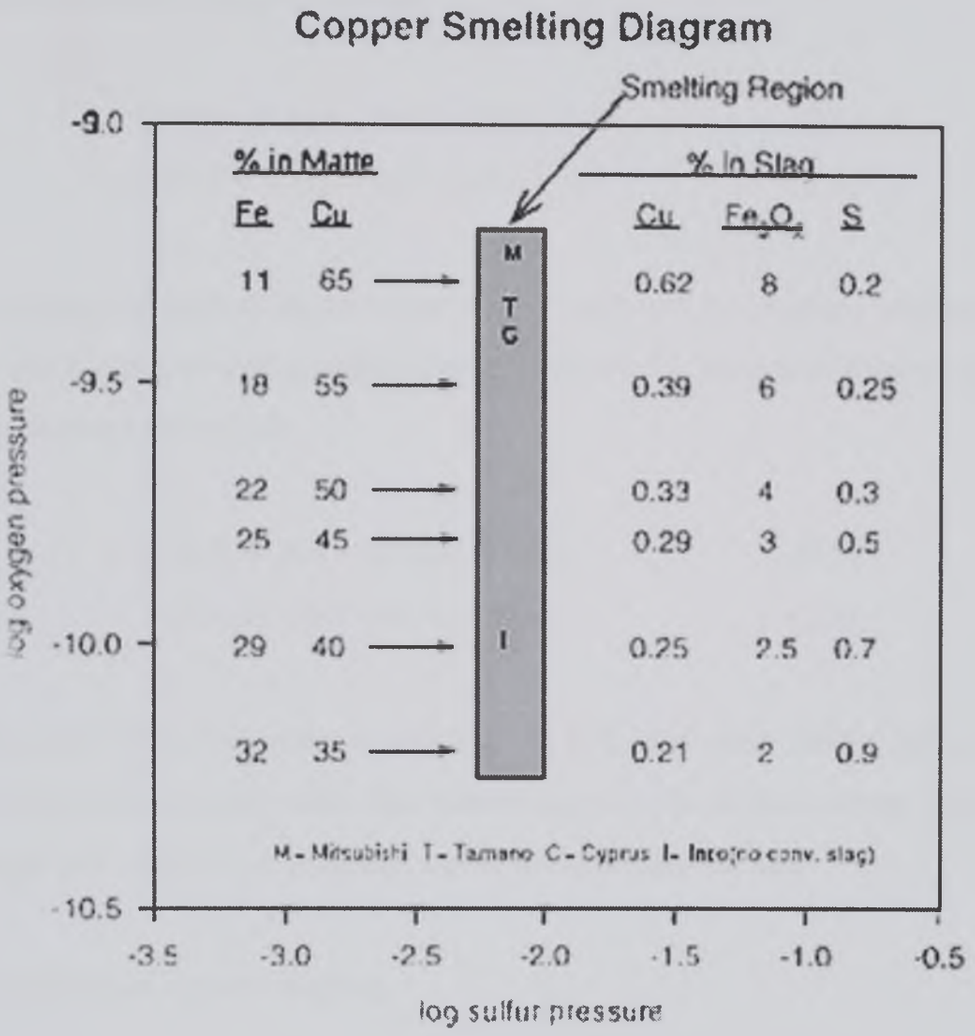

Figure 2.9 Copper smelting diagram (Sridhar et al. 1997a).

2.4.6 Converting of Matte

The converting of matte consists of the oxidation by air of the copper matte produced from the smelting stage. Converting is carried out in Pierce-Smith converters; the overall reaction is given as:

$$4(Cu_2S.FeS)_{(l)} + 10^1/_2\ O_{2(g)} + SiO_{2(s)} = 8Cu_{(s)} + 2FeO.SiO_2.Fe_2O_{3(s)} + 8SO_{2(g)} \qquad (2.2)$$

There are two aims to this process, the first aim of the process is to oxidise and slag off the iron from the matte, thus removing sulphur. The product from this stage is white metal, which is mainly copper sulphide.

$$2FeS + 3O_2 = 2FeO + 2SO_2 \quad (2.3)$$

$$2FeO + SiO_2 = 2FeO.SiO_2 \quad (2.4)$$

The second stage of converting involves sulphur removal by blowing oxygen producing a molten metallic phase with a copper grade of 99 wt. %, known as blister copper due to the blisters formed when cast.

$$2Cu_2S + 3O_2 = 2Cu_2O + 2SO_2 \quad (2.5)$$

$$2Cu_2O + Cu_2S = 6Cu + SO_2 \quad (2.6)$$

The waste gases from this process are high in SO_2 and need further processing. Any precious metals are retained within the molten copper. The blister copper produced from converting is too brittle to be used and needs to be refined further.

2.4.7 Continuous Copper Smelting

In conventional matte smelting and converting processes there are three steps to copper production, smelting of the concentrate followed by converting to white copper before blowing to form blister copper. In continuous smelting the concentrate is smelted and oxidised in one step to produce blister copper, sulphur dioxide and the slag phase (Johansen et al. 1970). The overall reaction for this process is given as:

$$4CuFeS_{2(conc.)} + 10½\ O_2 = 4Cu_{(l)(blister)} + FeO_{(l)(in\ silicate\ slag)} + Fe_3O_{4(s)(magnetite)} + 8SO_{2(g)} \quad (2.7)$$

Holeczy et al. (1964) concluded that continuous copper production is possible in two ways, firstly with the coexistence of two layers in the melt, copper and slag. Secondly with the coexistence of three layers in the melt, copper, white metal and slag. The minimum temperature for the production of copper from this process is given as 1250°C.

Such continuous copper converting operations include the Mitsubishi and Noranda processes (Nagamori and Mackey, 1978). The Noranda process is an example of continuous smelting and continuous copper conversion. The Mitsubishi is an example of continuous direct copper production from concentrates.

The sulphur content of the copper product at the end of the Mitsubishi continuous process is found to be higher than that of the conventional copper blow resulting in a need for additional sulphur removal by fire refining. Sridhar et al. (1997b) mentions that this disadvantage is outweighed by the excellent environmental control achieved by continuous converting.

2.4.8 Processing of SO_2 Gas

The offgases from smelting and converting are treated for SO_2 removal in sulphuric acid plants. The exception is offgas from reverberatory furnaces, in which the concentration of SO_2 is too dilute for economic acid manufacture; this is one of the reasons for closure of many reverberatory furnaces.

To manufacture H_2SO_4 the gases are cooled and cleaned of any dust and vapour impurities. The gas phase is then dried with 93% H_2SO_4/ 7% H_2O sulphuric acid. The SO_2 constituent is catalytically oxidised to SO_3 and is absorbed into the H_2O component of 98% H_2SO_4/ 2% H_2O sulphuric acid.

2.4.9 Refining of Blister Copper

Most of the blister copper from converters is electrorefined. In order to achieve this, the copper must be of a high enough grade to be cast into anodes smooth enough for interleaving with cathodes in the electrorefining cells. To obtain this grade, the copper is fire refined to remove most of the sulphur and oxygen (Baier and Kushma 1954). Typical concentrations of oxygen and sulphur in blister copper are 0.5-2% and 0.2-0.5% respectively.

To obtain a good conducting grade of copper the fire-refined copper is cast into anodes, which are placed into a Cu_SO_4 - H_2SO_4 - H_2O electrolyte solution with copper cathodes.

An electrical potential is applied across the electrolyte between the anode and cathode. The copper from the anode electrochemically dissolves into the electrolyte producing copper cations and electrons. The electrons and copper cations recombine at the cathode surface to produce the copper metal which plates onto the cathode. Impurities are prevented from plating onto the cathode by choosing an electrolyte in which the impurities can't dissolve.

A copper product relatively free of impurities is produced and the valuable impurities, such as gold and silver, are separated from the impure copper to be recovered elsewhere. The electrorefined copper, containing 20 parts per million impurities, is then melted and cast.

2.4.10 Recovery of Precious Metals

Gold, silver and the other precious metals do not dissolve in the electrolyte during electrorefining, they form as an anode slime that adheres to the anode surface or falls to the bottom of the electrolysis tank. These slimes are collected and sent for precious metal recovery if their concentration is sufficient to warrant treatment (Gilchrist 1989).

The anode slimes are leached and washed so they are as free as possible of metals such as copper, then roasted to eliminate or recover any Se or Te. The residue is melted down to an alloy of gold and silver with any of the other precious metals present (Dore metal). The Dore alloy can be electrolysed in a nitrate electrolyte where the silver is transferred to the cathode and is deposited as loose crystals. The gold and platinum group metals are refined at the anode in a fabric envelope or a specially positioned tray. To further refine the silver, the cathodic deposit is melted under charcoal and cast to form ingots of a very fine quality (Abdollahy 1996).

2.4.11 Control of Impurities during Copper Extraction

Impurities such as arsenic, antimony, lead and bismuth can be present in the chalcopyrite concentrate prior to smelting. These impurities can have a detrimental effect on the final copper metal produced, therefore it is important to eliminate these elements during the copper making process. These elements are difficult to remove by

oxidation into the slag and so are partially volatilised during smelting (Yazawa 1974). The matte is kept at a high temperature to increase the volatilisation of impurities and to aid this, the interfacial area between the liquid and gas is also kept large. The impurities not volatilised stay within the copper through the process until electrorefining where they are removed from copper and collect as part of the anode slimes.

CHAPTER THREE

The Reduction of Metal Sulphides and the Presence of Precious Metals and Impurities during Copper Extraction

3.1 Introduction

The reduction of metal sulphides can be achieved by the addition of solid carbon with a sulphur scavenger e.g. lime and heat treating under an inert atmosphere, or by using a reducing gas such as hydrogen or carbon monoxide in place of the solid carbon. This chapter details research carried out on this subject with particular emphasis placed on the phase equilibria relating to reduction of chalcopyrite.

Precious metals, especially silver, are important by-products of copper extraction and therefore important to research on reduction of chalcopyrite. A discussion of relevant research and phase equilibria is given here. Lastly the control of impurities during copper extraction is essential and is also related in this chapter.

3.2 Hydrogen Reduction of Metal Sulphides

Various authors have investigated the reduction of metal sulphides by hydrogen gas. Such a recovery of the metal by hydrogen is based upon the reaction:

$$MS_{(s)} + H_{2(g)} = M_{(s)} + H_2S_{(g)} \qquad (3.1)$$

The reaction is unfavourable (Cech and Tiemann 1969), as hydrogen does not react appreciably with metal sulphides, which can be seen by looking at the equilibrium constant for the reaction. At 800°C, the equilibrium constant, k, is in the range of 2×10^{-3} to 6×10^{-3} for the metal sulphides of Cu, Ni, Co and Fe.

To substantiate this, experiments carried out with the metal sulphide and hydrogen gas in an enclosed chamber, show negligible amounts of the metallic phase formed (Habashi

and Dugdale 1973). The hydrogen sulphide gas acts as an inhibitor to the reaction causing a low metal yield (Kor 1974). This is due to the low equilibrium constants; to overcome this, the equilibrium needs shifting to the right. To do this it is necessary to remove the hydrogen sulphide as soon as it has been produced. It was suggested that this could be achieved by maintaining a high enough gas flow for the H_2S to continually be carried away once produced (Habashi and Dugdale 1973). A better method is to add a reagent to the initial mixture, which reacts with the H_2S gas and removes it from the reaction site by forming H_2O and a solid sulphide compound. A basic oxide would do this, for example calcium oxide; lime has indeed been utilised by many researchers.

Lime is cheap and readily available and has a strong affinity for the H_2S gas, the reaction for which is:

$$CaO_{(s)} + H_2S_{(g)} = CaS_{(s)} + H_2O_{(g)} \qquad (3.2)$$

The addition of lime lowers the activation energy of the reaction giving an indication as to the effectiveness of lime as a sulphur scavenger (Sohn and Won 1985). The Gibbs free energy for reaction 3.2 is $-65{,}510.9 + 3.64T$ J mol^{-1} in the range of 750°C to 1425°C (Rosenqvist 1951).

As the sulphur is taken up as the solid calcium sulphide phase, the effluent gas stream should contain no sulphur (Cech and Tiemann 1969). This phase is also found not to inhibit the reaction site. The overall reaction is as follows:

$$MS_{(s)} + H_{2(g)} + CaO_{(s)} = M_{(s)} + CaS_{(s)} + H_2O_{(g)} \qquad (3.3)$$

The equilibrium constant for this reaction for copper sulphide is 1.7×10^3, which makes this reaction far more favourable than reaction 3.1 (Habashi and Dugdale 1973).

For the reduction of copper sulphide in the presence of lime, the reaction is:

$$Cu_2S_{(s)} + CaO_{(s)} + H_{2\,(g)} = 2Cu_{(s)} + CaS_{(s)} + H_2O_{\,(g)} \qquad (3.4)$$

At 1000°C in the absence of lime, slow reduction takes place with only 40% of the sulphur being eliminated, whereas at similar temperatures with lime added all of the sulphur is taken up as calcium sulphide. The formation of metallic copper is observed and the gaseous reaction product is exclusively water causing no pollution problems.

Copper metal can also be produced via hydrogen reduction from its complex sulphide mineral, chalcopyrite, the reaction for which is given as equation 3.5 (Habashi and Yostos 1977). Hydrogen reduction of natural chalcopyrite concentrates yield copper and iron metal in the form of filaments. Copper filaments form as a result of hydrogen reduction of copper sulphide in the temperature range of 550°C to 750°C (Sohn and Won 1985a).

$$CuFeS_{2\,(s)} + 2CaO_{(s)} + H_{2\,(g)} = Cu_{(s)} + Fe_{(s)} + 2CaS_{(s)} + 2H_2O_{(g)} \qquad (3.5)$$

From investigations into the reduction of nickel sulphide, increasing the molar ratio of CaO to nickel sulphide was found to give an increased effectiveness of H_2S removal, subsequently giving a faster rate of reduction (Sohn and Won 1985). Furthermore, coating the NiS pellets with lime also substantially increases the fixation of sulphur, showing that both the quantity and the distribution of lime through the pellet determine the fixation of sulphur to calcium sulphide. Increasing the temperature and the amount of lime both increase the rate of reduction (Rajamani and Sohn 1983).

Samples of reduced nickel sulphide were examined under the electron microscope to determine the physical characteristics of the metal phase produced (Thiam Chye Tan and Ford 1984). At lower temperatures, below 530°C, the nickel produced is in globular form. Above this temperature, the nickel begins to grow as fibres. Fibrous growth of metal was observed by Sohn and Won (1985a) from reduction of copper sulphide.

Byerley et al. (1972) investigated the kinetics of the reduction of nickel sulphide in the temperature range of 1133°C to 1300°C. The rate of reduction of nickel sulphide is second order with respect to sulphur concentration and half order to hydrogen pressure.

The authors conclude that the nickel in the molten sulphide may function as a catalyst promoting the reaction between S_2 and hydrogen. The theory of metals acting as the catalyst was furthered by Byerley et al (1973). The study was extended to Fe, Cu, Pb and Co sulphides investigated in the range of 1080°C to 1340°C. The order of catalytic activity is given as Ni ≈ Fe > Co > Cu > Pb. These catalytic metals adsorb the reacting molecules allowing the reaction to proceed via a path involving lower activation energy.

Due to SO_2 emissions, and hence environmental demands in the U.S, Cole et al. (1974) investigated the vapour phase reduction of lead sulphide. Complete reduction (>99%) is achieved by direct reduction of PbS vapour with hydrogen gas, with the minimum amount of gas needed to be 15 times the stoichiometric quantity. The residue from this process was found to contain potentially valuable by-products, such as Cu, Ag and Zn. Sulphur is removed as H_2S, which can be decomposed to elemental sulphur and water vapour.

Molybdenite (MoS_2) is reduced in hydrogen to produce molybdenum metal; again lime is used as the sulphur fixer (Mankhand and Prasad 1982). The best conditions to produce the metallic phase are to have high temperatures and to keep the hydrogen flow at a minimum. This observation had not been mentioned before and is an important result as minimising the flow rate discourages the production of H_2S.

3.3 Carbothermic Reduction of Metal Sulphides

Work of the most relevance to this thesis has been reported by Jha and co-workers (Jha et al. 1989, 1991, 1992a, 1992b) with the study of the reduction of synthetic chalcopyrite (Jha and Grieveson 1992b) being the most pertinent here. With respect to the reduction of chalcopyrite, $CuFeS_2$, the mineral may be seen as $Cu_2S.FeS$, therefore considerations of the reduction of Cu_2S (Jha et al. 1989) and FeS (Jha et al. 1991, 1992a) are highly applicable.

However, none of these references describe in detail selective reduction for achieving the preferential separation of copper and iron and no experimental data exists in the

literature. Furthermore, there have been no attempts to understand the distribution of gold and silver during the reduction process in these and other references. The recovery of gold and silver is of the utmost importance in a copper-making process because these two metals can be more valuable than the copper itself.

The production of metallic lead from lead sulphide is possible via the reduction process. An optimum yield of 80-86% lead can be achieved from direct reduction of lead sulphide at 900°C, utilising sodium carbonate as the sulphur scavenger as opposed to calcium oxide preferred by most other authors (Chesti and Sircar 1971). Lead sulphide reacts with sodium carbonate to facilitate the conversion of lead sulphide to a more reducible phase by eliminating sulphur. The lead oxide produced is then reduced by carbon monoxide to form lead, the purity of which is in the order of 99.2-99.6%.

$$PbS + Na_2CO_3 = PbO + Na_2S + CO_2 \qquad \Delta G^\circ_{1073K} = -33.49 \text{ kJ mol}^{-1} \qquad (3.6)$$

$$PbO + CO = Pb + CO_2 \qquad \Delta G^\circ_{873K} = -31.4 \text{ kJ mol}^{-1} \qquad (3.7)$$

Igiehon et al. (1992a) chose calcium oxide for sulphur capture during reduction of lead sulphide. The exchange reaction, equation 3.8, between lead sulphide and lime produces lead metal and calcium sulphide at reaction temperatures between 900°C and 1000°C.

$$3PbS_{(s)} + 2CaO_{(s)} = 3Pb_{(s)} + 2CaS_{(s)} + SO_{2\,(g)} \qquad (3.8)$$

In the presence of graphite, lead sulphide is reduced to lead metal in the temperature range of 900°C to 1000°C. However CaO and PbS are observed to be present in the resultant mixture, suggesting that the reaction has not gone to completion. This is assumed to be due to an accumulation of intermediate oxide phases formed from the exchange reaction between PbS and CaO. The production of intermediate phases is higher than the reduction of these intermediate phases hence leading to an accumulation.

Rao and El-Rahaiby (1985) determined that increased temperature during reduction of lead sulphide gives increased rates of reduction. 90% reduction occurs at 915°C for one hour, whereas at 849°C, 10 hours are needed to achieve the same degree of reduction.

The effect of temperature on the reduction of nickel sulphide also shows that an increase in temperature leads to an increased rate of reduction. Bronson and Son (1983) investigated nickel formation from its sulphide during reduction proving that the metal forms from this process. One aspect investigated was the effect of the size of the nickel sulphide particles. Below 1000°C, the finer sized particles react faster, but above this temperature there is little effect of particle size on the reduction rate. For a given particle size, the reaction rate increases with increasing temperature.

Machingawata et al. (1989) observed that metallisation of nickel can occur in the absence of the reducing agent, but the reaction would take a very long time to reach completion. The addition of a carbon source speeds up the reduction reaction considerably, especially so when coal is used, graphite being a slower reducing reagent than coal.

When plots of the reduction rate as a function of time for nickel sulphide are examined, a plateau is seen; this is a stage when a steady state of oxygen ion transport is established from the surface of the lime across the matte phase to the carbon surface. These plateaux have been noted in other reduction studies (Jha and Grieveson 1992b, Igiehon et al. 1992b).

Metallic iron is conventionally produced from the reduction of iron oxide ores; iron sulphide ores are exploited less for the extraction of metallic iron. Vert and Kamenstev (1956) carried out an early investigation on reduction of ferrous sulphide. The reaction of CaO and FeS was conducted in the presence of carbon that allowed for the production of iron:

$$CaO_{(s)} + FeS_{(s)} + C_{(s)} = CaS_{(s)} + Fe_{(s)} + CO_{(g)} \qquad (3.9)$$

But also prevented:

$$CaO_{(s)} + FeS_{(s)} = CaO.FeS_{(s)} \qquad (3.10)$$

Investigations were carried out on the reduction of pyrrhotite (Jha 1991, 1992a) with lime and carbon. Experiments were initially carried out on mixtures of FeS/CaO and FeO/CaS to investigate the exchange reaction between the S^{-2} and O^{-2} anions with Fe^{+2} and Ca^{+2} ions to produce $FeO/Fe_{1-x}O$ and CaS phases (Jha et al 1991). The exchange reaction is shown as:

$$FeS_{(s)} + CaO_{(s)} = FeO_{(s)} + CaS_{(s)} \qquad (3.11)$$

These two products combine to form intermediary oxysulphide compounds:

$$xFeO + yCaS = (FeO)x.(CaS)y \qquad (3.12)$$

Which are subsequently reduced by carbon:

$$FeO + C_{(gr)} = Fe + CO \qquad (3.13)$$

The combined reaction for the reduction of pyrrhotite is thus:

$$FeS_{(s)} + CaO_{(s)} + C_{(gr.)} = Fe_{(s)} + CaS_{(s)} + CO_{(g)} \qquad (3.14)$$

Different stoichiometric mixtures of FeS/CaO and FeO/CaS heated in argon form intermediary compounds. The two phases observed are named C_I and C_{II} where compound C_I has the formula 4FeO.3CaS and C_{II} is an equimolar compound FeS.CaO or FeO.CaS. The structure for the C_{II} oxysulphide phase is given in figure 3.1. The path of reduction of the compounds, C_I and C_{II} in the FeO-CaS-FeS-CaO quaternary diagram is given in figure 3.2.

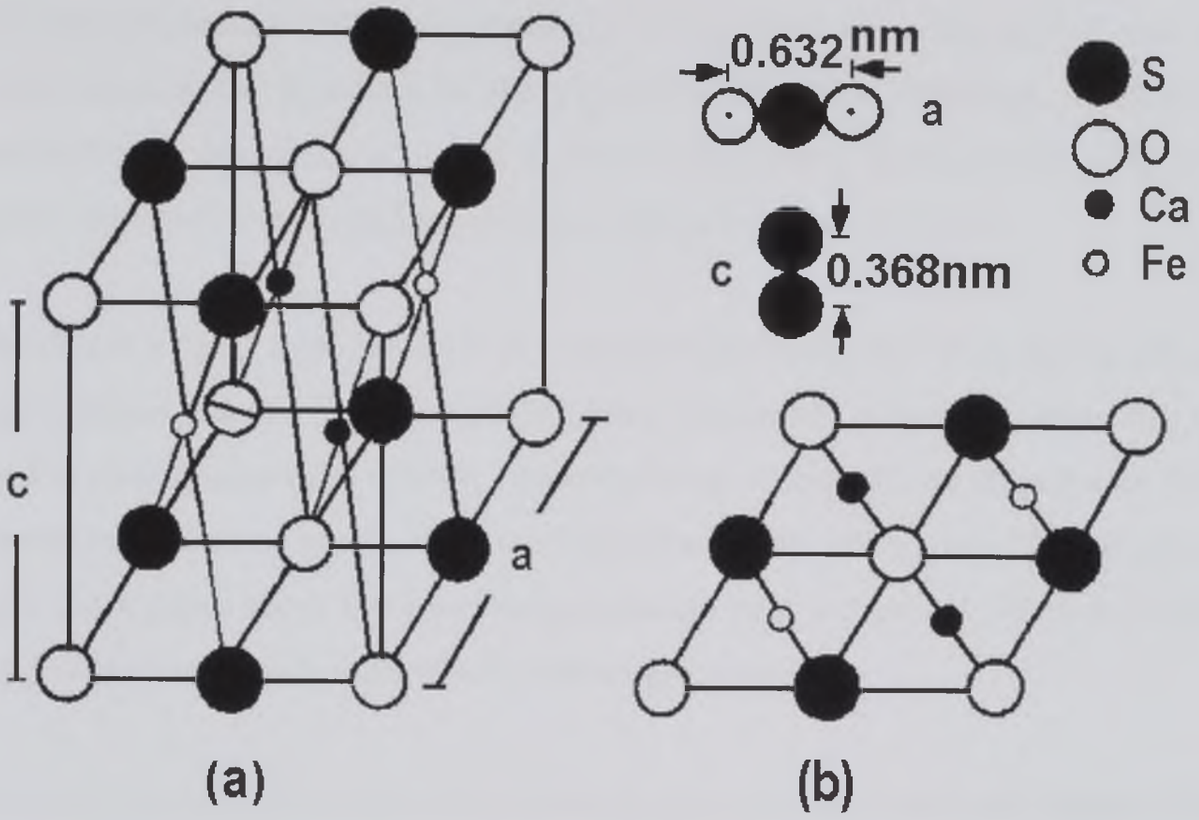

Figure 3.1 Structure for the C_{II} phase a) 3d–ideal lattice b) lattice sites for various ions. (Jha et al. 1991).

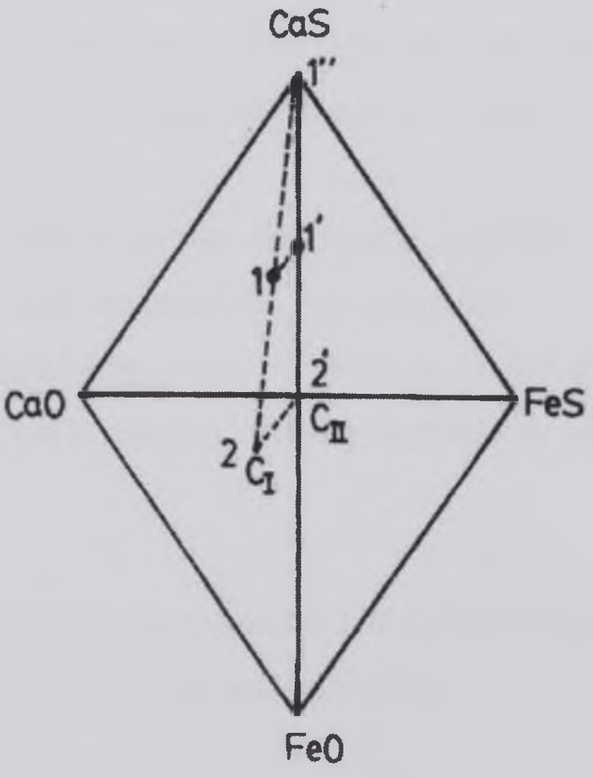

Figure 3.2 FeO-CaS-FeS-CaO quaternary phase diagram showing the path of reduction of compounds C_I and C_{II} (Jha and Grieveson 1992a).

Vert and Kamentsev (1956) suggested that the addition of carbon to FeS and CaO would prevent the formation of the C_{11} (FeS.CaO) phase. However, although the production of this phase is limited to lower temperatures during reduction it is not totally prevented from forming according to Jha and Grievson (1992a).

Metallic iron forms from reduction of synthesised pyrrhotite with lime and the reducing agent, carbon (Jha and Grieveson 1992a). Plots of degree of reduction against time were used to show comparisons of time, temperature and composition on the reaction. As the temperature increases so does the rate of reduction: below 900°C, only 38% reduction is achieved whereas above this temperature, a steady state is observed. The time taken to achieve this steady state reduces with increasing temperature.

Coal and graphite were both used as the reducing agent and produced varying effects (Jha and Grieveson 1992a). Although the reduction characteristics are similar for both the extent of reduction for coal is higher than for graphite, in agreement with the same comparison made during reduction of nickel sulphide (Machingawata et al 1989). When more lime is added during the reduction of pyrrhotite, the rate is higher due to an increase in surface area for the exchange reaction to take place.

From X-ray analysis it is found that the compound C_1 is present at lower temperatures whereas C_{11} is detected at all temperatures, indicating that C_{11} is the last phase to be reduced. These oxysulphide phases were not found to inhibit the degree of reduction although Igiehon et al. (1992c) suggest that oxysulphides do inhibit the reduction of lead sulphide.

Zinc sulphide can be reduced to zinc (equation 3.15) as investigated in the temperature range of 900°C to 1100°C (Abramowitz and Rao 1978).

$$ZnS_{(s)} + CaO_{(s)} + C_{(s)} = Zn_{(g)} + CaS_{(s)} + CO_{(g)} \qquad (3.15)$$

$$\Delta G^\circ = 376{,}907 + 33.70/\log T - 405T \text{ J mol}^{-1}$$

At 1079°C complete reduction is achieved after ~ 175 minutes. At 919°C for the same period of time only 35% reduction occurs. The effect of porosity and sample size shows that the optimum porosity for reduction is 58% and that for decreased sample size the rate of reduction appears to increase.

The formation of ZnCaSO from heat treatments in the Zn-Ca-S-O system was investigated with a view to investigating the reduction of zinc sulphide (Igiehon et al 1992c). Stoichiometric proportions of ZnS-CaO and ZnO-CaS were heat-treated to form the ZnCaSO compound. X-ray diffraction analysis of reacted samples show the presence of this compound at 900°C and 1000°C. ZnCaSO is assumed to be a hexagonal lattice as the crystallographic data for this compound of both calculated and observed d-spacings agree. Figure 3.3 is a diagram of the proposed idealised crystal structure for this compound showing that the structure of ZnCaOS is similar to that of FeCaOS (Figure 3.1) reported by Jha et al (1991). The likeness between these two compounds is explained by the similarity of the crystal ionic dimensions of Fe^{2+} and Zn^{2+}.

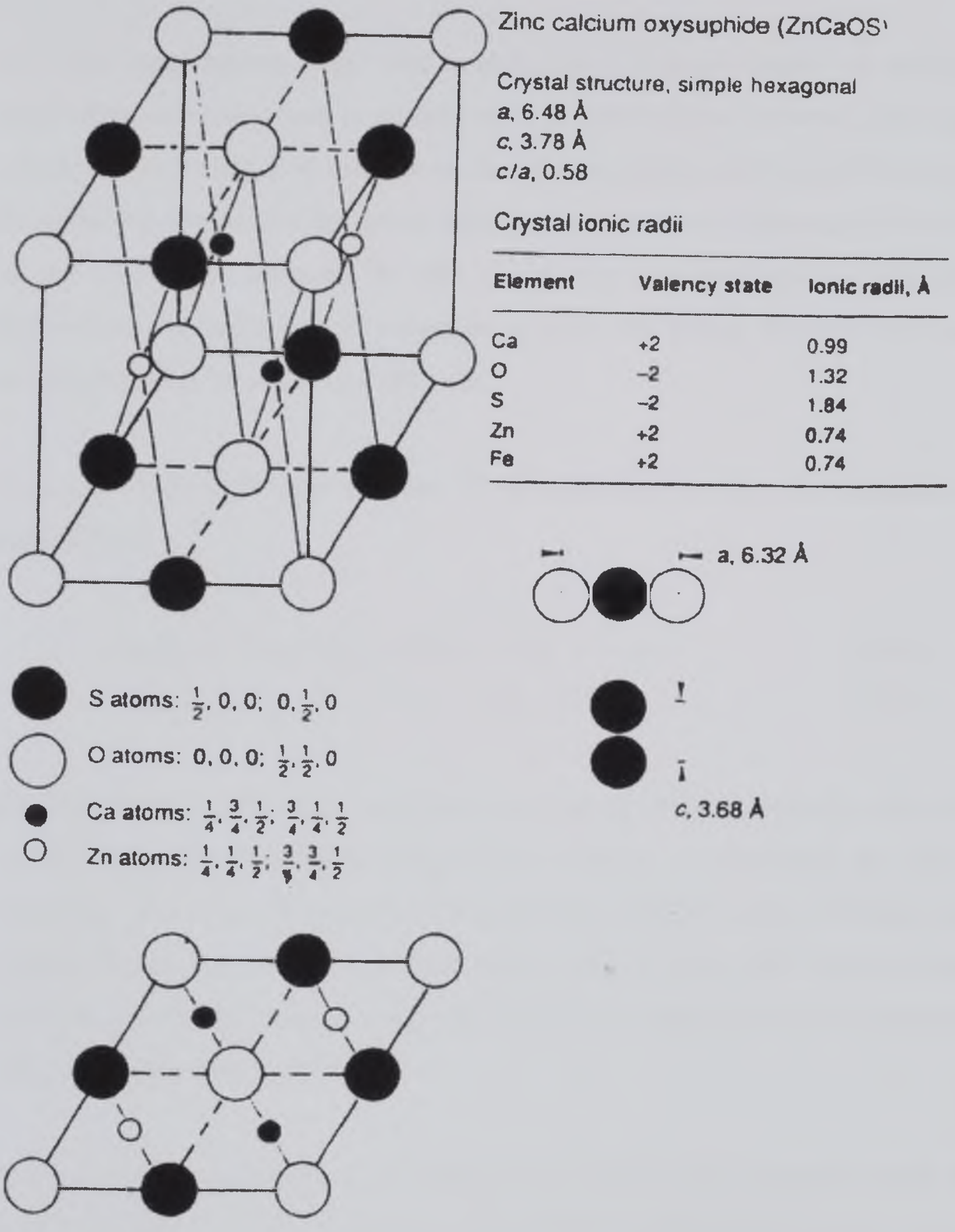

Figure 3.3 Idealised structure for the ZnCaSO compound (Igiehon et al 1992c).

At elevated temperatures the direct reduction of cuprous sulphide with carbon and lime is feasible (Moinpour and Rao 1985). The rate of reduction was determined from weight loss data, neither X-ray diffraction nor microscopy was employed in the investigation. The reduction kinetics are improved with increased lime and carbon quantities due to the favourable generation of gaseous species (CO and CO_2) which enhance reduction.

At lower temperatures larger size samples give a faster degree of reduction, as temperature increases there is no difference in reaction rate between small and large samples. This finding is at variance to that of Abramowitz and Rao (1978); they found for decreased sample size the rate of reaction increases for the reduction of ZnS to $Zn_{(g)}$. As the temperature increases the rate of reduction also increases and for any given temperature the initial rate of reduction is quite fast before dropping off. At lower temperatures this tail off is very obvious.

Jha et al. (1989) researched reduction of the sulphides of copper, the reactions for CuS and Cu_2S are:

$$Cu_2S_{(s)} + CaO_{(s)} + C_{(s)} = 2Cu_{(s)} + CaS_{(s)} + CO_{(g)} \quad (3.16)$$

$$CuS_{(s)} + CaO_{(s)} + C_{(s)} = Cu_{(s)} + CaS_{(s)} + CO_{(g)} \quad (3.17)$$

The individually synthesised sulphides were mixed stoichiometrically with lime and carbon, heat treated, and the weight loss recorded, to determine the kinetics of reduction. The main difference between the two sulphides is that, although copper is produced from the reduction in both cases, more is seen with Cu_2S as would be expected. As the temperature increases, so does the reduction rate, in agreement with other studies on metal sulphides.

Copper metal is gained from the reduction of tennanite and enargite, which are two copper arsenide compounds (Igiehon et al 1994b). Experimental analysis was carried out on synthetically derived forms of these compounds. Phase analysis of the reaction between tennanite ($Cu_{12}As_4S_{13}$) and calcium oxide shows the presence of CaS, copper sulphides, calcium arsenate (Ca-As-O) and copper-arsenic oxysulphide (Ca-As-S-O). The Ca-As-S-O compound is not properly identified due to lack of information on such compounds.

Reduction of tennanite and enargite was carried out by carbon in the form of coal and graphite. It is found that reduction by coal is complete only at higher temperatures, at

1000°C for 40 minutes. Reduction between 700°C and 900°C gives reaction products containing varying quantities of copper sulphide (Cu_2S or $Cu_{1.96}S$) leading to a conclusion of incomplete reduction. A similarity of results obtained from the reduction of tennanite and enargite was observed suggesting a similar reaction method for both sulphides occurred. Reduction for both tennanite and enargite is slower for graphite than with coal. After 90 minutes of reaction at 1000°C reduction is still incomplete for both sulphides.

Antimony sulphide can be reduced by carbon to antimony metal. Igiehon et al. (1994a) suggest that by reducing this sulphide in the temperature range of 700°C to 900°C, antimony metal could be produced. Comparison of reactions with MgO and CaO indicate that CaO is a more efficient exchange medium in the reduction of antimony sulphide (Igiehon et al 1992a)

The reaction of Sb_2S_3 with CaO showed the production of CaS and $Ca_3Sb_2O_6$ along with presence of an antimony oxysulphide. The actual composition is not concluded, the authors having assumed this compound to be a Sb-Ca-S-O quaternary oxysulphide. As with most references to these oxysulphide phases the authors state the limited available data on such phases.

Reduction of Sb_2S_3 results in CaS and Sb metal production. This reduction was carried out on synthetic and natural Sb_2S_3 (stibnite) concentrates. This study is found to be one of the few pieces of research carried out on a natural source of metal sulphide. Complete reduction is attained after 100 minutes at 800°C and 5 minutes at 900°C. Three natural ores were used with different Sb:S ratios, the higher the Sb:S ratio the quicker the rate of reduction.

Molybdenite can also be reduced by carbon to produce the metallic phase (Padilla et al 1997). Current molybdenum production is carried out in several stages. First the concentrate is roasted to produce molybdenum trioxide. The MoO_3 is purified by either hydrometallurgical or pyrometallurgical methods. Finally the MoO_3 is reduced by

hydrogen in two more stages. A direct reduction process would entail one process step and thus eliminate the time-consuming and energy-intensive stages.

As with many other direct reduction experiments by other researchers, lime was used as the sulphur capturer for molybdenum. Pellets of molybdenite, lime and carbon were used to investigate the reduction behaviour; this time nitrogen gas was used for the atmosphere. There was found to be no difference in the rate of reduction between mixtures as pellets or as powder, pellets only giving an ease of handling. The reaction mechanism discovered from these experiments shows that the sulphidisation of lime occurs by the direct oxidation of the mineral with CaO. This produces firstly MoO_2, then an intermediary oxide $CaMoO_4$, both of which are then reduced, by carbon initially and then by CO, to form metallic Mo or Molybdenum oxide. An oxysulphide or other complex compounds are thought to have formed, which is consistent with the work of Jha et al. (1989, 1991, 1992a, 1992b). The composition for such a compound is not given in the text.

The effect of temperature had a major influence on the reduction rate of molybdenite. An increase in the temperature from 900°C to 1100°C showed a marked increase in the rate such that, at 1200°C, the reaction is completed rapidly in less than 20 minutes. The amount of CaO is another factor that affects the rate of reduction. Excess is not needed: in fact it is likely to cause a decrease in reaction rate, due to an increased distance between MoS_2 and C particles and an enhanced production of $CaMoO_4$. However an excess of lime was found to increase reduction of pyrrhotite where it is argued that excess gives a larger surface area for reaction to occur (Jha et al. 1992a). An excess of carbon is found to increase the rate of reduction of molybdenite.

3.3.1 Carbon Monoxide Reduction of Metal Sulphides

Although in the reduction of CuS, hydrogen gas may be effective for the production of metallic copper, the cost of doing so on an industrial scale may be too expensive (Mohan et al 1987). Therefore, reduction by carbon monoxide has been investigated. The reaction for this is:

$$Cu_2S_{(s)} + CaO_{(s)} + CO_{(g)} = 2Cu_{(s)} + CaS_{(s)} + CO_{2(g)} \qquad (3.18)$$

The process is seen as a two stage reaction, the first being the evolution of a COS gas, leaving a metallic copper phase. The second, the desulphurisation of the gas by lime, differing from carbon reduction where the sulphide is desulphurised directly by lime leaving a metal oxide compound which is then reduced.

As the quantity of lime increases the amount of desulphurisation also increases, whereas an absence of lime slows the reaction rate. Increase in temperature increases the rate, as does the flow rate of CO but only until a limiting value is reached; this applies to all the controlling factors.

Udupa et al (1986) suggests that, according to the Boudouard reaction of equation 3.19, using carbon monoxide as the reducing agent can cause sooting to occur. Therefore it is necessary to know the limiting range of carbon monoxide needed to reduce any oxides, and so prevent sooting. The Boudouard reaction proceeds to the right above 670°C and rapidly from 950°C to 1050°C.

$$C + CO_{2\,(g)} = 2CO_{\,(g)} \qquad (3.19)$$

3.3.2 Effect of Catalysts

To increase the degree of reduction of metal sulphides two methods can be employed: firstly the temperature can be increased; secondly the addition of a catalyst can promote the degree of reduction (Rao 1983). Most authors mention the effect of temperature on reduction rates of metal sulphides. The consensus appears to be that an increase in temperature leads to an increase in rates of reduction. The addition of a catalyst can facilitate an increase in reduction rates as related here.

Catalysts in the form of Na_2CO_3, Na_2SO_4 and NaF were used to investigate their effect on the degree of reduction of ZnS (Abramowitz and Rao 1978). In the presence of

Na_2CO_3 the reaction rate increases with increased concentrations of the catalyst. 100% reduction occurs at 1080°C for 30 minutes with 1% Na_2CO_3. The addition of Na_2SO_4 also increases the reaction rate along with increase in concentration. Complete reduction is achieved with 1% Na_2SO_4 at 1086°C for 30 minutes. NaF is found to be a better catalyst, at 931°C complete reduction occurs after 800 minutes.

The investigation into the reduction of lead sulphides was furthered (El-Rahaiby and Rao 1984) by cell measurements of the reduction potentials of the gas phase that is evolved during the reduction reaction. The use of a catalyst on the rate of reaction was also examined. It is found that for the uncatalysed reaction, the reduction potential had values not far from the equilibrium CO/CO_2 ratio. With the addition of a catalyst, however, the reduction potentials are greatly enhanced towards the equilibrium for the Boudouard reaction.

Direct reduction of lead sulphide was undertaken under the influence of different catalysts (Rao and E-Rahaiby 1985). The catalysts used were K_2CO_3, Li_2CO_3, Na_2CO_3, Rb_2CO_3, NaF, Na_2SO_4 and the ternary $(K, Li, Na)_2CO_3$ eutectic.

Comparisons between Na_2SO_4, $(K, Li, Na)_2CO_3$ and NaF were made, NaF and $(K, Li, Na)_2CO_3$ appeared to be comparable whereas the $Na_2SO_4$was inferior to both at 850°C. Li_2CO_3, Rb_2CO_3 and $(K, Li, Na)_2CO_3$ exhibit nearly identical catalytic activities. K_2CO_3 is found to be nearly as effective as $(K, Li, Na)_2CO_3$ but Na_2CO_3 is definitely inferior. A ranking was made to these catalysts:

$$Li_2CO_3 > Rb_2CO_3 > (K, Li, Na)_2CO_3 = NaF = K_2CO_3 > Na_2CO_3 > Na_2SO_4$$

The effect of catalysts on the reduction of Cu_2S was initially studied in 1985 (Moinpour and Rao). The catalysts included K_2CO_3, Li_2CO_3, Na_2CO_3, NaF, Na_2SO_3 and $(K, Li, Na)_2CO_3$ eutectic. The preliminary investigations found that $(K, Li, Na)_2CO_3$ is the most effective followed by NaF, K_2CO_3, Na_2CO_3 and Li_2CO_3 with the least effective catalyst being Na_2SO_3.

Moinpour and Rao (1991) later furthered this study, when the catalysts used were the same as listed above and tested upon mixtures of Cu_2S:CaO:C and Cu_2S:4CaO:4C. As mentioned before the uncatalysed reduction of Cu_2S results in the formation of metallic copper. The catalysts listed above were found to enhance the degree of reduction at all temperatures studied. Gaseous intermediates, $CO_{(g)}$, $CO_{2(g)}$ and $COS_{(g)}$ are involved in the reaction. The Boudouard reaction is found to have an important influence on the kinetics of the uncatalysed reduction reaction. The rate of the Boudouard reaction is increased with the presence of the catalysts. The catalysts are given a ranking as to the effectiveness of enhancement on the reduction reaction:

$$(K, Li, Na)_2CO_3 > NaF > K_2CO_3 > Na_2CO_3 > Li_2CO_3 > Na_2SO_3$$

3.3.3 Reduction in a Plasma Environment

In a plasma medium an electric arc is maintained across a stream of gas passing between two electrodes, the potential difference across the gap is 500-7000V (Gilchrist 1989). From this the gas emerges as a jet of plasma of temperatures between 5000-7000°C. The plasma may be passed into a stream of ore or an ore and coal mixture, achieving an effect like flash smelting. The application of this technology has been investigated with respect to chromium and iron extraction. Selected research has utilised this technique for reduction of metal sulphides.

Udupa et al (1987) studied the use of plasma medium for carbothermic reduction of chalcopyrite. In this study the chalcopyrite utilised was a naturally occurring mineral from Massina, South Africa. The mineral concentrate was reduced by activated carbon 'in-flight' in a plasma environment in the presence of a desulphurising agent. Two such agents were used, CaO and Na_2CO_3, copper metallisation was higher when CaO was used. In the plasma medium a high degree of turbulence occurs breaking chalcopyrite particles and metallisation occurs at the fractures.

Molybdenum recoveries approaching 100% can be achieved in a plasma medium from molybdenum disulphide (Johnston and Pickles 1990). By reacting MoS_2 with CaO,

carbon and Fe, molybdenum can be recovered; the quantity increases with increased amounts of lime and carbon. However, excess addition of iron results in large amounts of ferromolybdenum forming.

3.4 Carbothermic Reduction of Chalcopyrite

Jha and Grieveson (1992b) suggest the possible separation of copper and iron from chalcopyrite can be achieved by carbothermic reduction of the concentrated mineral under controlled conditions. The theory for this observation is confirmed by examination of the Cu-Fe phase diagram (figure 3.4) discussed in more detail in section 3.5.1.

Synthesised chalcopyrite was made from stoichiometric amounts of CuS, oxide free metallic iron and elemental sulphur pressed into cylindrical pellets. The pellets were heat-treated in flowing argon to remove any residual oxygen.

Sulphur dioxide gas is evolved and metallic copper deposited from the reaction between chalcopyrite and lime. Metallic iron does not form from the exchange reaction and is found to be present as a quaternary oxysulphide, C_I or C_{II}, or as the quinary phase, C_{III}. The fraction of C_I found after heat treatment of chalcopyrite with lime is inversely related to the volume fraction of metallic copper. The oxygen potential needed to form metallic copper is lower than that in equilibrium with the C_I phase.

The quinary oxysulphide phase identified, C_{III}, has a structure broadly similar to that of the C_{II} phase (figure 3.1). The C_{II} phase is expected to have a range of solubility for copper ions so that a few copper ions will replace the iron ions within the crystal lattice. This exchange is possible because of the pseudo binary interaction in the Cu_2S-FeS system. This system is discussed in section 3.5.2.

Metallic copper and iron are produced from the reduction of chalcopyrite; neither lime nor the oxysulphide phases are found at the end of the reduction process. Partially

reduced pellets show no metallic iron deposition with this component only present as the oxysulphide compounds, C_{II} and C_{III}. Comparisons between CaO and Na_2CO_3 on the rate of reduction show that the presence of CaO leads to a higher degree of copper metallisation from chalcopyrite (Udupa et al 1984).

The results from these studies confirm that reduction of chalcopyrite yields metallic copper and iron. However the research carried out on the carbothermic reduction of chalcopyrite has been limited to the synthesised mineral. This has been true of most of the investigations into the carbothermic reduction of sulphides generally, the sulphides being stoichiometrically synthesised. When proposing new technology, it will be important to demonstrate its viability by studying natural mineral sulphides.

3.5 Phase Equilibria Relating to Carbothermic Reduction of Chalcopyrite

The reduction of chalcopyrite principally involves five main elements, copper, iron, calcium, sulphur and oxygen. In this section relevant systems containing some or all of these elements are discussed from existing literature. These systems provide a thermodynamic background to the phase equilibrium occurring during the reduction of chalcopyrite. Carbon is another main component of the reduction reaction, however this element is not discussed here.

3.5.1 Cu-Fe Binary Alloy

The Cu-Fe system, figure 3.4, contains two phases of particular interest, γ-iron and liquid copper. In the austenite phase, copper has a solubility of 12 %; there is also a large region of liquid-liquid immiscibility at high temperatures because of a large endothermic heat of mixing of the liquid alloy phase (Hultgren et al 1973).

The effect of this thermochemical property is seen in the low temperature solubility and consequent grain boundary segregation of metallic copper in ferritic and austenitic steel.

From the alloy physical chemistry it should be possible to determine a process that can physically separate copper and iron from the mineral concentrate.

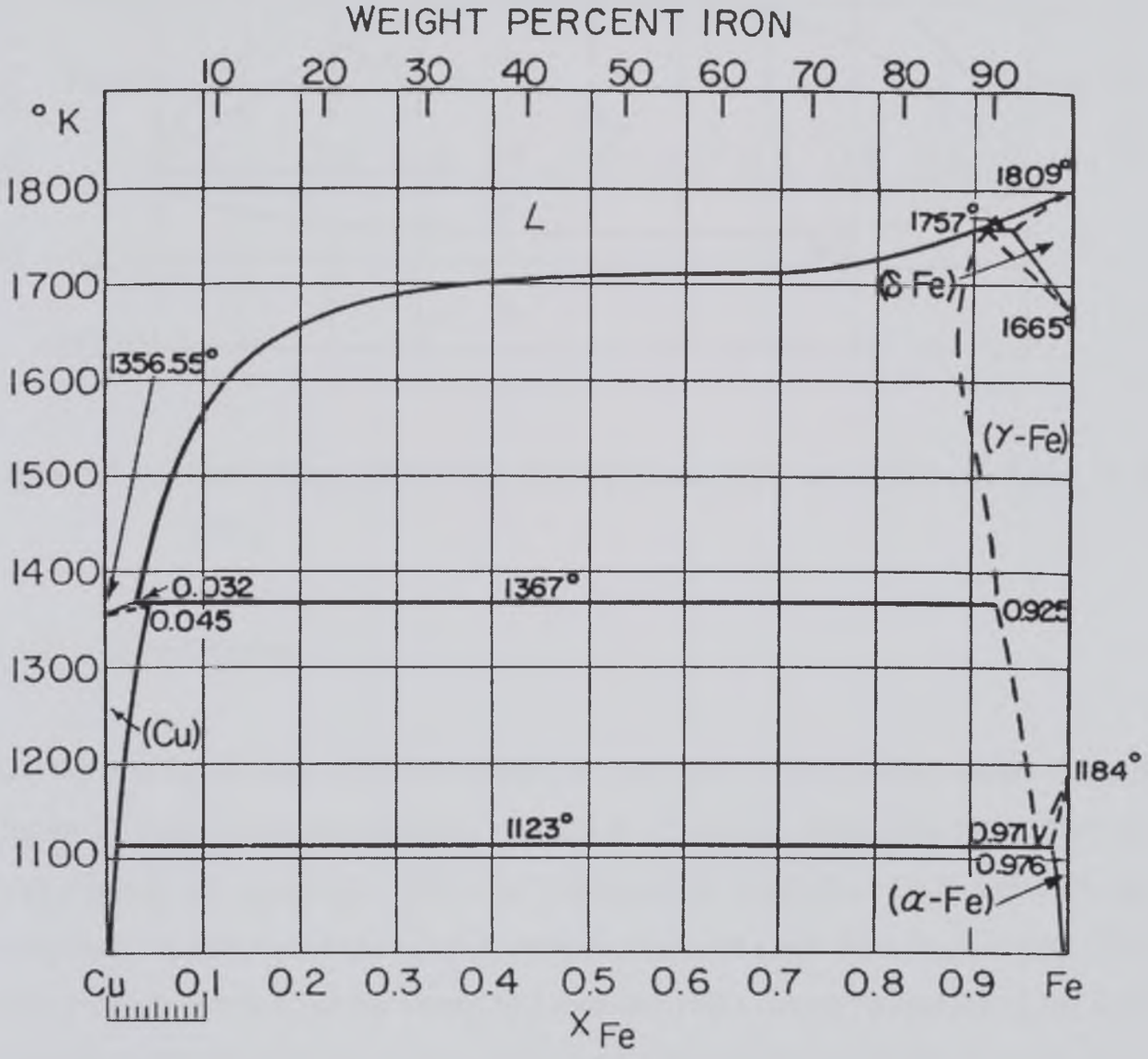

Figure 3.4 Copper-iron binary alloy phase diagram (Hultgren et al 1973).

The free energies of mixing were calculated by using equation 3.20:

$$\Delta G_{mix} = (X_{Cu} \,.\, \Delta G_{Cu}) + (X_{Fe} \,.\, \Delta G_{Fe}) \qquad (3.20)$$

The data (Hultgren et al. 1973) used for this calculation were determined at 1823 K. The diagram to show the free energy of mixing of the copper-iron alloy at 1823 K is shown in figure 3.5.

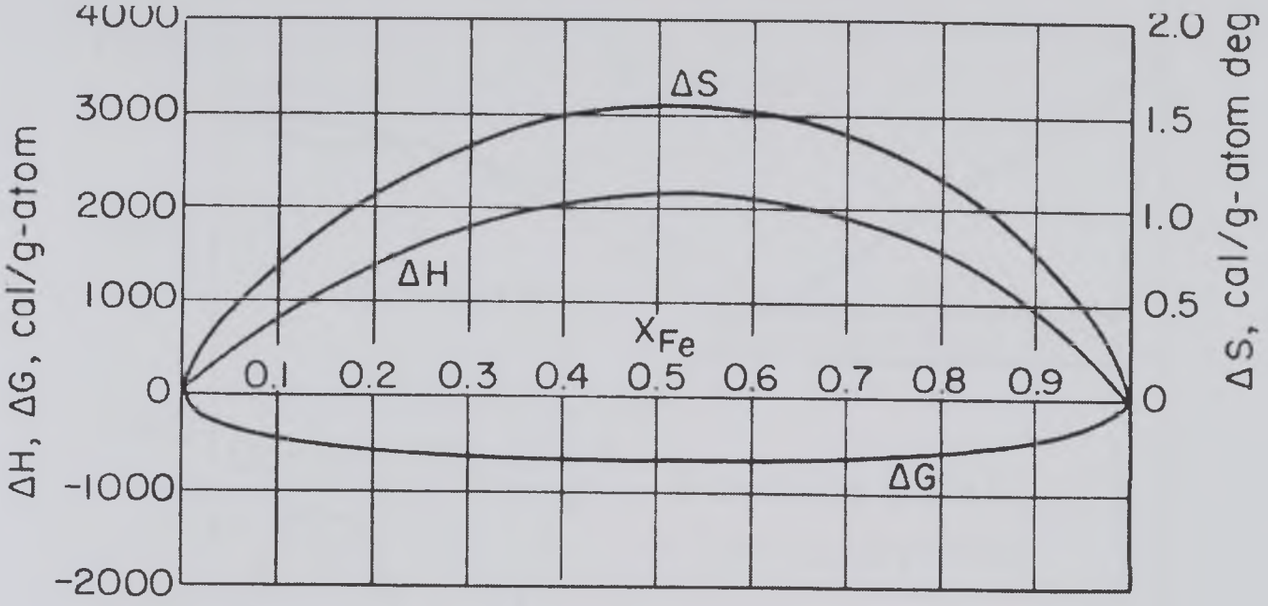

Figure 3.5 Free energy of mixing of copper-iron alloy at 1823K (Hultgren et al 1973).

3.5.2 Cu-Fe-S System

Krivsky and Schumann (1957) determined a large part of the Cu-Fe-S phase diagram (figure 3.6) over a temperature range of 1423 K to 1623 K. Within this range there are large regions of miscibility. The two stoichiometric sulphides, Cu_2S and FeS, are completely miscible and form a liquid matte covering the range from Cu_2S to FeS. They form an ideal solution, which means that their activities can be plotted using the ideal Temkin model. The activities of the components Cu_2S and FeS at 1200°C are plotted on figure 3.7 showing that these components follow closely the Temkin model. On the same figure the activities for Cu_2S and FeS determined by Bale and Toguri (1976) also show good agreement with the Temkin model.

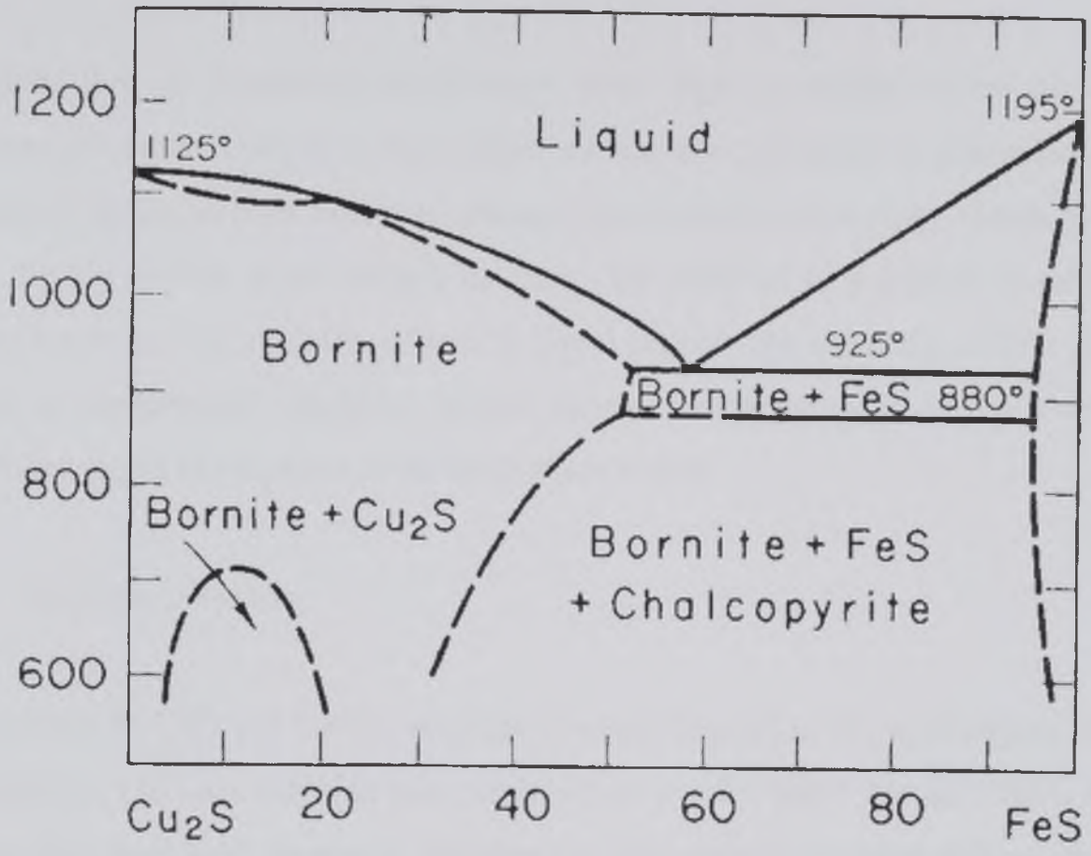

Figure 3.6 Cu_2S-FeS phase diagram (Levin et al 1969).

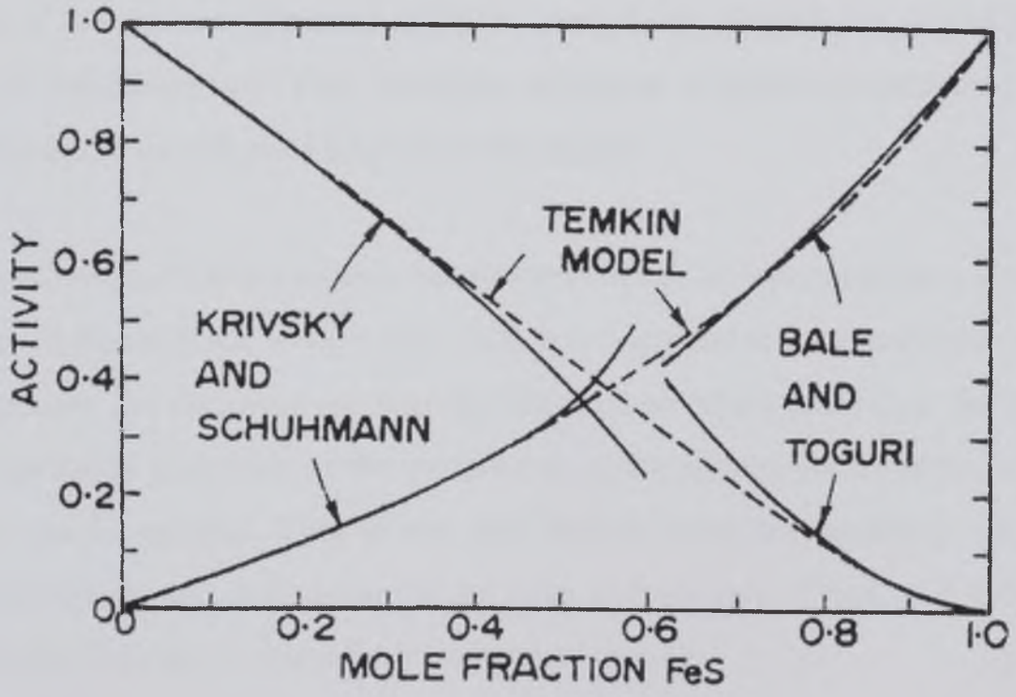

Figure 3.7 Comparisons of activities of the Cu_2S and FeS components of the pseudo-binary Cu_2S-FeS against the ideal Temkin model at 1200°C (Gaskell et al. 1990)

The formation of a separate liquid-matte phase high in copper occurs due to the reduction of sulphur content in high copper mattes. The γ-Fe phase is precipitated when the sulphur in low-copper mattes is reduced. Immiscibility of the two metals is shown along the Cu-Fe line of the ternary diagram. The addition of a critical percentage of sulphur increases the solubility of iron in liquid copper. The solubility of iron in liquid copper is temperature sensitive, which causes an enlargement of the two-liquid miscibility gap at the expense of the three-phase region.

3.5.3 Fe-Ca-S-O System

The reaction of CaO and ferrous sulphide was investigated in the temperature range of 400-1225°C. Calcium sulphide was observed as a solid phase around 400°C and its content increased with increased temperature. The authors assumed that at increased temperatures the CaO and FeS form a compound, Ca-O-Fe-S. An excess of CaO hindered the production of CaS (Vert and Kamenstev 1956).

Fusion of the mixture, observed at 840°C, leads to the dissociation of CaO.FeS, hence the CaS yield increased. CaS formation decreased at higher temperatures again, this time due to the formation of calcium ferrite phases.

Jha and Grievson (1992a) suggest that this system can be represented as a reciprocal salt mixture of the form AX + BY = AY + BX. It is important to understand this system as it characterises the exchange reaction that takes place before reduction. To estimate the thermodynamic properties of the components in the system, for example FeO, Flood's model can be applied. This model was derived from investigations of correlation between activity and composition in mixtures of fused salts (Flood et al 1953). Flood's activity for FeO can be determined from equation 3.21:

$$RT\ln a_{FeO} = RT\ln (X_{Fe}.X_O) + (X_{Ca}.X_S).\Delta G^\circ \qquad (3.21)$$

As ΔH becomes more negative, which implies that the change in energy is due to new associations of components, an increase in association fraction occurs. For the present system this indicates that there are more FeO-CaS pairs than FeS-CaO pairs.

3.5.4 Cu-Fe-S-Ca-O System

The carbothermic reduction of chalcopyrite occurs as a two step reaction: an exchange reaction and the reduction step. Sulphur and oxygen are the two chemical potentials that are lowered in the forward direction by forming CaS and CO. Therefore the system containing CaS has a lower chemical potential than with the sulphur as $CuFeS_2$ (Jha and Grievson 1992b).

To understand the melt chemistry of this system in order to devise a metal extraction route, it is important to define the activity of FeO within this quinary system. The activity of FeO can be defined as:

$$a_{FeO}^{(Cu\text{-}Fe\text{-}S\text{-}Ca\text{-}O)} = a_{FeO}^{(Fe\text{-}Ca\text{-}S\text{-}O)} \cdot a_{FeO}^{(Cu\text{-}Fe\text{-}S\text{-}O)} \qquad (3.22)$$

From the equations 3.23 and 3.24 the activity of metallic copper and iron have been calculated (Jha and Grievson 1992b):

$$Cu_2O_{(s)} + C_{(s)} = 2Cu_{(s)} + CO_{(g)} \qquad (3.23)$$

$$FeO_{(s)} + C_{(s)} = Fe_{(s)} + CO_{(g)} \qquad (3.24)$$

where at 1273K, $K_{(3.23)} = 5.34 \times 10^{6}$ and $K_{(3.24)} = 29.5$. For the formation of copper, the minimum activity for Cu_2O is 1.87×10^{-7} and for iron, 0.0034, for 1atm. of CO gas.

When considering the dissolved oxygen species in this system, the difference in free energy with respect to pure state as defined in equations 3.23 and 3.24 would determine the value of activities for the metallisation process.

3.6 Recovery of Precious Metals in Copper Extraction

Precious metals such as gold and silver enter the matte almost completely. These metals stay in the matte phase and are carried to the converter and are finally recovered as by-products when electrorefining copper.

At the electrorefining stage impure copper is cast into anodes and placed into an electrolytic cell. The copper anodes are dissolved electrochemically and the dissolved copper plates onto the cathode. The insoluble impurities from the anode including silver and gold collect at the bottom of the cell as anode slimes. These slimes can be treated for recovery of precious metals as valuable by-products of copper extraction processes.

The anode slimes are first treated for the removal of impurities such as Cu, Ni, Se and Te. The anode slimes are leached and washed so they are as free as possible of metals like copper, then roasted to eliminate or recover any Se or Te. The residue is melted down to an alloy of gold and silver with any other precious metals known as Dore metal. Schloen and Elkin (1950) describe the recovery of silver beginning with the Dore metal being cast into thin sheets and boiled with sulphuric acid. The resultant silver sulphate solution is diluted and silver is recovered by cementation on copper. In cells containing electrodes the silver dissolves into the electrolyte at the anode and deposits as crystals on the cathode. These crystals are non-adherent and can be brushed off. This method of silver recovery is also outlined by Hyvannen et al. (1984) as being utilised by the Outokumpu Puri refinery. Morrison (1985) mentions a similar process being used at the Canadian copper refineries.

3.6.1 Distribution and Phase Equilibria of Silver

Sinha et al. (1972) investigated the distribution of gold and silver between copper and matte. The distribution coefficient of gold, L_{Au}, is independent of gold concentration at 1400 and 1500K and is determined to be 102 and 127 respectively. In an iron bearing matte the distribution coefficient of gold decreases slightly with increased iron content.

The distribution coefficient of silver in the matte, L_{Ag}, is constant at constant temperature, and found to be 2.13 and 2.21 at 1400K and 1500K respectively. The distribution coefficient of silver increases slightly with increased temperature and iron content in the matte. Silver is assumed to be present in the matte as a sulphide, and that at dilute solutions silver should be represented as $AgS_{0.5}$ rather than Ag_2S.

Copper and matte phases are assumed to be Cu-Ag-Fe-S and Cu_2S-FeS-$AgS_{0.5}$ alloys respectively. The activities of Cu and Cu_2S were found to be 0.9634 and 0.8412 respectively. In copper mattes the three main constituents are copper, iron and sulphur therefore the phase relations between these components and silver are also discussed.

3.6.2 Cu-Ag Alloy

The Cu-Ag alloy behaves as a regular solution with a large exothermic heat of mixing. The phase diagram of this alloy shows a eutectic point at 1050K, the composition at this eutectic is 39.99% copper and 60.01% silver. Above the temperature at which the eutectic occurs there is a liquid copper and liquid silver miscibility region allowing one to dissolve in the other. The phase diagram for this alloy is shown in figure 3.8.

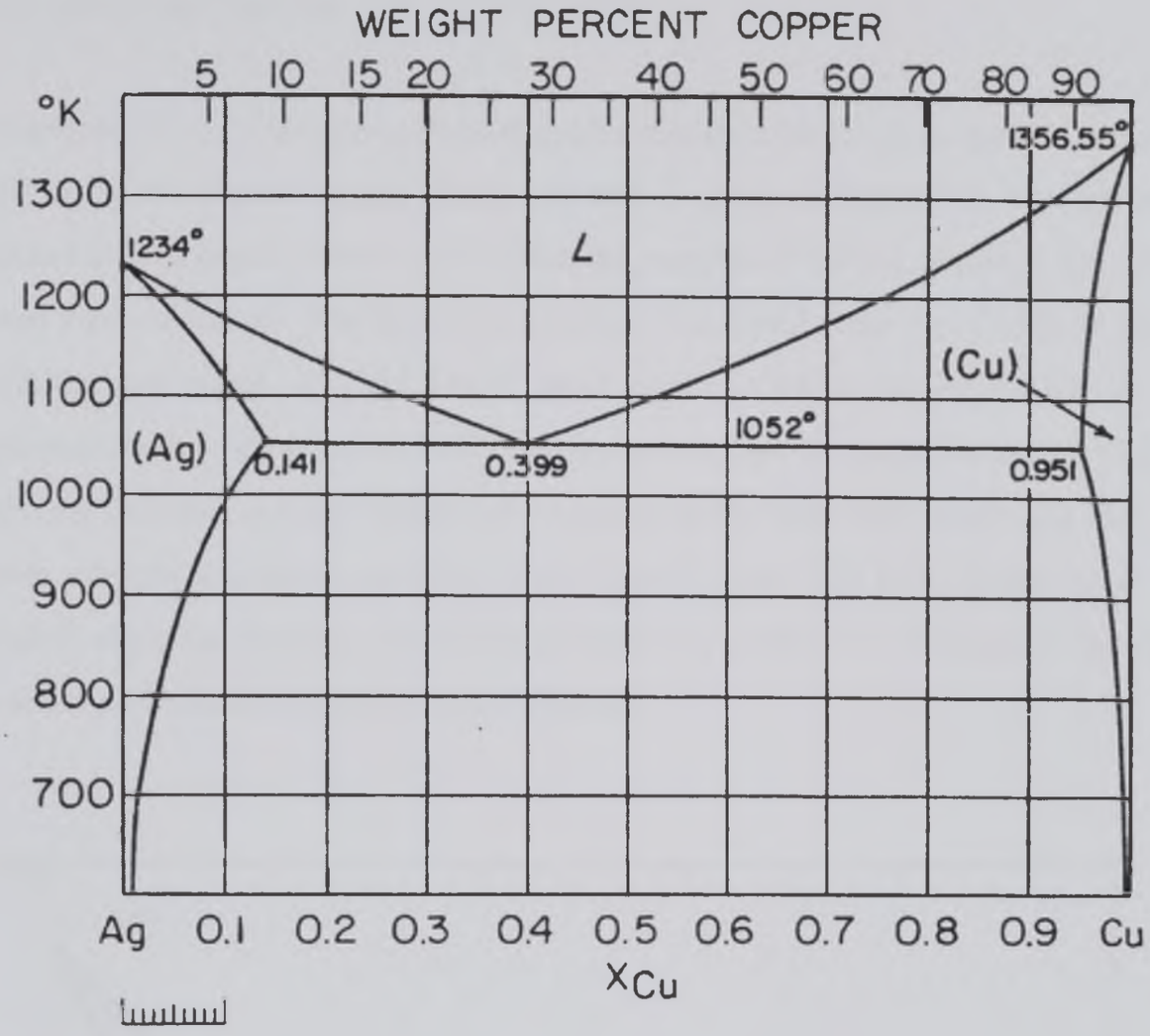

Figure 3.8 Phase diagram for the Cu-Ag binary alloy (Hultgren et al 1973).

Dokken and Elliot (1965) determined the partial molar heat of mixing for the Cu-Ag alloy from calorimetric measurements at 1100°C to 1200°C:

$$\text{Cu-Ag: } H^M [16.74 + 1.30\ X_{Ag}]\ X_{Ag}X_{Cu}\ \text{kJ mol}^{-1} \qquad (3.25)$$

The heats of fusion for copper and silver are given as:

$$\text{Cu: } \Delta H_m = 13771 \pm 1151\ \text{J mol}^{-1} \qquad (3.26)$$

$$\text{Ag: } \Delta H_m = 12097 \pm 104.65\ \text{J mol}^{-1} \qquad (3.27)$$

3.7.3 Cu_2S-Ag_2S System

Mendelevich et al. (1969) determined the phase equilbria for the chalcogenide system of Cu_2S-Ag_2S; the phase diagram for this system is given in figure 3.9. The system is assumed to be a regular solution, for which the energies of mixing, liquidus and solidus curves were calculated. The energy of mixing in the liquid phase is –13,688.22 J/mol^{-1} and in the solid phase, -2427.88 J/mol^{-1}, these values lie within the range $-2RT<V<2RT$ corresponding to complete miscibility of the components. The negative value of energy of mixing indicates stronger interactions between unlike molecules rather than like. The system exhibits a negative deviation from Raoult's law. The heat of mixing is also negative where the tendency for unlike molecules to combine is strongest in the liquid phase causing a minimum on the phase diagram.

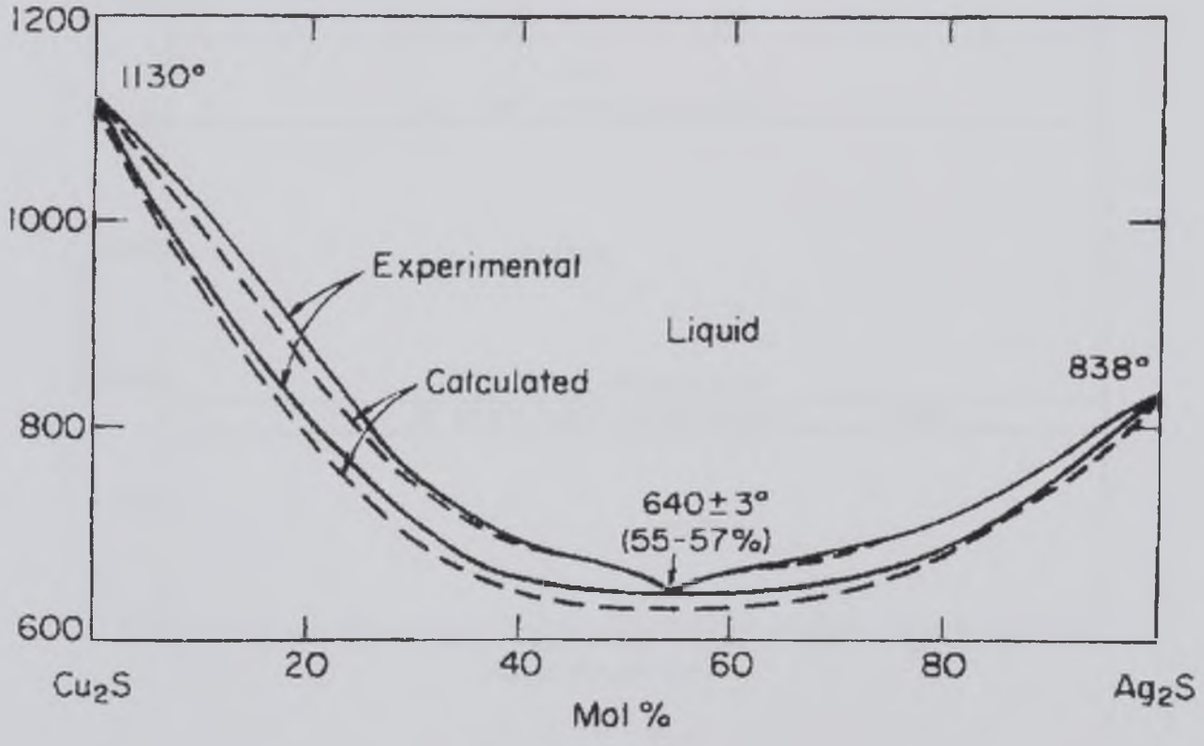

Figure 3.9 Phase diagram of the Cu_2S-Ag_2S system (Levin et al 1969)

3.7.4 Ag-Fe Binary Alloy

The information on the solubility of silver in liquid and solid iron is rare however Wreidt et al. (1973) presented a source. From the Ag-Fe phase diagram in figure 3.10, at

the reaction temperature there is a liquid + (γ-Fe) phase, where γ-Fe is in the fcc structure. It was discovered from Weidt et al. (1973) that the free energy change for the dissolution of silver in fcc iron is:

$$\underline{Ag}\ (l) = \underline{Ag}\ \text{(dissolved in iron)} \qquad (3.28)$$
$$\Delta G^\circ = 115{,}500 - 43.85\ T\ J/mol^{-1}$$

The authors also discovered that the silver content in γ-Fe is expressed as:

$$\log (\text{wt.\% Ag}) = -6{,}027\ T^{-1} + 2.289 \qquad (3.29)$$

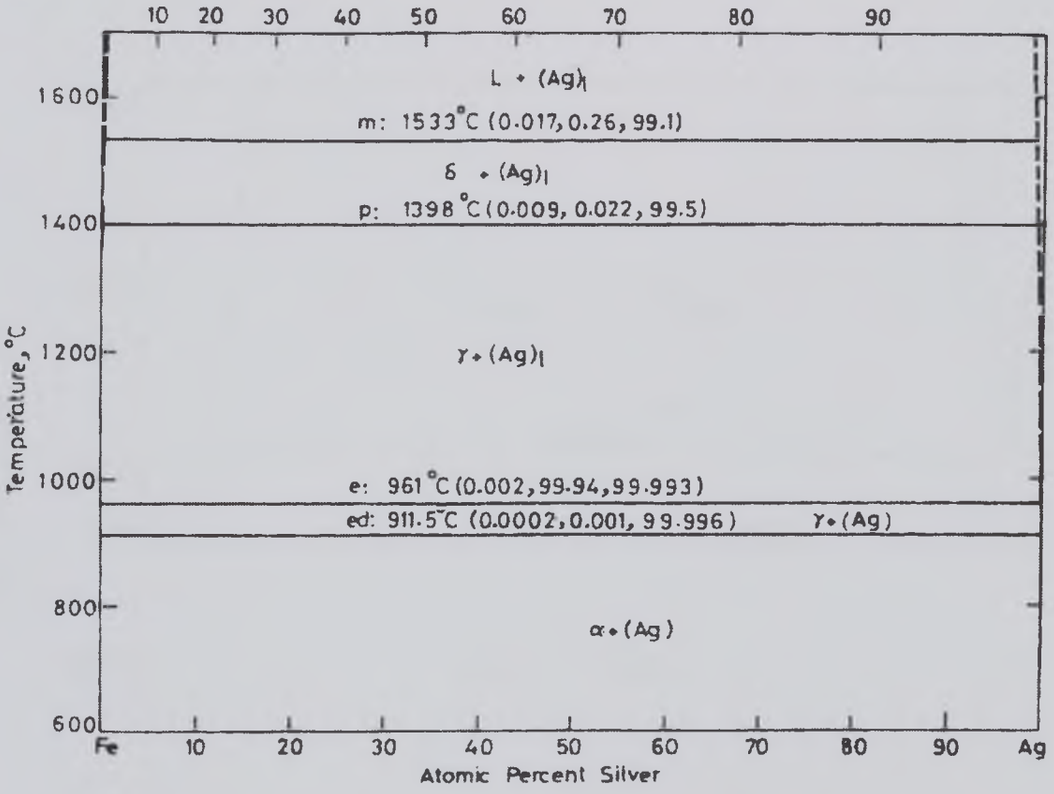

Figure 3.10 Phase diagram for the Ag-Fe binary alloy (Ragahavan 1973).

3.7.4 Ag-Fe-S System

Taylor (1970) determined phase relations of the Ag-Fe-S system between 700°C and 1200°C. The phase diagram of the Ag-FeS system is given in figure 3.11. At 1200°C a

continuous sulphur-rich two-liquid field completely spans the ternary system dominating the phase relations. In the temperature range of interest for this system several changes occur to the phase relations at 1200°C with decreasing temperature. At 1192°C $Fe_{1-x}S$ crystallises out, the ternary liquid-immiscibility field reaches the Ag-Ag_2S join at 1125 ± 25°C. At 1004°C a ternary singular point is defined by the reaction written as $L_t = L_{Ag} + FeS$.

The solubility of Ag in FeS_2 is less than 0.1 at.%: analysis determined the solubility to be approximately 500 ppm. The solubility of Ag in pyrrhotites of various compositions from reactions of Ag_2S and $F_{1-x}S$ was also found to be less than 0.1 at.%. The solubilities of $Fe_{1-x}S$ and FeS_2 in Ag_2S are limited with the solubility of Fe in Ag_2S less than 1.0 at.%.

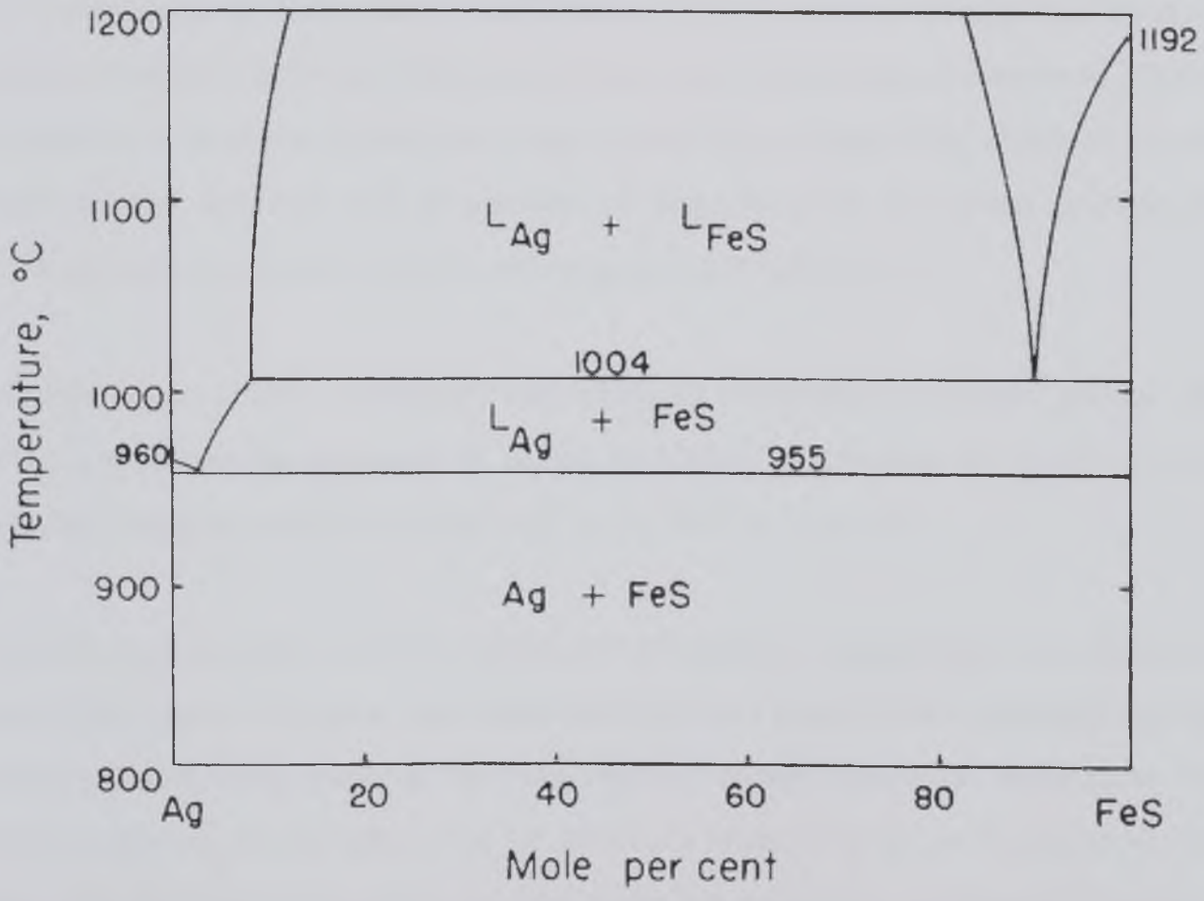

Figure 3.11 Phase diagram for the Ag-FeS system (Taylor 1988)

3.8 Activities and Control of Impurities in Copper Extraction and Relating Phase Equilbria

The elimination of impurities such as arsenic and antimony from copper during the process route is an important factor. These elements along with others such as bismuth, lead and zinc are difficult to remove by oxidation into the slag and so are volatilised during smelting and converting to produce flue dusts. Several authors have completed research into this area of copper extraction to assess the control and elimination of these elements.

3.8.1 Activities of Arsenic and Antimony in Copper Mattes

From determination of the activity coefficients of minor elements at infinite solutions in copper and copper mattes the behaviour of such trace elements can be assessed. This is of particular importance during the copper converting process. The effect of several factors on the activities and elimination of impurities has also been investigated including partial pressure of sulphur and oxygen and temperature.

Hino and Toguri (1987) investigated the behaviour of antimony in copper mattes. The activity coefficient for antimony in copper at 1100°C is given as 1.1×10^{-2} and by assuming a regular solution the value of γ°_{Sb} at 1150°C is 1.3×10^{-2}.

The authors studied the Cu-Sb-S system on two phases, a copper-rich and matte-rich phase. The copper-rich phase was observed to act as a reservoir for antimony and the sulphur pressure being constant when two melts of copper and copper matte exist. For identical antimony concentration, the Sb activity is found to be larger in the copper-rich phase. The effect of sulphur on arsenic activity is larger than that on antimony in molten copper.

The authors discuss the two-melt range as relating to the blister copper stage in copper making, in which the As and Sb activities are found to be relatively high. The two

elements are found to distribute more in the copper-rich phase. Therefore elimination is difficult at this stage of the copper extraction process but the impurities are removed during the matte smelting and slagging stage because of the large values of the activity coefficients in matte. The initial concentration of As in the charge affects the proportion of As in the matte, slag and gas phases whereas Sb is quite independent of its content in the charge (Itagaki and Yazawa 1985).

Roine and Jalkanen (1985) studied the activities of the sulphides of arsenic and antimony in copper mattes. The calculated activities are too low if the impurity components are also soluble in their metallic form. Arsenic and antimony have low affinities to sulphur at low pressures therefore they exist mainly as metallic species in the matte. The authors suggest that the sulphur to metal ratio is the most important factor influencing the activity coefficients of As and Sb in copper mattes. When the sulphur pressure increases, copper and iron activities decrease allowing As and Sb activities to increase. Chaubal and Nagamori (1988) suggest that in the converter the marked decrease in arsenic and antimony elimination at high matte grades is due to a decrease in partial pressure of sulphur. At high matte grades the copper activity is high and the partial pressure of $As_{(g)}$ decreases leading to decreased elimination.

Roine (1987) studied the effect of oxygen on activities of As and Sb. Although the effect on arsenic activity is negligible, oxygen does have a significant effect on As removal. This is due to the evaporation of AsO gas molecules in addition to that of sulphidic and elemental gas molecules. Oxygen does have an effect on antimony activity, at high oxygen concentrations Sb activities decrease due to the oxidation of Sb. This does not cause a decrease in antimony removal from matte as the amount of gaseous Sb compounds also increases.

Increased temperature leads to increased volatilisation of both arsenic and antimony from copper in converters. However the volatilisation of these elements during the blister making stage is negligible (Chaubal and Nagamori 1988).

3.8.2 Control and Removal of Impurities in Copper Extraction

Lau et al (1982) investigated the feasibility of capture of arsenic as calcium arsenate in reverberatory and Mitsubishi converter slags. The results indicated that the vaporisation of $Ca_3(AsO_4)_2$ proceeds primarily as:

$$Ca_3(AsO_4)_{2\,(s)} = Ca_3As_{(2-x)}O_{(8-x-2y)\,(g)} + x\,AsO_{(g)} + y\,O_{2\,(g)} \qquad (3.30)$$

Although $Ca_3(AsO_4)_2$ by itself is relatively non-volatile; the compound is reduced by reverberatory and Mitsubishi converter slags, yielding arsenic species as volatile products.

In the slag phase, iron is present as +2 and +3 oxidation states; the formation of each state is a function of temperature, oxygen partial pressure and overall slag composition. The pressure of oxygen is given from the CO/CO_2 ratios. The reduction of arsenic in the mix is given by:

$$5\,Fe^{2+} + As^{5+} = 5\,Fe^{3+} + As^{0} \qquad (3.31)$$

The authors deduced that the proposed scheme of recycling copper smelting flue dust with arsenic immobilised as $Ca_3(AsO_4)_2$ is not viable. The involatile arsenate compound is reduced by slag to volatile elemental arsenic. The reduction of arsenic oxide in contact with slag is proof that arsenic must dissolve in slag as elemental rather than oxide form.

Copper is assumed to exist in the slag phase as copper oxide, cuprous rather than cupric due to the high temperature of the process (Jimbo et al 1983).

$$Cu_{(in\ alloy)} + \tfrac{1}{4}\,O_2 = CuO_{0.5\ (in\ slag)} \qquad (3.32)$$

At high temperatures arsenic is stable as the oxide, $AsO_{1.5}$ and the authors found that as the solubility of arsenic approaches zero there is no elemental arsenic solubility in the slag.

$$As_{(in\ alloy)} + \tfrac{3}{4} O_2 = AsO_{1.5\ (in\ slag)} \qquad (3.33)$$

Also considered was the possibility that arsenic exists as AsO at low oxygen potentials.

$$As_{(in\ alloy)} + \tfrac{1}{2} O_2 = AsO_{(in\ slag)} \qquad (3.34)$$

The solubility of antimony in the slag was found to depend upon temperature and is found to exist as SbO.

$$Sb_{(in\ alloy)} + \tfrac{1}{2} O_2 = SbO_{(in\ slag)} \qquad (3.35)$$

Chaubal (1989) studied the effect of oxygen enrichment, on elimination of As, Sb and Bi during copper converting. Simulations of oxygen enrichment were carried out over different temperatures and oxygen concentrations, with the initial concentration of each impurity being 0.1 wt.% in the matte. Elimination of impurities is done initially by volatilisation of its sulphide; increased oxygen potential leads to a decrease in sulphur potential hence a decrease in volatilisation of the impurity.

The work carried out by Hang Goo Kim and Sohn (1988) agrees with the findings by Chaubal (1989). The authors predict that with increased oxygen enrichment, high elimination of impurities can be achieved by slagging. Low levels of elimination by volatilisation will occur at high oxygen potentials.

As the temperature increases then so too does the degree of removal of the impurities from the matte phase. At higher converting temperatures an increase in vapour pressure occurs which leads to an increase in volatilisation (Chaubal 1989).

Machingawata at al (1994) investigated the incorporation of arsenic into silicate slags as a disposal option. They discovered that large amounts of arsenic could be dissolved in

the silicate slag under mildly oxidising conditions. Arsenic was found to be present in crystalline phases, as calcium arsenate, in slags where crystalline iron oxide (primarily magnetite) is present. However this research did not suggest which non-ferrous applications this theory can be applied to.

The oxygen potential within the slag determines the state of dissolved arsenic, which can assume –3 to +5 oxidation states in slag melts.

$$As^{3+} + \tfrac{1}{2}\, O_2 + 3O^{2-} = AsO_4^{3-} \qquad (3.36)$$

At high O_2 potentials, As^{5+} is stable in the slag, forming anions such as AsO_4^{3-}. As^{3+} escapes to the gas phase as As_4O_6.

The oxygen potential in the slag is controlled by the ratio of Fe^{2+}/ Fe^{3+}.

$$AsO_4^{3-} + 2Fe^{2+} + 2O^{2-} = As^{3+}\ 2Fe^{2+} + 6O^{2-} \qquad (3.37)$$

$$As^{3+} + 3/2\ O_2 = AsO_{1.5} \qquad (3.38)$$

The SiO_2/CaO ratio is also an important factor in determining the basicity of the slag and the degree of polymerisation of the silicate structure. At high SiO_2/CaO ratios, the tetrahedral silicate structure is largely unbroken due to the deficiency of O^{2-} anions. The activity of the $As_{(111)}$ ion is high, resulting in a greater tendency for arsenic volatilisation as As_4O_6 for a fixed Po_2. There is a higher concentration of these anions in basic slags leading to a greater linkage between AsO_4^{3-} and SiO_4^{4-} rings, therefore the arsenic is stabilised as As^{5+}.

3.9 Summary

In this chapter literature has been reviewed on the reduction of metal sulphides. In particular relevance to this study the work by Jha and Grieveson (1992b) has been mentioned. This work was carried out only on synthetic chalcopyrite and at

temperatures only up to 1000°C. No considerations were made neither on sample size nor on the presence of precious metals in a mineral. Mention was made on the selective separation of the metallic phases but not on how to facilitate this. In the studies on other complex metal sulphides the selective separation of metallic phases were also not considered.

Very few sources mention reduction of natural mineral sulphides. The research appears to end with the synthetic sources of metal sulphides. None of the literature reviewed on the reduction reactions considered impurities, either for recovery as by-products or their elimination of. Very little literature exists on alternative methods to control and capture impurities from copper extraction in a safe disposable form. Those methods that do exist are still in the early stages of development.

The phase equilbria relevant to the reduction reaction and presence of silver during reduction are given in this chapter. Theoretical considerations relating to these systems are given in chapter four.

CHAPTER FOUR

Theoretical Considerations

4.1 Introduction

In chapter three the phase equilibria for different systems relevant to the research of this thesis are reviewed. In this chapter pertinent calculations were made to provide information for the selection of the experimental parameters given in chapter five. In addition the phase equilibria determined in this chapter were completed to compliment the results obtained in chapter six.

Two areas of interest are concentrated upon in this section. The reduction equilibrium for the extraction of copper and iron from chalcopyrite is initially considered. Secondly, the thermodynamics of the Ag-Cu binary alloy were determined with respect to the reduction of chalcopyrite.

4.2 Phase Equilbria for the Cu-Fe-Ca-S-O System

Two diagrams were constructed to thermodynamically explain the reduction of chalcopyrite: a Gibbs free energy diagram and a log P_{SO_2} partial pressure diagram. These figures provide information relevant to the experimental conditions used for the reduction of chalcopyrite and for the determination of the selective separation of copper and iron from chalcopyrite.

4.2.1 Gibbs Free Energy Diagram

The reduction of chalcopyrite to the metallic species by carbon in the presence of lime occurs at high temperatures. The characteristic equilibrium for this system is demonstrated by the Gibbs free energy diagram of figure 4.1.

From enthalpy (ΔH) and entropy (ΔS) values obtained from Turkdogan (1980) the Gibbs free energy values (ΔG) were determined using equation 4.1 for each reaction equation detailed in table 4.1.

$$\Delta G = \Delta H - T\Delta S \qquad (4.1)$$

Reaction Equation	ΔG ($Jmol^{-1}$)	log Pso_2 (atm)
$CaS_{(s)} + 3CaSO_{4(s)} = 4CaO(s) + 4SO_{2(g)}$	233,020.72-159.11T	-12,170/T + 8.31
$Cu_2S_{(s)} + 2CaSO_{4(s)} = 2Cu_{(l)} + 2CaO_{(s)} + 3SO_{2(g)}$	23,670 - 151.8 T	-12,152 /T + 7.93
$3Cu_2S_{(s)} + 2CaO_{(s)} = 6Cu_{(l)} + 2CaS_{(s)} + SO_{2(g)}$	269,157 – 60.8 T	-14,064 /T + 3.54
$FeS_{(l)} + 2FeO_{(s)} = 3Fe_{(l)} + SO_{2(g)}$	357,568 - 132.4 T	- 18,675 /T + 6.9
$3FeS_{(s)} + 2CaO_{(s)} = 3Fe_{(s)} + 2CaS_{(s)} + SO_{2(g)}$	287,302 – 107.22T	-15005/T + 5.6

Table 4.1 Free energy values and SO_2 partial pressures for the pertinent phase equilibria of metal extraction relevant to reduction of chalcopyrite.

From equation 4.1 it is possible to determine the equilibrium temperature for each reaction, i.e. the temperature above which the reaction can proceed. A plot of the free energy changes against temperature for these reactions is shown in figure 4.1. By examining this graph it is possible to determine the temperature at which the free energy becomes zero. At temperatures greater than the equilibrium temperature the reaction should proceed. This type of information can be applied practically: no experiments should be carried out below the equilibrium temperature, as the reaction can not proceed.

4.2.2 SO_2 Partial Pressure Diagram

The thermodynamic equilibrium for the multicomponent system, Cu-Fe-Ca-S-O, can be represented by the univariant plot given in figure 4.2. This type of plot is used to show the significance of the relevant phase equilibria for metal extraction, especially for reducing conditions.

To calculate the log of the partial pressures of SO_2 for the diagram, equation 4.2 is used:

$$\log Pso_2 = \frac{1}{2.303}\left[\frac{-\Delta G}{RT}\right] \qquad (4.2)$$

The ΔG values per mole of SO_2 and the calculated log of the partial pressures of SO_2 are presented in table 4.1, and the values of log Pso_2 are plotted against the reciprocal of temperature in figure 4.2. In table 4.1 the conditions that favour the metallisation of copper from Cu_2S and iron from FeS are defined. Figure 4.2 enables the determination of the conditions for which selective separation of these metal phases can be achieved. The stability regions of CaS, $CaSO_4$ and CaO are evident from this figure indicating CaS as the most stable. There exists a difference in chemical potential between the metallisation of copper and iron, thus indicating the difference in chemical potential is significant for preferential separation.

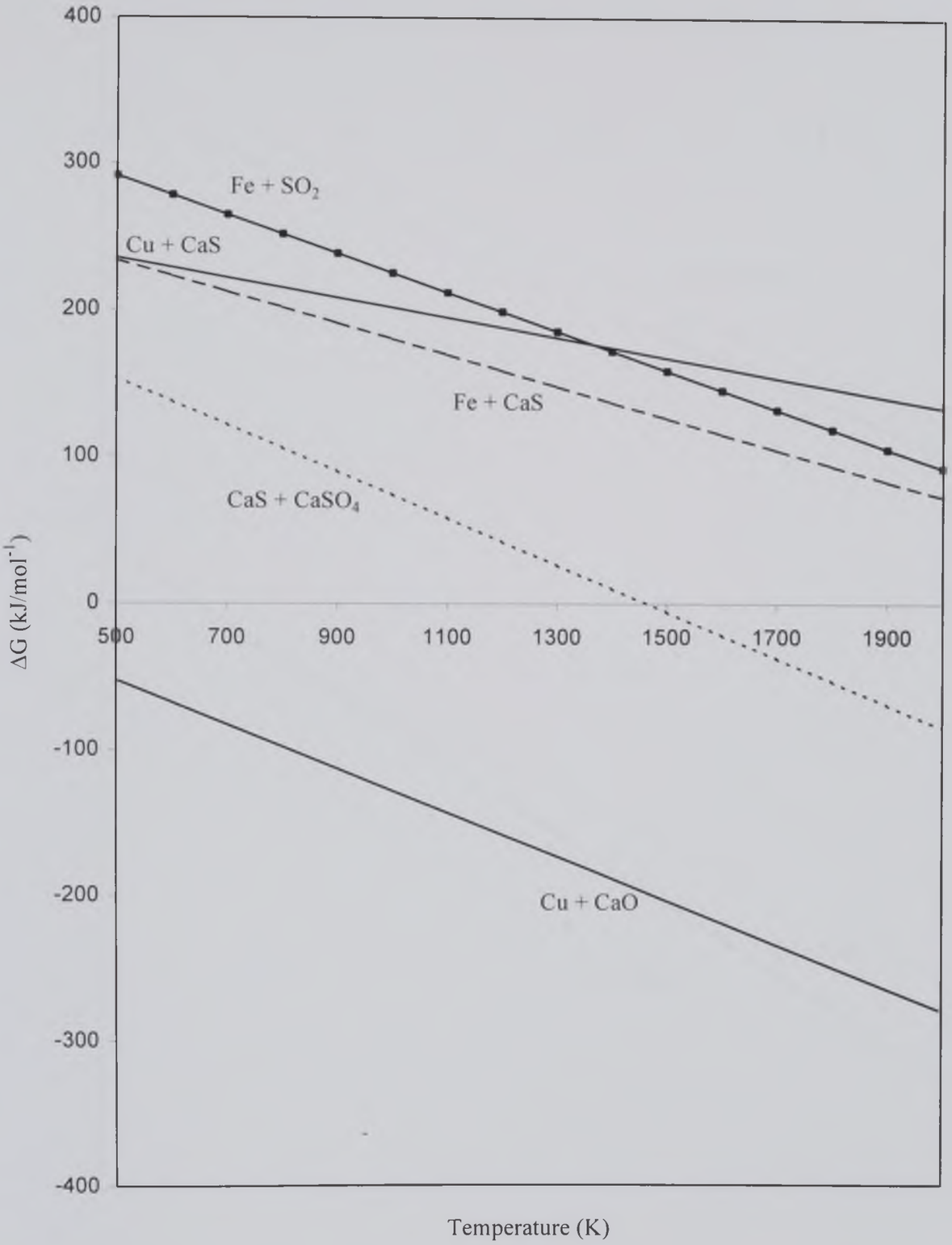

Figure 4.1 A plot of the Gibbs free energy functions in table 4.1 against temperature.

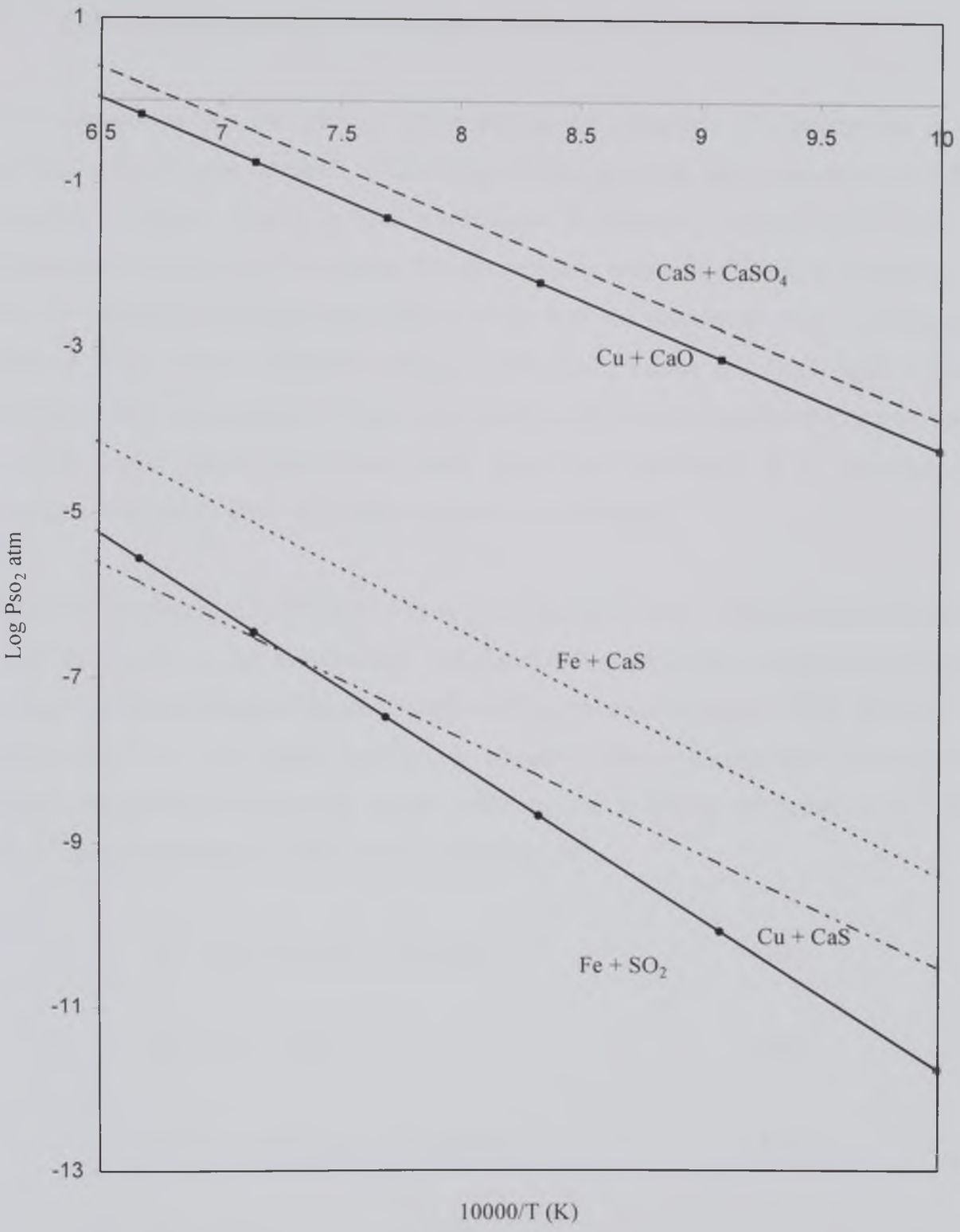

Figure 4.2 A plot of log Pso_2 values for the functions in table 4.1 against the reciprocal of temperature.

4.3 Calculations relating to the Presence of Silver during Reduction

The investigation into the path of silver during the reduction of chalcopyrite is an important aspect to the research of this thesis. Silver is an important by-product of the extraction of copper details, a brief explanation is given in section 2.4.9 which is elaborated in section 3.6. In section 3.6 the relevant phase equilibria for presence of silver in chalcopyrite during the reduction reaction are discussed. Four systems are reviewed from existing literature, Cu-Ag, Cu_2S-Ag_2S, Fe-Ag and Fe_2S-Ag_2S. It was established from examination of these systems that silver would preferentially segregate out with copper rather than iron. Based upon this conclusion it is important to understand the binary alloy of copper and silver in particular.

This alloy was described in chapter 3 as being a regular solution with a large exothermic heat of mixing. A regular solution can be defined as one where the entropy of mixing is the same for that of ideal solutions (Swalin 1972; Darken and Gurry 1953). The heat of mixing may have any value, positive or negative. For a binary alloy, Cu-Ag for example, the solution of A and B which exhibit regular behaviour the values of G^M, H^M and S^M can be expressed in terms of mole fractions as:

$$G^M = RT\,(N_A \ln a_A + N_B \ln a_B) \qquad (4.3)$$

$$H^M = G^M + TS^M \qquad (4.4)$$

$$S^M = -R\,(N_A \ln N_A + N_B \ln N_B) \qquad (4.5)$$

The heat of mixing for the binary alloy (H^M) can be expressed as:

$$H^M = RT\,[N_A \ln (a_A/N_A) + N_B \ln (a_B/N_B)] \qquad (4.6)$$

The mole fraction and activity of a component can be related to the activity coefficient (γ) by:

$$a_A/N_A = \gamma_A \qquad (4.7)$$

Therefore:

$$H^M = RT\ (N_A \ln \gamma_A + N_B \ln \gamma_B) \qquad (4.8)$$

The heats of mixing for both components can be expressed as:

$$H^M{}_A = RT \ln \gamma_A \qquad (4.9)$$

$$H^M{}_B = RT \ln \gamma_B \qquad (4.10)$$

The value for $H^M{}_A$ is positive when a positive deviation from ideality is positive (i.e $\gamma >$ 1) and if the deviation from ideality is negative (i.e $\gamma_M < 1$) the value for $H^M{}_A$ is negative. In general in practice the value of $H^M{}_A$ usually varies with temperature.

If there is an absence of experimental data for an alloy the equations for the regular solution can be applied to determine the values of activities at different temperatures when measurements are available at one particular temperature. The data can also be used to find the activities in liquid solutions from the liquidus and solidus lines on the phase diagram.

The thermodynamic data available for the Cu-Ag system gives values for activity of silver in a silver-copper alloy at 1423K for a range of compositions where X_{Ag} = 0-1 (Hultgren et al. 1973). For this information to have any bearing on the investigation in hand the values of the activity of silver in a silver-copper alloy was determined for different temperatures from equation 4.11 where T_2 = 1423K.

$$T_1 \ln \gamma_1 = T_2 \ln \gamma_2 \qquad (4.11)$$

At different compositions of silver and copper RT lna is plotted against temperature. From this graph of figure 4.3 the activity of silver in the alloy can be determined for any temperature thus giving an indication as to the segregation of silver into copper at the reaction temperatures for the reduction of chalcopyrite.

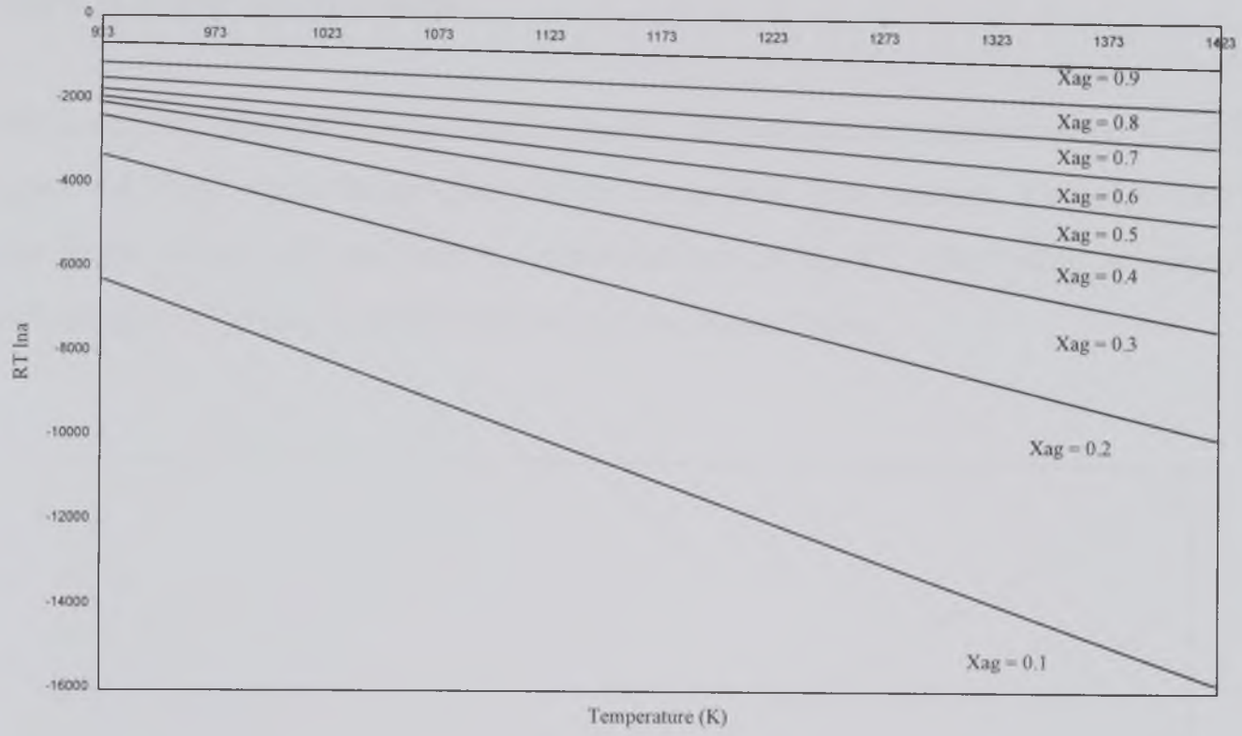

Figure 4.3 A graph of calculated values of RT lna as a function of temperature (K) for a range of compositions of Ag in the Cu-Ag alloy.

4.3.2 Calculation of Ω

The next stage in the calculations is the determination of the value of Ω; this value represents the degree of interaction between molecules, in the alloy. For a binary alloy of components A and B there are three types of interactions, A-A, A-B and B-B. This value of Ω can be determined from the equation:

$$\ln(1-X_2) + \Omega/RT.\ (X_2)^2 = -\Delta H_{f\,1}/R\ .\ (1/T - 1/T_{f.1}) \qquad (4.12)$$

If the solution is regular as is the copper-silver binary alloy is then:

$$\ln\ (a_A/X_A) = \Omega/RT\ (1-X_A)^2 \qquad (4.13)$$

And:

$$\ln\ (a_B/X_B) = \Omega/RT\ (1-X_B)^2 \qquad (4.14)$$

Where A is silver and B is copper.

For silver the values of $(1-X_B)^2$ and ln (a_B/X_B) are calculated, and plotted on a graph, figure 4.4, from which the gradient can be determined. The gradient is equal to Ω/RT and found to be 1.22 and can be expressed as: $\Omega=10.14T$. This value is positive indicating $\gamma_i > 1$ giving a positive deviation from Raoult's law.

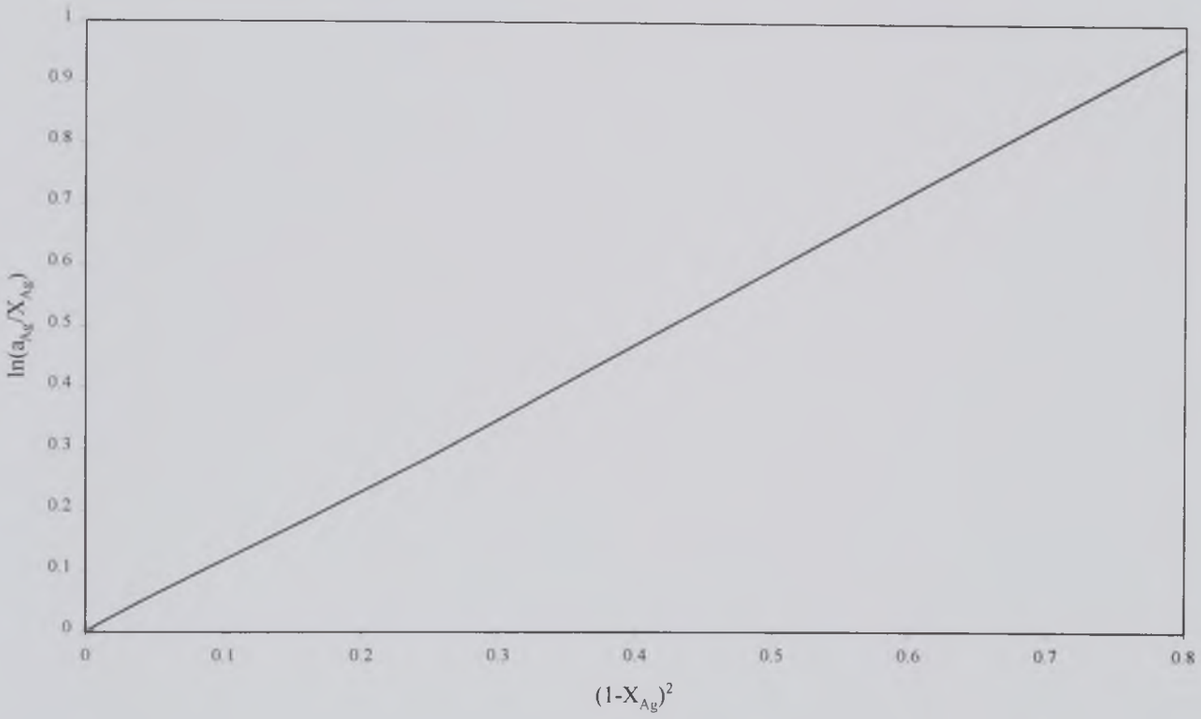

Figure 4.4 A graph of ln (a_B/X_B) against $(1-X_B)^2$ to determine Ω from the gradient, Ω/RT.

4.4 Summary

The calculation of phase equilbria of the relevant reactions for the reduction reaction has been completed in this chapter. The free energy diagram has allowed for the determination of reaction conditions (i.e. temperature) for the experiments investigating the reduction of chalcopyrite. The construction of the stability diagram in figure 4.2 allowed for the determination of the condition for metallic phase separation for example by controlling the partial pressure of SO_2.

The evaluations of the Cu-Ag alloy give information regarding the activity of silver within this alloy for any temperature, the graph for which is given in figure 4.4. In addition to this evaluation the interaction value of Ω is determined as 10.14T.

CHAPTER FIVE

Experimental Procedures and Analysis

5.1 Introduction

The following chapter describes the experimental set and procedures undertaken along with the analysis carried out for each set of experiments. Tables are presented with the parameters for each reaction, detailing the sample identification, composition, time and temperature. The chalcopyrite mineral concentrate from the Ghatsila Mines in Bihar, India was used for the experiments, the chemical analysis of which is listed in table 5.1.

Constituents %	Chalcopyrite Concentrate
Cu	25.20
Fe	28.28
S	31.60
Ni	0.43
Co	0.15
Mo	0.09
MgO	0.50
SiO_2	7.44
Al_2O_3	4.84
Moisture	2.71
ppm Au	20.00
ppm Ag	1.50

Table 5.1 Chemical analysis of the natural chalcopyrite mineral used for all experiments, obtained from the Ghatsila Mines in Bihar, India.

5.2 Investigation into the Carbothermic Reduction of Chalcopyrite

The reduction of chalcopyrite was carried out in a number of different ways, all designed to gain a detailed profile of the process. The reduction of mineral sulphides is seen to proceed in two steps, as reported in chapter three. The reduction of synthetic chalcopyrite as reported by Jha and Grievson (1992b) proceeds as two steps. The first experiments completed were the simple reactions between chalcopyrite and lime. The next step was the introduction of a reducing agent in the form of graphite. At this stage, as well as investigations of the reduction rate, an extensive phase analysis was conducted. Activated carbon replaced graphite in order to gain a comparison of reducing agent on the reduction reaction.

The study proceeded with reduction on a larger scale to verify the reproducibility of results obtained from small scale trials and adaptability to possible industrial scale. The control of separation of metallic phases was considered by taking oxygen potential measurements during reduction. Silver metal and silver sulphide were added in appreciable amounts to the reduction mix prior to heat treatment in order to analyse the path of silver during reduction.

5.2.1 Heat Treatment of Natural Chalcopyrite with Lime

The natural chalcopyrite mineral concentrate used for this set of experiments was obtained from the Ghatsila mines in India, the average chemical composition of which is listed in table 5.1. The other chemical component, CaO, was obtained from Aldrich and was of 99.9 wt.% purity.

For each experiment, a 2g mixture was produced from mixing natural chalcopyrite with the stoichiometric amount of lime. The stoichiometric ratio of chalcopyrite concentrate to lime was 1:2 in order to keep the comparison with the ratio for reduction reactions (see section 5.2.2). The chalcopyrite and lime mixtures were reacted in a muffle furnace whilst maintaining an inert atmosphere of argon, the reaction conditions employed for each sample are listed in table 5.2. The temperature range was chosen to allow comparison with the anticipated range for the reduction reactions (850°C to 1200°C).

The procedure used for these experiments is given in section 5.4.1. Two of the reaction samples listed in table 5.2 are larger in size at 50g in weight. These samples were reacted in a clay crucible in a retort furnace under an inert atmosphere. These experiments were carried out to provide a comparison between 2g and 50 g samples whilst showing the first step to the reduction reaction on a larger scale. The procedure for the retort furnace is given in section 5.4.3. For each sample heat treated X-ray analysis was completed and selected samples were analysed using a scanning electron microscope, details for both techniques are given in section 5.5.

Sample Composition $CuFeS_2$:CaO	Temperature (°C)	Time (mins)
1:2	850	5
1:2	850	30
1:2	850	60
1:2	850	90
1:2	850	120
1:2	900	60
1:2	950	60
1:2	1000	60
1:2 (50g)	1000	120
1:2	1100	60
1:2 (50g)	1100	180
1:2	1200	120

Table 5.2 Reaction conditions employed for the heat treatment of chalcopyrite with lime.

5.2.2 Carbothermic Reduction of Chalcopyrite in the Presence of Lime

As in the previous set of experiments the concentrate composition is listed in table 5.1, the other chemical components, CaO and C, were obtained from Aldrich, and were of 99.9 wt.% purity each. For each reactant sample, a 2g powder mixture was produced

from mixing natural chalcopyrite with stoichiometric amounts of carbon and lime. The stoichiometric ratio of chalcopyrite concentrate: CaO: C is 1:2:2 derived from equation 5.1.

$$CuFeS_{2(s)} + 2CaO_{(s)} + 2C_{(s)} = Cu_{(s)} + Fe_{(s)} + 2CaS_{(s)} + 2CO_{(g)} \qquad (5.1)$$

$$\Delta G^\circ = 234040\text{-}296.5T \text{ J mol}^{-1}$$

The parameters for each experiment are given in table 5.3. The samples were heat treated in the muffle furnace under an inert argon atmosphere, the method is given in section 5.4.1. Before and after reduction the samples were weighed to measure the weight loss caused by the reduction reaction. The weight loss results allowed the percentage of reduction to be determined from the equation detailed in section 5.5.1. After reduction each sample was prepared for X-ray diffraction with selected samples prepared for SEM and EPMA analysis, all described in section 5.5.

Sample Composition $CuFeS_2$:CaO:C	Temperature (°C)	Time (mins)
1:2:2	850	5
1:2:2	850	30
1:2:2	850	60
1:2:2	850	90
1:2:2	850	120
1:2:2	900	5
1:2:2	900	30
1:2:2	900	60
1:2:2	900	90
1:2:2	900	120
1:2:2	950	5
1:2:2	950	30
1:2:2	950	60
1:2:2	950	90
1:2:2	950	120
1:2:2	950	180
1:2:2	1000	5
1:2:2	1000	30
1:2:2	1000	60
1:2:2	1000	90
1:2:2	1000	120
1:2:2	1050	60
1:2:2	1050	120
1:2:2	1100	60
1:2:2	1100	120
1:2:2	1100	180

Table 5.3 Reaction conditions for the carbothermic reduction of chalcopyrite in the presence of lime.

5.2.3 Weight Loss Measurements

Although weight loss was recorded for each reaction, accurate measurements could not always be achieved, therefore experiments were carried out on the thermogravimetric (TGA) furnace under an inert atmosphere to compliment the results from individual weight loss measurements on the muffle furnace. Samples of $CuFeS_2$, CaO and graphite, with the ratio of 1:2:2, were prepared to a total weight of 1g. Each sample was heat treated at a selected isotherm for 120 minutes during which time the weight loss was measured every five seconds to give a smooth reading. Three temperatures were chosen as a comparison for this set of experiments, 900°C, 1000°C and 1100°C. The procedure for these reactions is given in section 5.4.2 and the calculation (equation 5.3) in section 5.5.1 was applied to the weight loss data to give values of percentage reduction.

5.2.4 Reduction by Activated Carbon

The reduction of chalcopyrite by activated carbon was carried out to obtain a comparison between different reducing agents. As in previous experiments the composition of the chalcopyrite used is given in table 5.1. The CaO powder and activated carbon were obtained from Aldrich at 99.9 wt.% purity. Table 5.4 lists the experiments undertaken to develop the comparison. The ratio for the reaction powders was kept at 1:2:2 for $CuFeS_2$: CaO: C, these powders were prepared to give 2g samples. The samples were heat treated in the muffle furnace in an inert gas atmosphere over a temperature range of 850°C to 1100°C, the procedure for which is given in section 5.4.1. The last sample given in this table was 50g in size and heat treated in the retort furnace, the procedure for which is given in section 5.4.3. For each sample X-ray analysis was completed and selected samples were examined microscopically under the scanning electron microscope, these analyses are described in section 5.5.

Sample Composition $CuFeS_2$:CaO:C	Temperature (°C)	Time (mins)
1:2:2	850	60
1:2:2	900	60
1:2:2	950	60
1:2:2	1000	60
1:2:2	1050	60
1:2:2	1100	60
1:2:2	1100	180
1:2:2 (50g)	1100	180

Table 5.4 Reaction conditions for the reduction by activated carbon in the ratio of 1:2:2 of $CuFeS_2$: CaO: C.

5.2.5 Medium Scale Experiments

These experiments were carried out to investigate and verify the reproducibility of the phases produced from the small scale (2g) experiments to a larger scale (50g). The ratio of $CuFeS_2$:CaO:C was kept the same as for the small scale trials, 1:2:2. For each experiment 50g of the mixture was reacted in a retort furnace under an inert argon atmosphere according to table 5.5. The procedure for these reactions is given in section 5.4.3. After each experiment samples were analysed by X-ray diffraction and electron microscopy, these methods are both given in section 5.5.

Sample Composition $CuFeS_2$:CaO:C	Temperature (°C)	Time (mins)
1:2:2	900	180
1:2:2	1000	120
1:2:2	1000	180
1:2:2	1100	120
1:2:2	1100	180
1:2:2	1200	120
1:2:2	1250	180

Table 5.5 Reaction conditions for the reduction of $CuFeS_2$ in the presence of lime for 50g samples.

5.2.6 Silver and Silver Sulphide Additions

In the copper extraction industry, silver is a valuable by-product. It is recovered from the anode slimes residue from electrorefining of copper. Therefore when investigating new process technology for the extraction of copper, the behaviour of silver should also be determined.

To facilitate the investigation of the path of silver during reduction of chalcopyrite, reaction mixtures were either enriched with silver sulphide powder or silver metal. The experimental conditions are presented in table 5.6. In the mineral concentrate the naturally occurring silver component is too small to investigate clearly under the scanning electron microscope. Therefore significant amounts, 1 wt.%, of Ag_2S and Ag metal, were added to allow examination under the electron microscope. For these experiments the ratio of $CuFeS_2$: 2CaO: 2C was kept the same and two sample sizes were used. Small samples, 2g in weight, were reacted in an inert atmosphere in the muffle furnace, the procedure is given in section 5.4.1. Larger samples of 50g were heat treated in the retort furnace under an inert argon atmosphere and, as before, the process is in section 5.4.3. For each sample, X-ray analysis was employed, not to detect silver

phases but to conclude that reactions had occurred in the same manner as for the reduction reactions of section 5.2.2. Each sample was looked at under the electron microscope with an example of Ag_2S doped samples examined on the electron microprobe analyser (EPMA). These techniques are detailed in section 5.5.

Sample Composition	Temperature (°C)	Time (mins)
$CuFeS_2$ + 2CaO + C + 1wt.% Ag_2S (2g)	1100	180
$CuFeS_2$ + 2CaO + C + 1wt.% Ag_2S (50g)	1100	180
$CuFeS_2$ + 2CaO + C + 1wt.% Ag_2S (50g)	1150	180
$CuFeS_2$ + 2CaO + C + 1 wt.% Ag (2g)	1100	180
$CuFeS_2$ + 2CaO + C + 1 wt.% Ag (50g)	1150	180

Table 5.6 Experimental conditions for the reduction of $CuFeS_2$ with silver metal and silver sulphide additions

5.3 Investigation of the Reaction of Chalcopyrite with Calcium Sulphate and Silica

Unlike the ore from India, many chalcopyrite concentrates contain significant amounts of impurities such as arsenic and antimony. Although reduction of chalcopyrite in the presence of lime to produce copper is achievable, this does not solve the problem for the control of and the elimination of these elements. In current copper extraction processes these elements are either volatilised from the process or extracted as anode slimes at the electrorefining stage of copper extraction.

The investigation into the possible control for the elimination of these elements was contemplated. The addition of calcium sulphate and silica will contain the iron

component as the slag phase but also entrain the impurities within it. In a partially reducing atmosphere metallic copper will also be produced as given in equation (5.6).

$$2CuFeS_2 + 3CaSO_4 + 4O_2 + 2SiO_2 + C =$$
$$2Cu + 2FeO.SiO_2.3CaO.SiO_2 + 7SO_2 + CO \qquad (5.2)$$

This set of experiments was carried out to investigate the basis for this reaction. The first reactions completed were the calcination of chalcopyrite followed by the addition of silica to the reaction mixtures. The results from this stage of the research provide the basis for the future investigation into the control and elimination of impurities from chalcopyrite whilst producing copper metal.

5.3.1 Reaction of Chalcopyrite with Calcium Sulphate

The experiments of chalcopyrite and calcium sulphate were carried out as a precursor to those containing $CaSO_4$ and SiO_2. The composition of the chalcopyrite concentrate is given in table 5.1, the other chemical component, $CaSO_4$ was obtained from Aldrich of 99.9 wt.% purity. Samples of 4g were mixed thoroughly in a ratio of 1:2 of $CuFeS_2$ to $CaSO_4$. The reaction conditions are given in table 5.7. These samples were heat treated in an argon atmosphere in the induction furnace, see section 5.4.4. Each sample was analysed by X-ray diffraction to determine the phases present.

Sample Composition $CuFeS_2$:$CaSO_4$	Temperature (°C)	Time (mins)
1:2	850	60
1:2	900	60
1:2	950	60

Table 5.7 Reaction conditions for the heat treatment of $CuFeS_2$ and $CaSO_4$.

5.3.2 Study of the Reaction of Chalcopyrite with Calcium Sulphate and Silica

The reactants for this set of experiments are the same as section 5.3.1, in addition the SiO_2 was obtained from Aldrich. Samples of these reactants were prepared in 2g weights, the experimental compositions are listed in table 5.8. Each mixture was heat treated in the induction furnace (section 5.4.4) with the exception of the 50g sample that was calcined in the retort furnace, section 5.4.3. X-ray analysis was completed for each sample and selected samples were examined under the electron microscope, see section 5.5.

Sample Composition $CuFeS_2$:$CaSO_4$:SiO_2	Temperature (°C)	Time (mins)
1:2:1 (2g)	1000	180
1:2:1 (2g)	1100	180
1:2:1 (50g)	1100	180
1:2:1 and Cu layer (2g)	1100	180
1:3:2 (2g)	1100	180

Table 5.8 Experimental conditions for the heat treatment of $CuFeS_2$ with $CaSO_4$ and SiO_2.

5.4 Experimental Procedures

5.4.1 Procedure for Experiments Carried out on the Muffle Furnace

For each experiment carried out in the muffle furnace the stoichiometric amounts of powders were mixed and ground thoroughly in a ceramic pestle and mortar. The mixture was packed and compressed inside the alumina crucible with a steel plunger. The experimental apparatus employed is shown in figure 5.1. The crucible was suspended from a hook at the top of the silica tube arrangement by a heat resistant iron-chromium alloy wire. The height of the crucible inside the silica tube was maintained in a constant temperature zone by adjusting the length of the wire. Prior to the experiment, the length of the constant temperature zone in the Lenton molybdenum disilicide

furnace was determined by using a Pt - Pt 13% Rh thermocouple. The temperature variation within this zone was ± 5°C

The glassware was held above the furnace by a clamp. After the system was set up and closed, the silica reactor tube was purged with argon for 15 minutes. This was necessary to ensure that the concentration of residual oxygen gas inside the reactor was sufficiently low not to adversely affect the reduction reaction equilibrium. The flow of argon gas was maintained at a rate of 200ml min^{-1} for the duration of the experiment.

The silica tube was then lowered slowly in the upright position into the furnace until the crucible was within the constant temperature zone region. The powder mixture was allowed to react at the pre-selected isotherm for different time periods, which varied between 5 and 180 minutes. After the reaction, the silica tube was withdrawn slowly from the hot zone and the heat treated mass was allowed to cool. The heat treated material was then analysed for new phases produced by using X-ray powder diffraction, scanning electron microscope (SEM) and electron microprobe analysis (EPMA) techniques.

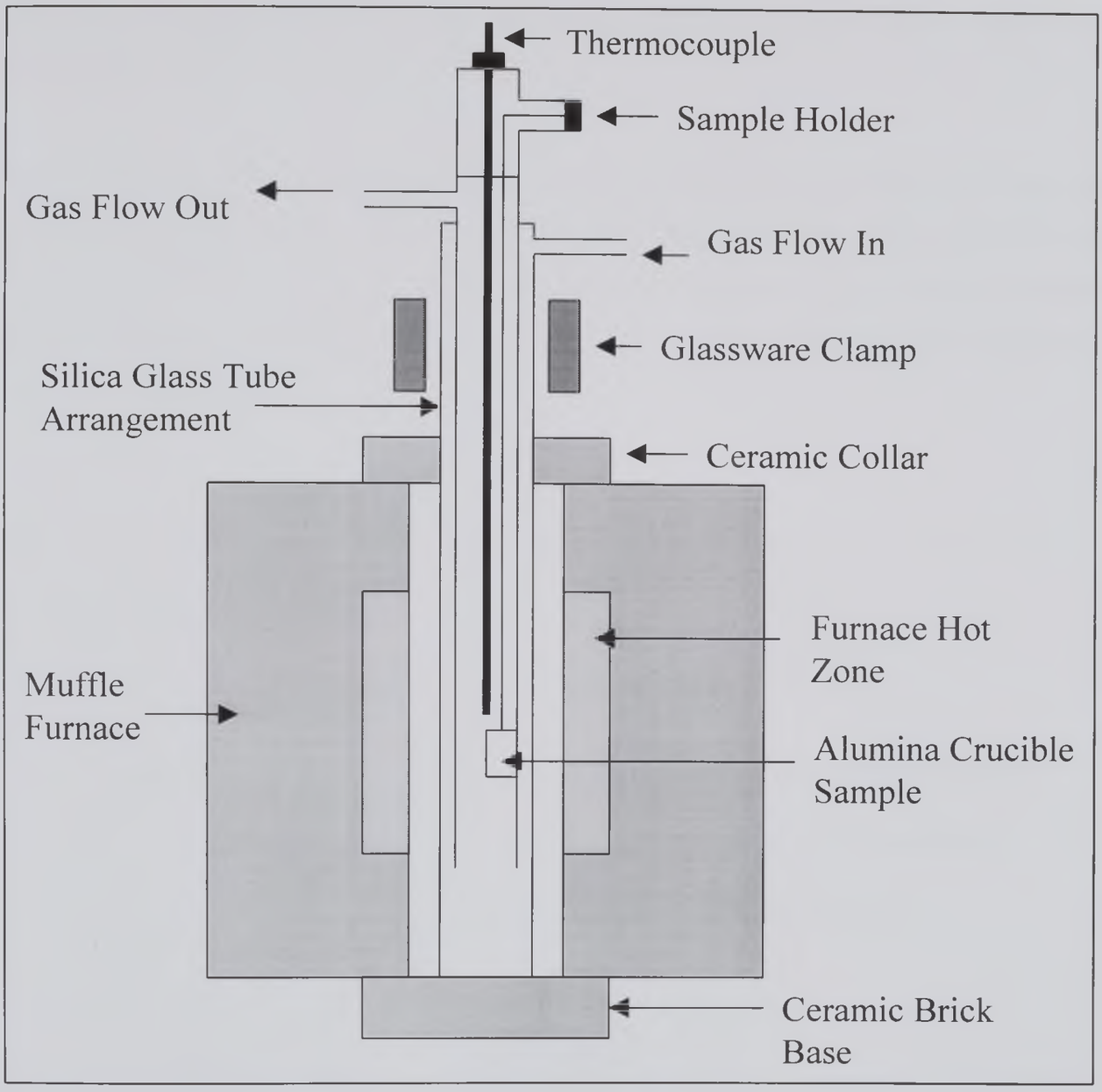

Figure 5.1 Schematic diagram of the experimental apparatus for the muffle furnace.

5.4.2 Thermogravimetric Analysis

The schematic diagram for the thermogravimetric apparatus is shown in figure 5.2. A stoichiometric powder mixture was made of chalcopyrite concentrate, lime and carbon to a weight of 1g and pressed by a steel plunger into alumina crucibles. The crucible was suspended from a platinum wire attached to the TGA balance. Inside the silica tube an inert atmosphere was maintained by passing a stream of argon gas at a rate of 200ml min^{-1}. The furnace was kept at the selected isotherm for two hours whilst regular weight measurements, every 5 seconds, were recorded by a computer. A counter balance was

used from which the weight loss was determined kept to the same weight as that of the unreacted mixture.

From the data recorded by the computer, weight loss data throughout the trial time was determined for each reaction and converted to percentage reduction, details of which are given in section 5.5.1. These results were plotted on graphs as percentage reduction against time and compared with the weight loss results obtained from individual reduction experiments.

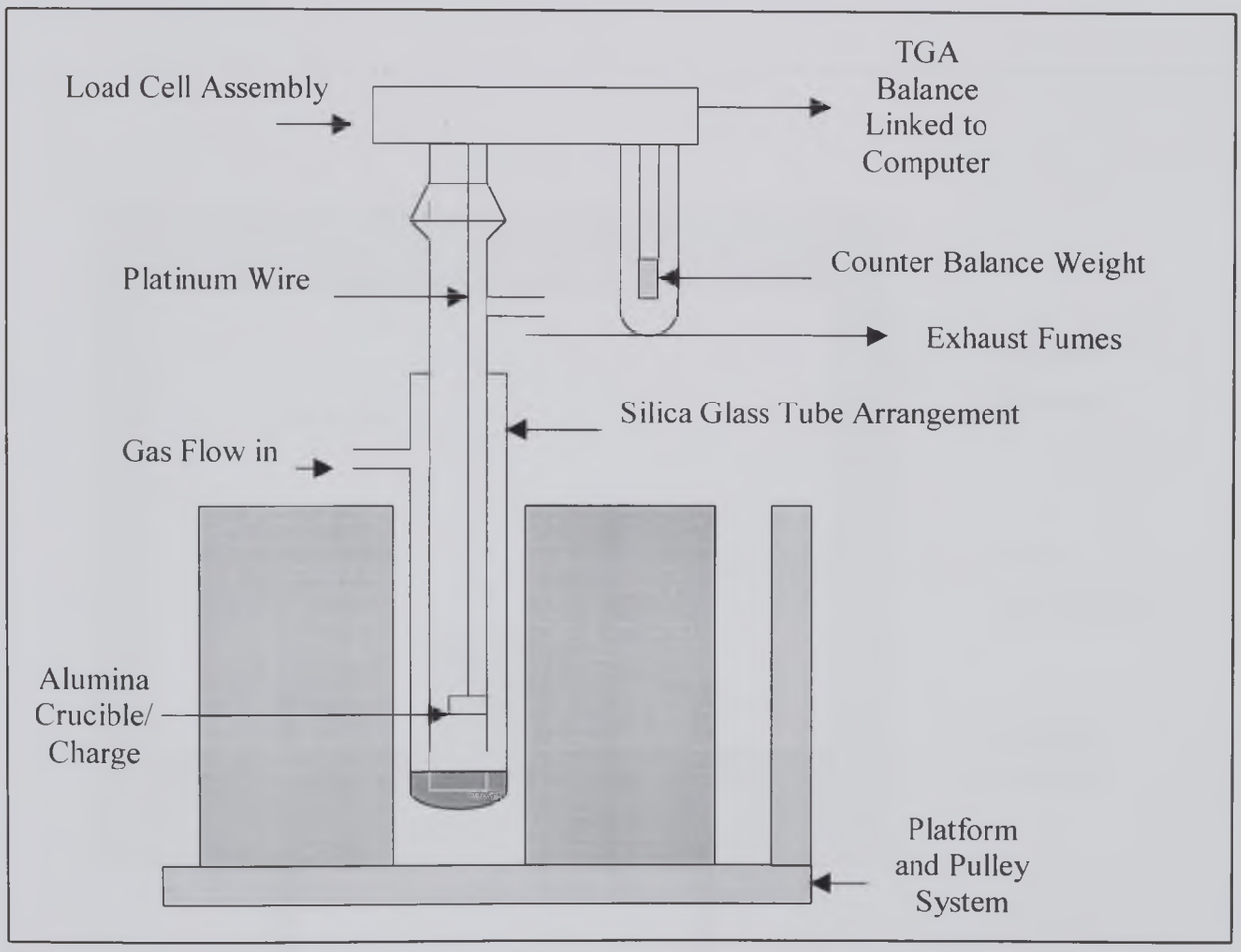

Figure 5.2 Schematic diagram for the thermogravimetric apparatus used for the kinetic study of the reduction reaction.

5.4.3 Procedure for Experiments Carried out on the Retort Furnace

The charges to be used in retort furnace experiments were thoroughly mixed in a mortar and pestle before being compacted into graphite crucibles and placed in the retort furnace. A stream of argon was introduced to provide an inert atmosphere inside the retort chamber. The furnace was heated to a pre-selected isotherm at which it was held for a fixed period of time. The sample was allowed to cool down after the experiment in the flowing gas atmosphere before being analysed by X-ray powder diffraction analysis, SEM and EPMA microscopic techniques.

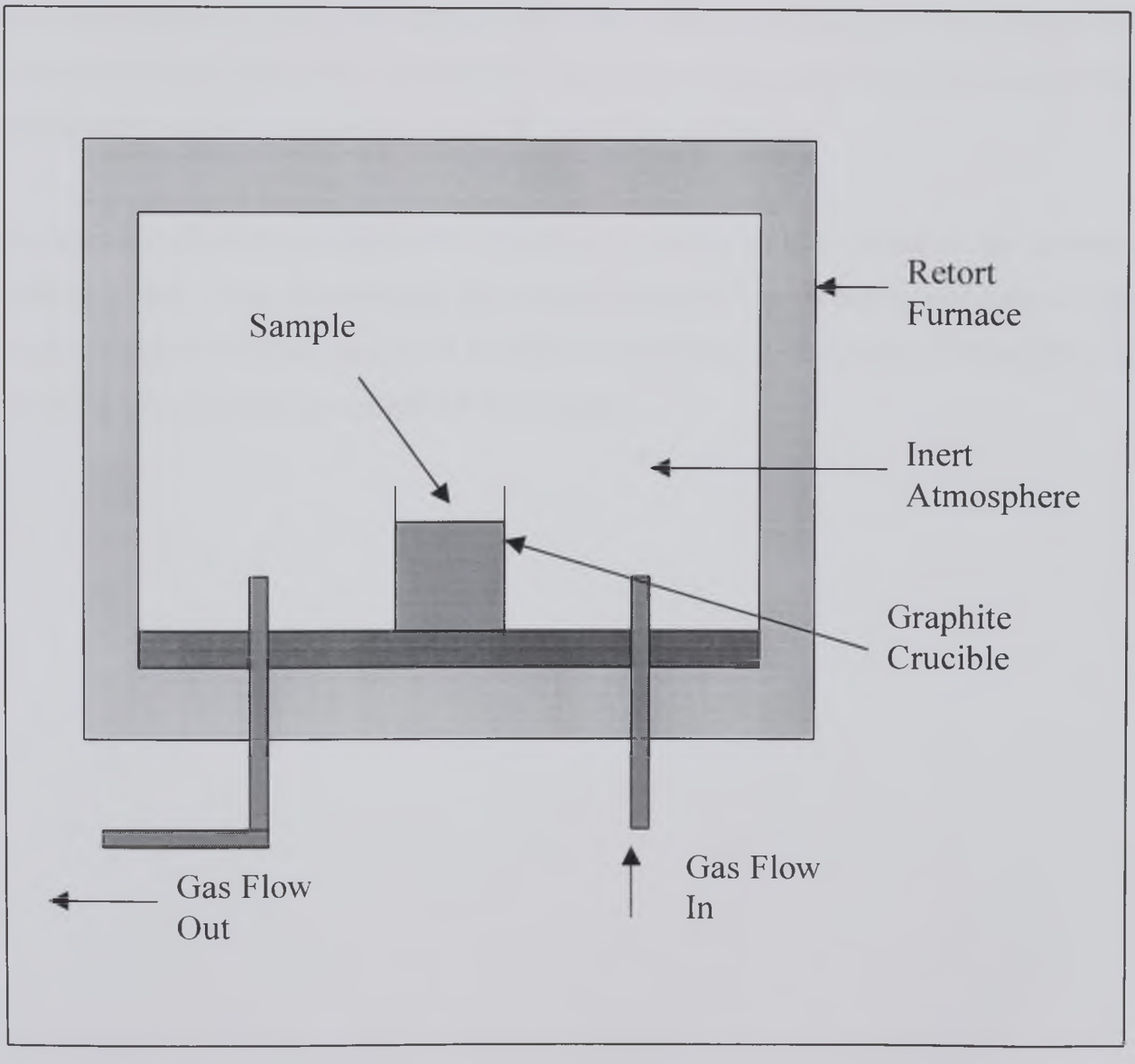

Figure 5.3 Schematic diagram of the experimental set-up for the retort furnace.

5.4.4 Procedure for Experiments Carried out on the Induction Furnace

Each charge prepared for experiments carried out in the Induction furnace was mixed and ground thoroughly in a ceramic pestle and mortar. The mixture was packed and compressed with a steel plunger to compact the powder inside the alumina crucible. The experimental apparatus employed is shown in figure 5.4. The crucible position inside the silica tube was maintained in a constant temperature zone by adjusting the height of a Pt-13%Rh thermocouple.

The glassware was held in the apparatus by a clamp, at the base of the tube, that also held the thermocouple in place. After the system was set-up and closed, a flow of argon gas was maintained inside the silica reactor tube, which was purged with argon for 15 minutes to ensure that the concentration of residual oxygen gas inside the reactor was sufficiently low not to adversely affect the reaction equilibrium.

The powder mixture was allowed to react at the predetermined isotherm for different lengths of time. After the reaction, the sample was cooled in the argon atmosphere. The reacted material was then analysed for new phases using X-ray powder diffraction and scanning electron microscope (SEM) techniques.

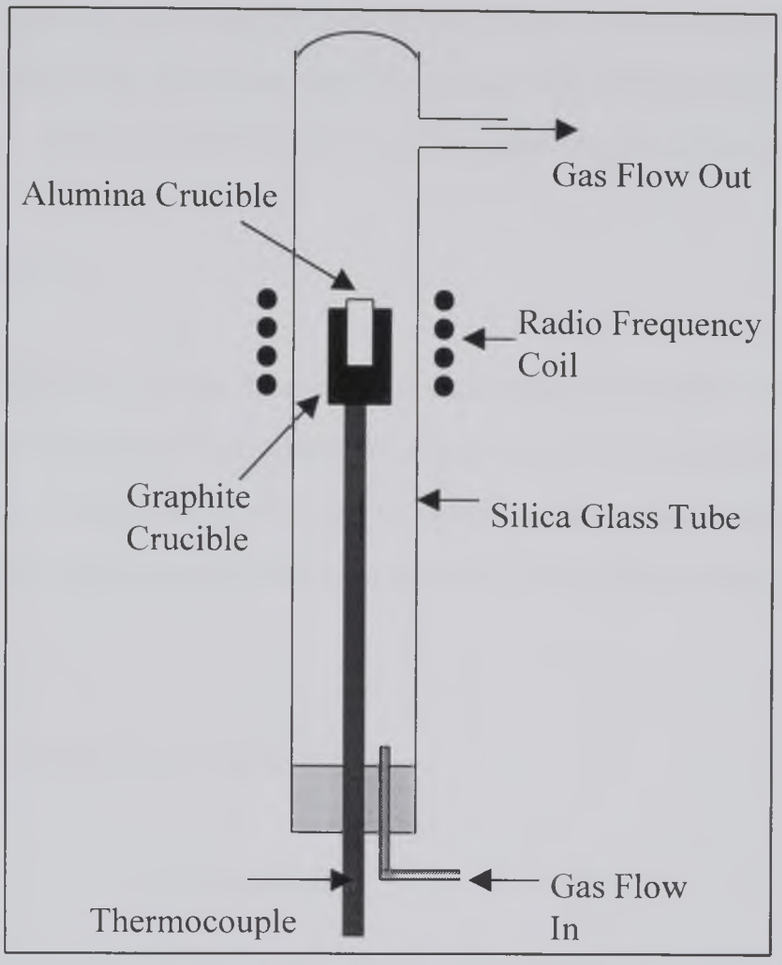

Figure 5.4 Schematic diagram of the experimental apparatus for the induction furnace

5.5 Analysis Techniques Employed

5.5.1 Percentage Reduction

The percentage reduction of a reaction is calculated from the weight loss during the experiments expressed as a percentage of the theoretical loss, as shown in equation 5.3:

$$\% \text{ Reduction} = W_a / W_s \times 100 \qquad (5.3)$$

Where W_a is the actual weight loss and W_s is the calculated stoichiometric weight loss based on the equation for the appropriate reduction reaction for the samples. By calculating the percentage reduction profile, the degree of reduction can be determined

at a specific temperature and time. A plot of percentage reduction against time can be utilised to investigate the reduction rate for a particular temperature over a range of times. In this way, various reduction rates can be compared for different temperatures.

5.5.2 X-ray Analysis

X-ray powder diffraction of the heat-treated and reduced samples was carried out to determine the phases present. The procedure adopted involved grinding a representative part of the sample, loading the powder into a sample holder and scanning using Cu Kα radiation. A Philips Automated Diffraction system 1700 diffractometer was used for all X-ray work.

X-ray diffraction is based upon Bragg's law:

$$\lambda = 2d_{hkl} \sin\theta_{hkl} \qquad (5.4)$$

Where λ = wavelength of the X-ray

d_{hkl} = inter planar spacing of the hkl planes in the lattice

$2\theta_{hkl}$ = diffraction angle

The analyses were carried out over the range 2θ = 20-90°, the wavelength of Cu Kα radiation being 0.15406 nm. A powder diffraction pattern is obtained by examining the intensities of the reflected X-rays as a function of 2θ, the diffraction pattern forming a fingerprint by which phases can be identified. From matching peak positions on the diffraction trace to documented data, i.e. the JCPDS files, phases can be identified.

5.5.3 Scanning Electron Microscopy

A Camscan Series 4 scanning electron microscope (SEM) operating at 20 keV was used for all SEM and EDX work. The microscope was fitted with a Link LZ5 X-ray detector and a Link 860 Series II Energy Dispersive X-ray (EDX) analysis system.

Some samples were placed directly on stubs and gold coated for SEM analysis of the microstructure. Others samples were vacuum impregnated with Araldite resin, polished finely to 1μm, carbon coated and then used for elemental analysis (EDX) on the electron microscope. Back-scattered electron imaging (BSE) was employed to gain contrast between different phases present within the sample. Elemental dot maps were produced on selected samples to further investigate the phases produced from the reactions. The elemental distribution within the sample can be studied using this method; the elements are pinpointed on micrographs.

5.5.4 Electron Probe Microanalysis

Specimens were vacuum impregnated in Araldite resin and polished to a 1 μm finish and carbon coated prior to examination on the microscope. A Cameca SX-50 Electron Probe Micro-analyser fitted with three wavelength dispersive spectrometers containing an Oxford Microanalytical Division Link 10/55 EDS system was used operating at 25 keV with a 50nA beam current.

CHAPTER SIX

Results

6.1 Introduction

This chapter presents the results obtained from the experiments outlined in chapter 5. Initially the results from the reduction of chalcopyrite with lime are reported. The reduction of chalcopyrite is detailed including a discussion of the effect of activated carbon, the sample size, and the addition of both silver sulphide and silver metal. The measurement of oxygen potentials during reduction is given in appendix 2. After the data for the reduction of chalcopyrite has been presented then the next stage of this result chapter will present the results of the analysis carried out on samples of chalcopyrite reacted with calcium sulphate. These are presented together with a discussion of the reaction of chalcopyrite with calcium sulphate and silica.

6.2 Reaction of Natural Chalcopyrite Mineral Concentrate and Lime

The reaction between chalcopyrite and lime is thought to occur as an exchange reaction, and is the initial stage of the reduction reaction. Therefore it is important to characterise this reaction in order to understand the reduction mechanism. The equation for the proposed exchange reaction between chalcopyrite and lime is given in equation 6.1. The reaction products are expected to be copper and iron oxides with calcium sulphide with any weight loss due to the evolution of oxygen.

$$2CuFeS_{2\,(s)} + 4CaO_{\,(s)} = Cu_2O_{\,(s)} + 2FeO_{\,(s)} + 4CaS_{\,(s)} + \tfrac{1}{2}\,O_{2\,(g)} \qquad (6.1)$$

The reaction between chalcopyrite and lime was studied in the temperature range 850°C to 1200°C. Samples of a 1:2 mixture of chalcopyrite and lime were reacted in a flowing inert argon atmosphere. Increase in temperature resulted in increased weight loss, the data for which is given in table 6.1. The samples prior to heat treatment were light grey in colouration, after reaction the samples became darker. At 1100°C a red colouration was observed at the top of the reacted mass. The results detailed in this

section for the exchange reaction indicates that the reaction does not proceed as in the reaction given in equation 6.1.

6.2.1 X-ray Diffraction Analysis

X-ray diffraction analysis was carried out on every sample. The phases identified as present are given in table 6.1. A comparison of selected X-ray diffraction patterns is given in figure 6.1. The phases were identified by X-ray analysis from the JCPDS powder diffraction files. The relevant card files numbers and peak data for each phase are given in appendix 1.

Temperature (°C)	Time (mins)	% Sample Lost	Phases Analysis with Relative Intensity					
			CaS	C_{III}	CaO	Cu	C_{II}	Fe
850	5	7.57	VS	WM	S			
850	30	8.66	VS	S	S			
850	60	7.69	VS	S	S			
850	90	9.92	VS	S	M			
850	120	9.78	VS	S	M			
900	60	8.54	VS	MS			W	
950	60	10.55	VS	MS			W	
1000	60	12.52	VS	M			W	
1000	120	17.56	VS	M		W	W	
1100	60	13.45	VS	M		M	M	
1100	180	18.21	VS	M		M	M	
1200	120	13.76	VS	M		M	M	

Table 6.1 Summary of the X-ray analysis carried out on samples of natural chalcopyrite reacted with lime in the ratio of 1:2 (VS-very strong, S-strong, MS-medium strong, M-medium, WM-weak medium, W-weak).

Calcium sulphide is identified as being present in each sample heat treated and is the most prevalent of all the phases observed. On these patterns presented in figure 6.1, CaS is the strongest peak identified for all reaction conditions. The peak data from the X-ray diffraction patterns correspond well with the peak data in the JCPDS file. This phase

was first identified in the sample heat treated at 850°C for 5 minutes, indicating that this phase as well as being predominant is the first product of the exchange reaction.

Unreacted lime was detected from the X-ray analysis of these samples in reaction at 850°C. Although found with the reaction product, calcium sulphide, the presence of lime indicates that the exchange reaction does not reach completion at this temperature. As shown by table 6.1 CaO was present in all samples at 850°C but did not appear at 900°C. At this temperature and above, all of the CaO reacts with chalcopyrite to form either CaS or the intermediary oxysulphide compounds, C_{II} and C_{III}. The longer the time period the samples were reacted for at 850°C the weaker the presence of lime becomes.

Unreacted chalcopyrite was not detected from experiments at any temperature. The mineral is not expected to still be present in this temperature range as it not stable at such high temperatures. Without the presence of lime chalcopyrite would decompose to produce bornite and pyrrhotite as shown by equation 6.2. However the presence of lime means that the reaction of equation 6.2 is not observed as demonstrated by the lack of either of the two products of equation 6.2 in the X-ray diffraction patterns.

$$5CuFeS_{2\,(s)} = Cu_5FeS_{4\,(s)} + 4FeS_{\,(s)} + S_{2\,(g)} \qquad (6.2)$$

The quinary oxysulphide phase (C_{III}) was identified by X-ray phase analysis as occurring at all temperatures in all of the samples reacted. The presence of this phase in samples heat treated at 850°C was initially weak but the intensities became stronger for longer times and at higher temperatures. The C_{III} phase is a quinary compound with the general formula CuFeCaSO and the production from chalcopyrite can be represented by the reaction of equation 6.3.

$$CuFeS_{2\,(s)} + 2CaO_{\,(s)} = CuFeCaSO_{\,(l)} + CaS_{\,(s)} + \tfrac{1}{2}\,O_{2\,(g)} \qquad (6.3)$$

The reaction in equation 6.3 differs considerably from the theoretical reaction of equation 6.1 for the reaction of chalcopyrite and lime. The gaseous evolution from equation 6.1 is assumed to be oxygen only whereas in reality the gaseous phases

evolved are a mixture of O_2 and SO_2 gases. Therefore the weight loss observed in table 6.1 is due to the evolution of these gases.

The quinary oxysulphide was given the notation, C_{111}, by Jha and Grieveson (1992b). However the d-spacings published for this phase were at variance with those observed from X-ray powder diffraction patterns obtained in the current study. A comparison of the d-spacings is presented in table 6.2. An investigation was carried out to re-define the peaks and structure for this phase. The details and results for this investigation are given in section 6.3. All identification of the C_{111} compound is made from the data given in this section and not from the previously published data.

D-spacing values for published C_{111}	D-spacing values from experimental data
5.20	—
4.95	—
3.45	3.5123
—	3.3057
3.12	3.1713
2.70	2.7206
2.66	2.6890
2.54	2.5360
2.37	—
2.18	—
1.91	1.9389
1.83	—
1.55	—

Table 6.2 Comparison between d-spacing values for published (Jha and Grieveson 1992b) and experimental values.

Another oxysulphide phase, C_{11}, was observed from X-ray diffraction analysis. This phase has the formula FeO.CaS, the published d-spacings from which this phase is identified were reported by Jha and Grieveson (1992b). The d-spacings for the C_{11} phase are given in appendix 1, with relative intensities. This phase was first observed at

900°C and at all higher temperatures. The presence of this phase was not as strong as the C_{111} phase.

Copper and iron at the lower temperatures of 850°C, 900°C and 950°C are tied up as the intermediary phases, C_{11} and C_{111}; other compounds of neither iron nor copper were apparent from the X-ray diffraction analysis as demonstrated by figure 6.1. At higher temperatures metallic copper is identified as forming from the reaction of chalcopyrite with lime. The presence of this metal is shown by the diffraction pattern of figure 6.1c for chalcopyrite reacted with lime at 1100°C. The production of copper from the reaction is given in equation 6.4.

$$CuFeS_{2\,(s)} + 2CaO_{\,(s)} = Cu_{\,(s)} + FeO.CaS_{\,(s)} + CaS_{\,(s)} + \tfrac{1}{2}\,O_{2\,(g)} \qquad (6.4)$$

Metallic iron does not form as a result of this reaction and is not observed in any of the X-ray diffraction patterns. The iron component is always found as one of the two oxysulphide phases, C_{11} and C_{111}.

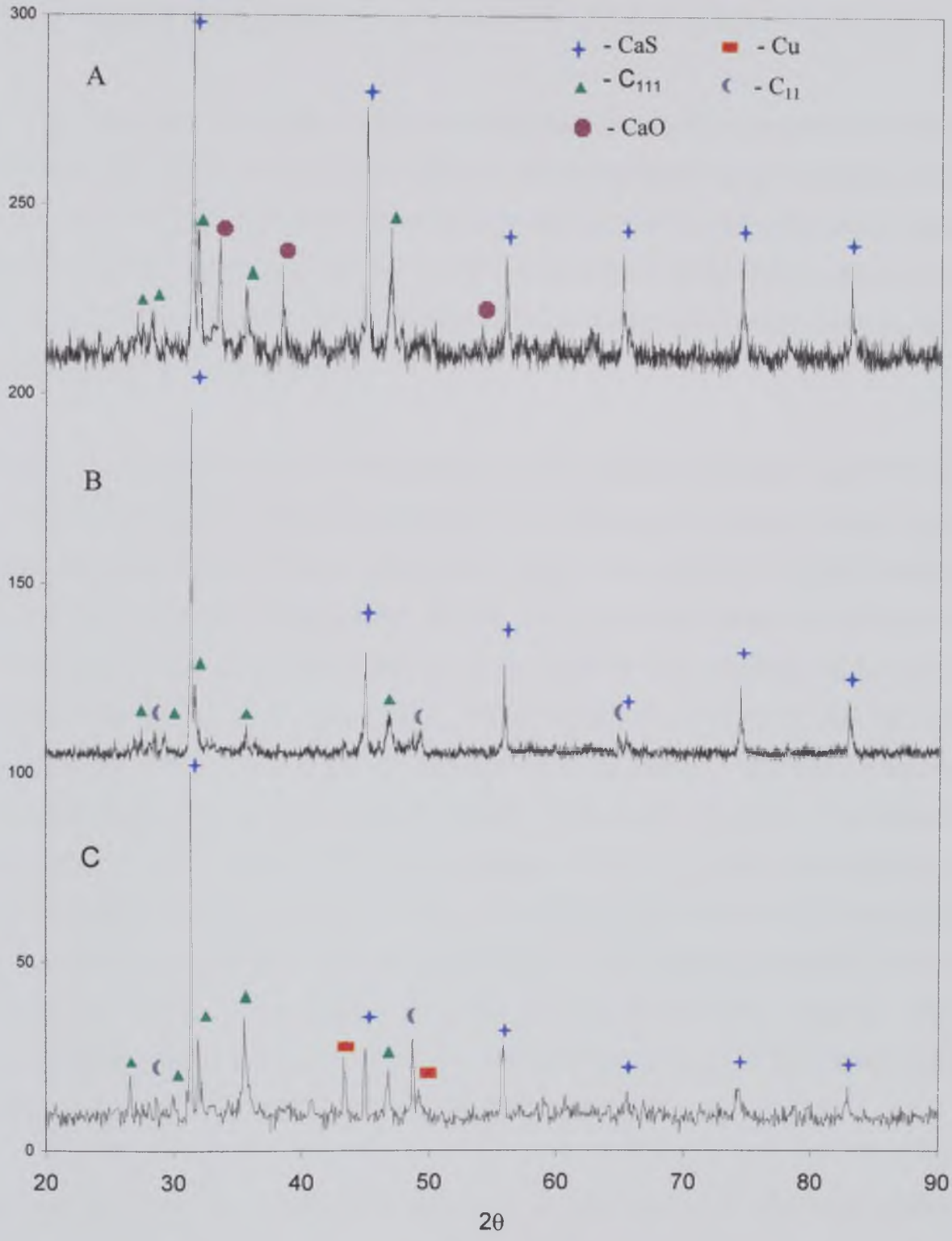

Figure 6.1 X-ray powder diffraction patterns for the heat treatment of chalcopyrite and lime at A-850°C, B-1000°C and C-1100°C for 60 minutes.

6.2.2 Electron Microscopy

It was important to investigate the phase structure produced as a result of the reaction between chalcopyrite and calcium oxide to aid on understanding the phases produced from the reduction of chalcopyrite. Thus, samples of heat treated chalcopyrite and lime were examined under the scanning electron microscope (SEM). Both scattered electron imaging (SEI) and back scattered electron (BSE) imaging with energy dispsersive X-ray analysis (EDX) were employed.

Figure 6.2 is a back scattered electron image of a sample heat treated at 850°C for 60 minutes. The phase distribution observed from this image is typical of that observed throughout the sample. Phase analysis, by energy X-ray dispersive (EDX) analysis of this sample, indicated the presence of CaS. This phase was observed on the electron microscope in all heat treated samples as expected from X-ray analysis. In figure 6.2 the lighter widespread phases are typical of CaS (dark) surrounded by the lighter C_{111} oxysulphide phase. The larger grey areas are silica, a naturally occurring component of the chalcopyrite concentrate. Figure 6.3 shows in particular the darker CaS phase with the lighter C_{111} compound. The identification of the C_{111} phase was established by taking elemental dot maps for Cu, Fe, Ca and S. In regions where all of these elements are present the assumption that the area is the C_{111} oxysulphide compound was made. This phase was not as readily observed as CaS through the samples. The C_{11} oxysulphide phase was not detected from electron microscopy of the reacted samples although it was identified in the X-ray diffraction patterns.

At low temperatures, typified by figure 6.2, in agreement with the X-ray diffraction analysis there was no evidence of metallic phases. At higher temperatures metallic copper is produced as a result of the reaction between natural chalcopyrite and calcium oxide, as identified by X-ray diffraction analysis. The formation of metallic copper was observed at 1100°C and can be seen in figures 6.4, 6.5 and 6.6. Figure 6.4 typifies the microstructure observed at the top of the reacted mass. Figure 6.5 focuses particularly on a region of metallic copper globules surrounded by the darker calcium sulphide phase. The presence of metallic copper explains the reddish colouration observed at the

top of the reacted chalcopyrite when first removed from the furnace. Figure 6.6, also taken at the top of the sample reacted at 1100°C, shows a metallic region in which the centre is metallic copper. The surrounding metallic phase contains both copper and iron but there was no detection of calcium nor sulphur. This region would appear to be a combination of metallic copper and iron oxide. The darker phases surrounding this metallic region are calcium sulphide. Iron oxides were not detected from X-ray analysis suggesting the presence of this compound in the sample is minimal.

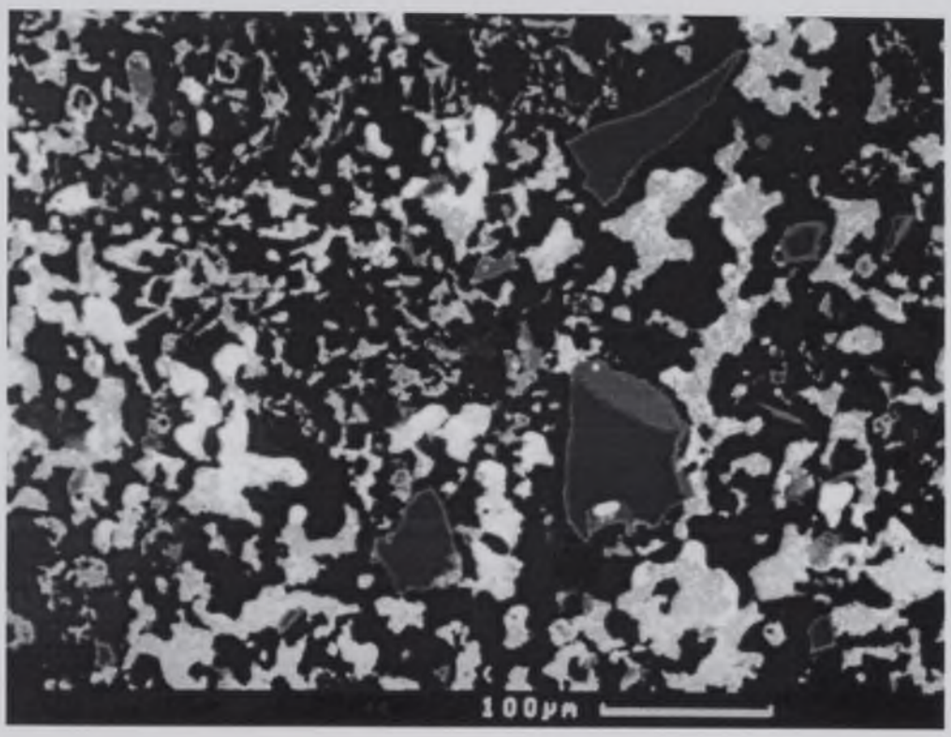

Figure 6.2 BSE image of general microstructure observed from $CuFeS_2$:2CaO heat treated at 850°C for 60 minutes.

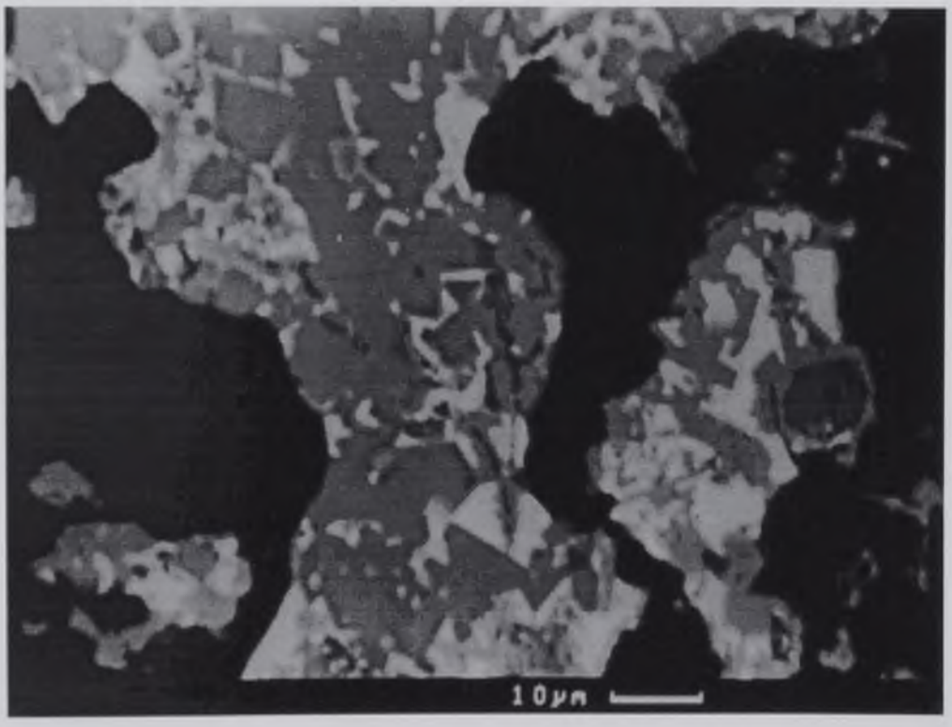

Figure 6.3 BSE image of figure 6.2 at a higher magnification showing CaS (dark grey) surrounded by the C_{111} phase (lighter region).

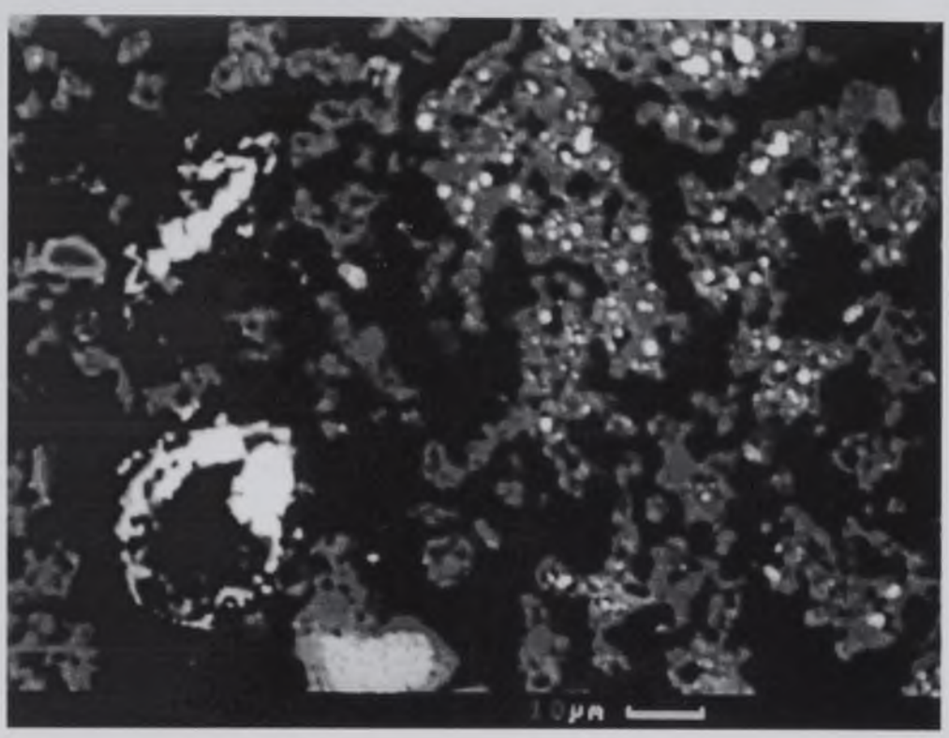

Figure 6.4 BSE of the microstructure observed from the heat treatment of chalcopyrite and lime at 1100°C for 120 minutes.

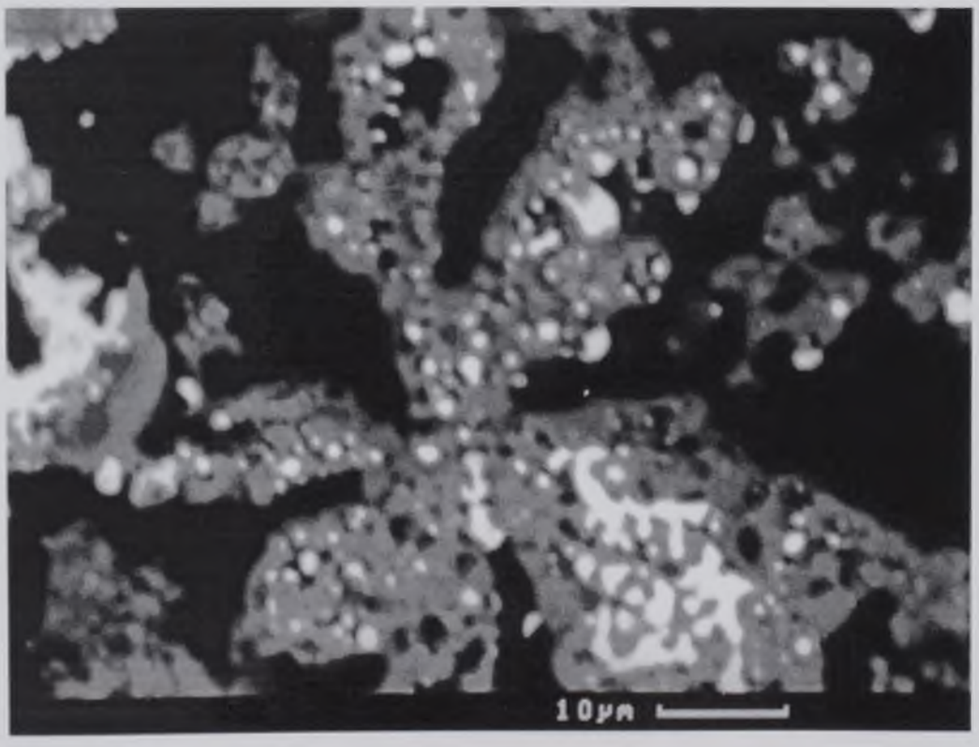

Figure 6.5 BSE microstructure observed in figure 6.4 at a higher magnification, the light regions are metallic copper surrounded by darker CaS.

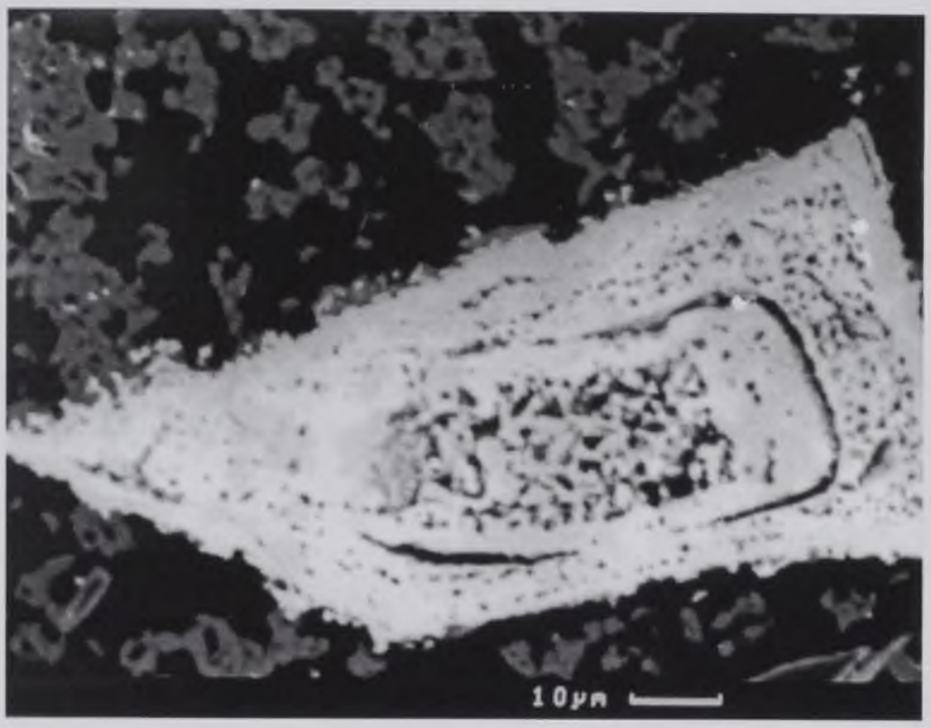

Figure 6.6 BSE image from $CuFeS_2$:2CaO reacted at 1100°C for 120 minutes.

6.3 C_{111} Oxysulphide Phase Determination

When the X-ray diffraction patterns were analysed to identify the phases produced from heat treatments with lime and carbon it became obvious that some d-spacings were not found in the JCPDS files which allow for determination of known compounds. The d-spacings are listed in tables 6.3 and 6.4. These unidentified d-spacings did not correlate with any data previously published. The compound type that these d-spacings were thought to correspond with was a copper-iron oxysulphide. This assumption was based on preliminary investigations on the electron microscope. The use of EDX analysis indicated the presence of compounds containing copper, iron, calcium, sulphur and oxygen.

Previously published work of the discovery of d-spacings for such intermediary compounds gave them the notations C_1, C_{11} and C_{111}, where C_1 represents the formula 4FeO.3CaS and C_{11} is identified as FeO.CaO. Jha and Grieveson (1992b) reported data on the C_{111} compound, giving the relative intensities of peaks and d-spacing data from powder diffraction analysis on synthesised chalcopyrite reduced by carbon in the presence of lime.

Comparison of the published data for the C_{111} compound and the experimental data, given in table 6.2, reveals that the published C_{111} phase is not present in the X-ray diffraction patterns. Nevertheless the unidentified phase was still regarded to be similar in shape and structure to that of the C_{111} phase. This assumption is made because although the peaks for the unidentified phase do not match with the published values (see table 6.2) a similarity is observed. Therefore re-evaluation of this compound was necessary to facilitate thorough analysis of the X-ray diffraction data for all the sets of experiments.

An X-ray diffraction analysis was completed for every experiment. Tables 6.3 and 6.4 show the unidentified d-spacings for various selected experiments. From these tables patterns emerged as to which d-spacings would most likely belong to the intermediary oxysulphide phase. These d-spacings were observed at 850°C and 900°C for samples of chalcopyrite heat treated with lime. On the patterns of those samples which had

undergone their reaction at 850°C, similar d-spacings were detected for chalcopyrite reduced by carbon in the presence of lime. Although these d-spacings were observed elsewhere from other sets of reactions, the investigation was limited to those mentioned above. The calculations completed for each unidentified d-spacing were fairly involved and to complete these calculations for every value would have been too time consuming therefore representative sets of data were used.

5 mins	30 mins	60 mins	90 mins	120 mins
3.5045	3.4689	3.5123	3.5042	3.5082
3.3151	3.3187	3.3057	3.2928	3.2961
3.1655		3.1713	3.1686	3.1562
2.7152	2.7024	2.7206	2.7182	7.7194
2.6853	2.6692	2.6892	2.6863	2.6876
2.5367	2.5260	2.5417	2.5378	2.5409
1.9296	1.9311	1.9389	1.9346	1.9306

Table 6.3 Comparison of unidentified d-spacings obtained from X-ray diffraction patterns of $CuFeS_2$: 2CaO reacted at 850°C.

5 mins	30 mins	60 mins	90 mins	120 mins
3.5604	3.5028	3.4930		
3.3015	3.3051	3.3030	3.2943	3.2788
3.1702	3.1672	3.1576	3.1620	3.1598
2.7020	2.7184	2.7152	2.7188	2.7108
2.6890	2.6878	2.6867	2.6818	2.6957
2.5360	2.5407	2.5388	2.5399	2.5215
1.9312	1.9311	1.9337	1.9346	1.9306

Table 6.4 Comparison of d-spacings from X-ray diffraction analysis obtained from the reduction of chalcopyrite, $CuFeS_2$: 2CaO: 2C at 850°C.

The C_{111} phase is assumed to be hexagonal in structure and hence the determinations of the hkl values and lattice parameters from the experimental d-spacings were made based upon this assumption. The premise that the C_{111} phase is hexagonal was based upon the

C_{11} phase also being hexagonal. The C_{111} phase is regarded as differing from the C_{11} compound by the addition of copper in the crystal lattice. The changes in d-spacings observed for the C_{111} compound depend upon the extent of Fe replacement by Cu.

Different approaches to the structure were made. Firstly the structure was determined from looking at the d-spacings of the X-ray diffraction patterns, tables 6.3 and 6.4. The d-spacings and hkl values for the compound were assigned from comparing the experimental d-spacings to those of the C_{11} phase. Once determined, these d-spacings were used to calculate the values for a and c in the hexagonal structure. These values were derived from equation 6.4 for the interplanar spacings of the hexagonal structure. A summary of calculated a and c values is presented in table 6.5, here ranges of values are given. It is not possible to ascertain single values of a and c due to the calculations being dependant upon X-ray diffraction patterns from different experiments.

$$\frac{1}{d^2} = \frac{4}{3}.\frac{h^2 + hk + k^2}{a^2} + \frac{l^2}{c^2} \qquad (6.5)$$

Experimental Condition	Range of values for a	Range of values for c
1:2 @ 850°C for 60 mins	6.653 - 6.70	3.72 – 3.95
1:2 @ 900°C for 60 mins	6.29 – 6.65	3.67 - 3.88
1:2:2 @ 850°C for 60 mins	6.60 – 6.72	3.73 – 3.96
C_{11}	6.32	3.68

Table 6.5 Selected calculated ranges of values for lattice parameters a and c for the C_{111} compound, compared to published data for the C_{11} phase.

Comparisons of the ranges of values for the lattice parameters a and c indicate good agreement. However these findings are not conclusive enough to be able to determine the crystal structure.

The second approach to determine the structure of the C_{111} phase was to use the analytical method prescribed by Cullity (1959). If the structure of an unknown phase is to be determined via the non-graphical method then an assumption has to be made first on the crystal system to which the phase belongs. As already stated this system is

assumed to be hexagonal, therefore calculations are made based on this assumption. The first step in such a determination is to calculate the $\sin^2\theta$ values for each angle, arithmetical manipulation of these values leads to observations of relationships.

The first step of the arithmetical manipulation of the $\sin^2\theta$ values is to find values of $\sin^2\theta$ divided by 3, 4 and 7. An example of this procedure is given in table 6.6 which shows calculations from d-spacings obtained from X-ray analysis of chalcopyrite reacted with lime at 850°C for 60 minutes. From the integrals of $\sin^2\theta$ comparisons are made to find like values. In table 6.6 a like value is found for $\sin^2\theta/3$ and $\sin^2\theta/4$, equal to 0.0180 therefore giving $\sin^2\theta = 0.054 = A$. For hexagonal crystals the $\sin^2\theta$ values are linked to the miller indices (hkl) by equation 6.6:

$$\mathrm{Sin}^2\,\theta = A(h^2 + hk + k^2) + Cl^2 \qquad (6.6)$$

The hkl value for $\sin^2\theta = 0.054$ is 100 and 110 is assigned to $\sin^2\theta = 3.3114$. Once the value for A is determined the next stage is to find the value for C. Calculations of values for $\sin^2\theta$ - A and $\sin^2\theta$ -3A are made, from which relationships are made in the ratio of 4, 9 and 16. From table 6.6 the value for C is determined as 0.411, hence the $\sin^2\theta$ is equal to A + C therefore this peak is assigned the hkl value of 101.

2 θ	d	I	$\mathrm{Sin}^2\theta$	$\mathrm{Sin}^2\theta/3$	$\mathrm{Sin}^2\theta/4$	$\mathrm{Sin}^2\theta/7$	d-A	d-3A	hkl
25.40	3.5042	8.78	0.0483	0.0161	0.0121	0.0069	0.0303		
26.90	3.3114	6.96	0.0541	0.0181	0.0135	0.0077	0.0361		110
28.14	3.1686	10.50	0.0591	0.0197	0.0148	0.0084	0.4110	0.0050	101
31.21	2.8616	10.22	0.0724	0.0241	0.0181	0.0134	0.4001	0.1938	200
31.96	2.7982	15.12	0.0758	0.0253	0.0189	0.0108	0.0577	0.0217	
33.41	2.6800	24.08	0.0826	0.0275	0.0207	0.0118	0.0646	0.0285	
35.34	2.5378	12.06	0.0921	0.0307	0.0230	0.0132	0.0741	0.0380	111
47.07	1.9290	13.72	0.1595	0.0532	0.0399	0.0228	0.1414	0.1054	002

Table 6.6 Example of determination of hkl values from X-ray diffraction using the Cullity method for a sample of chalcopyrite heat treated 850°C for 60 minutes.

From derived values for A and C the lattice parameters a and c can be calculated for the hexagonal structure from equations 6.7 and 6.8. The values for $(h^2 + hk + k^2)$ are found tabulated in Cullity (1959).

$$A = \lambda^2 / 3a^2 \qquad (6.7)$$

$$C = \lambda^2 / 4c^2 \qquad (6.8)$$

To check the validity of the values for the lattice parameters, graphs of a and c against $\sin^2\theta$ were constructed, an example is given in figure 6.7. The lines for a and c are given for a sample reduced at 850°C for 60 minutes. The values were extrapolated to $\sin^2\theta = 1$ from which the values for a and c are determined at unity, a = 4 and c = 6.75.

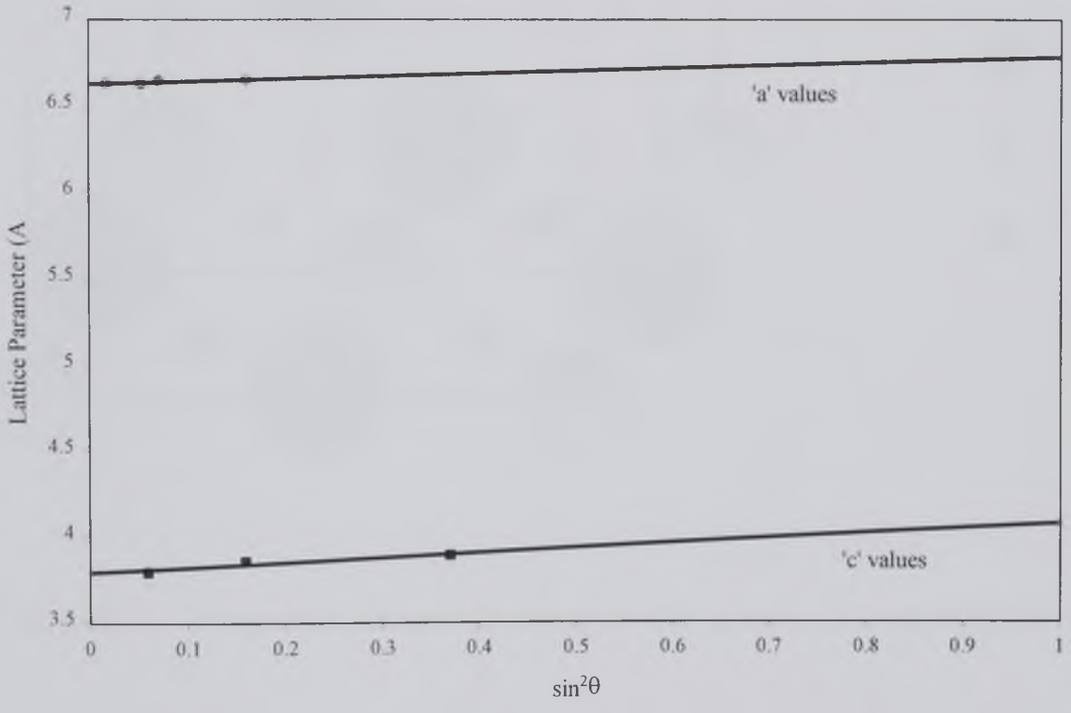

Figure 6.7 Example of determined a and c parameters for the C_{111} phase for chalcopyrite heat treated at 850°C for 60 minutes.

A proposed structure for the C_{111} phase is given in figure 6.8. The structure is based on the determined a and c lattice parameters and the crystal structure for the published C_{11}

compound. The C_{111} phase is thought to be a solid solution phase. The lattice parameters and hence the d-spacings change depending upon experimental conditions and due to the extent of Fe replacement by Cu. Therefore the structure presented in figure 6.8 is an idealised structure that would change depending upon temperature and reaction condition, i.e. with or without carbon.

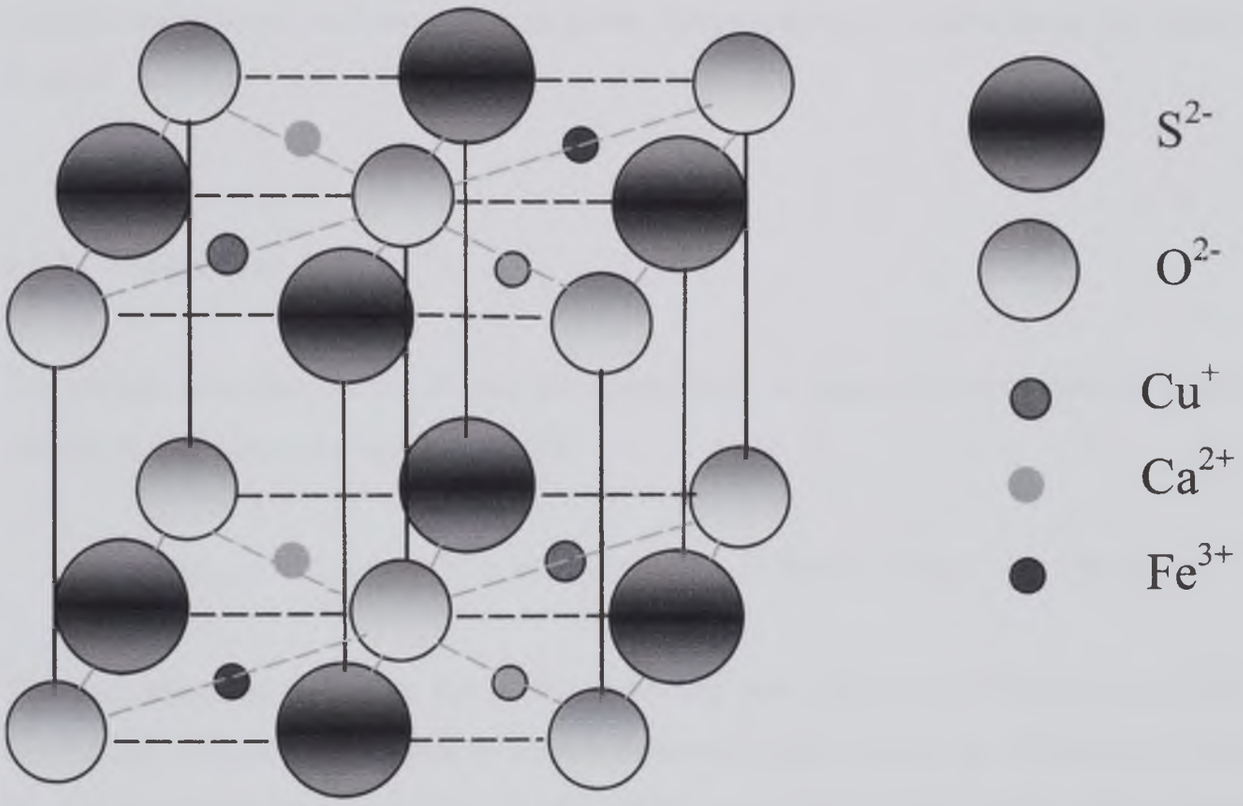

Figure 6.8 Proposed idealised structure for the quinary C_{111} oxysulphide compound.

6.4 Reduction of Chalcopyrite with Carbon in the Presence of Lime

Samples of 1:2:2 mixtures of natural chalcopyrite concentrate, lime and carbon were heat treated in the temperature range of 950°C to 1250°C in an inert flowing argon atmosphere. The weight loss for each experiment was measured and hence the percentage of reduction was determined. The value of measured weight loss as a percentage is given in table 6.6 for each sample with the calculated percentage of reduction. The phases formed were analysed by X-ray diffraction; the results are summarised in table 6.7. Selected reacted samples were observed under the scanning electron microscope and the electron probe microanalyser to characterise the phases formed.

6.4.1 Weight Loss Data

The weight loss that occurs during the experiment is due to the evolution of carbon monoxide gas according to equation 6.9.

$$CuFeS_{2(s)} + 2CaO_{(s)} + 2C_{(s)} = Cu_{(s)} + Fe_{(s)} + 2CaS_{(s)} + 2CO_{(g)} \qquad (6.9)$$

The percentage of reduction for each experiment was determined from the measured weight loss. Figure 6.9 is a graph of these determined percentages as a function of time plotted for values taken at 850°C, 900°C, 950°C and 1000°C. Evaluation of the degree of reduction for each temperature was determined from this figure. An increase in time and temperature gave an increase in reduction. This trend can be accepted for all the lines if the deviations seen on the graphs are ignored. For the lines of 850°C and 900°C the anomalies are relatively small and are put down to experimental error when the samples were weighed. However, the anomalies observed for the 950°C line are too large to put down to experimental error. On the outside of the crucible, after a reaction when excessive weight loss occurs, a discolouration was noticed which explains this loss in weight. During the reaction the matte creeps over the edge of the alumina crucible and falls to the bottom of the glassware, so discolouring the crucible and resulting in excessive weight loss. For the line of 1000°C the reaction conditions were

adapted by using smaller samples hence the results give a smoother line. This graph does not contain any data at temperatures above 1000°C because at this temperature the percentage of reduction exceeded 100% due to sample loss from the crucible.

Temperature (°C)	Time (mins)	% Weight Loss	% Reduction
850	5	7.21	41.11
850	30	7.37	42.05
850	60	8.76	50.00
850	90	9.70	55.33
850	120	14.07	80.23
900	5	7.24	41.35
900	30	9.23	53.12
900	60	14.81	84.57
900	90	12.97	73.97
900	120	16.81	95.96
950	5	9.25	52.80
950	30	15.92	90.83
950	60	25.23	144.02
950	90	19.64	112.02
950	120	25.20	145.45
950	180	20.22	115.57
1000	5	10.26	58.56
1000	30	17.89	102.11
1000	60	20.80	118.74
1000	90	21.13	120.61
1000	120	21.29	121.49
1050	60	24.01	137.04
1050	120	26.21	149.60
1100	60	27.01	151.52
1100	120	25.89	147.77
1100	180	26.83	153.14

Table 6.7 Summary of weight loss and percentage reduction data for samples of $CuFeS_2$:2CaO:2C.

It would appear from the graph of figure 6.9 that two obvious stages occur in the reduction. The initial step, witnessed between 0 and 5 minutes, is characterised by a relatively rapid rate of reduction. The lines then continue to rise but at a much lower rate of reduction from 5 until 120 minutes. From the shape of the 950°C line it is deduced that complete reduction was attained at this temperature by heat-treating the sample for 60 minutes. Below this time and temperature complete reduction was not achieved.

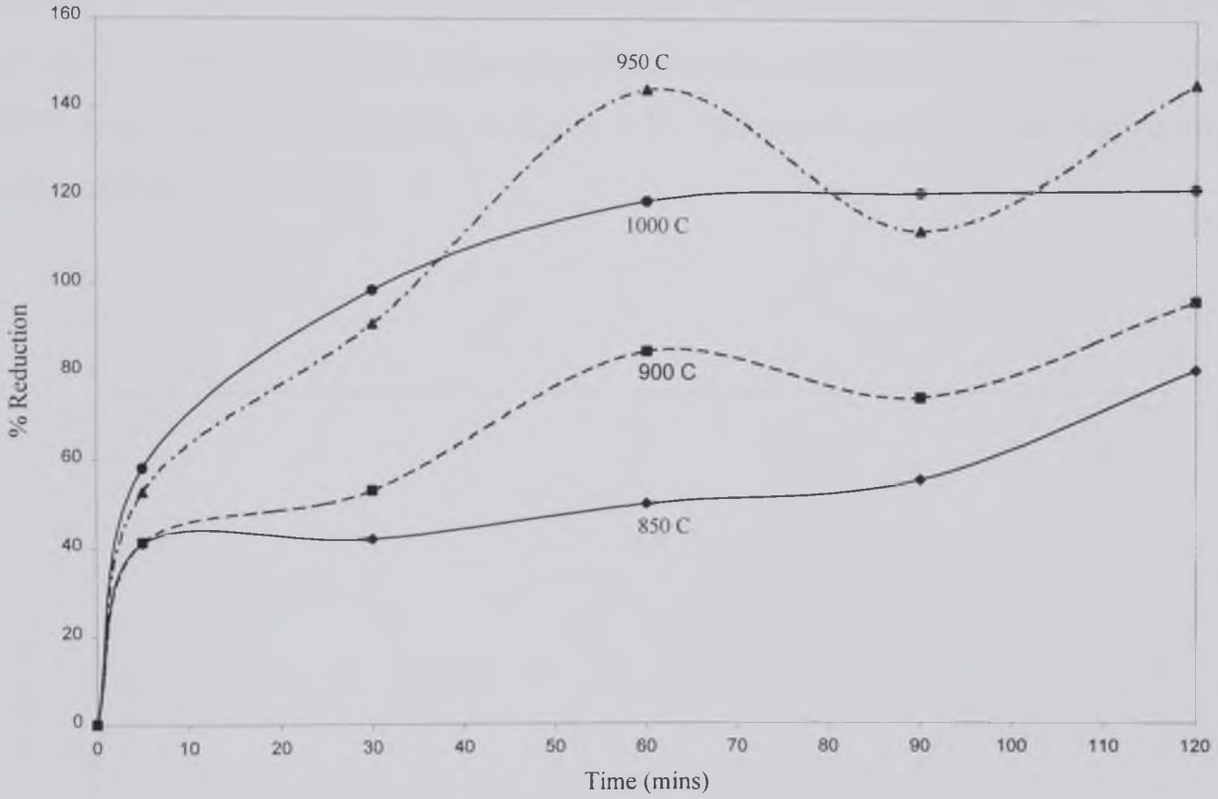

Figure 6.9 Percentage reduction as a function of temperature from data given in table 6.7 for samples of $CuFeS_2$:2CaO:2C heat treated in the muffle furnace.

6.4.2 TGA Weight Loss

The investigation into weight loss and hence the degree of reduction was continued by carrying out experiments in the T.G.A. furnace in a flowing argon atmosphere. The use

of this furnace allows for detailed analysis of the rate of reduction at different temperatures over a time period of 120 minutes. Weight loss readings were taken every five seconds, therefore a large amount of data was obtained for each experiment. This could not be tabulated but is instead presented graphically.

The initial experiment, carried out on the TGA furnace, was the reduction of chalcopyrite through a temperature range of 20°C to 1100°C. The results from this reaction allowed for the determination, experimentally, of the temperature range in which reduction occurs. Figure 6.10 is a graph of the percentage of reduction as a function of temperature. Small amounts of weight loss occurred at low temperatures, between 100°C and 400°C; this was due to slight disturbances in the laboratory and not reduction. A steady reduction began at around 600°C, continuing until 1050°C where 100% was achieved. According to figure 6.10, reduction occurs in the temperature region of 600°C to 1050°C.

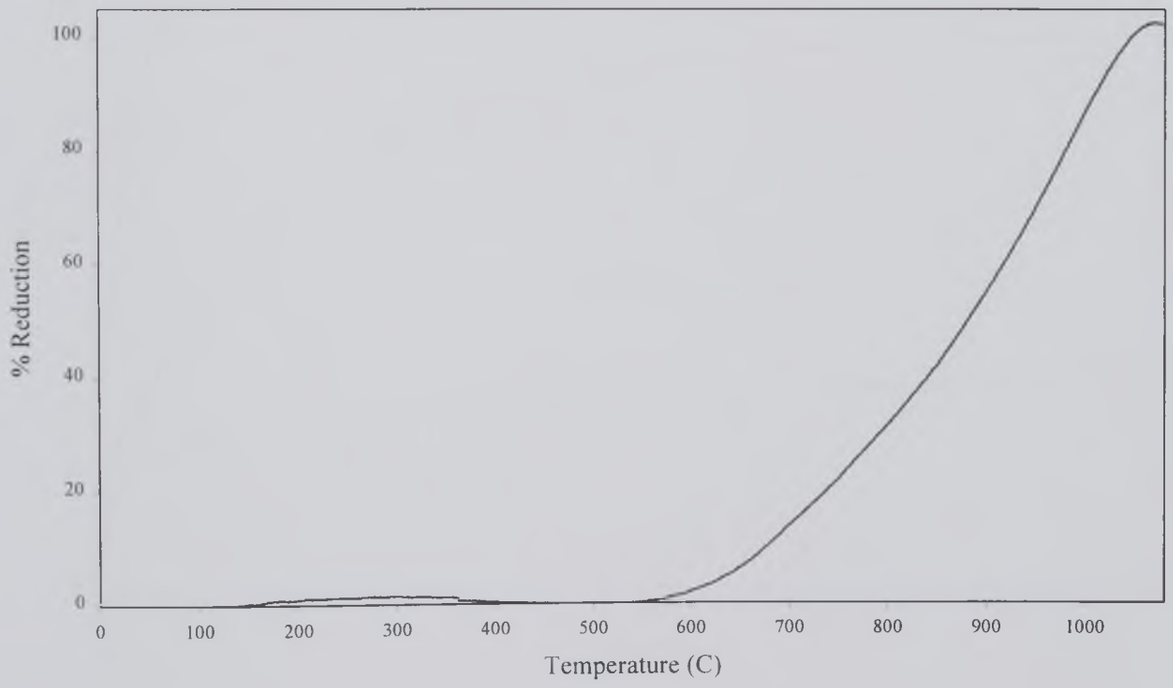

Figure 6.10 Rate of reduction of chalcopyrite with carbon from 20°C to 1100°C.

The weight loss experiments represented by figure 6.11 were carried out at temperatures in the range where reduction was achieved in figure 6.10; 900°C, 1000°C and 1100°C.

The weight losses for these experiments are expressed as a function of time. Each experiment was conducted at the selected isotherm for 120 minutes in an argon atmosphere.

There appear to be two distinct stages in the reduction process as indicated in figure 6.11, the initial step occurred during the first five minutes of reduction. During this period of reduction the rate was very rapid before slowing to a steadier rate. A low percentage of reduction resulted at 900°C that never rose above 40% throughout the duration of the experiment. Complete reduction was achieved at 1000°C after 100 minutes of reaction. At 1100°C the reduction rate was considerably improved, complete reduction being observed after just 10 minutes. The general trend observed from these reactions is that increased temperatures lead to an increase in reduction rates.

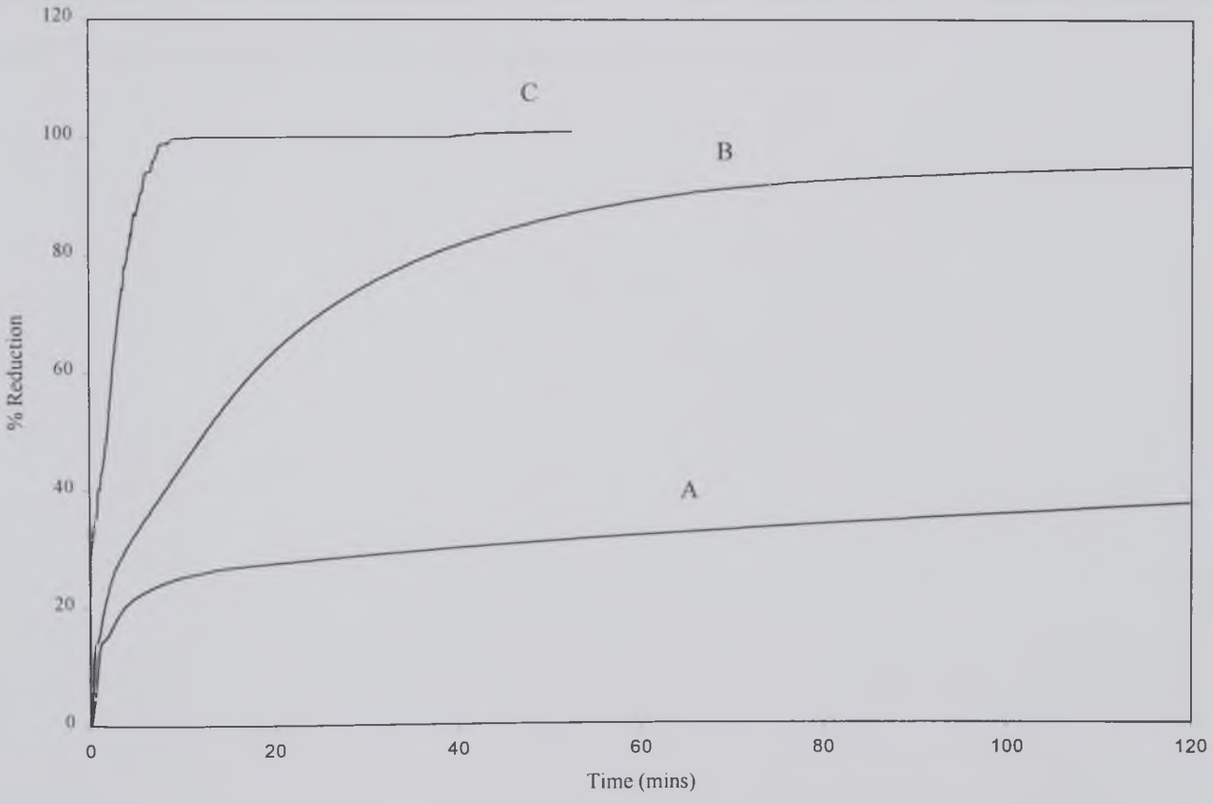

Figure 6.11 Percentage of reduction of chalcopyrite with carbon at, A-900°C, B-1000°C, C-1100°C.

The weight loss analyses carried out on the TGA furnace gave considerably more accurate results than those determined from individual readings taken from experiments carried out on the muffle furnace (Muf.). Figure 6.12 presents a comparison of the percentage reduction as a function of time for both sets of weight loss analyses. The difference between percentage reduction for individual and TGA experiments under the same nominal conditions is quite marked. However, the trends of the lines on the graph are similar.

Whilst analysis of samples from the TGA furnace appears to be the most reliable of the two, the information obtained from individual reactions in the muffle furnace is still valid. Both sets of experiments reveal that increased temperatures gave a higher rate of reduction until complete reduction was achieved. In addition, increased time also gave higher rates of reduction. According to results from the muffle furnace, complete reduction occurred at 950°C for 60 minutes, but that at 1000°C complete reduction was achieved in 30 minutes. Results from those samples from the TGA work indicated that 1100°C for 10 minutes was the optimum condition for reduction.

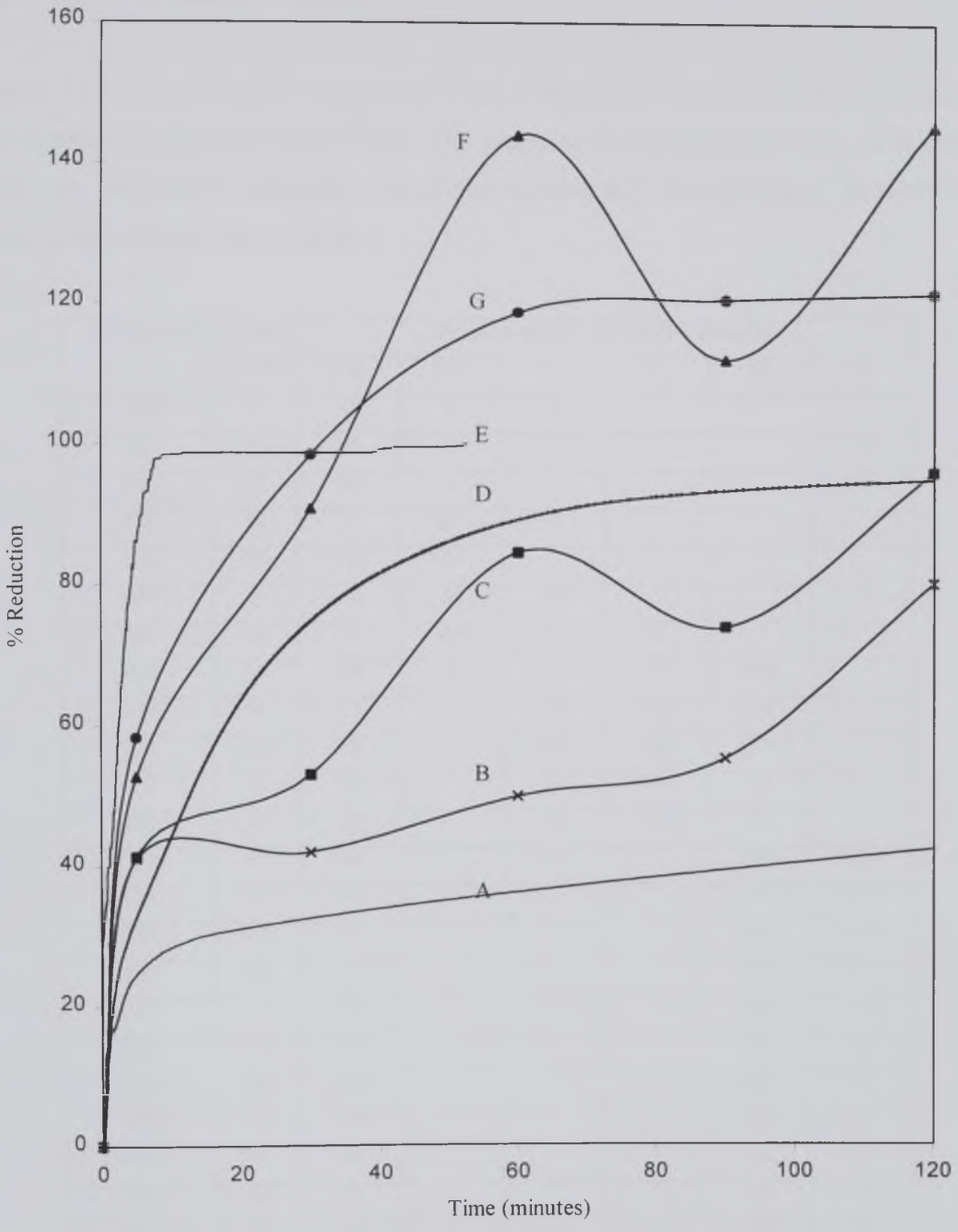

Figure 6.12 A comparison of the rate of reduction of chalcopyrite with carbon determined from individual (Muf.) measurements and continual TGA measurements: A-900°C (TGA.), B-850°C (Muf.), C-900C (Muf.), D-1000°C (TGA), E-1100°C (TGA), F-950°C (Muf.), G-1000°C (Muf.).

6.4.3 X-ray Diffraction Analysis

Figure 6.13 is a comparison of selected X-ray diffraction patterns from the reduction of chalcopyrite in the presence of lime. The phase analyses from the X-ray diffraction traces are presented in table 6.8. The phases in table 6.8 were identified from JCPDS files, which are given in appendix 1.

Temperature (°C)	Time (mins)	Phases Analysis with Relative Intensity					
		CaS	CaO	C_{111}	C_{11}	Cu	Fe
850	5	VS	S	W			
850	30	VS	S	S			
850	60	VS	S	S			
850	90	VS	MS	S			
850	120	VS	M	S			
900	5	VS	M	MS			
900	30	VS	WM	MS	W		
900	60	VS	W	M	W	MW	
900	90	VS		M	MW	MW	
900	120	VS		M	MW	MW	
950	5	VS		W	MW	M	
950	30	VS		W	MW	M	
950	60	VS		W		MS	WM
950	90	VS				MS	WM
950	120	VS				MS	WM
950	180	VS				MS	WM
1000	5	VS				MS	WM
1000	30	VS				MS	M
1000	60	VS				MS	M
1000	90	VS				MS	M
1000	120	VS				MS	M
1050	60	VS				MS	M
1050	120	VS				MS	M
1100	60	VS				MS	M
1100	120	VS				MS	M
1100	180	VS				MS	M

Table 6.8 Summary of phases identified from X-ray diffraction analysis of $CuFeS_2$:2CaO:2C (VS-very strong, S-strong, MS-medium strong, M-medium, WM-weak medium, W-weak).

X-ray analysis revealed that calcium sulphide was the predominant phase formed at all temperatures and for all time periods. This phase is also produced as a result of the exchange reaction discussed previously. Calcium oxide was observed at the lowest temperature, 850°C, indicating that the experiments did not reach completion at this temperature. This was in agreement with the conclusions drawn from the weight loss analysis. At 900°C CaO was also observed for reactions of 5, 30 and 60 minutes in length and at this temperature only 40% reduction was achieved after 120 minutes. When temperatures were raised above 900°C all of the calcium oxide reacted to form either calcium sulphide or the intermediary phases.

At 850°C the intermediary compound, C_{111}, was detected which was seen at both this temperature and at 900°C for any time duration. At 950°C the compound was observed for reactions of 5, 30, and 60 minutes in length but was not apparent after reactions of longer time periods or after reactions at higher temperatures. The C_{11} oxysulphide phase was observed at 900°C and at 950°C. This phase was produced when copper was present but was not apparent when metallic iron was present.

The formation of metallic copper was first observed at 900°C after 60 minutes and was detected in all samples of reduced chalcopyrite that were reacted for longer time periods at this temperature. It was also detected in all samples that were reacted at temperatures higher than 900°C regardless of the duration of those reactions. Metallic iron was first observed at 950°C for a reaction time of 60 minutes and was also identified after reactions at all higher temperatures regardless of the time of reaction.

The X-ray diffraction patterns of figure 6.13D and 6.13E are of $CuFeS_2$ reduced at 1000°C and 1100°C respectively for 60 minutes. Three phases were identified as being present in both patterns; Cu, Fe and CaS. None of the oxysulpides are observed. Complete reduction appears to have occurred at these temperatures. At 1000°C after a reaction of 60 minutes, the weight loss data revealed 90% reduction had occurred. The lack of oxysulphide phase was due to the relative intensities of these phases being too low to be detected by X-ray analysis. At 1100°C after a reaction of 60 minutes, complete reduction was achieved. The fact that a complete reduction had taken place explains the lack of any oxysulphide phase.

In figure 6.14 a comparison is made between chalcopyrite heat-treated with lime and chalcopyrite reduced with carbon in the presence of lime. Both samples were heat treated for 60 minutes at 1000°C. This comparison indicated the difference in phases produced when carbon was added. The X-ray phase analysis is less complicated when carbon was added due to the absence of oxysulphide phases. In the reduced sample only three phases were identified, CaS, Cu and Fe. These were the expected products from the reduction reaction.

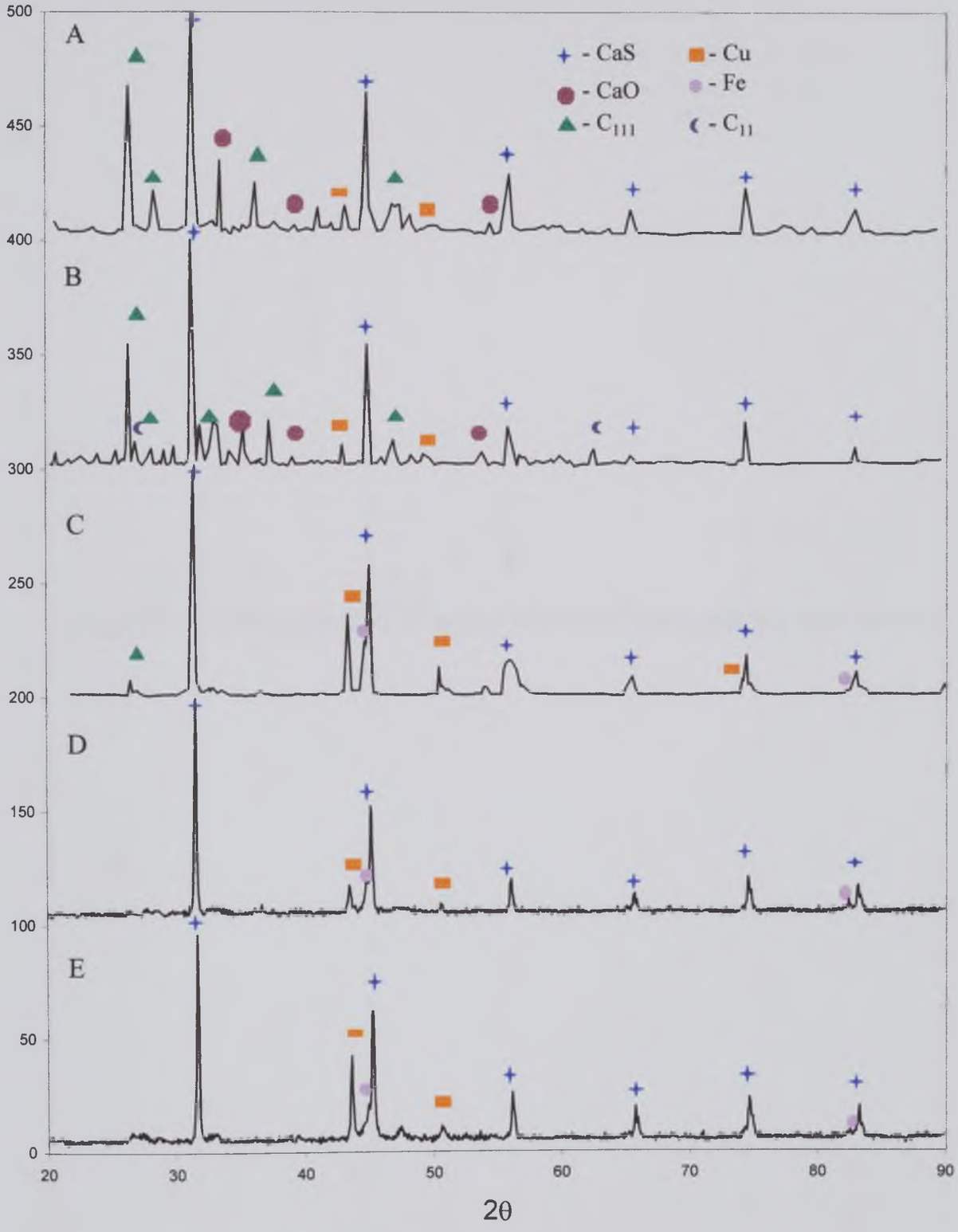

Figure 6.13 Comparison of selected X-ray diffraction patterns for $CuFeS_2$:2CaO:2C heat treated for 60 minutes: A-850°C, B-900°C, C-950°C, D-1000°C, E-1100°C.

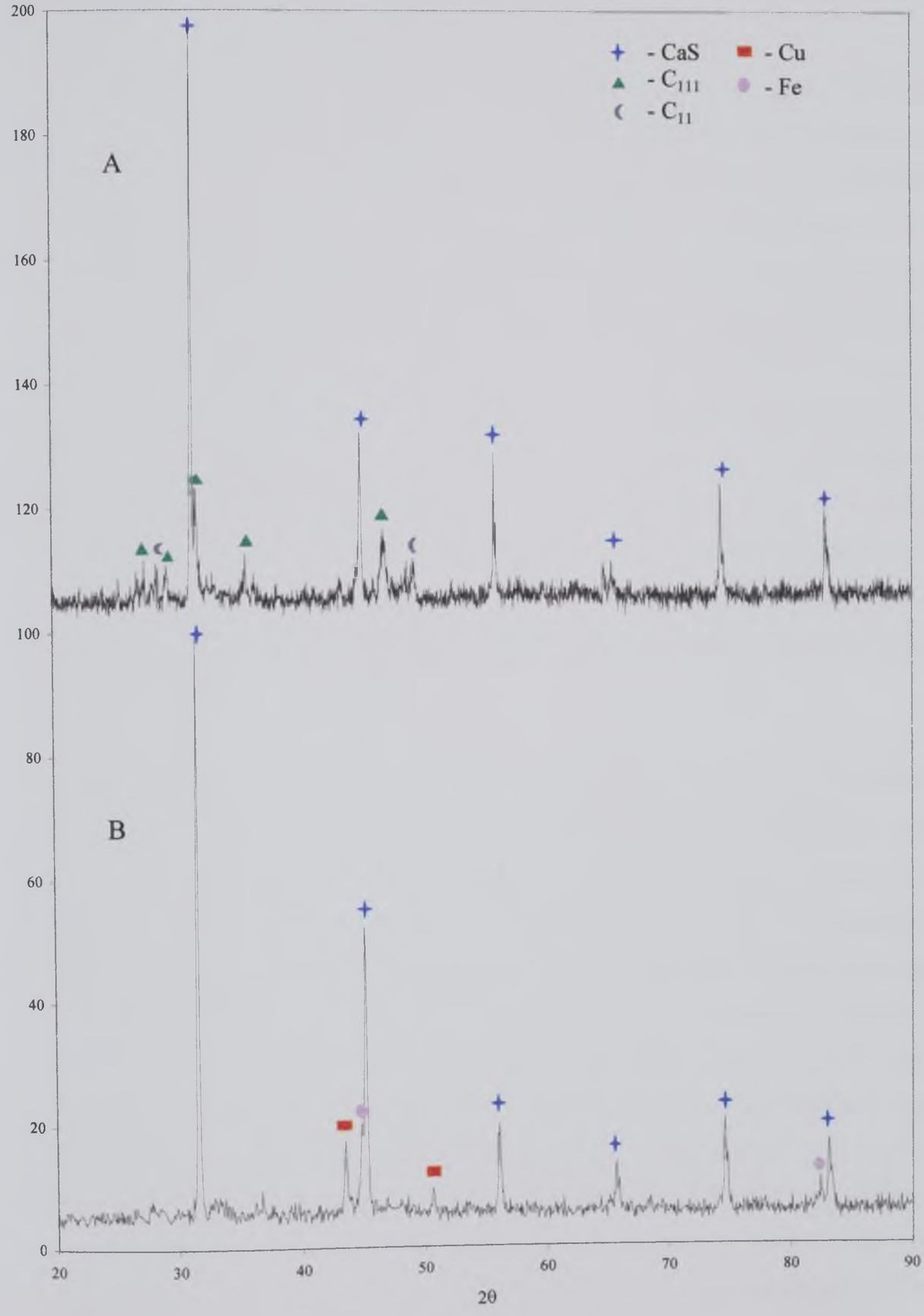

Figure 6.14 Comparison of phases produced from heat treatment of chalcopyrite with lime at 1000°C/60 minutes: A-without carbon and B-with carbon.

6.4.4 Electron Microscopy

Samples of reduced chalcopyrite were examined under the electron microscope using secondary electron imaging (SEI) and back scattered electron (BSE) imaging with energy dispersive X-ray analysis (EDX). As determined from the X-ray diffraction analysis, metallic copper and iron are products of the reduction reaction. Figure 6.15 is a BSE image of the distribution of metallic particles in the calcium sulphide-rich phase for chalcopyrite reduced at 950°C for 60 minutes. This figure depicts the typical phase distribution through the sample at this temperature. The lightest phase in the image is metallic copper, the next lightest being metallic iron. In some areas the magnification and contrast are such that there is no differentiation between the copper and iron therefore the brightest phase is actually copper and iron not just copper. The medium grey phase is calcium sulphide and was seen in high quantities through the samples. The other darker grey areas are combinations of intermediary phases and silica phases that occurred as a result of the chalcopyrite being a natural mineral sample with a silica content of 7.44 wt.%.

Figure 6.16 depicts, at a higher magnification, specifically the formation of the metallic copper and iron phases at 950°C with a clearer contrast. It was noticed that the copper and iron form together as separate metallic species with no miscibility. Figures, 6.16a and 6.16b are the corresponding elemental dot maps of copper and iron respectively for figure 6.16. Metallic copper and iron are found together throughout the reacted samples and this figure is typical of this characteristic. Figure 6.17 is another example of metallic copper/ iron formation isolated from the other phases. Figure 6.18 is a higher magnification of this area showing quite clearly the two separate metals. Metallic iron is nearly always found surrounded by the metallic copper as seen in figure 6.18, where the brightest phase is copper and the darker region iron. The size of metallic species formed varies through the samples observed for chalcopyrite reduced at 950°C. The larger metallic regions, usually isolated from CaS, are approximately 60-100μm across whilst the smaller regions usually appearing with CaS are 5-20 μm across.

Figure 6.19 is a typical secondary electron image (SEI) of the chalcopyrite reduced at 950°C for 60 minutes. Fewer images were taken by secondary electron imaging as most

samples were polished for BSE imaging. However the image of figure 6.20 does show the typical microstructure observed in reduced chalcopyrite. A micrograph (fig. 6.3) of a sample of chalcopyrite heat treated with lime, was taken to show the formation of the quinary oxysulphide compound C_{111}. This compound was observed in relation to calcium sulphide and without any metal formation. Figure 6.20 is a SEI image obtained from a sample of $CuFeS_2$ reduced at 900°C for 60 minutes. Figure 6.21 is of the same area but at a higher magnification. These images depict the formation of metallic copper from the C_{111} compound. The small protrusions were identified as copper by EDX. The phase, labelled as A, in figure 6.21, from which copper is formed, is identified as containing copper, iron, calcium and sulphur thus indicating the presence of C_{111}. The region labelled B is that of calcium sulphide.

Silica is a naturally occurring component of the chalcopyrite mineral concentrate and is observed throughout all of the reacted samples. Figure 6.22 is such an area found within chalcopyrite reduced at 950°C for 60 minutes. The central darkest phase is the silica and is surrounded by a lighter phase; this is typical of most of the silica contained within the sample. The phase surrounding the silica is calcium rich and appears to form as a result of the calcium from calcium oxide attacking the silica during reduction. Therefore the silica in the centre is the remainder of the silica, found naturally in chalcopyrite, not yet affected by the presence of the calcium. In some areas where the silica occurs metallic copper is found in small quantities embedded within the surrounding calcium-rich phase. This inclusion of copper is seen in figure 6.22 where the brightest phase is copper. Metallic iron is also found in the silica but only when in the presence of copper, never on its own. However metallic copper is found on its own in this calcium rich phase.

Another structure appeared different to those already mentioned and is shown in figure 6.23 surrounded by the typical microstructure of metallic copper and CaS phases observed in the reduced samples. Figure 6.24 is an image of this area at a higher magnification. The phases already seen in figures 6.15 to 6.22 form a layered structure. The layers are found to be the metallic species bound between calcium sulphide and regions of the silica/ calcium rich phases.

Reduced chalcopyrite was examined under the electron probe microanalyser (EPMA). Figure 6.25 is a back scattered electron image of $CuFeS_2$ reduced at 950°C for 60 minutes. The brightest phases are identified as metallic regions. Figure 6.26 is an elemental map for iron showing these metallic regions clearly. The bright orange areas of figure 6.25 are CaS regions with the darker orange areas being the calcium-rich phases surrounding the silica. Figure 6.27 is an elemental map for calcium, the highest intensity of which is for calcium sulphide.

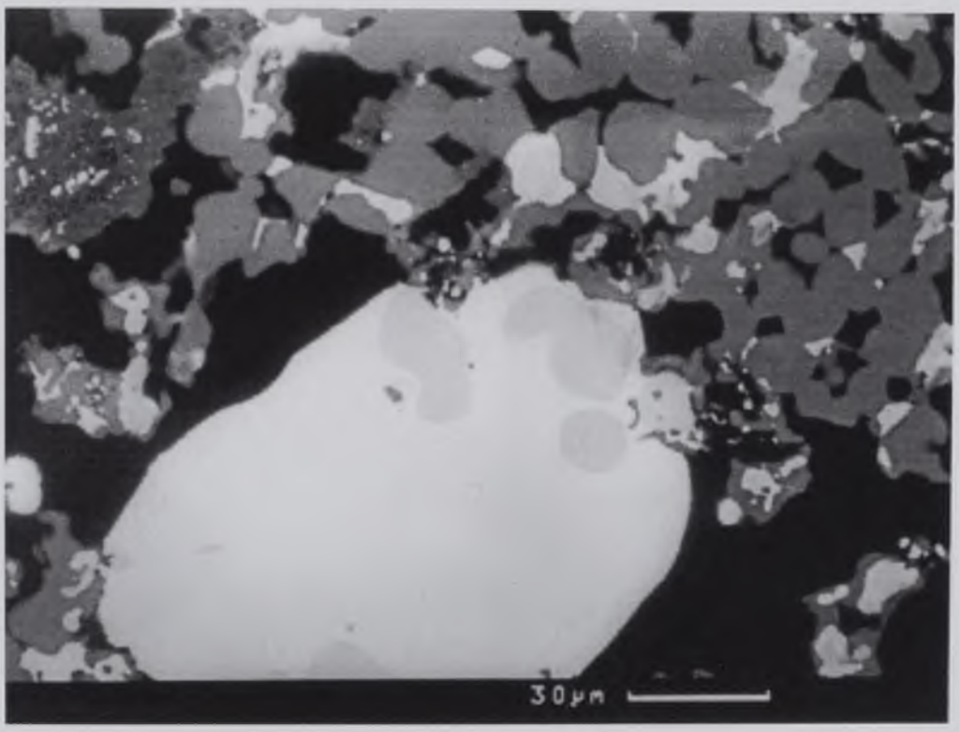

Figure 6.15 BSE image of the general microstructure observed from the reaction of $CuFeS_2$:2CaO:2C at 950°C for 60 minutes, the lighter region is metallic copper and iron surrounded by CaS and silica phases.

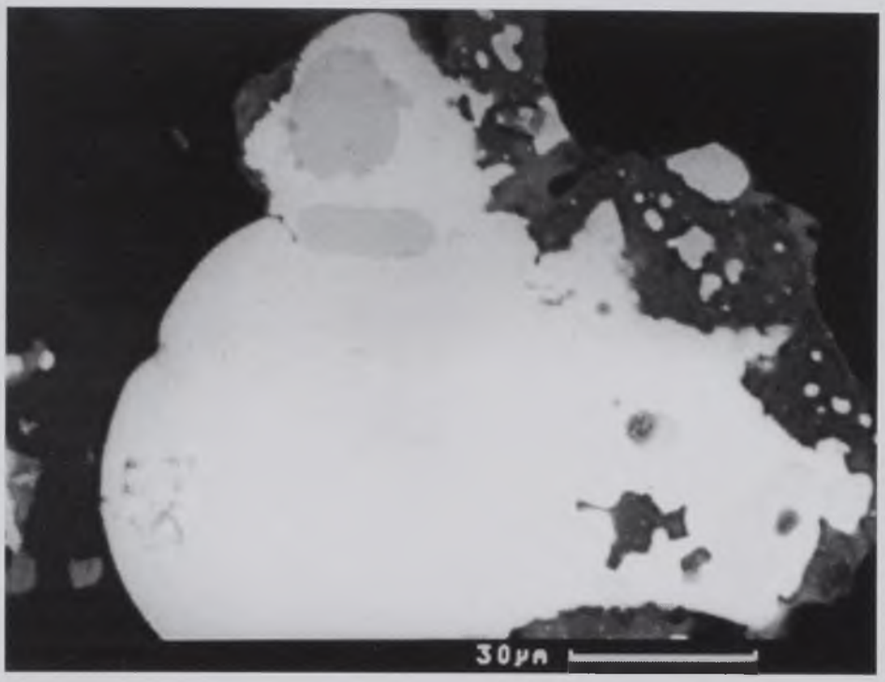

Figure 6.16 BSE image of the metallic microstructure of iron surrounded by copper from chalcopyrite reduced at 950°C for 60 minutes with a) and b) copper and iron elemental dot maps respectively.

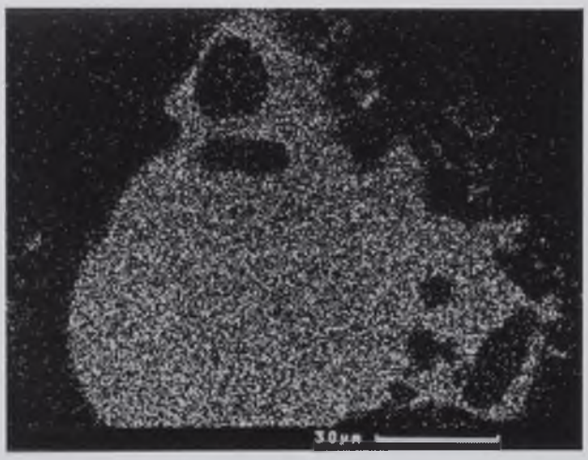

(a)

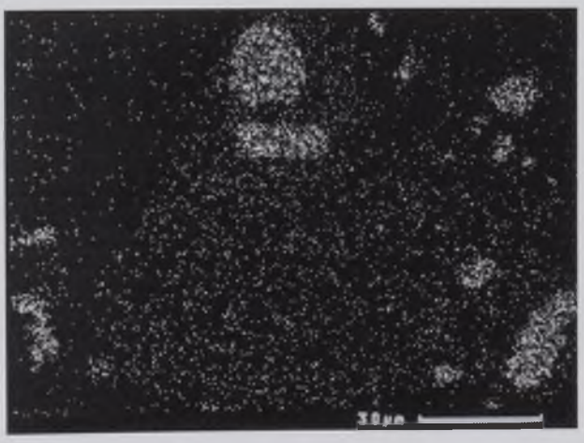

(b)

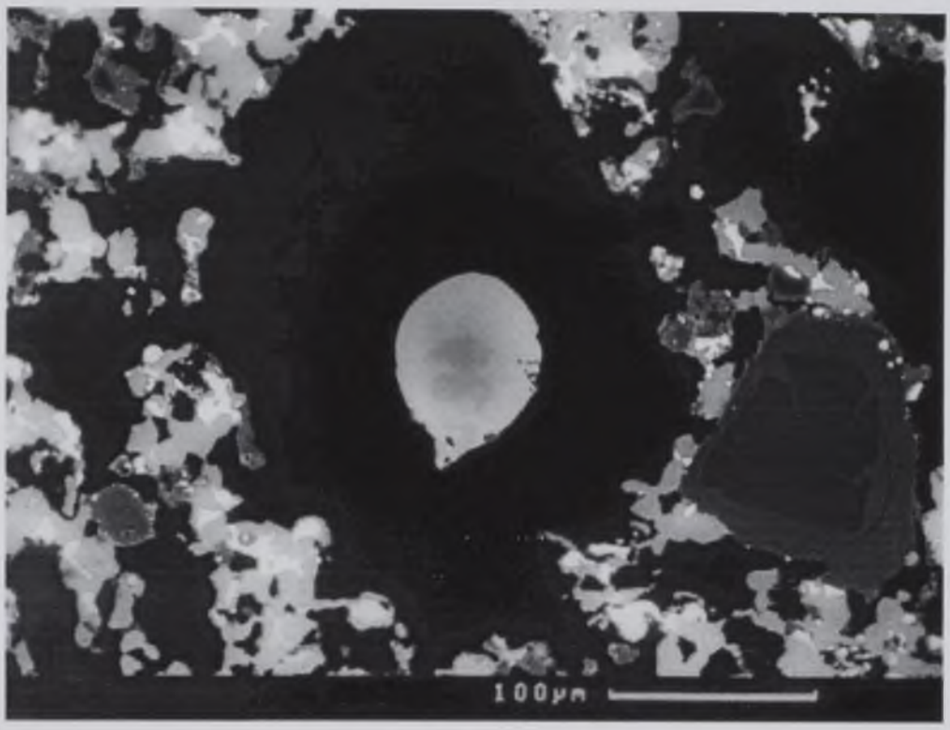

Figure 6.17 BSE image of the isolated production of metallic copper and iron from the reduction of chalcopyrite with carbon at 950°C for 60 minutes surrounded by CaS, silica and metallic phases.

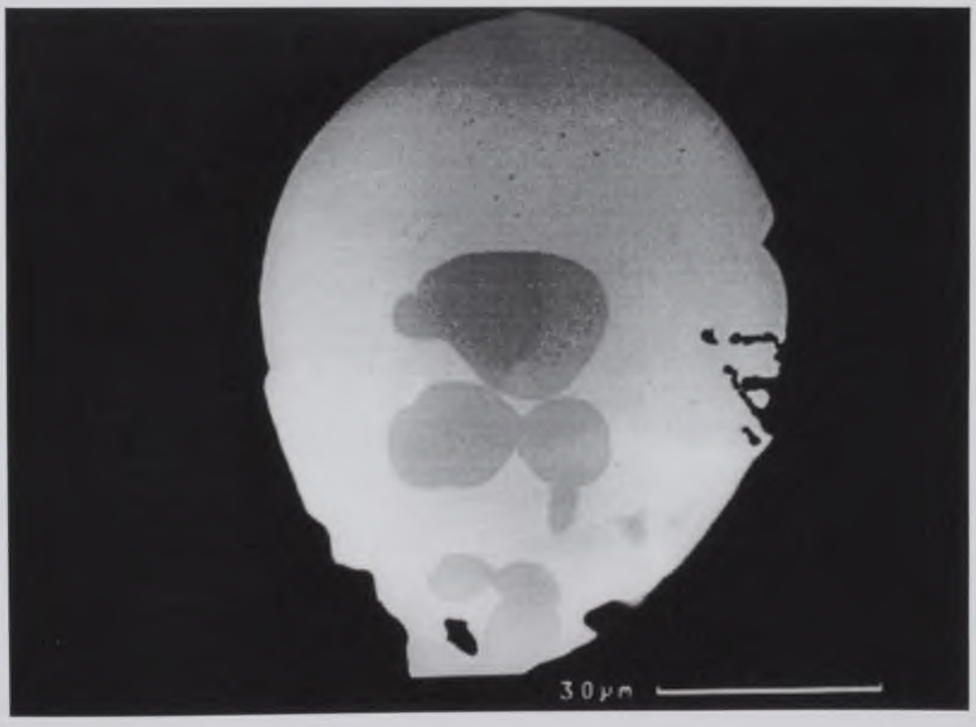

Figure 6.18 BSE image of the metallic phase observed in figure 6.17 at a higher magnification of iron surrounded by copper.

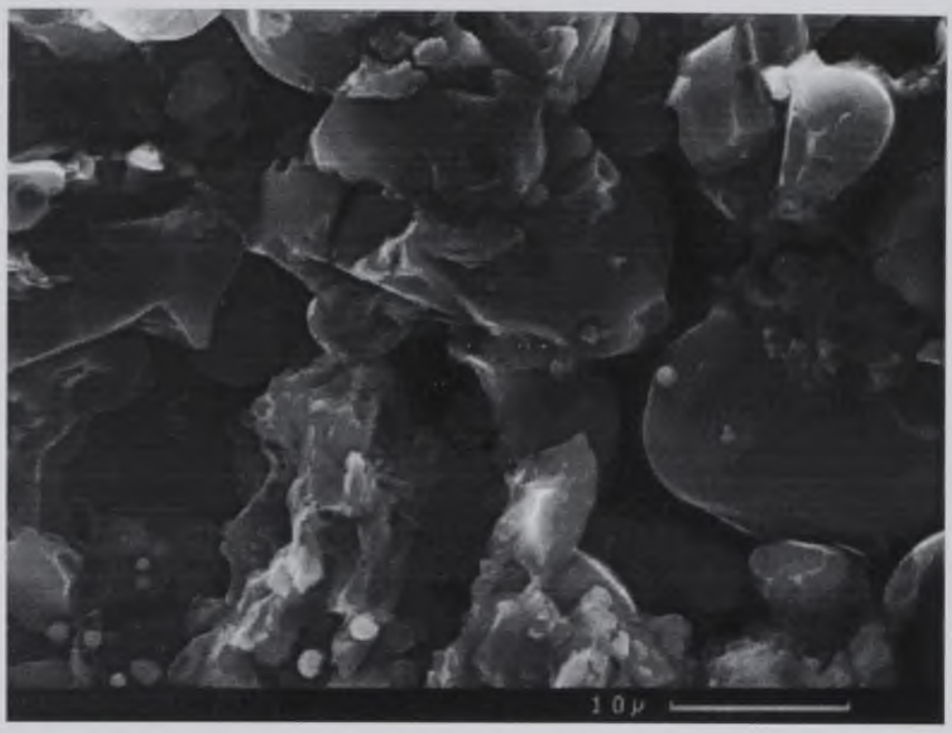

Figure 6.19 SEI of the reduction of chalcopyrite with carbon 950°C for 60 minutes.

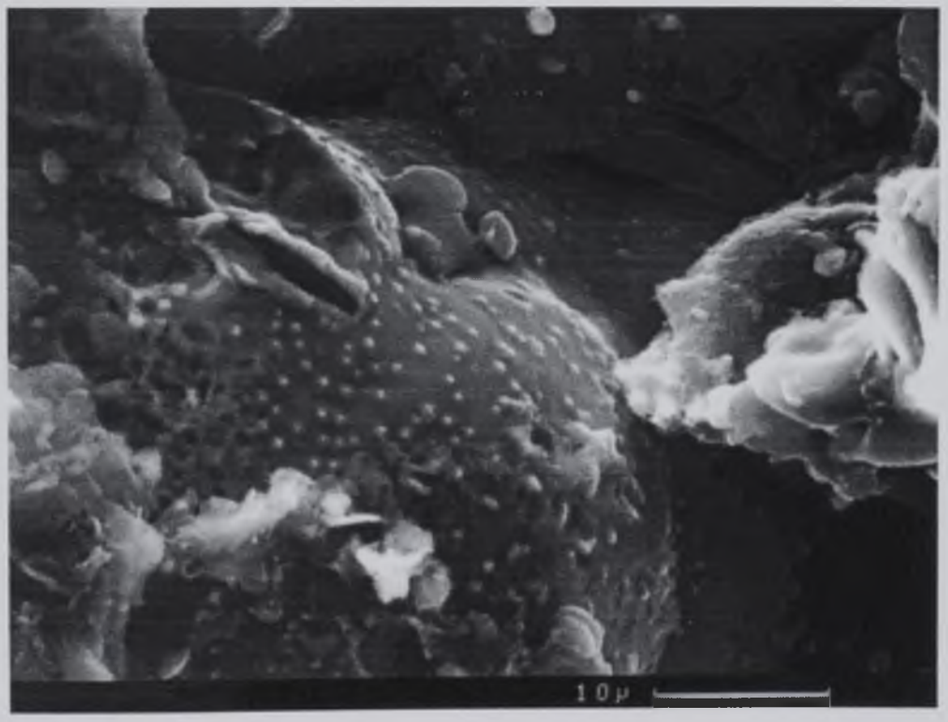

Figure 6.20 SEI of the reduction of chalcopyrite with carbon at 900°C for 60 minutes.

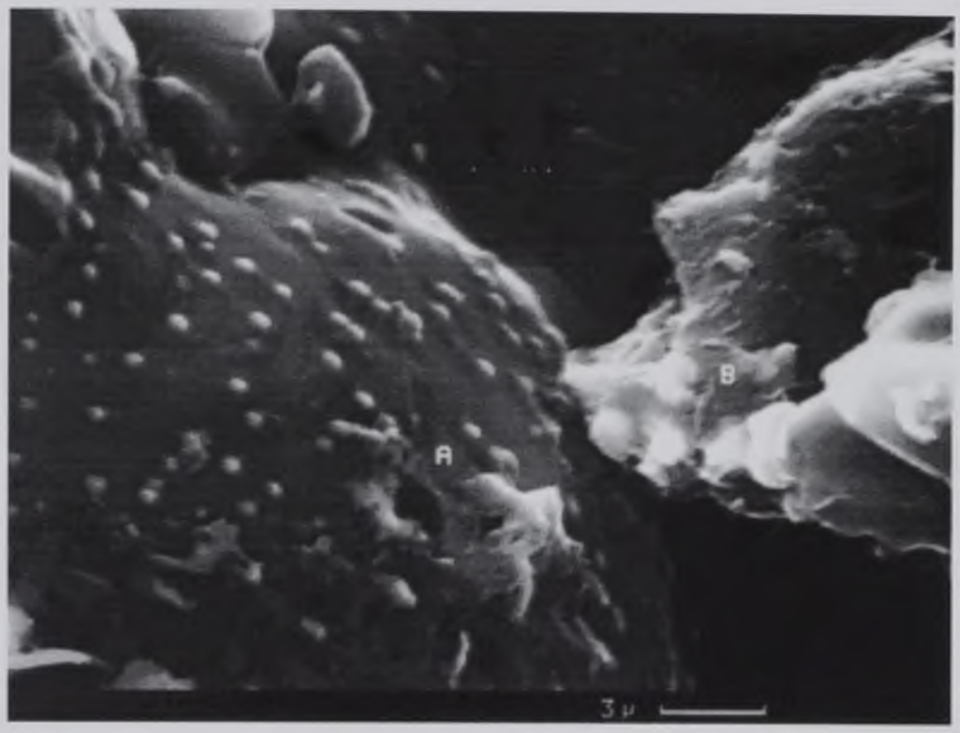

Figure 6.21 SEI of the region observed in figure 6.20 at a higher magnification), A – C_{111} oxysulphide phase and B – CaS.

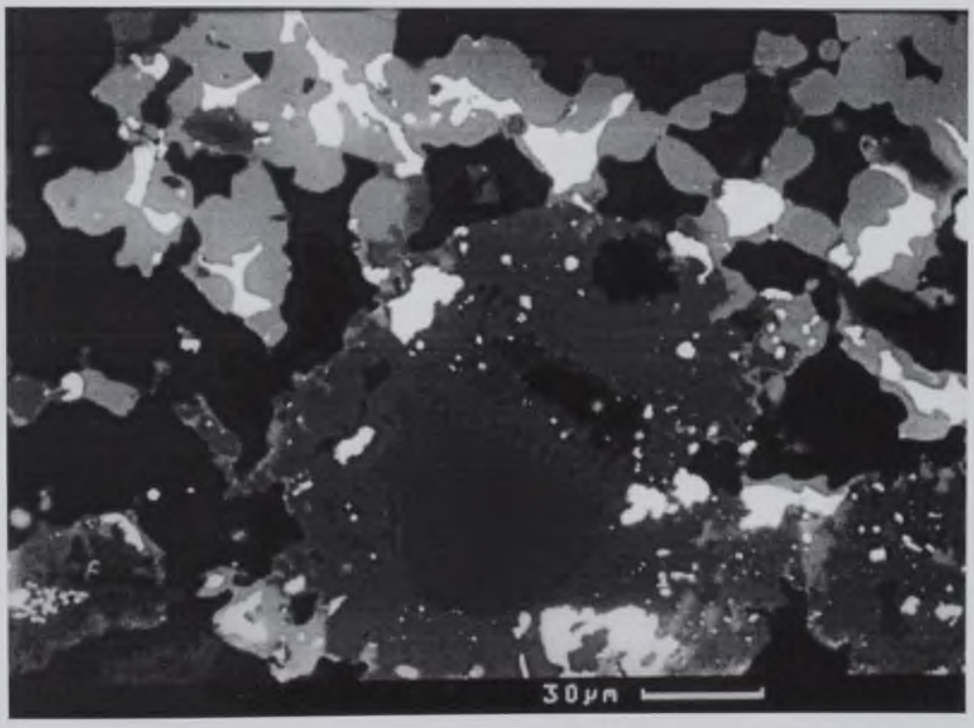

Figure 6.22 BSE image of the microstructure of silica phases observed from chalcopyrite reduced at 950°C for 60 minutes.

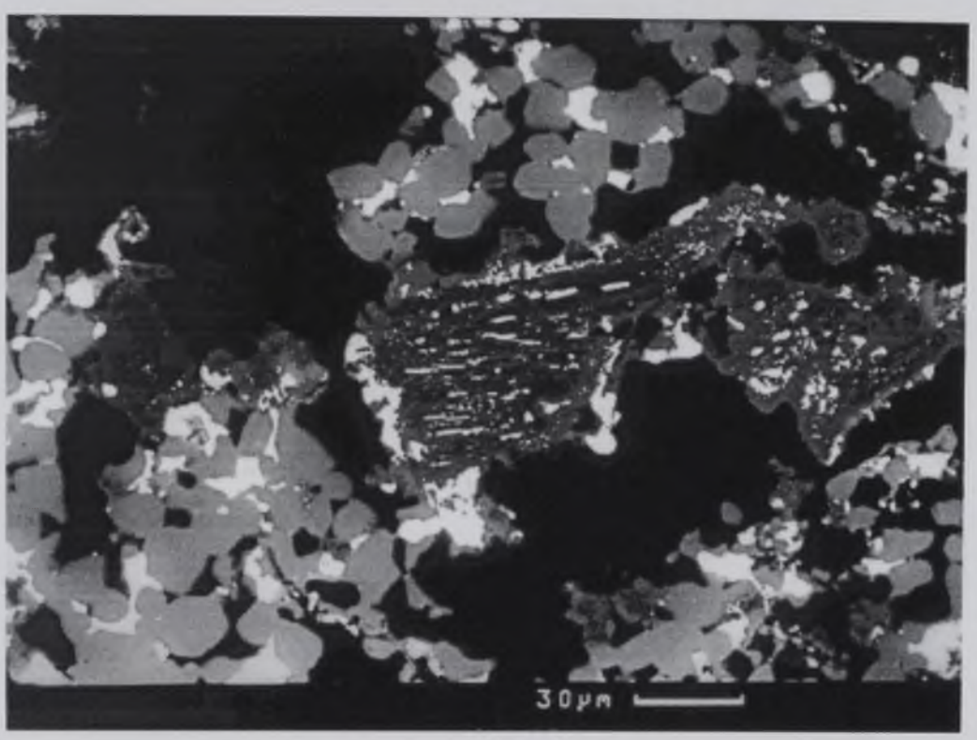

Figure 6.23 BSE image of chalcopyrite reduced at 950°C for 60 minutes illustrating silica, metallic and CaS phases.

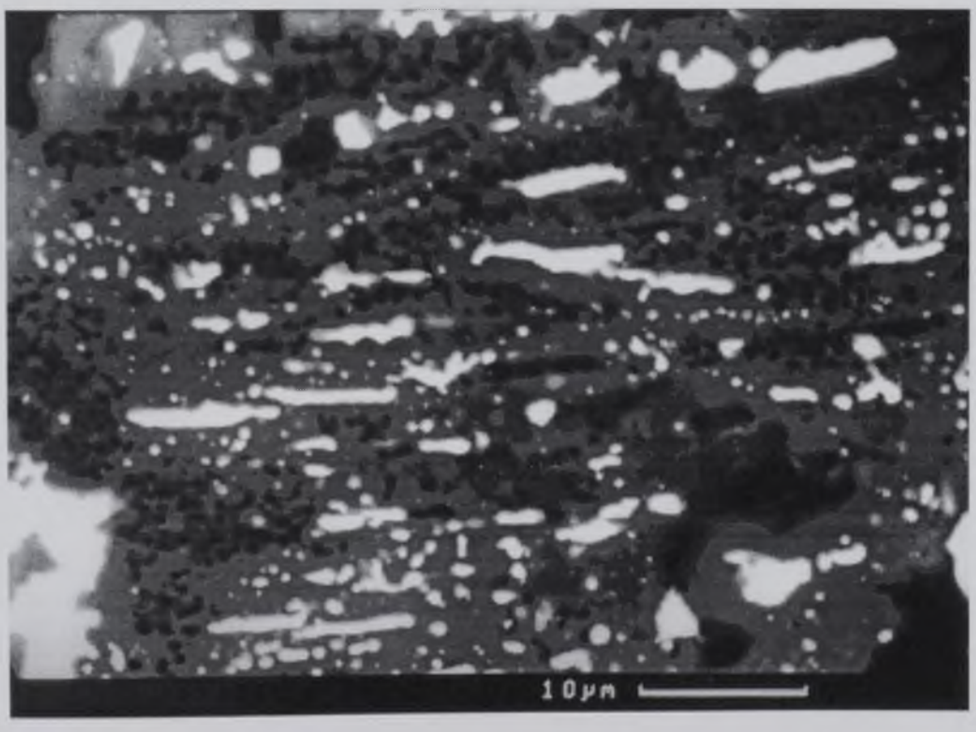

Figure 6.24 BSE image of figure 6.23 at a higher magnification.

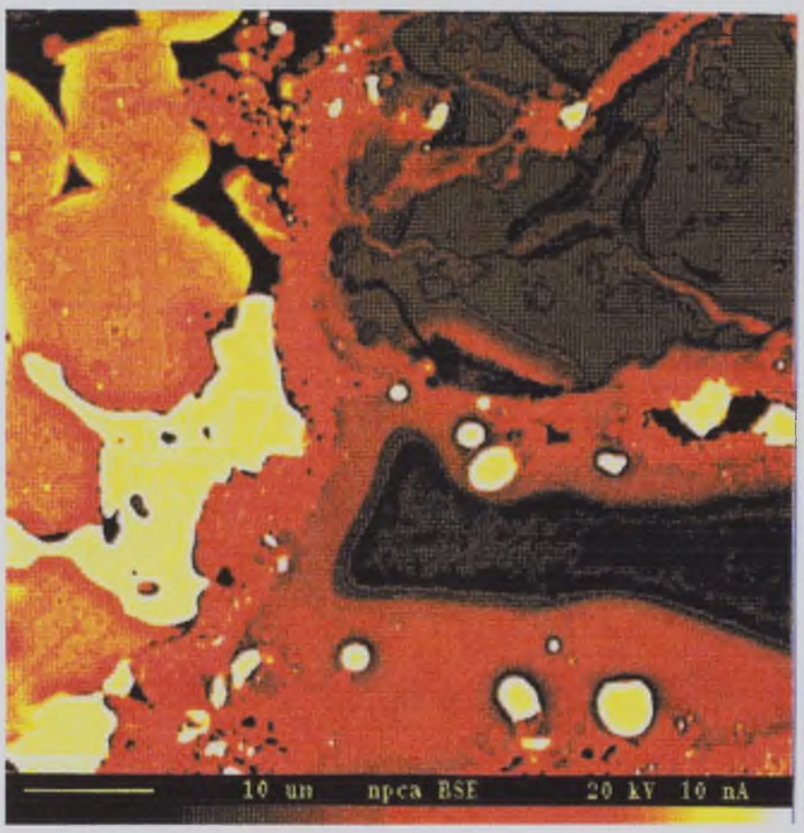

Figure 6.25 EPMA back scattered electron image of the reduction of chalcopyrite with carbon at 950°C for 60 minutes.

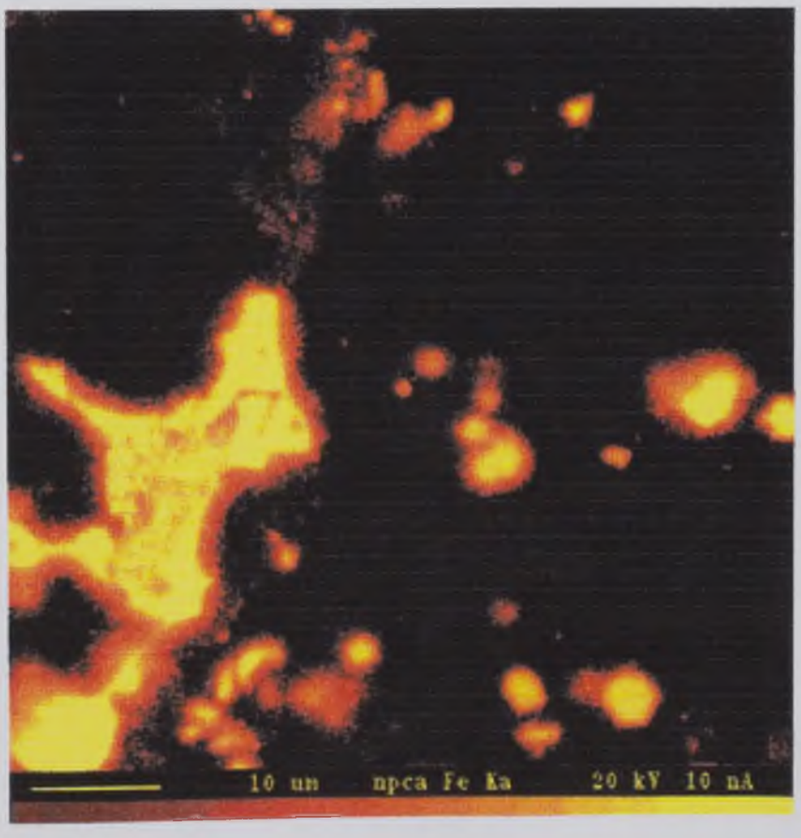

Figure 6.26 Iron elemental dot map for the BSE image in figure 6.25.

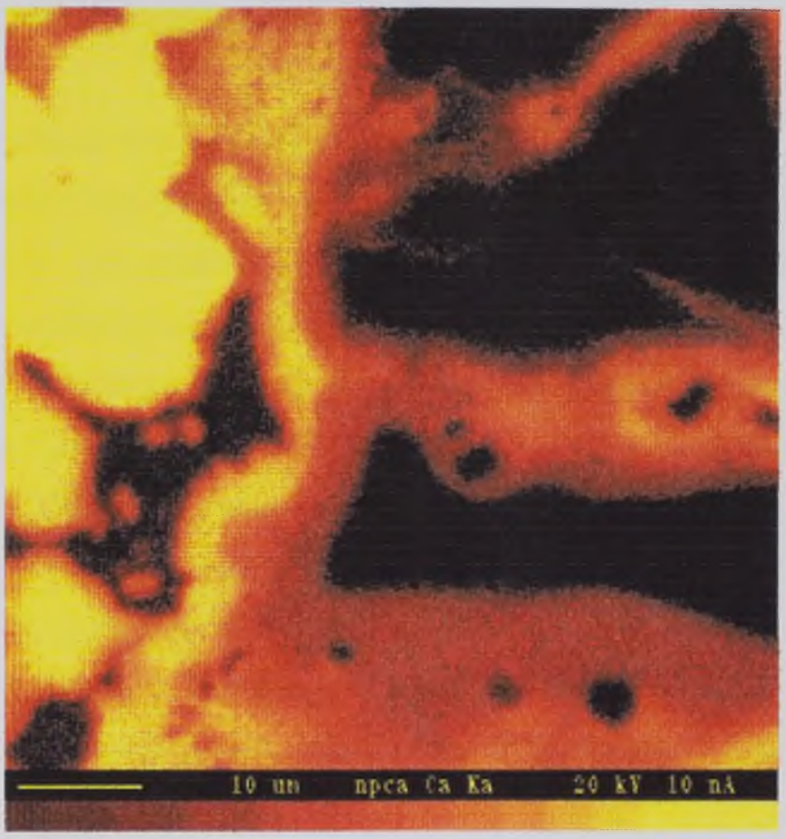

Figure 6.27 Calcium elemental dot map for the BSE image in figure 6.25.

6.5 Reduction of Chalcopyrite with Activated Carbon in the Presence of Lime

A series of experiments were carried out to study the effect of activated carbon on the reducibility of natural chalcopyrite in the presence of lime. Activated carbon has a higher surface area than graphite carbon, which means that the surface area for the overall reduction reaction is greater, leading to a higher rate of completion of reaction 6.3. The reaction conditions for each experiment are given in table 6.9. The general appearance of the reacted samples to those from the reduction of chalcopyrite with non-activated carbon differed. The samples of chalcopyrite reduced with carbon, after heat treatment, had turned from a light grey powder mixture to a dark grey sintered mass. The samples after reduction with activated carbon were well sintered but with a different colour appearance. The samples changed from a red colouration at the top to grey, lighter grey and finally brown at the bottom of the sample.

6.5.1 Weight Loss Results

For each experiment the weight loss was measured. The degree of reduction was thus determined as a percentage of theoretical reduction. The values obtained are given in table 6.9. Fewer experiments were carried out with activated carbon than with carbon. This set of experiments was designed to give a comparison of the effect the two sources of carbon made on the rate of reduction.

Temperature (°C)	Time (mins)	% Weight Loss	% Reduction
850	60	12.32	70.42
900	60	18.65	106.60
950	60	22.62	129.11
1000	60	26.90	153.54
1050	60	26.95	153.82
1100	60	24.31	138.76
1100	180	27.9	159.24
1100 (50g)	180	27.9	159.24

Table 6.9 Weight loss and percentage reduction data for samples of $CuFeS_2$: 2CaO: 2C (activated).

A series of values for the percentage of reduction was attained for a temperature range of 850°C to 1100°C with intervals of 50°C. Figure 6.28 is a graph plotted from this data and used as a comparison to a similar series of data determined from reduction with non-activated carbon.

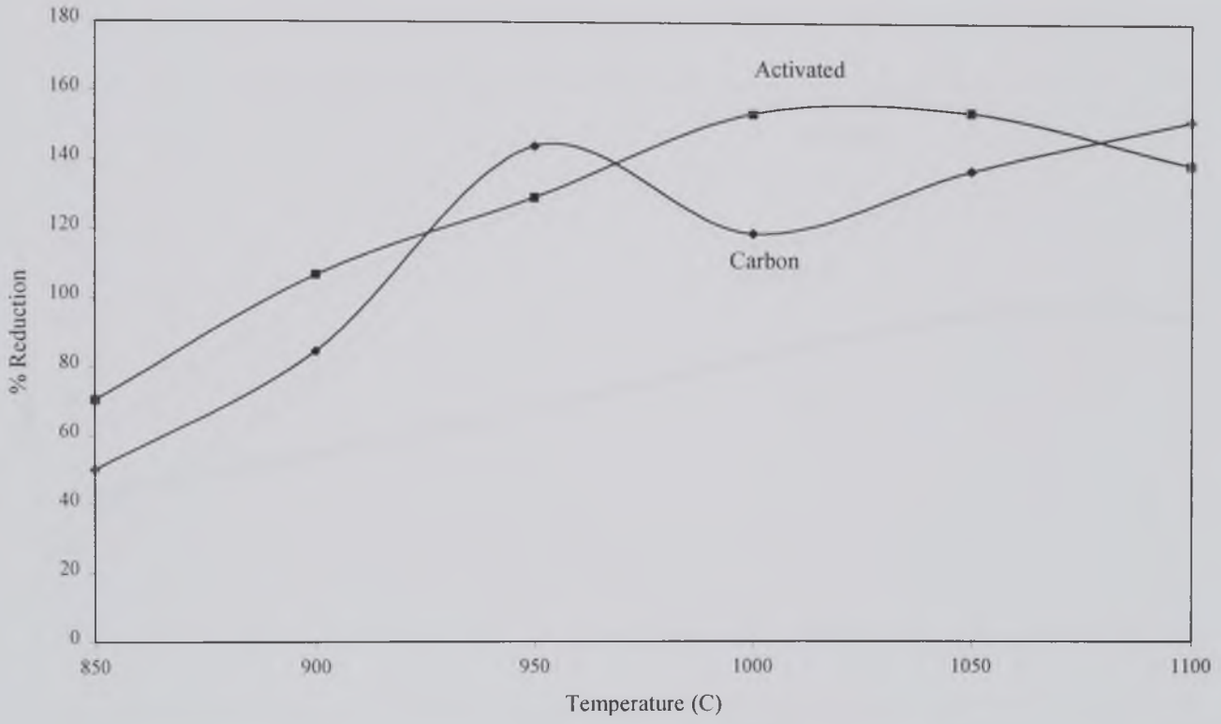

Figure 6.28 A graph to show the comparison of rates of reduction of chalcopyrite with carbon (non-activated) and activated carbon from 850°C to 1100°C.

The general trend observed from this graph was that with an increase in temperature an increase in the percentage of reduction occurred. All the values used for this graph were from samples heat treated for 60 minutes to give comparability for each temperature. The line plotted for non-activated carbon reduction is not a smooth line due one point being out. As discussed previously this anomalous point was as a result of the weight loss being due to excess material loss out of the crucible as well as of carbon monoxide evolution. However the trend of the line is still evident and it can be seen that the use of activated carbon increases the degree of reduction across this temperature range.

Figure 6.29 compares data for the percentage of reduction as a function of temperature for data obtained from weight loss measurements of individual experiments carried out on the muffle furnace and continual readings from the TGA analysis. For the relevant temperature range the rate of reduction is lower for reduction in the TGA furnace. However, the shape and therefore trend of the lines for these sets of data compare agreeably well.

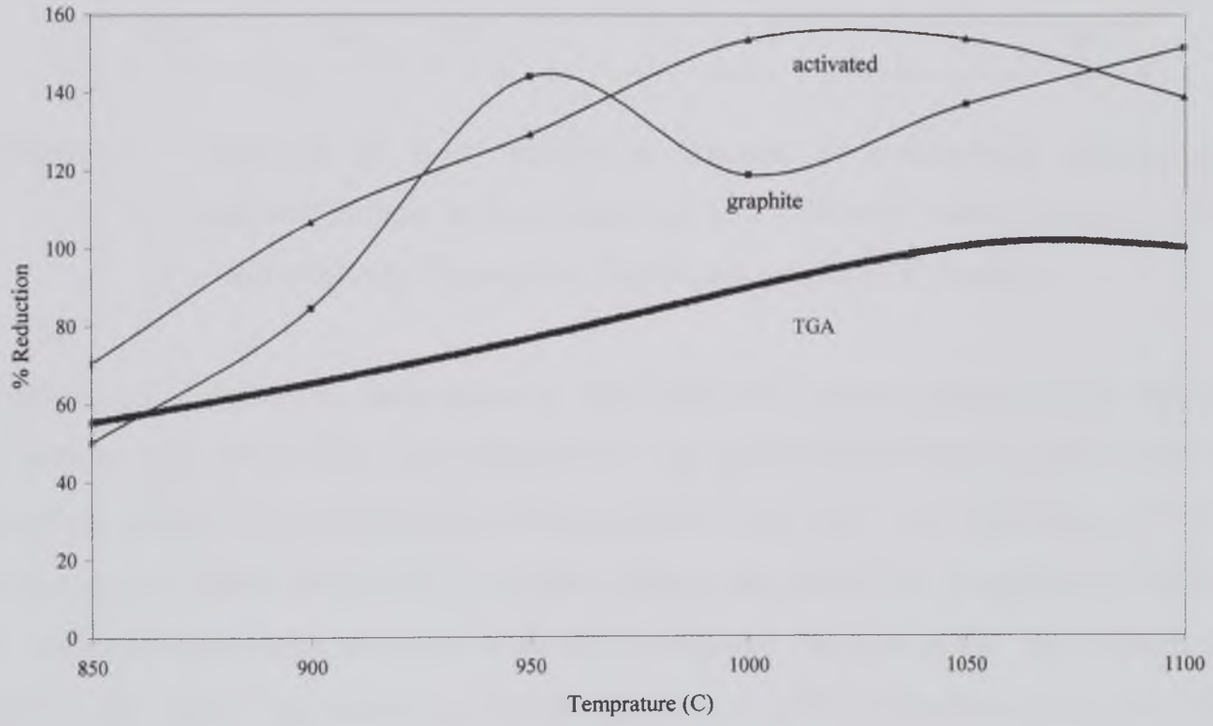

Figure 6.29 Comparison of weight loss data gained from individual experiments and data from the TGA furnace.

6.5.2 X-ray Analysis

The phases formed as a result of reduction by activated carbon are summarised in table 6.10. These phases are identified from the JCPDS files given in appendix 1. Similar phases were observed in X-ray diffraction patterns obtained from samples of chalcopyrite reduced with activated carbon as were observed from samples reduced by carbon. Figure 6.30 is a comparison of X-ray powder diffraction patterns for chalcopyrite reduced by activated carbon at 900, 1000 and 1100°C

Temperature (°C)	Time (mins)	Phases Identified with Relative Intensity					
		CaS	CaO	C_{III}	C_{II}	Cu	Fe
850	60	VS		WM	W		
900	60	VS		W		M	WM
950	60	VS				M	M
1000	60	VS				M	M
1050	60	VS				MS	M
1100	60	VS				MS	MS
1100	180	VS				S	MS
1100	180	VS				S	MS

Table 6.10 Summary of X-ray diffraction analysis of chalcopyrite reduced by activated carbon in the presence of lime (VS-very strong, S-strong, MS-medium strong, M-medium, WM-weak medium, W-weak)

Analysis of weight loss data indicated that activated carbon increased the rate of reduction. This observation is supported by the phases identified in table 6.10. In samples reduced by non-activated carbon metallic iron was first observed at 950°C. However, in $CuFeS_2$ reduced by activated carbon, the metal was identified at 900°C. For non-activated reduction (see table 6.8) unreacted calcium oxide was present at 850°C and 900°C. Reduction by activated carbon at lower temperatures ensured the conversion of all the lime to CaS and the intermediary phase occurred. The combination of these observations leads to the conclusion that activated carbon increases the rate of reduction.

The intermediary oxysulphides were only present at low temperatures. The C_{III} phase was present at 850°C and 900°C, but not above this temperature, the C_{II} phase was also present at 850°C and 900°C and not above this temperature.

A comparison of X-ray analysis for chalcopyrite reduced by carbon and activated carbon at 900°C for 60 minutes is given in figure 6.31. The main differences observed from this figure include the presence of iron in figure 6.31B (activated C) and not in 6.31A (non-activated C). Also observed was the C_{II} phase present in figure 6.31A and not in 6.31B.

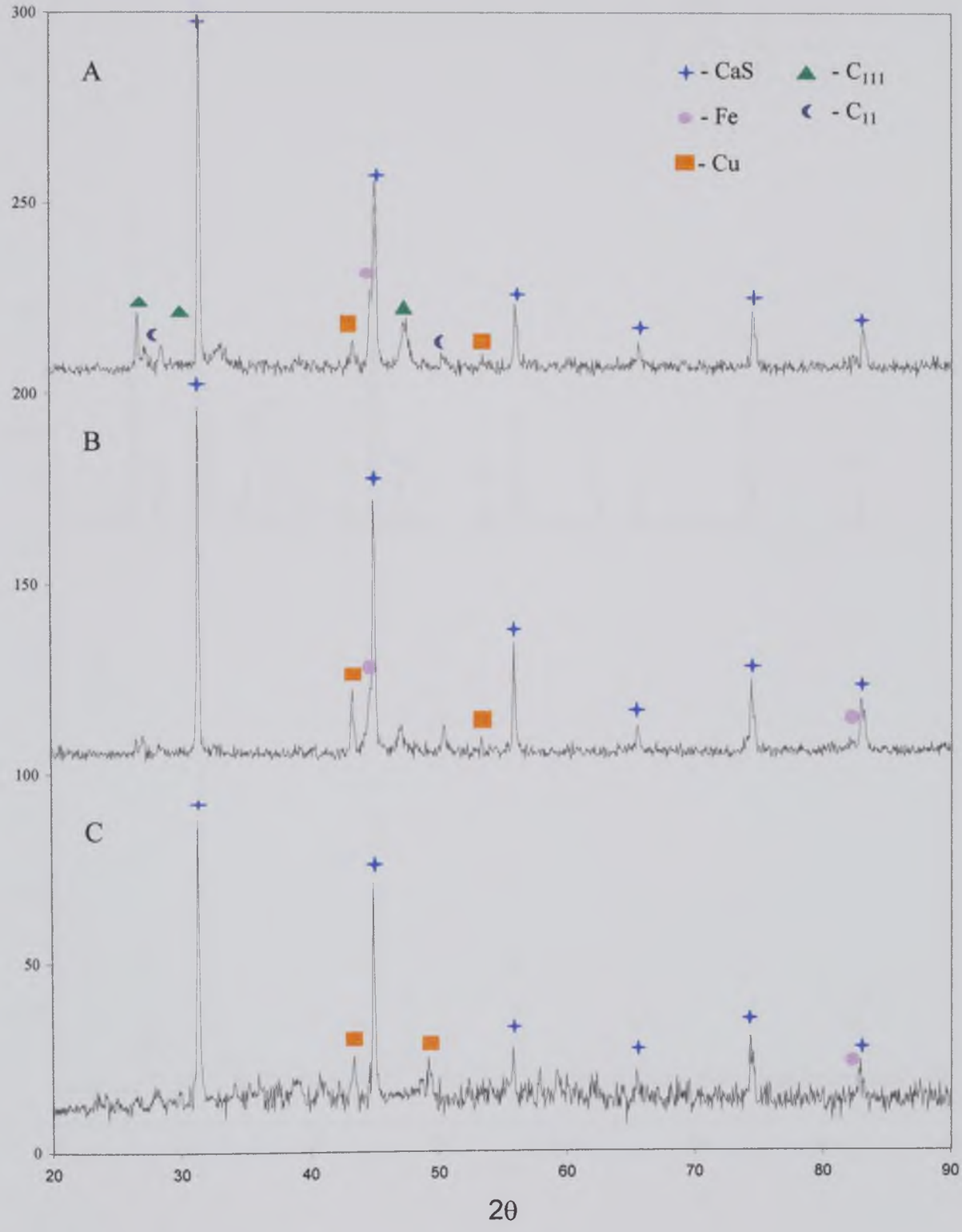

Figure 6.30 Comparison of X-ray diffraction patterns for chalcopyrite reduced by activated carbon for 60 minutes at A-900°C, B-1000°C and C-1100°C.

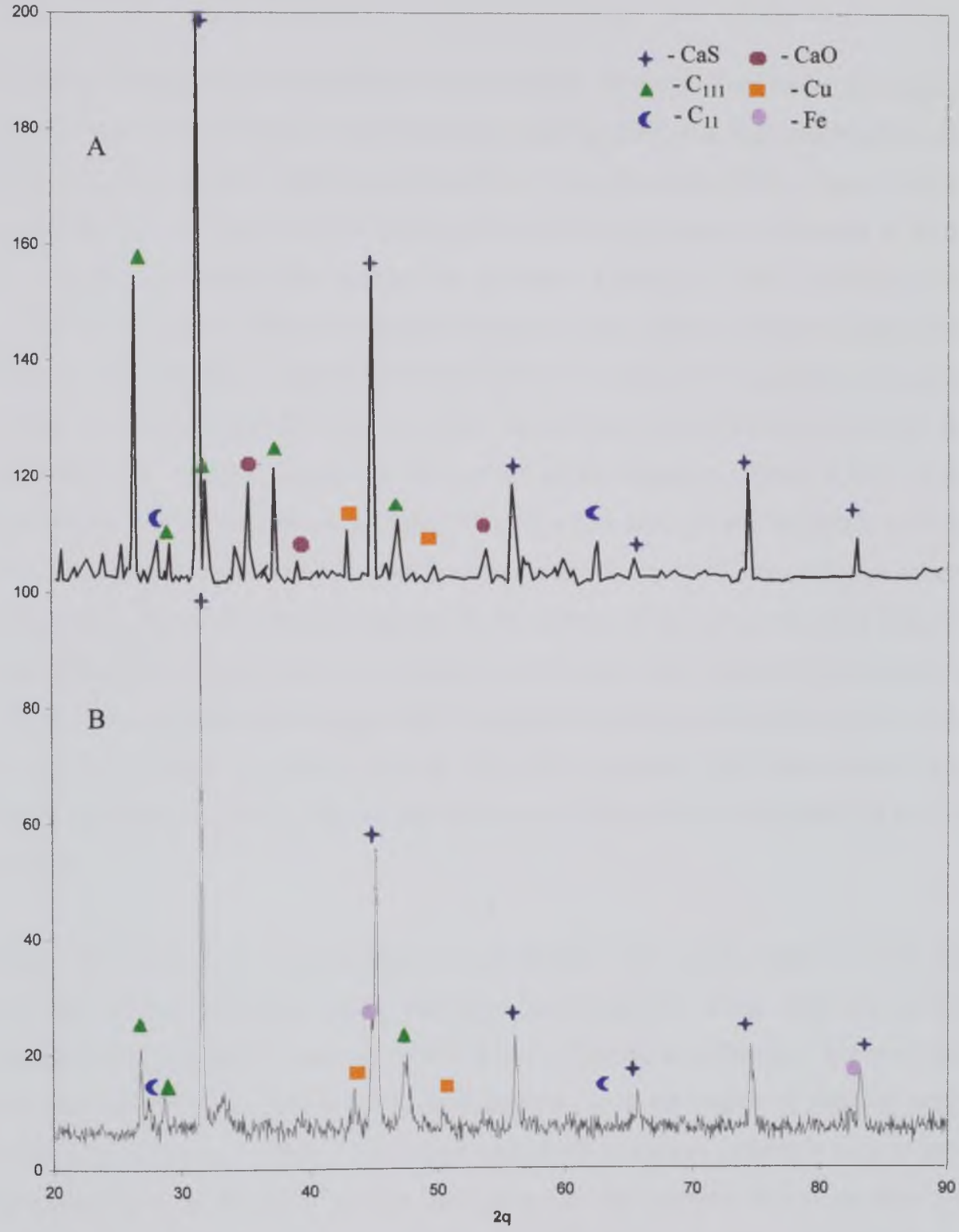

Figure 6.31 Comparison of X-ray patterns for chalcopyrite reduced by carbon (A) and activated carbon (B) at 900°C for 60 minutes.

6.5.3 Electron Microscopy

Samples of chalcopyrite reduced by activated carbon were examined under the scanning electron microscope using secondary electron imaging (SEI) and back scattered electron (BSE) imaging together with energy dispersive X-ray analysis (EDX). Figure 6.32 is a secondary electron image (SEI) depicting the typical microstructure observed at the top of a sample of chalcopyrite reduced by activated carbon at 950°C. Initially before analyses were carried out on the reacted samples it was obvious, by observation of the samples, that metallic copper had formed. On the surface of the reacted samples a copper colouration was observed, on closer inspection this colouration was seen as a small layer of metallic copper on the surface of the samples. Figure 6.33 is a SEI micrograph of this surface on a higher magnification than shown in figure 6.32 and shows the growth of metallic copper from the sample. At 950°C, on samples reduced with carbon, this metallic copper growth on the surface of the sample was not observed, thus indicating a higher degree of copper metallisation was achieved using activated carbon. This metallisation of copper was noticed in all samples of chalcopyrite reduced by activated carbon, especially near the top of the samples. This characteristic is not dependent upon the size of sample thus reduced as it was observed in both 2g and 50g samples.

Figure 6.15 shows the typical phase microstructure in samples reduced with non-activated carbon. Metallic copper and iron occur together along with the calcium sulphide and naturally occurring silica phases. The main difference between non-activated and activated carbon reduction appears to be in the degree of metallic copper production. Although readily produced as a result of reduction, copper is seen at lower temperatures with activated carbon and grows on the surface of the sample. This migration of copper to the surface results in low levels of metallic copper observed within the lower part of the sample. In samples of chalcopyrite reduced with non-activated carbon, metallic copper and iron are seen in similar quantities, whereas reduction by activated carbon shows a higher amount of metallic iron than copper throughout the samples below the surface, due to the migration of copper metal to the surface of the sample.

Figure 6.34 is a BSE image depicting, in particular, the production of metallic iron from chalcopyrite at 1100°C. The lightest phase is identified as iron with the next slightly darker shade being calcium sulphide. Figure 6.35 is a BSE image demonstrating an eutectic of calcium sulphide surrounded by the calcium sulphide in its normal form. Figure 6.36 demonstrates this eutectic structure at a higher magnification.

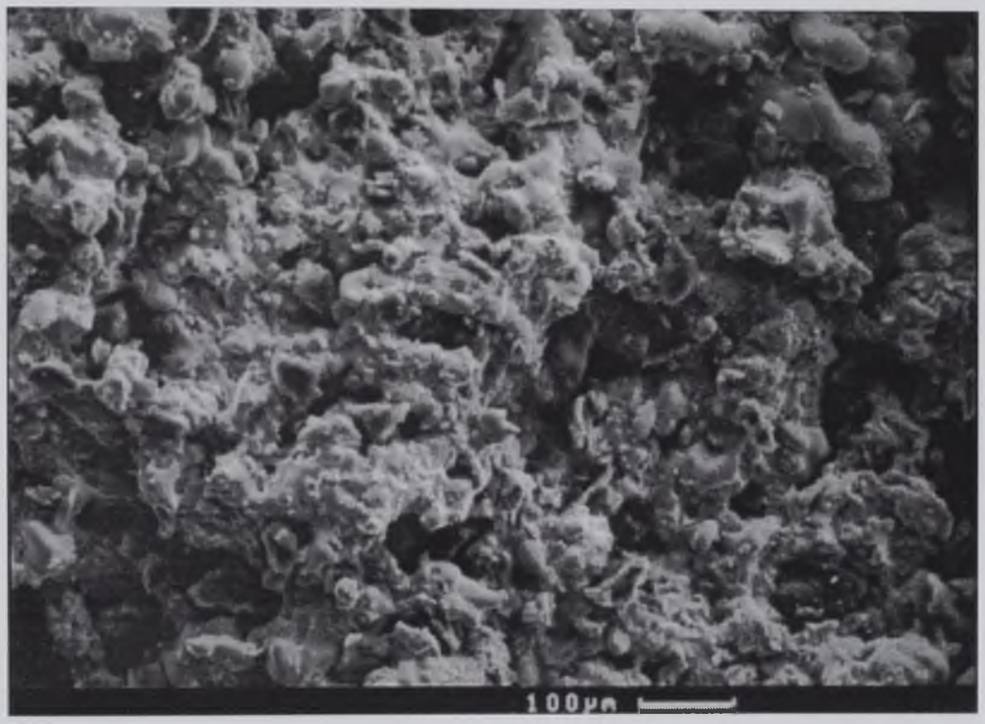

Figure 6.32 SEI micrograph of the top of a sample of the reduction of chalcopyrite with activated carbon at 950°C for 60 minutes.

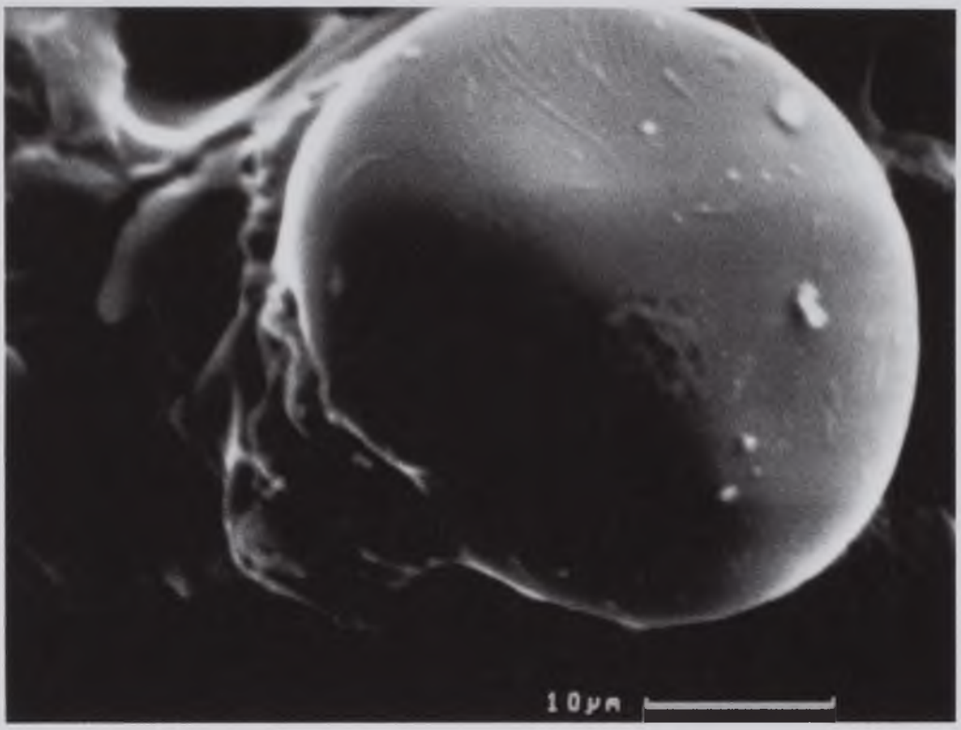

Figure 6.33 SEI micrograph of metallic growth from the surface of a sample of chalcopyrite reduced by activated carbon at 950°C for 60 minutes.

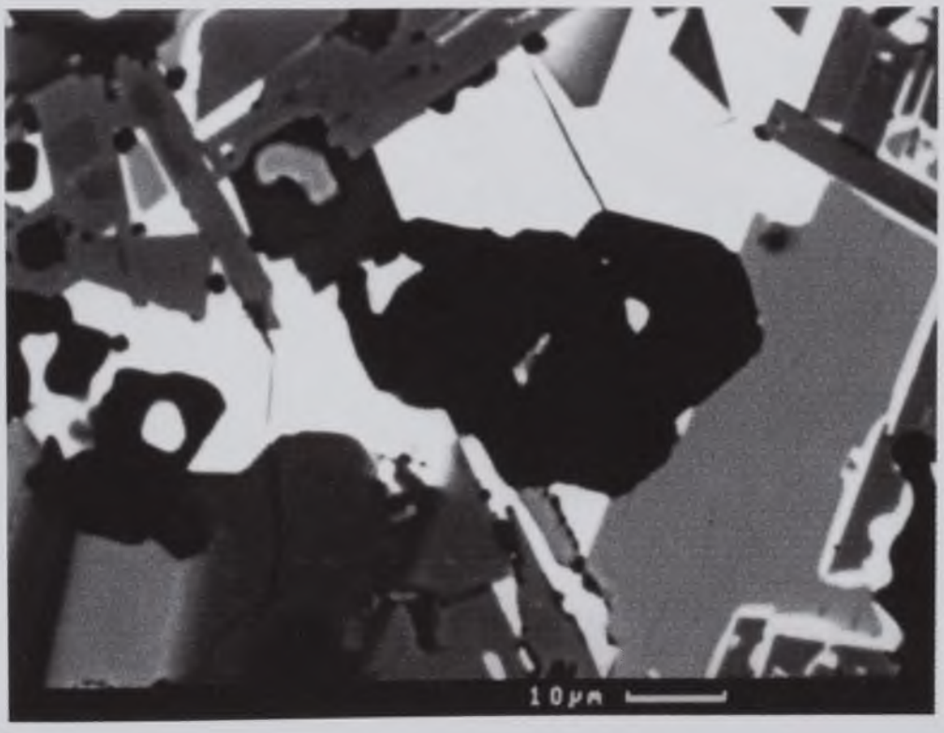

Figure 6.34 BSE image of the microstructure observed from the reduction of chalcopyrite with activated carbon at 1100°C for 180 minutes indicating CaS (darker regions) and metallic iron (lighter).

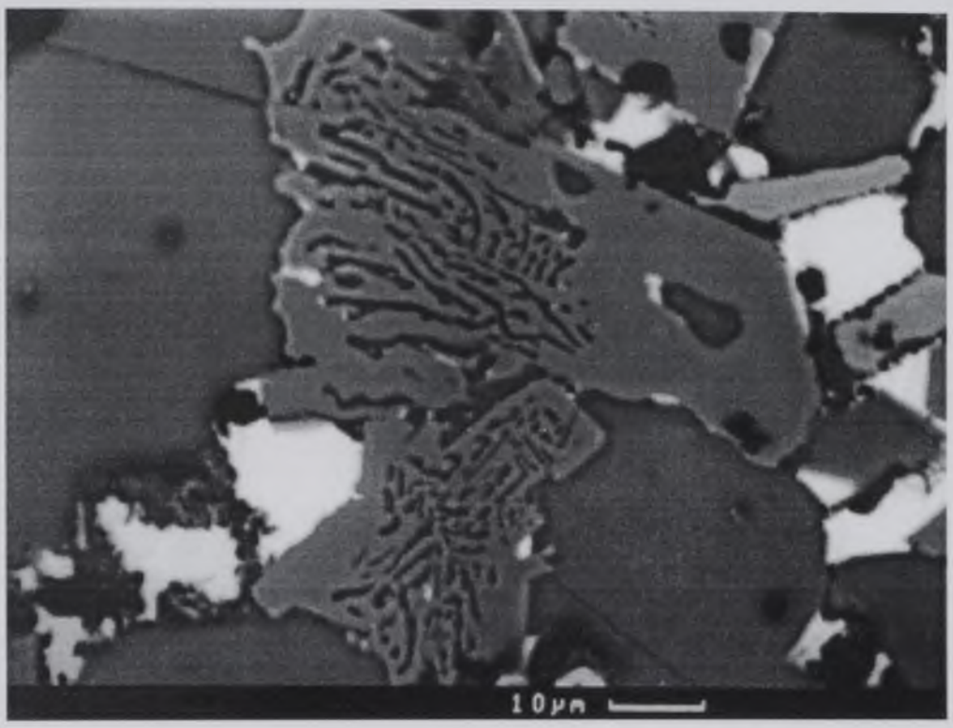

Figure 6.35 BSE image of a sample of chalcopyrite reduced with activated carbon at 1100°C for 180 minutes showing the formation of CaS with the eutectic of CaS.

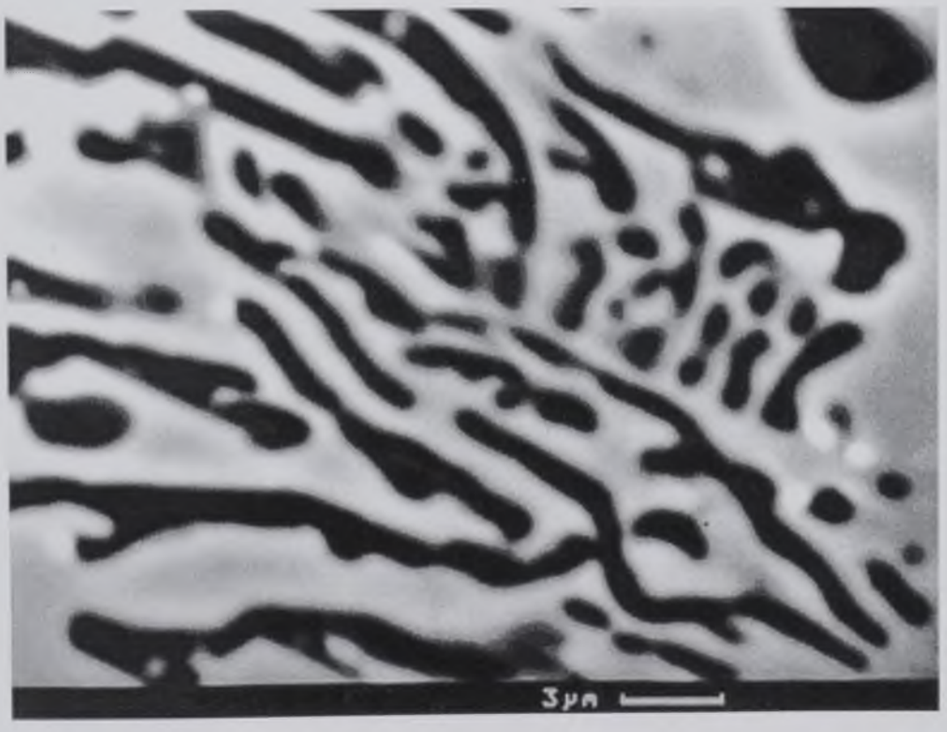

Figure 6.36 BSE image of the eutectic of CaS observed in figure 6.35 at a higher magnification.

6.6 Reproducibility of Phases on a Larger Scale

Samples of chalcopyrite, lime and carbon, each 50g in weight, were mixed in a ratio of 1:2:2 and heat treated in a retort furnace in which an atmosphere of argon was maintained. The aim of these experiments, now using 50g of material, was to verify the reproducibility of phases formed in the 2g experiments on a larger scale. The 50g heat treated samples, were in appearance, similar to the samples from small scale experiments. The initial powder mixture was light grey in colour, after reduction the colour was dark grey and the samples were sintered.

6.6.1 X-ray Diffraction

A comparison of X-ray diffraction patterns for samples 50g in size is presented in figure 6.37. The phases from this set of reactions are summarised in table 6.11 and agree well with data from small scale experiments. The phases in table 6.11 were identified from JCPDS files given in appendix 1.

Temperature (°C)	Time (mins)	Phases Identified with Relative Intensity					
		CaS	CaO	C_{111}	C_{11}	Cu	Fe
900	180	VS	WM	MS			
1000	120	VS	W	M	WM	W	
1000	180	VS		M		W	W
1100	120	VS		WM		WM	W
1100	180	VS		W		M	W
1200	120	VS				M	WM
1250	180	VS				M	WM

Table 6.11 Summary of X-ray diffraction analysis for 50g samples of $CuFeS_2$:2CaO:2C (VS-very strong, S-strong, MS-medium strong, M-medium, WM-weak medium, W-weak).

Calcium sulphide is the predominant phase recognised from X-ray analysis appearing in all X-ray diffraction patterns. The next strongest phase occurring was the oxysulphide phase, C_{111}, which was observed in the temperature range 900°C-1100°C but not above this temperature. The oxysulphide phase, C_{11}, was noticed after a reaction at 1000°C for 120 minutes but not after a reaction at 180 minutes. Unreacted lime was observed at 900°C but not above this temperature.

Metallic copper was first detected in chalcopyrite reduced at 1000°C for 120 minutes. Iron was also present in chalcopyrite reduced at 1000°C but only after 180 minutes. Both of these metallic phases were present in samples reacted above 1000°C.

X-ray analysis was carried out on different parts of selected samples. After the reaction at 1100°C, the first, most noticeable observation, was the red colouration at the top of the sample. X-ray diffraction indicates that the colouration is due to copper being the most predominant phase in the top part of the sample, second only to calcium sulphide. Metallic iron was not detected in this part of the sample but was seen in the middle and bottom parts along with copper and CaS.

Figure 6.38 is a comparison of X-ray diffraction patterns for 2g and 50g samples reduced for 120 minutes. The most obvious difference between the two sample sizes is the presence of the oxysulphide phases C_{111} and C_{11} in the 50g sample but not in the smaller sample. The second difference is the presence of iron for the 2g sample but not for the 50g sample. This comparison indicates that although the reproducibility of phases from 2g to 50g samples is reasonable the rate at which they occur is lower in the larger samples.

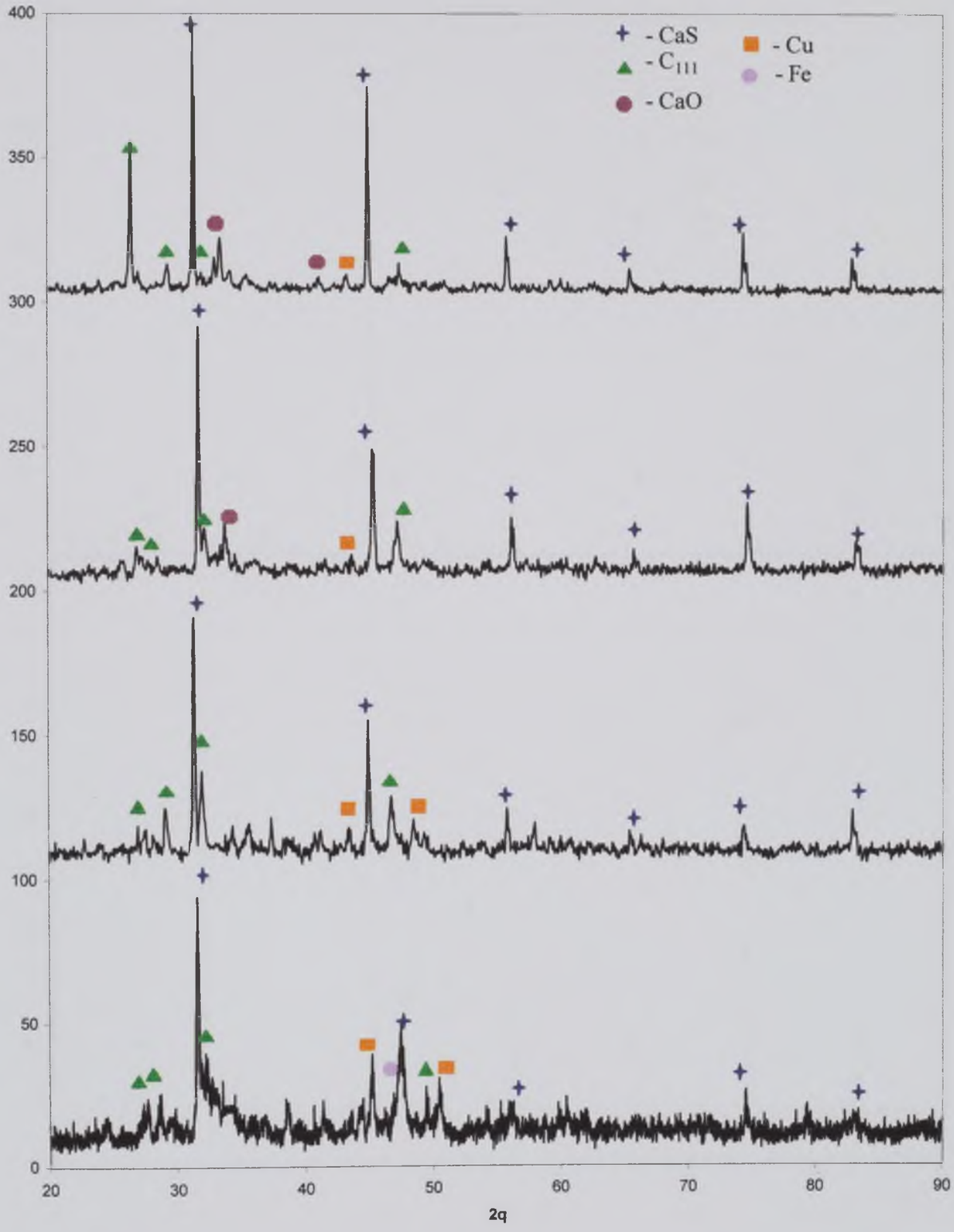

Figure 6.37 Comparison of X-ray diffraction patterns for medium scale samples of $CuFeS_2$ reduced at A-900°C, B-1000°C, C-1100°C and D-1250°C for 180 minutes.

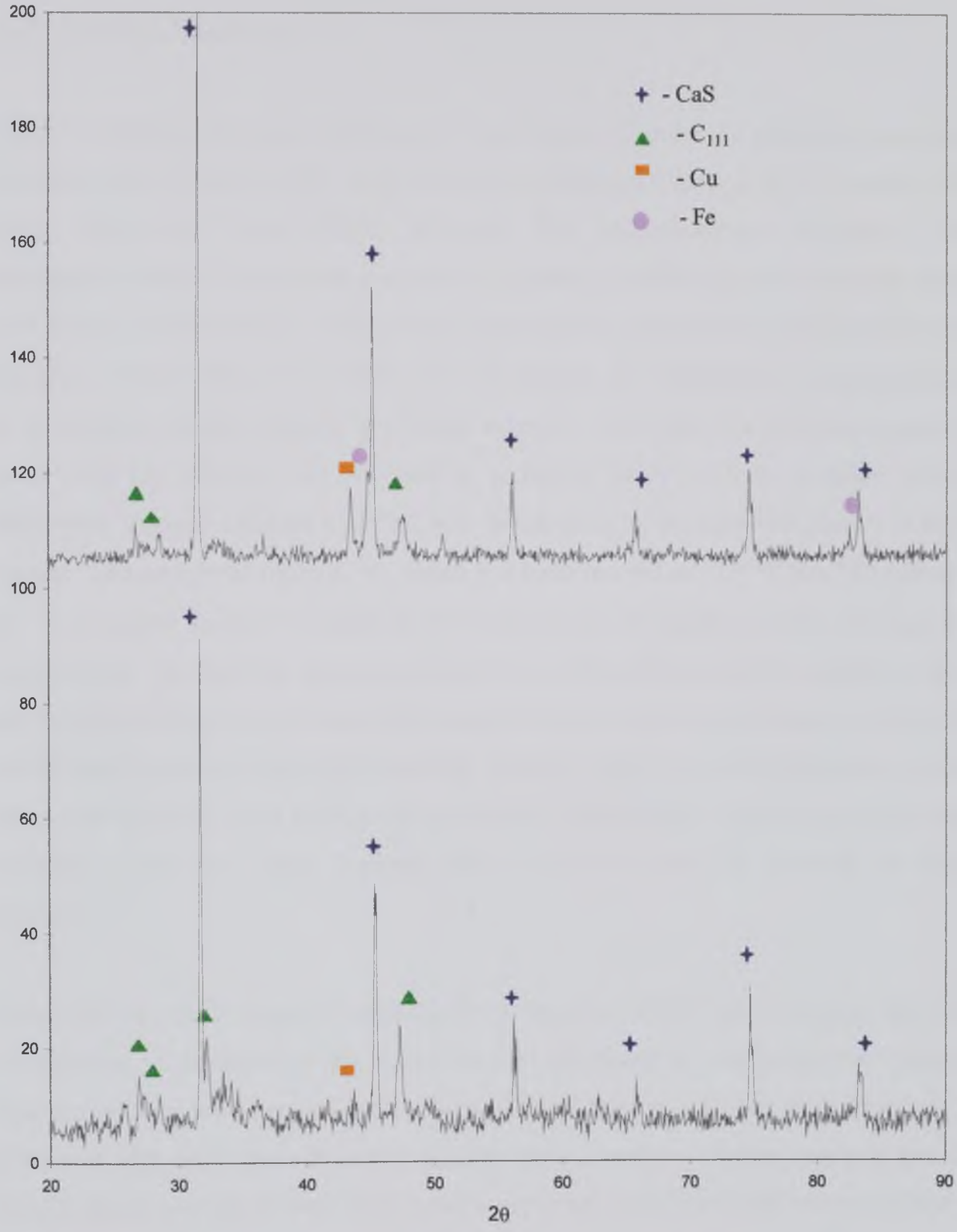

Figure 6.38 Comparison of X-ray diffraction patterns for chalcopyrite reduced at 1000°C/120 minutes for samples of A-2g and B-50g.

6.6.2 Electron Microscopy

Selected samples of reduced chalcopyrite were examined under the electron microscope using secondary electron (SEI) imaging and back scattered electron (BSE) imaging with energy dispersive X-ray (EDX) analysis. The microstructures discerned from chalcopyrite reduced on a larger scale are very similar to those reported from the small-scale trials. Figure 6.39 is a BSE image demonstrating the typical phase distribution through a sample reduced at 1100°C for 180 minutes. In similarity to phases produced in 2g samples metallic species are found together with CaS. For the micrograph of figure 6.39 the contrast was adjusted to show the fairly uniform metallic species distribution through reduced $CuFeS_2$. The distribution of the metallic phases is fairly uniform. The sample of figure 6.40, which had been reacted at 1100°C for 180 minutes, was investigated further to establish the distribution of metallic phases through the reacted mass. The findings agreed with the X-ray diffraction analysis. Metallic copper was found principally at the top of the sample but found to a lesser degree through the middle and bottom regions of the material. Metallic copper was still observed to occur along with iron but not at the top of the sample. Metallic iron was seen only in small quantities at the top, which explains why its presence was not detected by X-ray analysis.

Figure 6.41 is a BSE image of chalcopyrite reduced at 1250°C and indicates that with the increase in temperature the microstructure produced is one previously unseen. Figures 6.42 and 6.43 are images of this microstructure at a higher magnification. In agreement with the X-ray diffraction analysis of this sample calcium sulphide and the metallic species are identified. These phases are observed to form differently to those at lower temperatures. It appears that the lighter metallic phases are found between the darker bladed calcium sulphide phases.

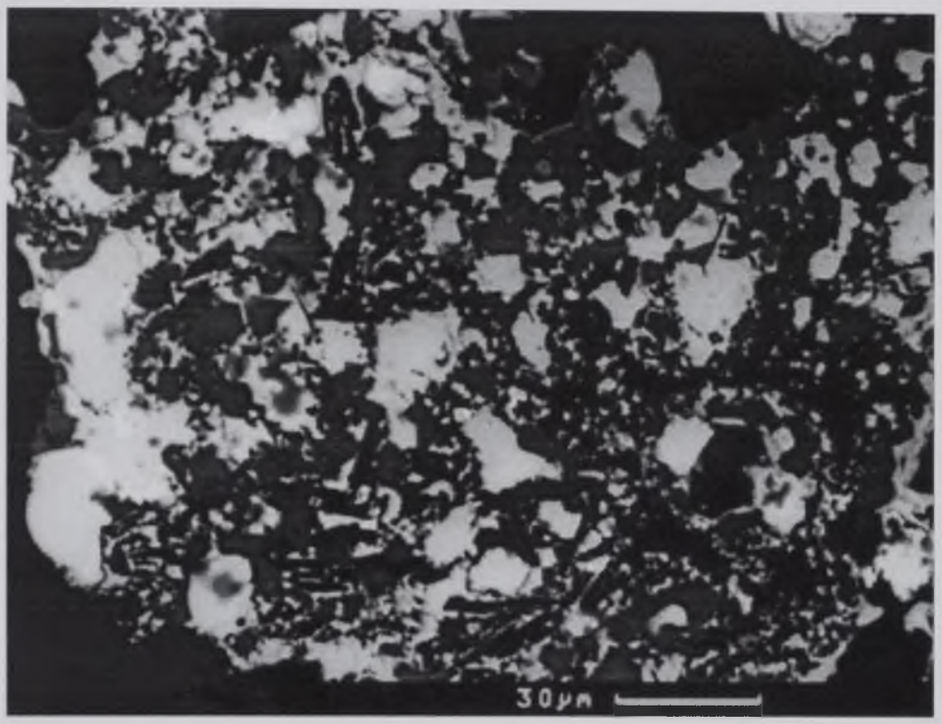

Figure 6.39 BSE of the typical microstructure observed from a 50g sample of $CuFeS_2$:2CaO:2C heat treated at 1100°C for180 minutes.

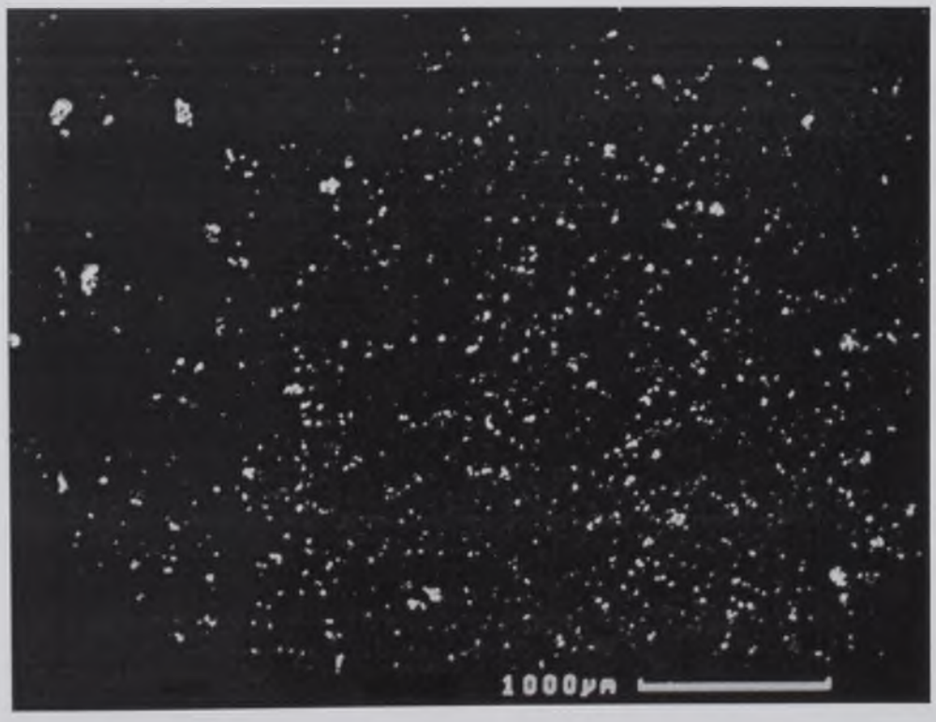

Figure 6.40 BSE image of a 50g sample of $CuFeS_2$:2CaO:2C heat treated at 1100°C for180 minutes showing in particular the metallic phase production.

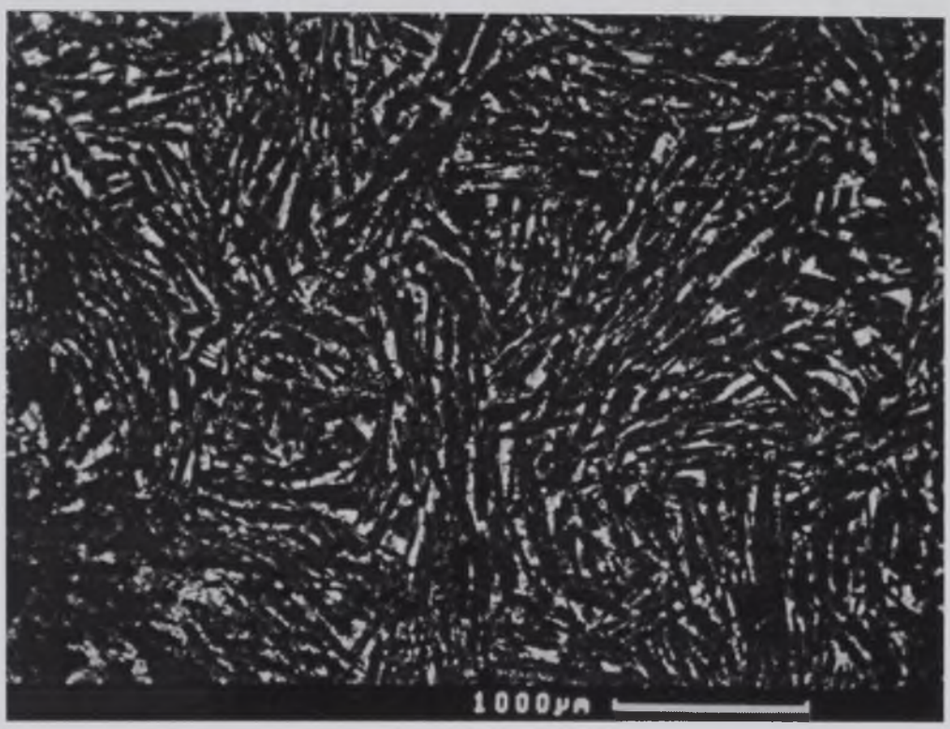

Figure 6.41 BSE of the microstructure of a 50g sample of $CuFeS_2$:2CaO:2C heat treated at 1250°C for 120 minutes.

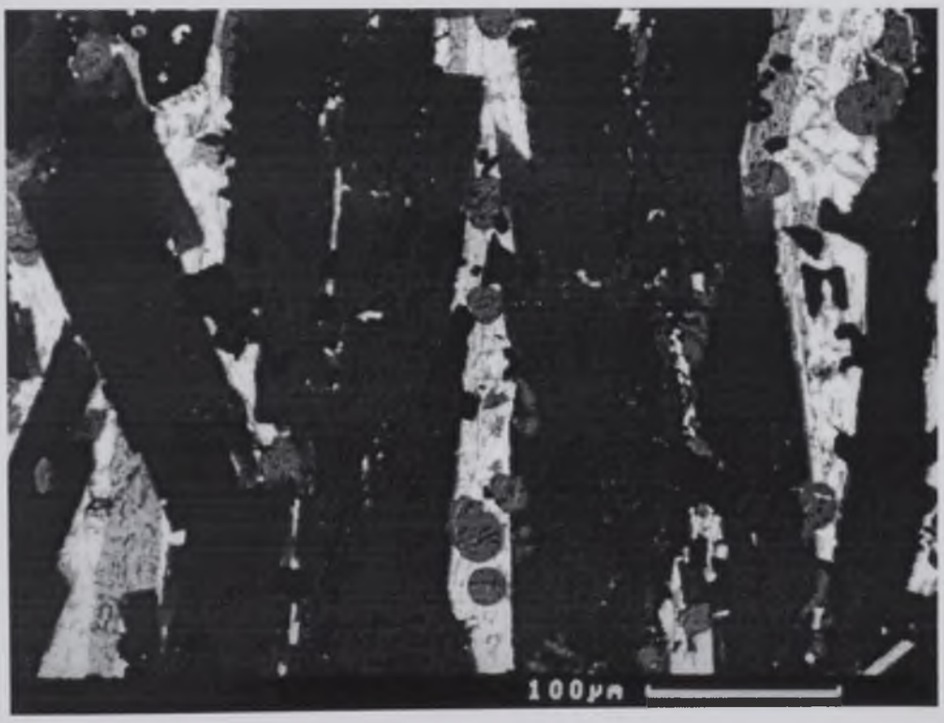

Figure 6.42 BSE image of the microstructure observed in figure 6.41 at a higher magnification.

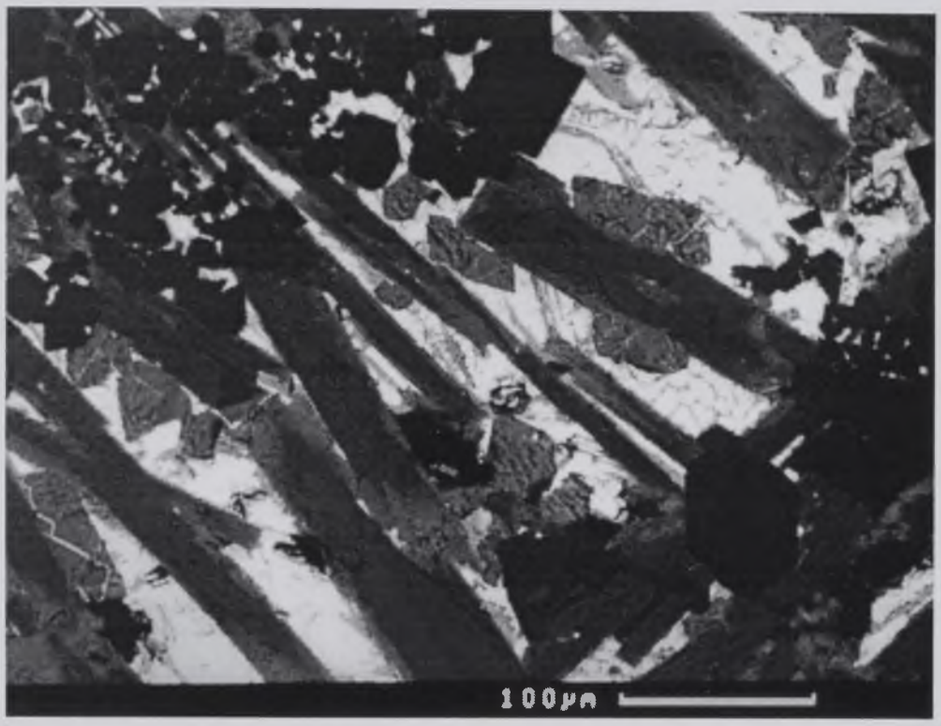

Figure 6.43 BSE image of the microstructure observed in figure 6.41 at a higher magnification.

6.7 The Reduction of Chalcopyrite with Silver and Silver Sulphide Additions

Silver is an important by-product of copper extraction. It is therefore important to understand the behaviour of silver during the carbothermic reduction of natural chalcopyrite. Silver and silver sulphide additions of 1 wt. % were made in different mixtures of $CuFeS_2 + 2CaO + 2C$. The amounts of silver and silver sulphide added were significantly large enough to enable the detection of silver by electron microscopical methods. The various sample compositions with the experimental conditions are listed in table 6.12.

Sample Composition	Temperature (°C)	Time (mins)	Phases Identified					
			CaS	CaO	C_{111}	C_{11}	Cu	Fe
$CuFeS_2 + 2CaO + C +$ 1wt.% Ag_2S (small)	1100	180	VS				M	M
$CuFeS_2 + 2CaO + C +$ 1wt.% Ag_2S (50g)	1100	180	VS				M	M
$CuFeS_2 + 2CaO + C +$ 1wt.% Ag_2S (50g)	1150	180	VS				M	M
$CuFeS_2 + 2CaO + C +$ 1 wt.% Ag (small)	1100	180	VS				M	M
$CuFeS_2 + 2CaO + C +$ 1 wt.% Ag (50g)	1150	180	VS				M	M

Table 6.12 Phase identification for $CuFeS_2$:2CaO:2C with additions of 1 wt.% silver metal and 1 wt.% Ag_2S (VS-very strong, M-medium).

6.7.1 X-ray Analysis

The analysis, by X-ray diffraction analysis, of the reduction of chalcopyrite with silver sulphide and silver metal, was carried out to investigate the effect on the phases produced from the reduction of chalcopyrite by the presence of these additions. It also acted as a control to ensure that the reduction of chalcopyrite proceeded as it had in previous reduction experiments. This analysis was not used to understand what happens to the silver additions as the amounts of these substances were not of significant quantities to be observed on X-ray diffraction patterns. This aspect was covered using

electron microscopy as stated above. Table 6.12 lists the phases identified, from the JCPDS files given in appendix 1, as present in each sample after reduction.

Calcium sulphide was the predominant phase identified in all samples, either those doped with silver sulphide or with silver metal. This phase was identified clearly in figure 6.44 where a comparison between X-ray diffraction patterns for silver sulphide and silver additions is given. Metallic copper and iron are detected in all of the samples of the reduction of chalcopyrite with silver sulphide and silver metal additions. Neither one of the C_{11} nor C_{111} phases are present in the X-ray diffraction patterns. For all of these reactions complete reduction had occurred.

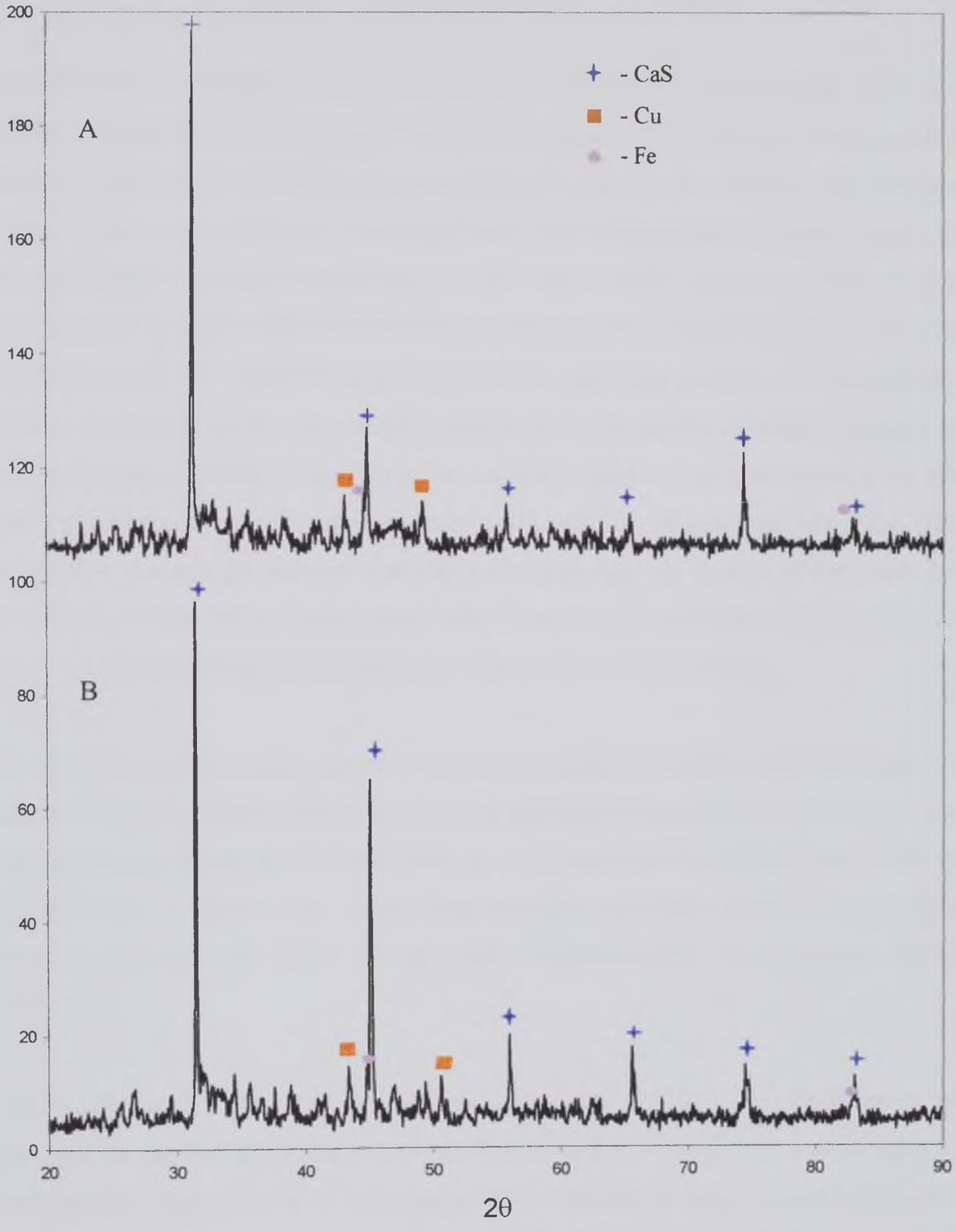

Figure 6.44 Comparison of X-ray diffraction patterns for chalcopyrite reduced at 1150°C for 180 minutes with A-1 wt.% Ag_2S and B-1wt.% Ag.

6.7.2 Electron Microscopy of Chalcopyrite Reduced with Ag_2S

Metallic silver is produced as a result of the reduction of chalcopyrite with silver sulphide additions at 1150°C for three hours. Figure 6.45 shows a back-scattered electron image of the typical microstructure obtained from this reaction. The brightest, smallest phases are detected as metallic silver. The next brightest phase is copper and the third lightest phase is metallic iron. Within the metallic region no other elements were detected by EDX. The darker region surrounding this metallic region is identified as calcium sulphide. Therefore, as a result of the reduction reaction, silver sulphide is reduced to metallic silver, in a process similar to the formation of metallic copper and iron from their sulphides. Throughout the sample metallic silver was observed to have been produced and was found in location with metallic copper and iron. The phase distribution through the reduced samples containing Ag_2S is similar to that seen from the reduction trials. As the experiments were carried out at such high temperatures none of the oxysulphide phases were present as indicated by X-ray analysis.

The silver appears to form at the grain boundaries between copper and iron. Figure 6.46 depicts this characteristic where the brightest phase is silver, the next lightest is copper with the darkest being iron. Figure 6.46a is a dot map for silver and figure 6.46b is a map for iron. It appears that silver does segregate into the metallic copper phase, however this was not clear enough from microscopy on the scanning electron microscope.

Chalcopyrite and 1 wt.% silver sulphide reduced at 1150°C for three hours was examined on the EPMA. Figures 6.47, 6.48, 6.49 and 6.50 depict the results from this investigation. Figure 6.46 is a BSE image of the sample showing a region of metallic phases produced from the reaction. Figures 6.48, 6.49 and 6.50 are the elemental dot maps of iron, copper and silver respectively. Metallic silver is found at the boundary between copper and iron, this characteristic was also noticed in samples analysed on the electron microscope, see figure 6.45. The metallic silver alloys itself to the metallic copper at the grain boundary and is also found to segregate within the copper phase. This segregation into copper is seen clearly from the silver elemental dot map of figure 6.50. From the elemental dot maps it appears that no miscibility is observed between the

iron and silver, as it is also true that miscibility does not occur between metallic copper and iron as observed from the reduction reactions

Further investigations were made on the electron microscope of the phases produced from the addition of Ag_2S to chalcopyrite reacted at 1100°C for 180 minutes. The top of the sample was investigated and figures 6.51, 6.52 and 6.53 are typical of the microstructure observed. The calcium sulphide appears as the darkest phase, iron forms as the slightly lighter bladed structure with metallic copper and silver found in between as the lightest phase. Larger metallic regions, as typified in figure 6.54, were observed in this sample. The microstructure, observed in figure 6.54, was previously unseen from the other samples of reduced chalcopyrite. Figure 6.55 is an image taken at a higher magnification than of figure 6.55. As with other samples, silver (lightest phase) is found at the grain boundaries between the metallic phases. In figure 6.46a silver is found at a several points between copper and iron. In figure 6.55 silver is found at all boundaries and particularly with iron.

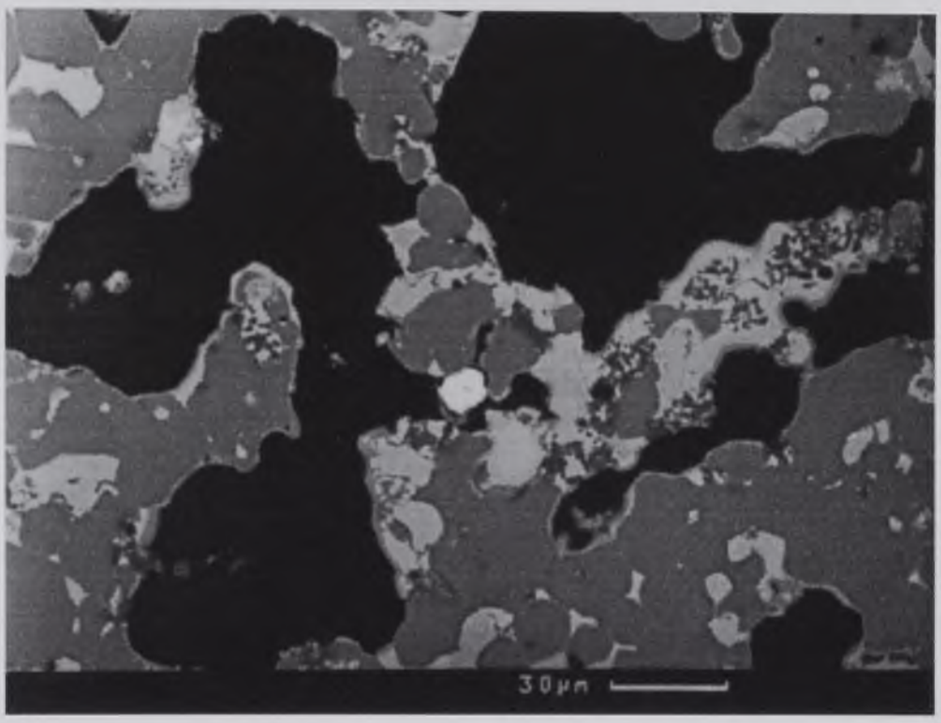

Figure 6.45 BSE image of the reduction of chalcopyrite with 1 wt.% Ag_2S at 1150°C for 180 minutes showing copper (light) and iron metallisation (dark) with silver (brightest) metal formed at the phase boundaries between copper and iron.

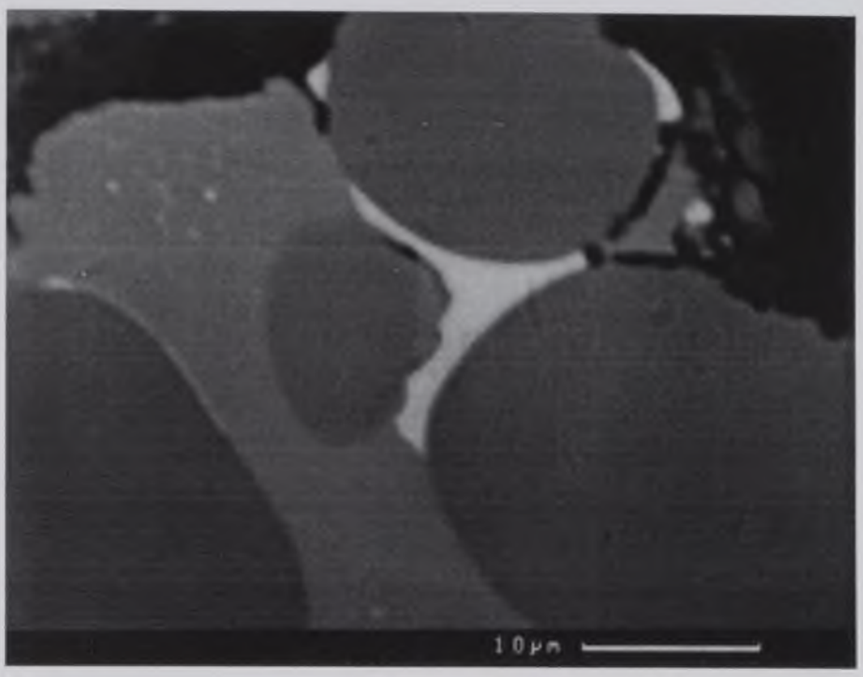

Figure 6.46 BSE image of metallic silver (lightest) produced at the grain boundary between copper (medium) and iron (darkest) from the reduction of chalcopyrite at 1100°C for 120 minutes with a) and b) elemental maps of the region for Fe and Ag respectively.

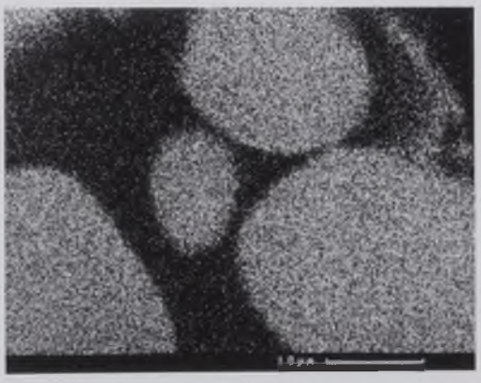

(a)

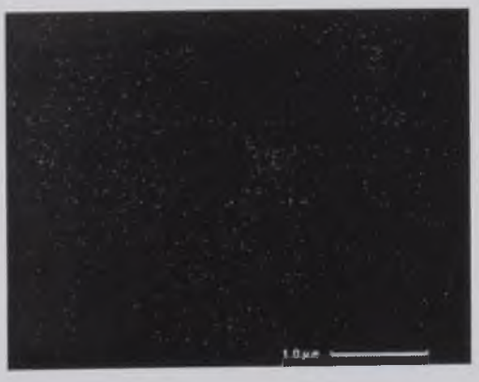

(b)

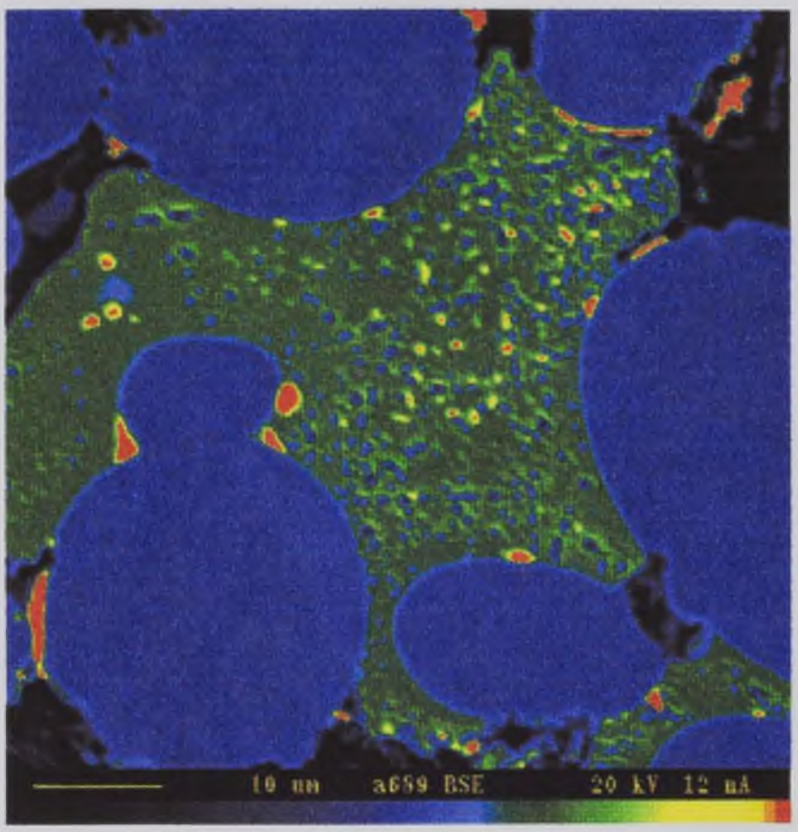

Figure 6.47 EPMA back scattered electron image of chalcopyrite reduced with 1 wt.% Ag_2S at 1150°C for 180 minutes.

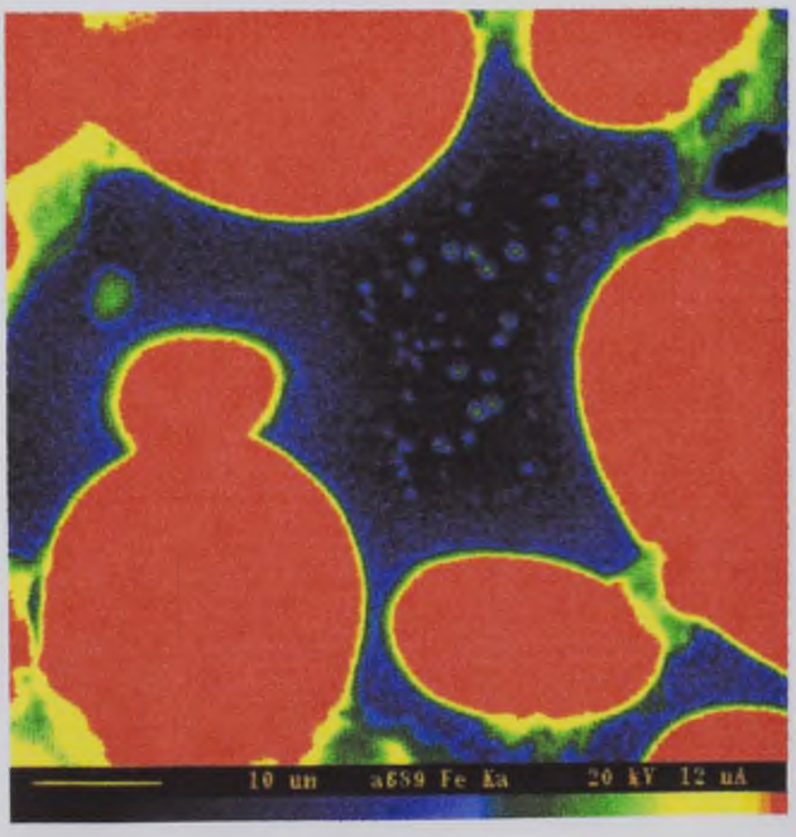

Figure 6.48 Iron elemental map for the metallic region in figure 6.47.

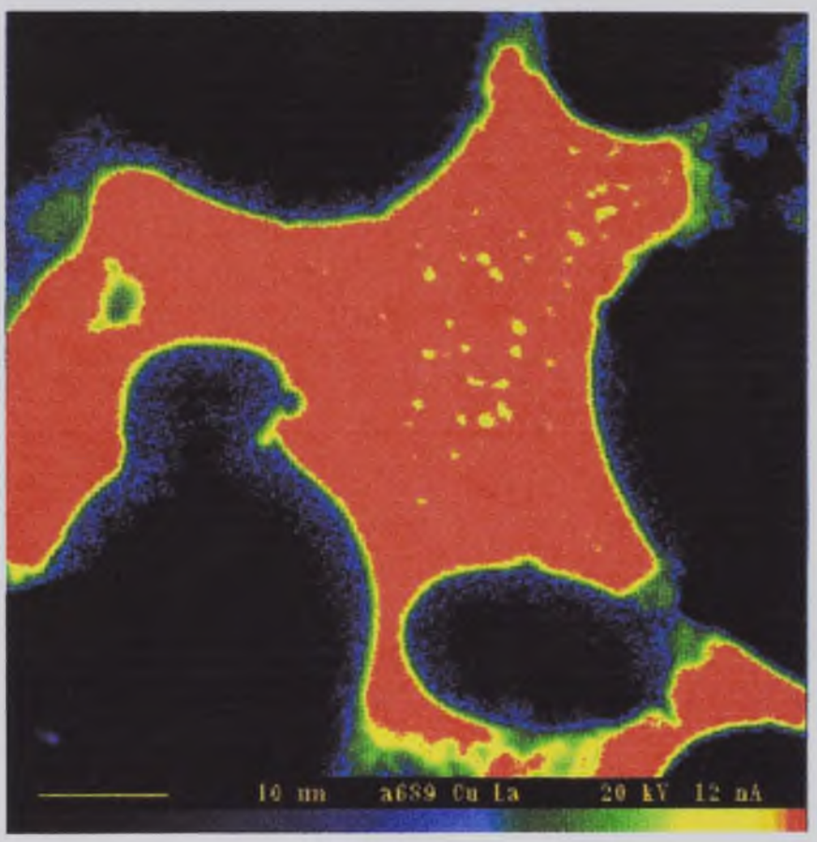

Figure 6.49 Copper elemental map for the metallic region of figure 5.47.

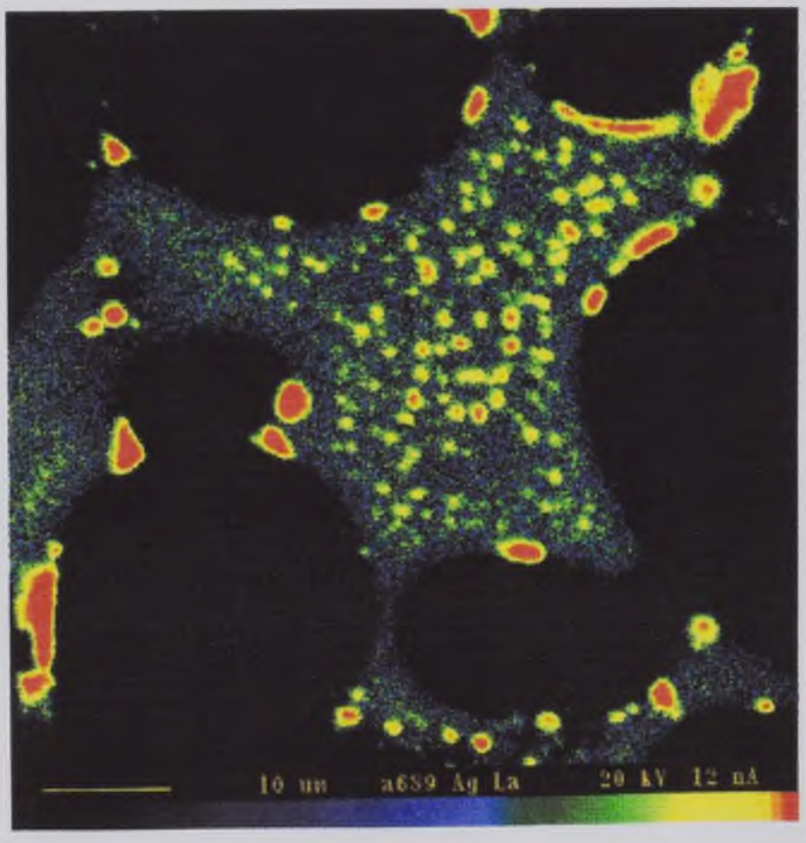

Figure 6.50 Silver elemental map for the metallic region of figure 5.47.

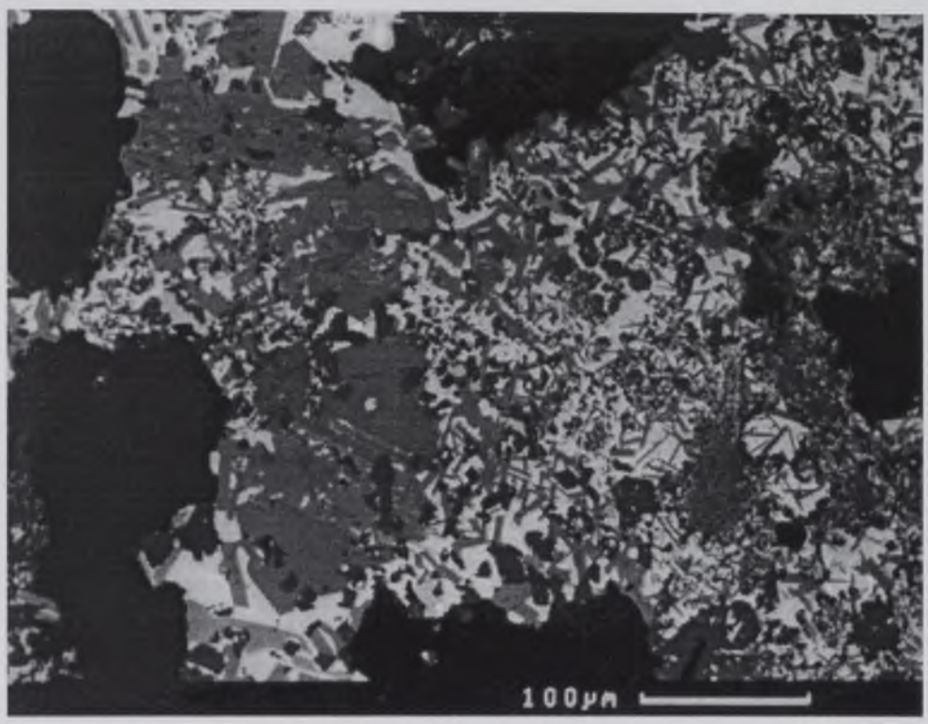

Figure 6.51 BSE image of the microstructure of chalcopyrite reduced with 1 wt.% Ag_2S at 1100°C for 180 minutes.

Figure 6.52 BSE image at a higher magnification for the region of figure 6.51.

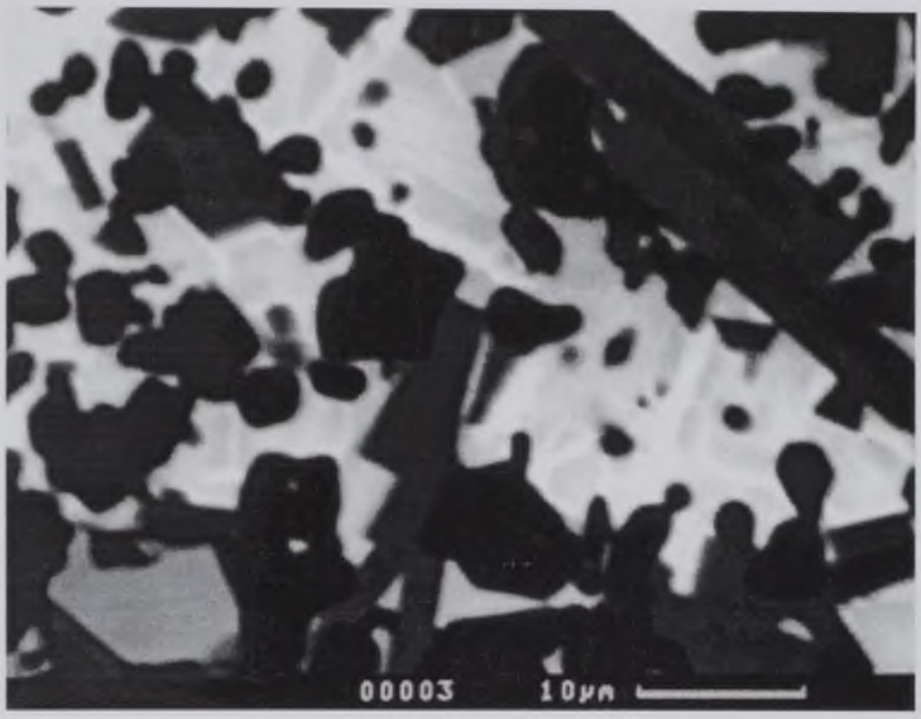

Figure 6.53 BSE image at a higher magnification for the region of figure 5.51.

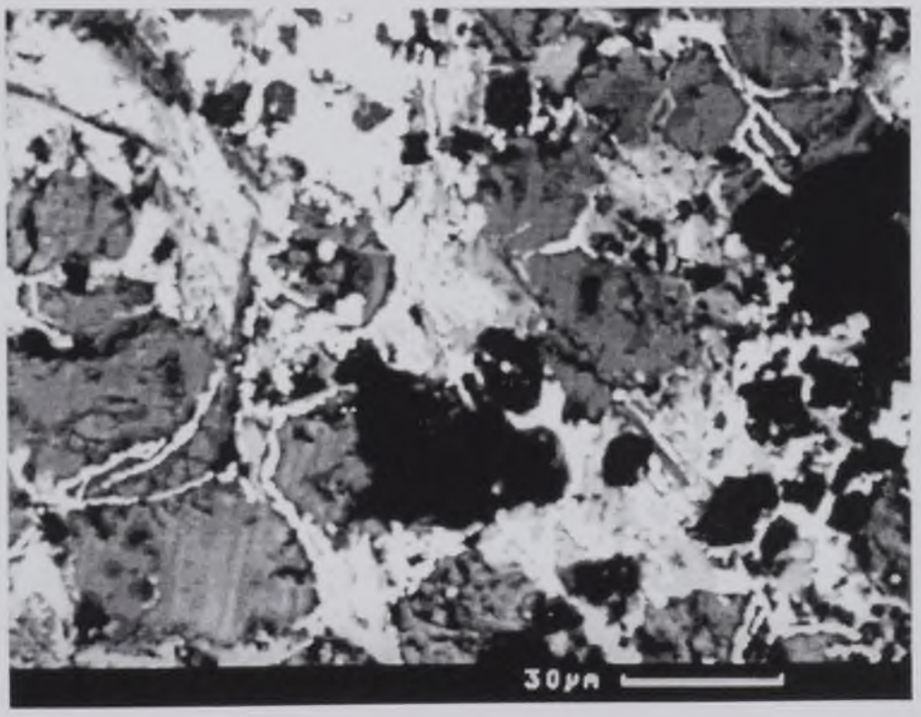

Figure 6.54 BSE image of the microstructure observed from the reduction of chalcopyrite with 1 wt.% Ag_2S at 1150°C for 180 minutes.

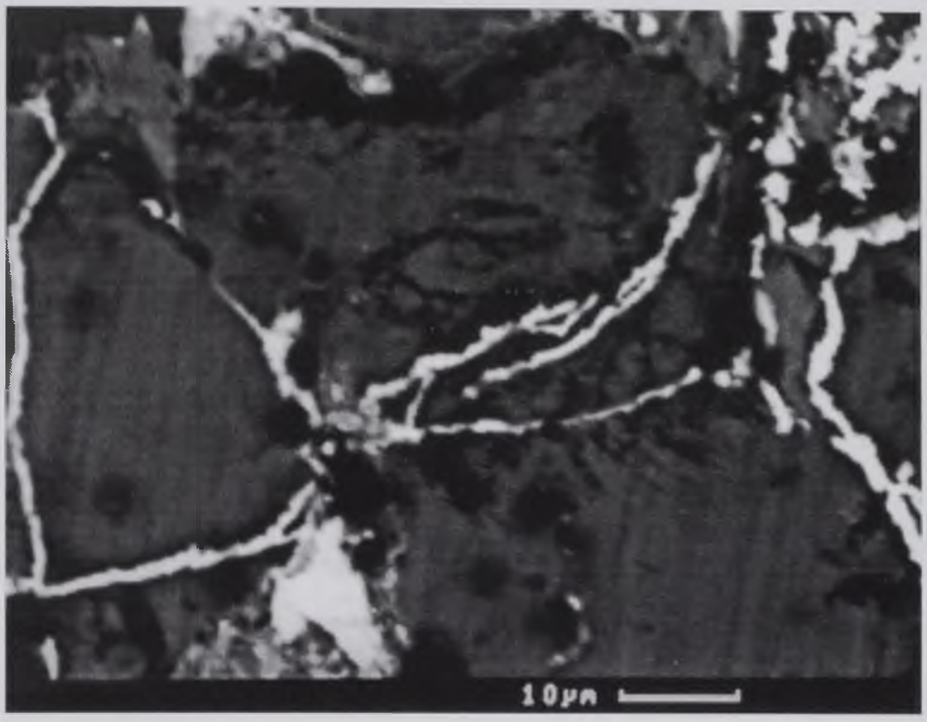

Figure 6.55 BSE image of the microstructure of figure 6.54 at a higher magnification.

6.7.3 Electron Microscopy of Chalcopyrite with Silver Metal

The microstructure observed after the reduction of chalcopyrite with the addition of silver differs to that of reduced and silver sulphide doped samples. Figure 6.56 shows the microstructure formed from the reaction with silver, where an eutectic of silver and copper was observed in the sample when reacted at 1150°C. Figures 6.56a and 6.56b are elemental dot maps of silver and copper respectively. Figure 6.57 is a higher magnification of the eutectic seen in figure 6.56. Figures 6.57a and 6.57b are elemental dot maps for silver and copper for the area of figure 6.57. This eutectic was observed in all areas where the silver metal had been added and is a silver rich phase where the copper metal is embedded in the silver metal. This eutectic is observed at a higher magnification in figure 6.58. The lightest phase is silver metal with darker copper embedded within it.

Figure 6.59 shows another area where metallic copper and silver are found together. This area differs in that it is not, for the main part, in whole, a eutectic between the two

metals. In the silver rich phase the eutectic occurs but in the copper rich phase the silver appears to be embedded within the copper. This copper rich phase is similar to the metallic copper regions seen in samples with silver sulphide additions. These two phases are seen more clearly in figure 6.60 taken at a higher magnification. Figures 6.60a and 6.60b are elemental dot maps for silver and copper respectively for figure 6.60. On investigation, through the rest of the sample, metallic copper was in little evidence. The majority of the metallic copper produced as a result of the reduction reaction is found as the two regions shown in figures 6.56 and 6.59.

As confirmed by X-ray analysis results metallic iron was formed from this but was not found in the vicinity of the copper/ silver regions. In fact metallic iron was not found at all with the silver phase. In the samples observed from the reduction reaction, metallic copper and iron were seen together along with the calcium sulphide and the silica containing regions. Here, in these silver metal doped samples, the majority of metallic copper is not found with the iron, instead the iron is found with the calcium sulphide phase and the non-metallic regions. Figures 6.61 and 6.62 show examples of the copper depleted regions. The lighter phases observed in these figures belong to metallic iron and the darker regions are calcium sulphide. Figure 6.63 is a SEM image of the microstructure observed away from the silver/ copper metallic regions. Within this figure two iron droplets were observed. Figure 6.64 is a micrograph of these droplets at a higher magnification. The surrounding phase is calcium sulphide.

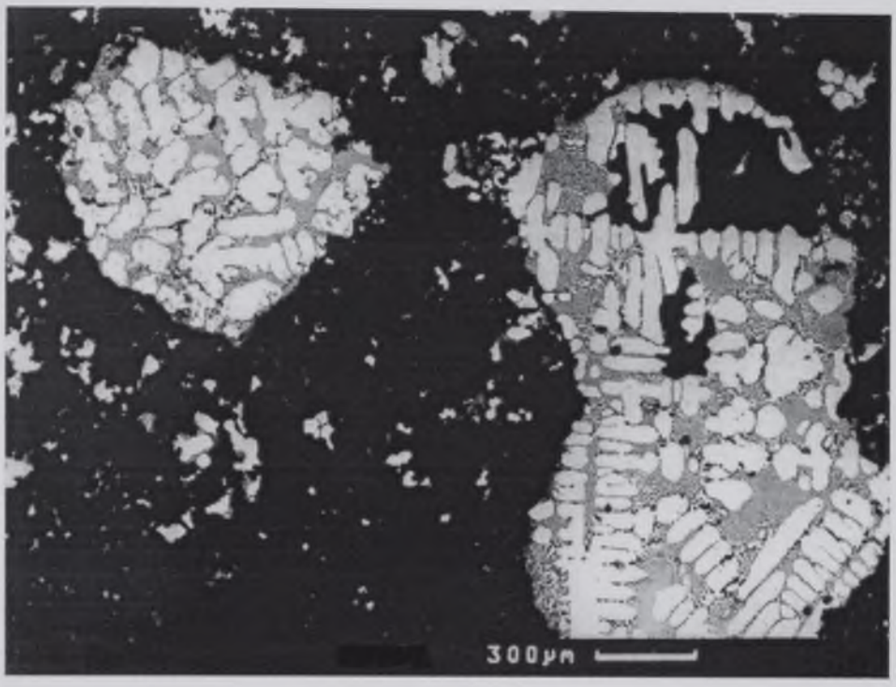

Figure 6.56 BSE image of the silver-copper eutectic observed from the reduction of chalcopyrite with 1 wt.% Ag at 1150°C for 180 minutes with a) and b) Ag and Cu elemental dot maps respectively for the eutectic phase.

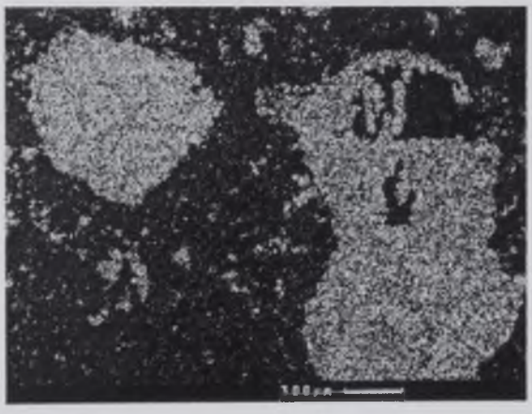

(a)

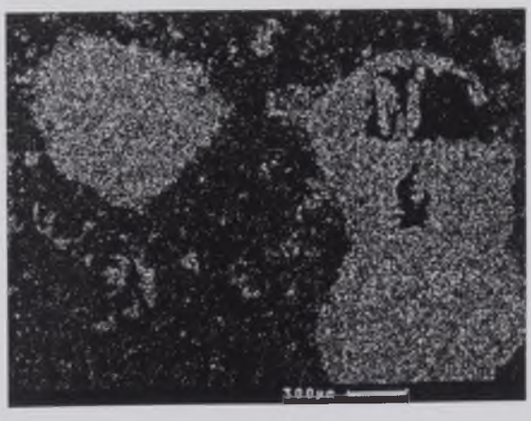

(b)

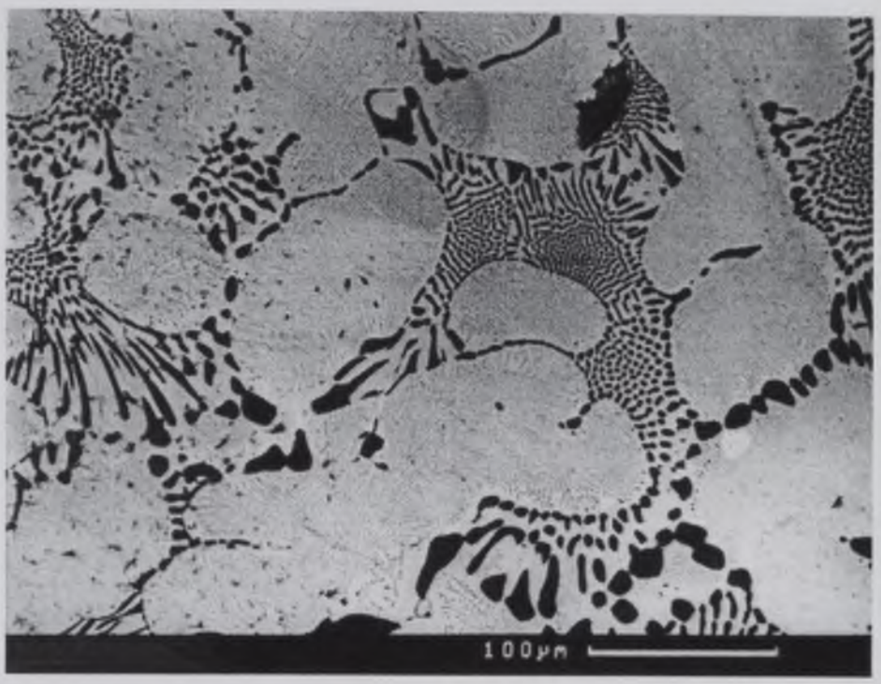

Figure 6.57 BSE image of the phases from figure 6.56 at a higher magnification with a) and b) the elemental dot maps of silver and copper respectively.

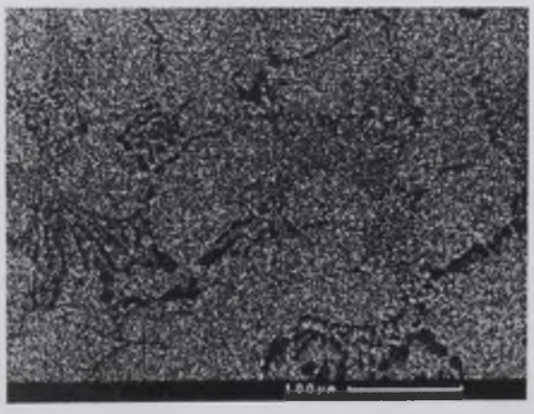

(a)

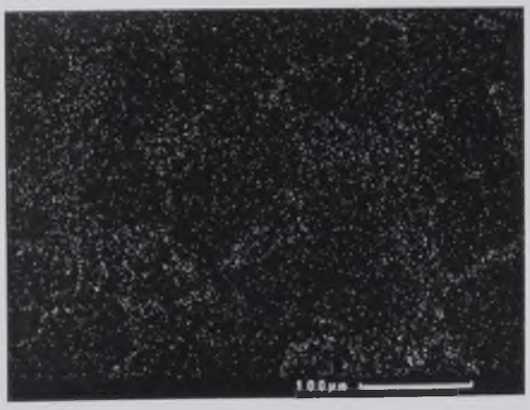

(b)

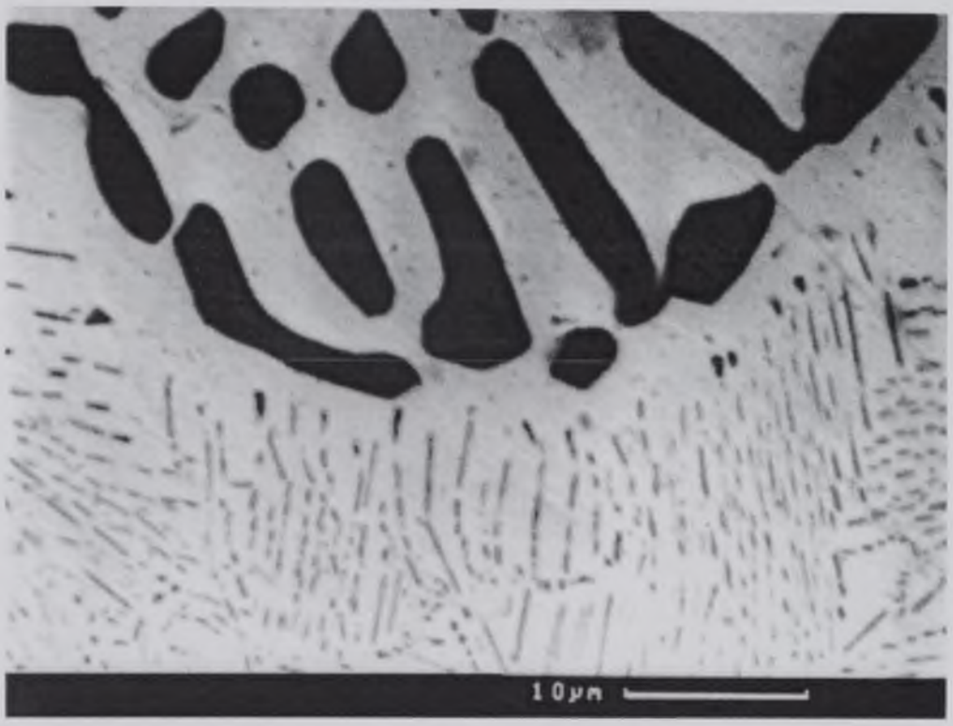

Figure 6.58 BSE image of the Ag-Cu eutectic observed in figures 6.56 and 6.57 at a higher magnification with the lightest region silver and darkest copper.

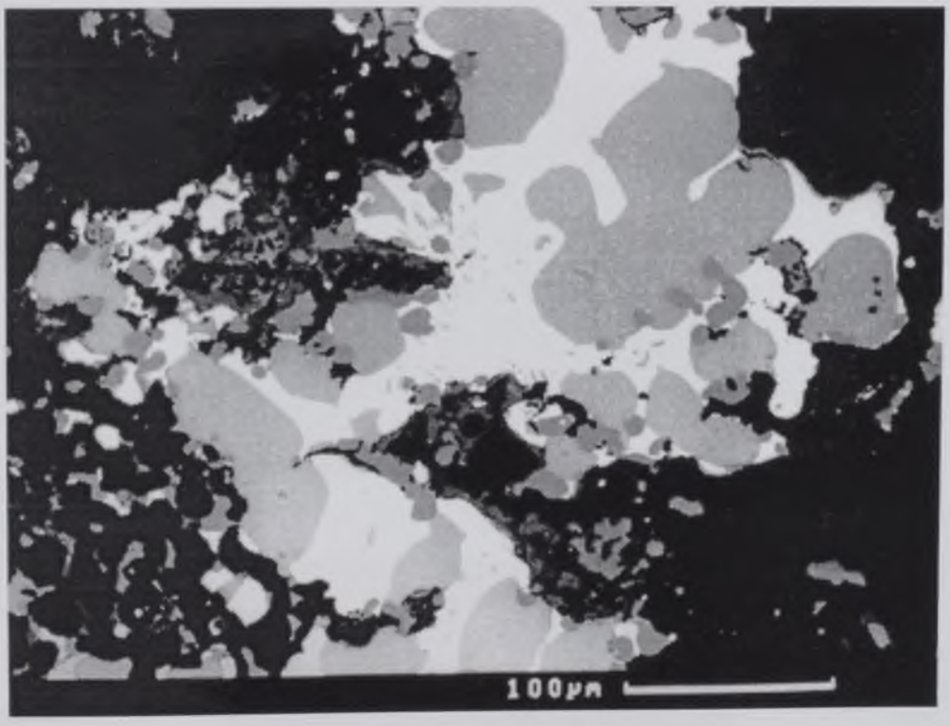

Figure 6.59 BSE image of the microstructure of chalcopyrite with 1 wt.% Ag at 1150°C for 180 minutes showing a copper-silver region where the darker region if copper and lighter silver.

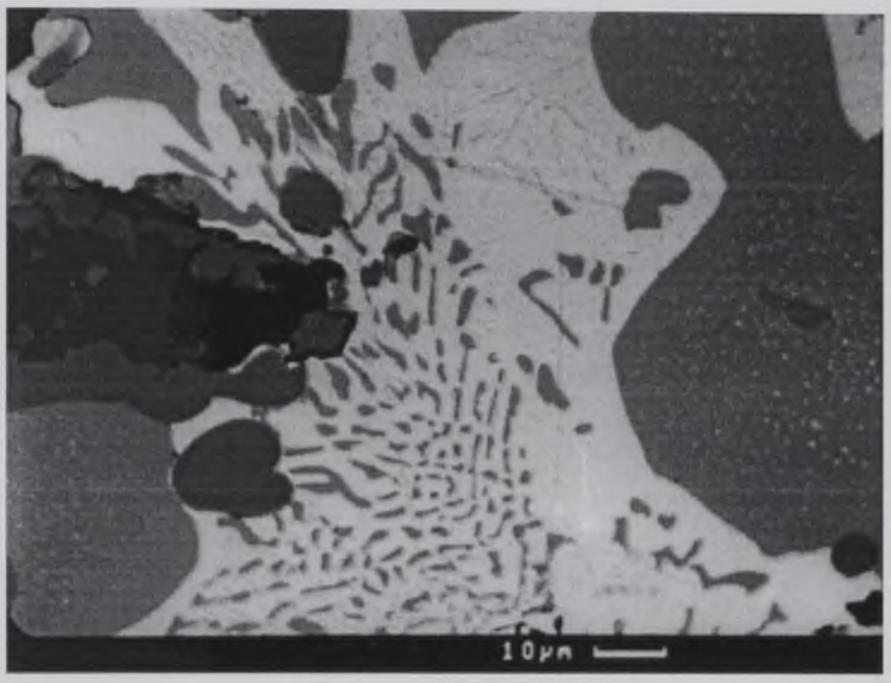

Figure 6.60 BSE image of the copper/silver region in figure 6.59 at a higher magnification, the light phase is silver and dark phase copper with a) and b) the elemental maps for Ag and Cu respectively.

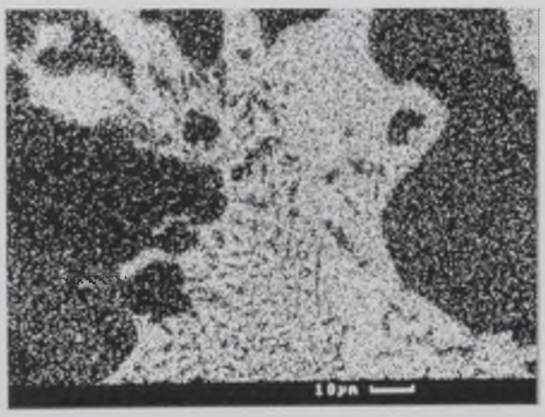

(a)

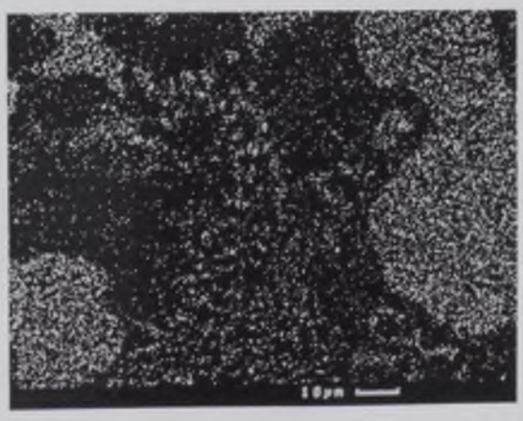

(b)

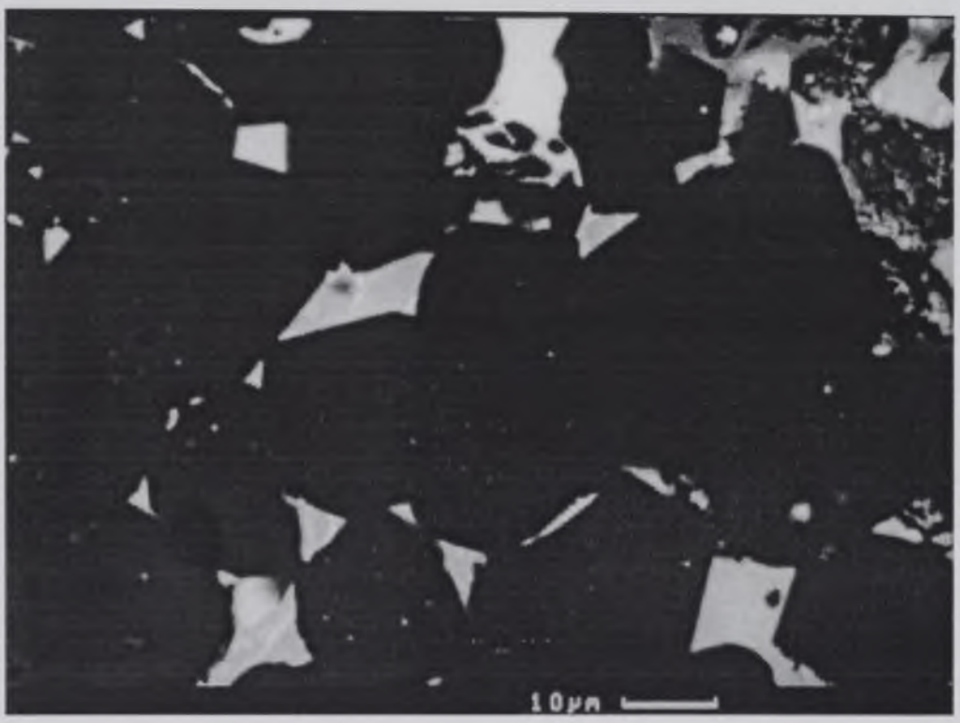

Figure 6.61 BSE image of the microstructure observed from the reduction of chalcopyrite with 1 wt.% Ag at 1150°C for 180 minutes, the darkest phase is CaS appearing with metallic iron.

Figure 6.62 BSE image of metallic iron (light) and CaS (dark) formation from the reduction of chalcopyrite with 1 wt.% Ag at 1150°C for 180 minutes.

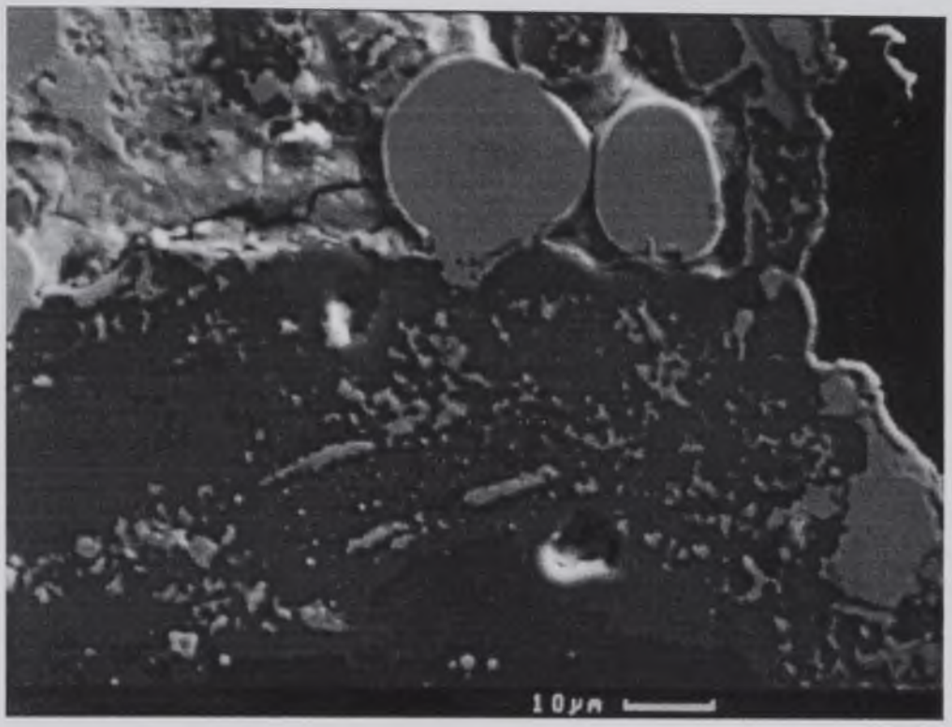

Figure 6.63 SEI of chalcopyrite with 1 wt.% Ag reduced at 1150°C, the small globules are iron surrounded by CaS and silicate phases.

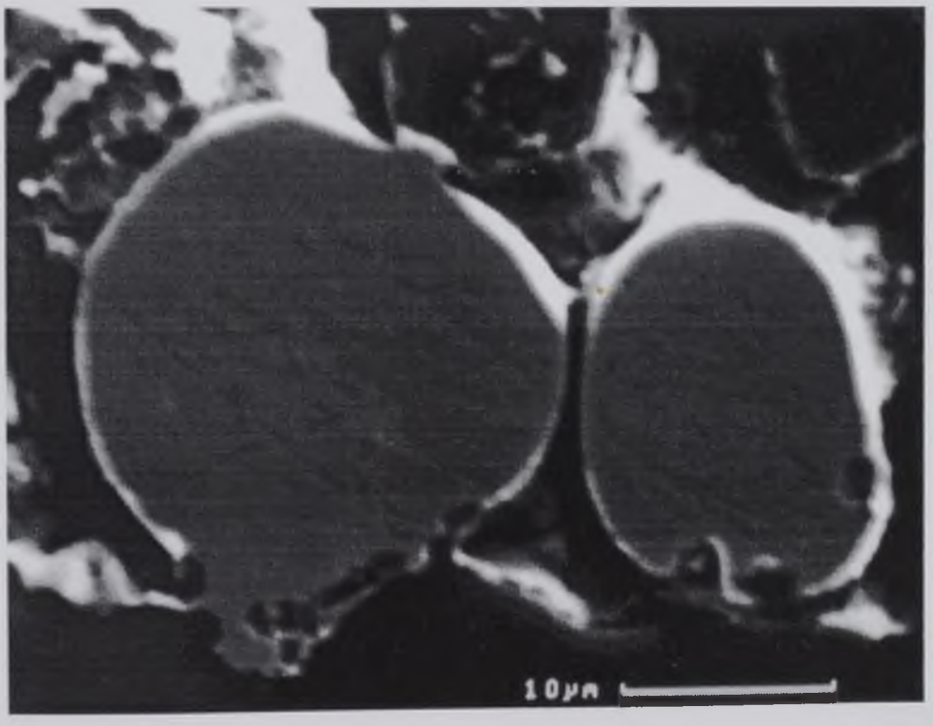

Figure 6.64 SEI of iron globules observed from figure 6.63 at a higher magnification.

6.8 Calcination of Chalcopyrite by Calcium Sulphate and Silica

In some chalcopyrite ores there are impurities present such as arsenic and antimony that are removed during copper extraction via volatilisation from the matte or during electrorefining. One possible method is to entrap these impurities together with the iron component as calcium iron silicate phases. This theory was considered in this set of experiments initially by the reaction of chalcopyrite and calcium sulphate and then by the addition of silica.

6.8.1 X-ray Analysis for Chalcopyrite with Calcium Sulphate

To help establish the reaction of chalcopyrite, calcium sulphate and silica, experiments were carried out initially on chalcopyrite and calcium sulphate. This set of experiments was carried out in a flowing argon atmosphere. The reaction conditions and the X-ray phase analysis are presented in table 6.13. The phases were identified from the JCPDS files given in appendix 1.

Temperature (°C)	Time (mins)	Identified Phases
850	60	CaS, C_{111}, $Cu_{1.96}S$, $Ca_3Fe_2(SiO_4)_3$, Ca_2SiO_4, Cu-S, $Ca_2Fe_2O_5$
900	60	CaS, C_{111}, $Cu_{1.96}S$, $Ca_3Fe_2(SiO_4)_3$, Ca_2SiO_4, $Ca_2Fe_2O_5$, Ca_3SiO_5
950	60	CaS, $Ca_3Fe_2(SiO_4)_3$, C_{111}, $Cu_{1.96}S$, Ca_2SiO_4, $Ca_2Fe_2O_5$, Ca_3SiO_5 Cu-S

Table 6.13 Summary of identified phases in descending order of intensity from X-ray diffraction analysis of heat treated mixtures of chalcopyrite and: calcium sulphate.

Figure 6.65 compares X-ray diffraction patterns for the reaction between chalcopyrite and calcium sulphate at 850°C and 950°C. These X-ray diffraction patterns are very complicated containing many peaks. Not every peak has been identified because no matches could be found in the JCPDS files. Nevertheless from the peaks analysed, compounds containing all the relevant elements have been identified.

As with the exchange reactions of chalcopyrite and lime, CaS was the predominant phase produced. This phase was found at all the reaction temperatures. The X-ray analysis revealed the formation of calcium silicates although no silica was added prior to the experiments. These compounds formed because of the silica content naturally occurring in the mineral content. The two calcium silicates identified are Ca_3SiO_5 and Ca_2SiO_4, both observed at all three temperatures.

The iron component of chalcopyrite was found in three compounds; the C_{111} oxysulphide phase, $Ca_3Fe_2(SiO_4)_3$ and $Ca_2Fe_2O_5$. At 850°C and 900°C the C_{111} phase was predominant over the other two phases but at 950°C the $Ca_3Fe_2(SiO_4)_3$ compound becomes stronger. Copper was found as the quinary oxysulphide phase C_{111}, occurring at all three temperatures. Two different forms of copper sulphide were observed from this reaction. Both $Cu_{1.96}S$ and Cu-S were observed at the three temperatures with $Cu_{1.96}S$ the predominant phase of the two.

The presence of calcium silicates, calcium iron silicates and calcium ferrites was at variance to the phases analysed from the exchange reaction between chalcopyrite and lime at similar temperatures. None of the above mentioned compounds were observed from the exchange reaction.

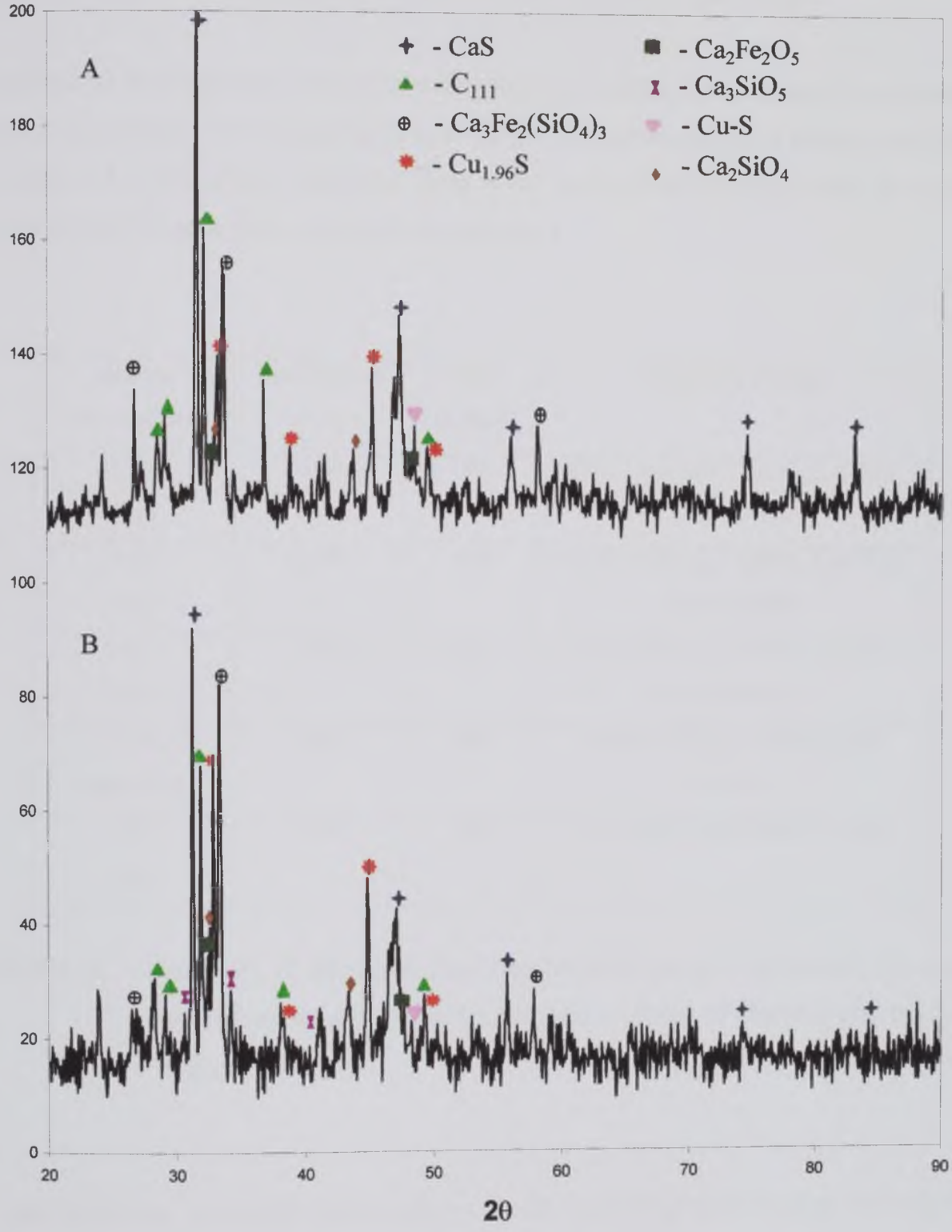

Figure 6.65 Comparison of X-ray patterns for $CuFeS_2$:$2CaSO_4$ samples reacted for 60 minutes at A-850°C and 950°C.

6.8.2 X-ray Analysis of Chalcopyrite with Calcium Sulphate and Silica

Samples of chalcopyrite with calcium sulphate and silica were reacted in a flowing argon atmosphere. The compositions and reaction conditions for each sample are listed in table 6.14. The phases identified from X-ray analysis are given in table 6.14; the JCPDS files for each phase are given in appendix 1.

Sample Composition	Temperature (°C)	Time (mins)	Identified Phases
1:2:1 (2g)	1000	180	CaS, $Ca_3Fe_2(SiO_4)_3$, C_{111}, Cu-S, Ca_2SiO_4
1:2:1 (2g)	1100	180	$Ca_3Fe_2(SiO_4)_3$, Ca_3SiO_5, Ca_2SiO_4, Cu-S, Fe_2SiO_4
1:2:1 (50g)	1100	180	$Ca_3Fe_2(SiO_4)_3$, Ca_3SiO_5, Ca_2SiO_4, Cu-S, $Ca_3Si_2O_7$
1:2:1 and Cu layer (2g)	1100	180	$Ca_3Fe_2(SiO_4)_3$, Ca_3SiO_5, CuS, Ca_2SiO_4
1:3:2 (2g)	1100	180	$Ca_3Fe_2(SiO_4)_3$, Ca_3SiO_5, CuS

Table 6.14 Summary of identified phases in descending order of intensity from X-ray diffraction analysis of heat treated mixtures of chalcopyrite, calcium sulphate and silica.

A comparison of X-ray diffraction patterns for this set of experiments is given in figure 6.66. These patterns are very complicated as with those from the reaction between chalcopyrite and calcium sulphate. A reasonable amount of phases were identified and are presented in table 6.14. Some peaks have not been assigned phases as matches could not be made to the JCPDS files. Despite this, the phase analysis of heat treated samples of chalcopyrite, calcium sulphate and silica indicated the phases present containing all of the elements present in the initial mixtures.

At 1000°C CaS is the predominant phase observed from X-ray analysis. However above this temperature this phase was not observed. The C_{111} phase was also present at this temperature and as with CaS was not observed above 1000°C. These two phases were formed with $Ca_2Fe_2(SiO_4)_3$, Cu-S and Ca_2SiO_4. All of these phases are similar to those observed at 950°C for the reaction between chalcopyrite and calcium sulphate. Copper was only observed to be present as one sulphide from X-ray analysis of the mixture of chalcopyrite, calcium sulphate and silica heat treated at 1000°C. Copper was also found at its sulphide phase at 1100°C, when copper shot was added prior to the reaction at 1100°C copper is found present as the CuS form of copper sulphide.

At 1100°C the predominant phase observed was $Ca_3Fe_2(SiO_4)_3$. This calcium iron silicate was found as the predominant phase for experiments at 1100°C, with additions of copper shot and change in ratio of $CuFeS_2$:$2CaSO_4$:SiO_2 to $CuFeS_2$:$3CaSO_4$:$2SiO_2$. Calcium ferrites were not observed from this set of experiments. Three calcium silicate phases were observed: Ca_2SiO_4, Ca_3SiO_5 and $Ca_3Si_2O_7$.

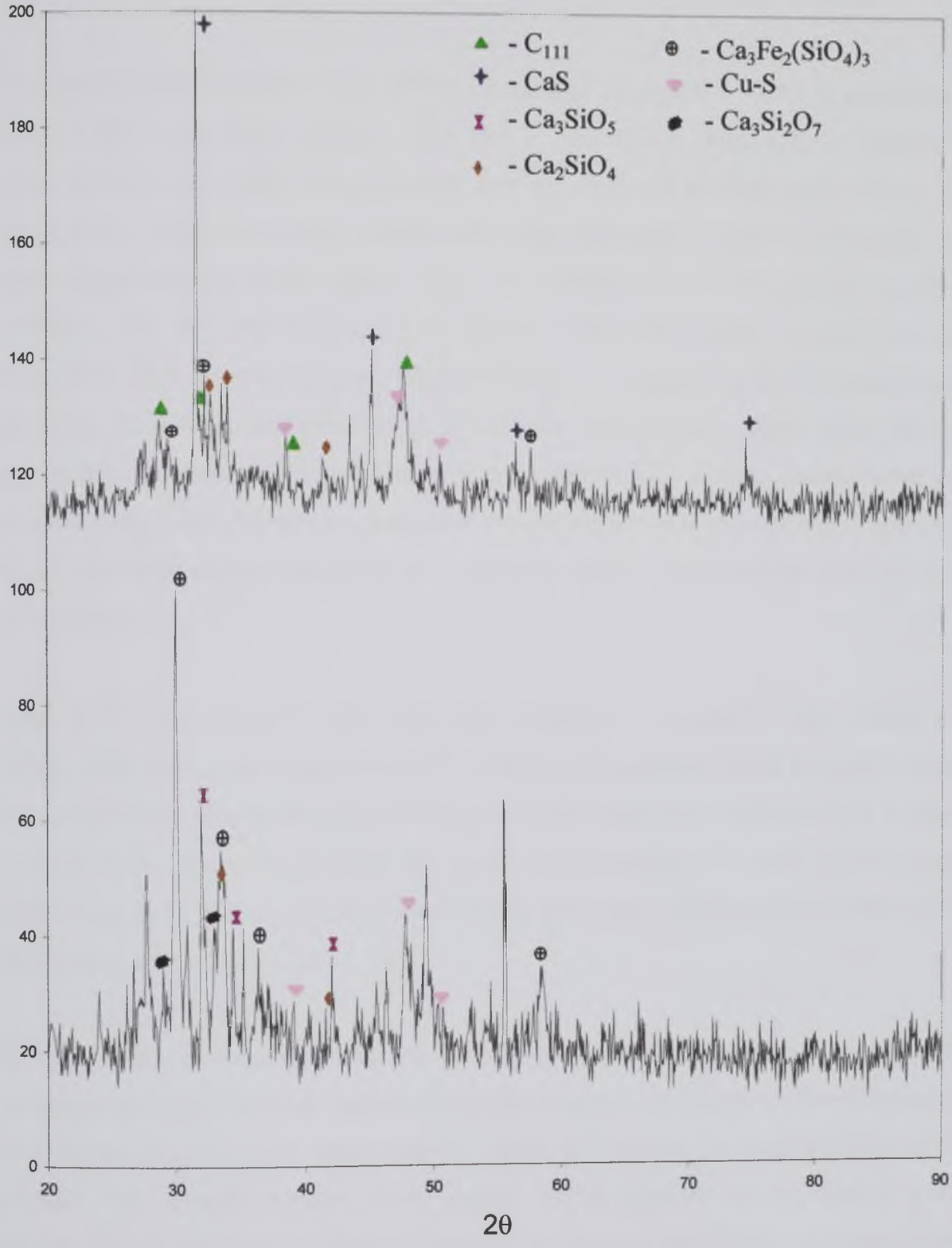

Figure 6.66 Selected X-ray diffraction patterns for chalcopyrite heat treated with $CaSO_4$ and SiO_2; A-1000°C/180 mins, B-1100°C/180 mins and C-1100°C/180 mins (I wt.% Cu).

6.8.3 Electron Microscopy of Chalcopyrite Calcined in the Presence of Silica

The general microstructure observed from a sample reacted at 1100°C is presented in figure 6.67. A dendritic phase is observed in this figure. Figure 6.68 depicts the microstructure on a higher magnification; here the dendrites are seen more clearly with the primary dendrites running horizontally along the image. Figure 6.69 again is a higher magnification of the region, this time to demonstrate the composition of the dendrites. The dot map of figure 6.70 indicates that this dendrite phase is an iron compound. EDX analysis suggests this compound to be an iron oxide. The surrounding light grey phase to the dendrites in figure 6.69 is a calcium ferrite phase whilst the dark grey phase is calcium silicate. These calcium ferrite and silicate phases were also detected from X-ray diffraction analysis of the samples prior to microscopy. Figure 6.71 shows the large region identified as containing copper and sulphur assumed to be copper sulphide.

Figure 6.72 is an image of nearly the whole sample of chalcopyrite heat treated with $CaSO_4$, SiO_2 and copper metal at 1100°C. The lightest areas are where the added copper metal was found. One such region of copper was chosen for investigation and is shown in figure 6.73. According to EDX the reaction did not affect the bulk of the copper added. Copper sulphide was found surrounding the copper. This phase was detected by EDX analysis shown by figure 6.74.

Figure 6.75 is a micrograph of the top of the copper metal, the lightest areas are of the metallic copper and these are surrounded by the copper sulphide phase. There appears to be a channel leading to the copper metal. Figure 6.76 is a higher magnification of this channel. This channel leading to the copper metal, depicted as the darkest phase, appears to be calcium iron silicate. The lightest phase is identified as calcium ferrite whilst the medium grey phase is calcium silicate. EDX analysis of this area did not give any detection of copper nor copper sulphide. In other regions of the sample the silicate and ferrite phases are in evidence. No further observations of copper were found other than regions similar to that of figure 6.73.

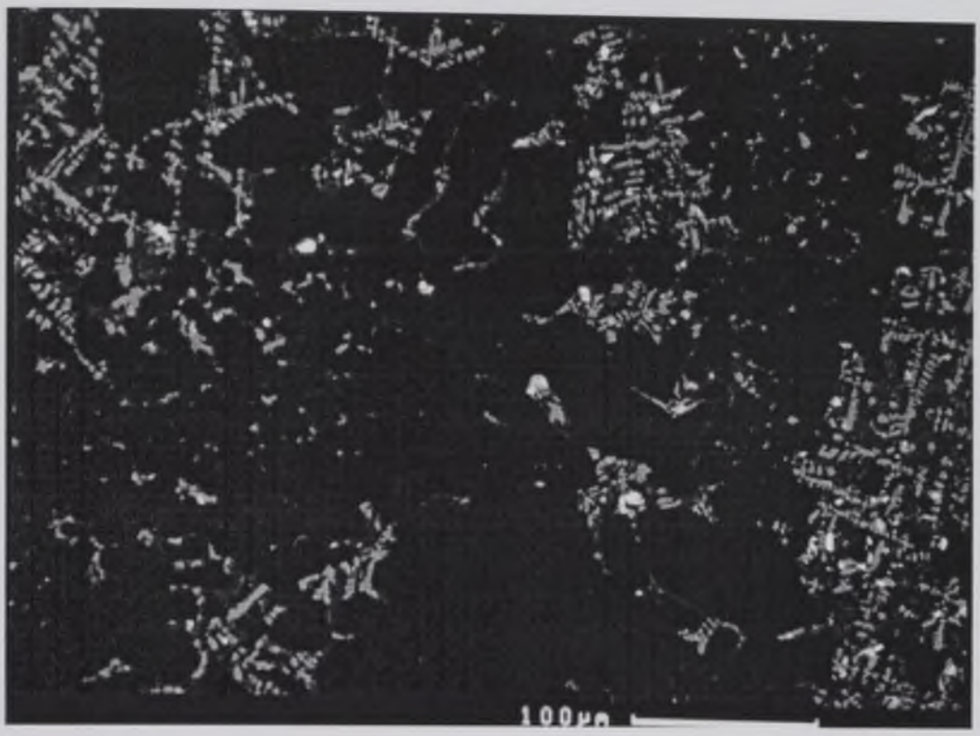

Figure 6.67 BSE image of the general microstructure observed from the heat treatment of $CuFeS_2$:$2CaSO_4$:SiO_2 at 1100°C for 180 minutes.

Figure 6.68 BSE image of the microstructure observed in figure 6.67 at a higher magnification showing dendritic iron oxide formation.

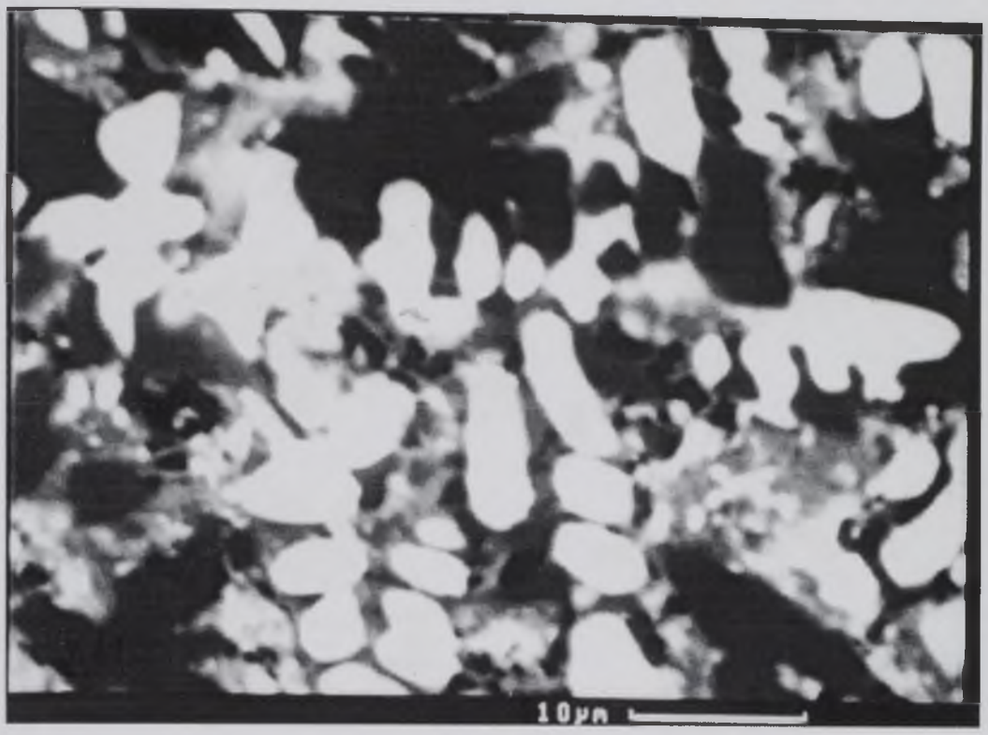

Figure 6.69 BSE image of the dendritic structure of figure 6.68 at a higher magnification.

Figure 6.70 Iron elemental dot map for figure 6.69 of the dendritic phase.

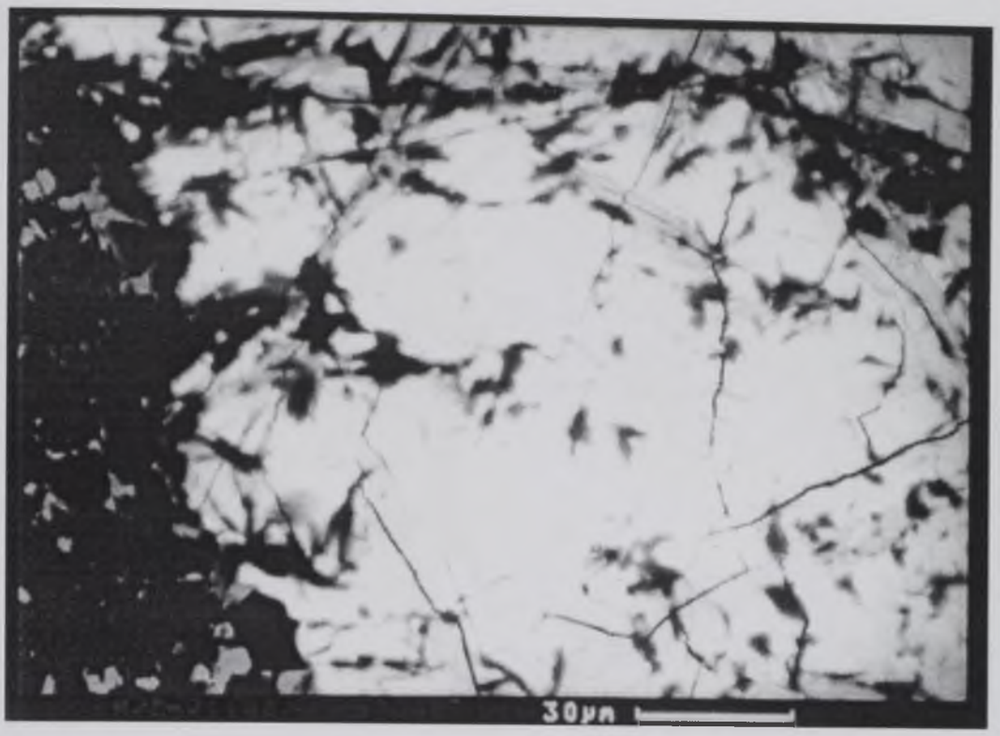

Figure 6.71 BSE image of the microstructure observed from the heat treatment of $CuFeS_2$:$2CaSO_4$:SiO_2 at 1100°C for 180 minutes, showing the formation of copper sulphide.

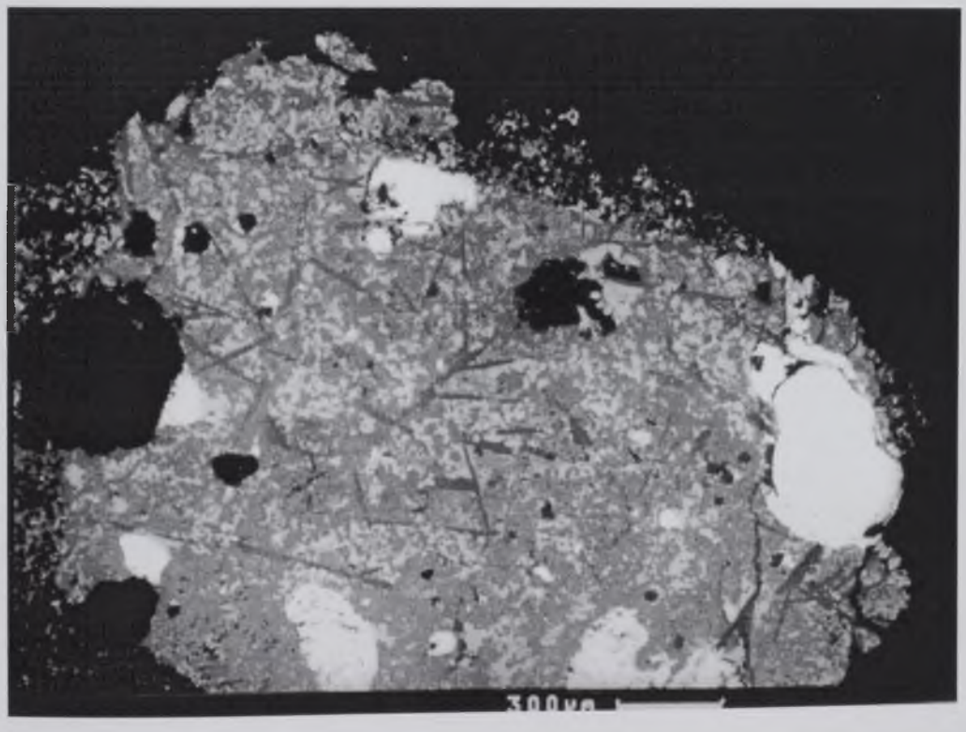

Figure 6.72 BSE image of the sample of $CuFeS_2$:$2CaSO_4$:SiO_2 with added Cu metal heat treated at 1100°C for 180 minutes.

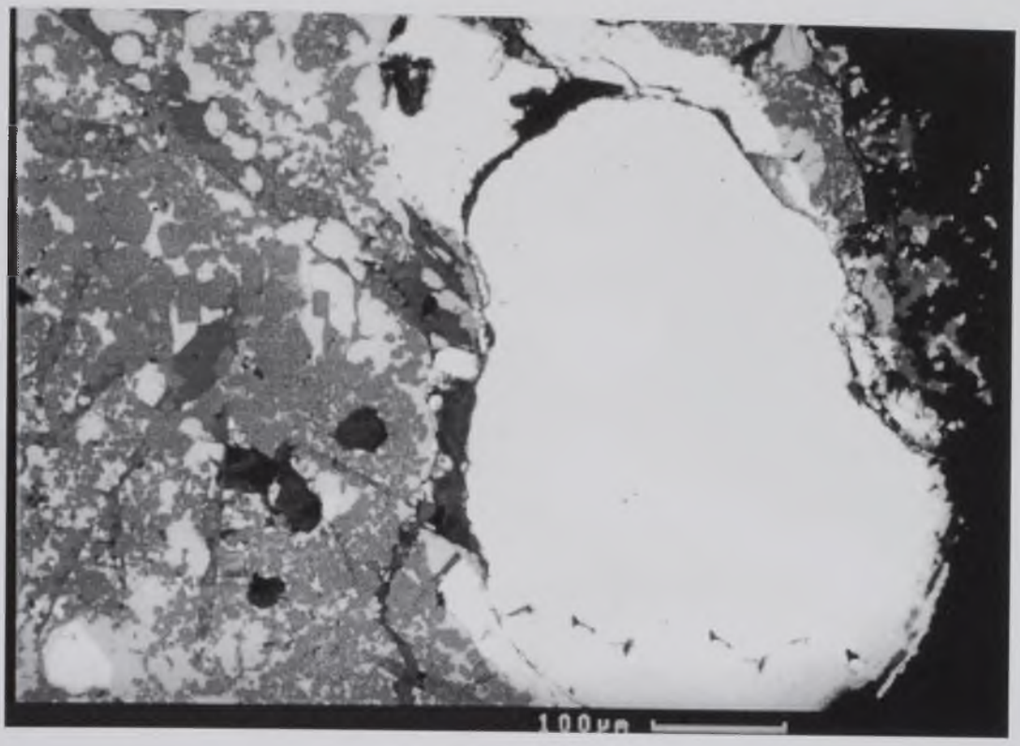

Figure 6.73 BSE of a region of added copper from figure 6.78 at a higher magnification.

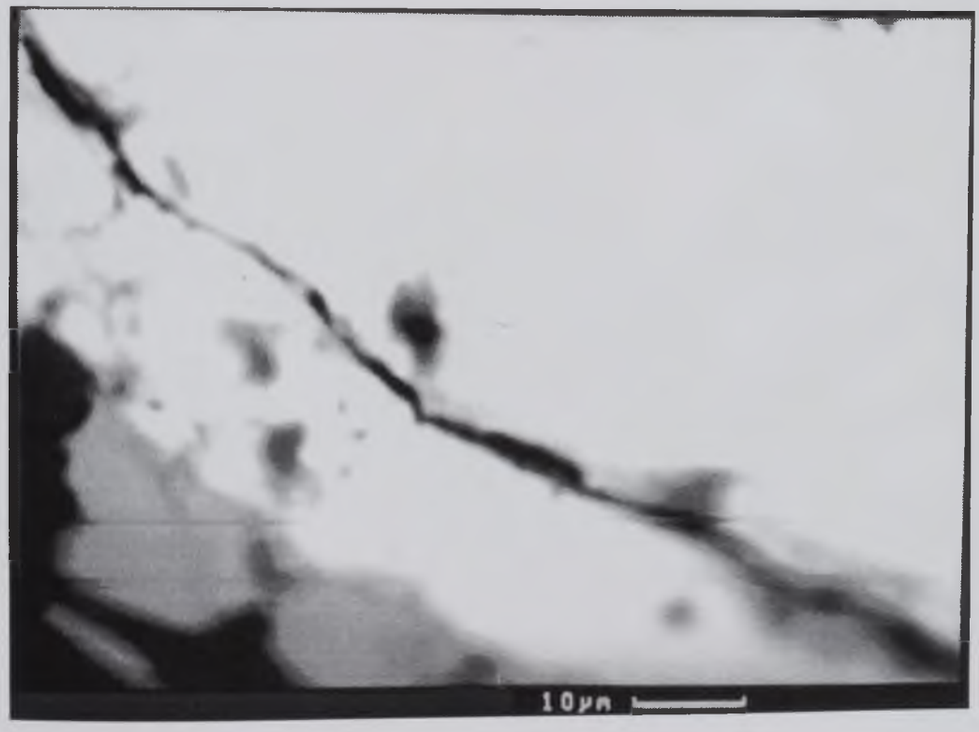

Figure 6.74 BSE image of the boundary to the copper region of figure 6.73 showing copper metal surrounded by a layer of copper sulphide.

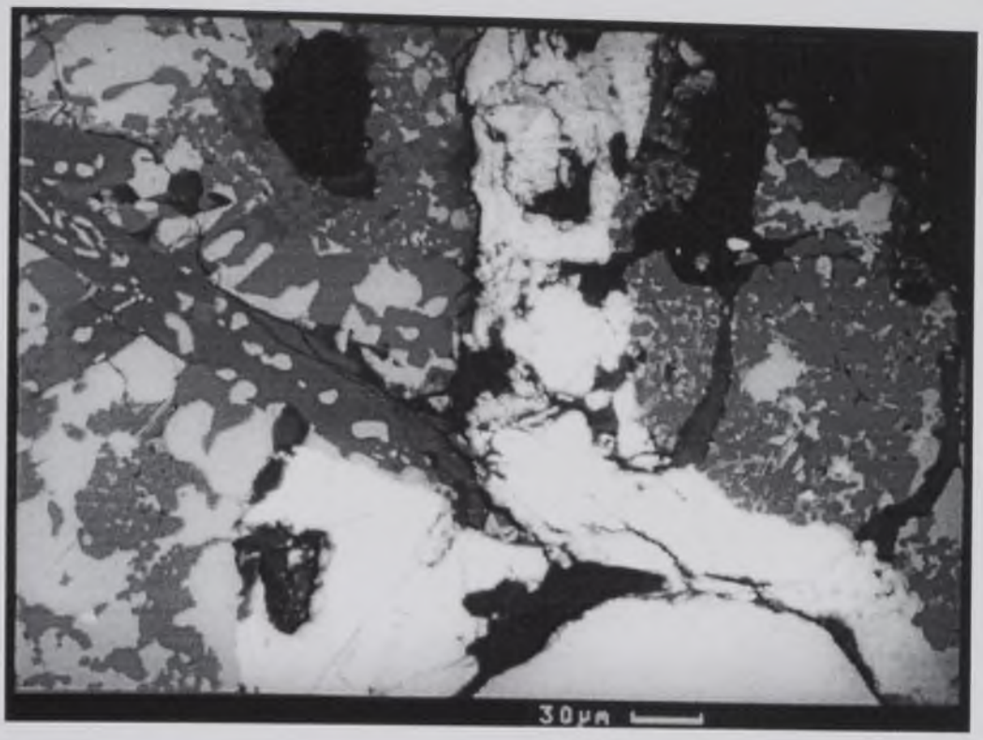

Figure 6.75 BSE image taken at the top of the copper region of figure 6.73.

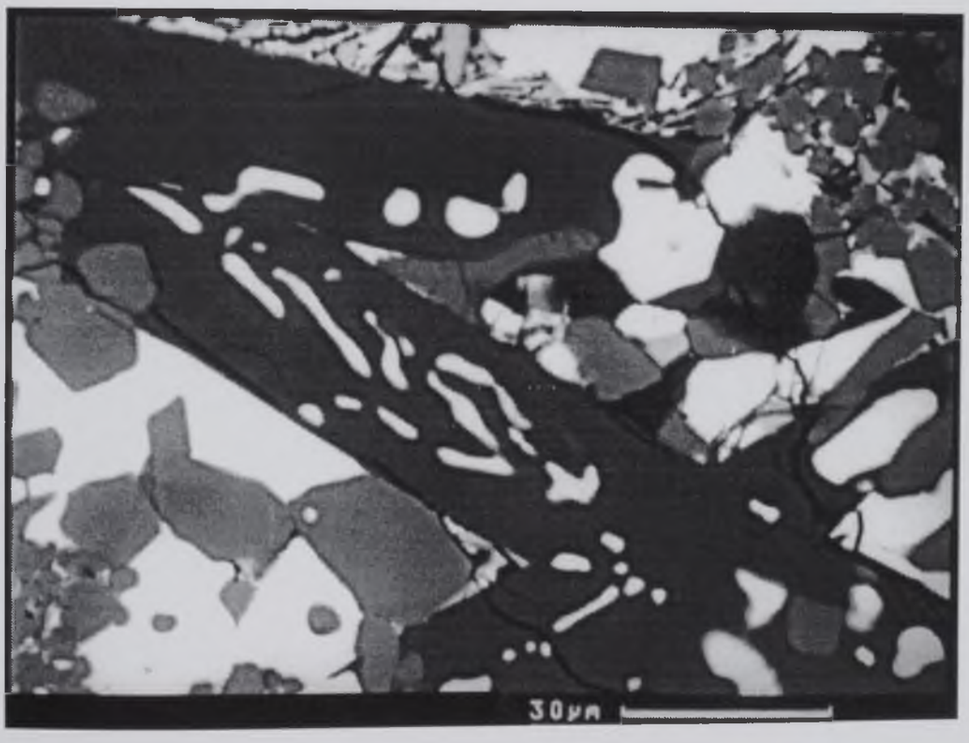

Figure 6.76 BSE image at a higher magnification of the region leading to the top of the copper region in figure 6.73.

CHAPTER SEVEN

Discussion

7.1 Introduction

A discussion of the results presented in chapter six is given in this chapter. Section 7.2 will offer a discussion of the results pertaining to the reduction of chalcopyrite. In section 7.3 the results from reactions of chalcopyrite, calcium sulphate and silica are given.

7.2 Carbothermic Reduction of Chalcopyrite in the Presence of Lime

The results relating to the reduction of natural chalcopyrite are discussed in this section. Initially the discussion deals with the heat treatment between chalcopyrite and lime. A discussion of the reduction reaction follows with emphasis placed on the effects of activated carbon, sample size, Ag_2S and Ag additions on the reduction reaction.

7.2.1 Reaction between Chalcopyrite and Lime

In theory the reaction between a metal sulphide and lime should yield calcium sulphide and the metal oxide as shown in equation 7.1. The reaction results in the exchange of S^{2-} and O^{2-} ions between the sulphide and lime.

$$MS_{(s)} + CaO_{(s)} = MO_{(s)} + CaS_{(s)} \qquad (7.1)$$

However, in practice this does not happen for most metal sulphides especially complex sulphides. Certainly from the reaction between the natural chalcopyrite concentrate and lime, neither copper oxide nor iron oxide form although CaS does. One of the few sulphides reacted with lime to yield the metal oxide is nickel sulphide (Machingawata et al. 1989). Most authors observed the production of intermediary oxysulphide phases

along with CaS. For example the reaction between ZnS and CaO yielded ZnCaSO (Igiehon et al. 1994c).

The main product of the reaction between the natural chalcopyrite mineral concentrate and lime is calcium sulphide. The compound is found as the predominant phase forming from the reaction in the temperature range 850°C to 1200°C. The copper and iron components of the mixture are partially oxidised as a result of this reaction and combine with CaO to form intermediate oxysulphide phases. These are C_{III} and C_{II}, the C_{III} phase occurs at all temperatures in the range 850°C to 1200°C whereas the C_{II} phase is only identified from 900°C to 1200°C.

Jha and co-workers (1992b, 1992a) previously identified the C_{III} and C_{II} phases. Jha and Grieveson (1992b) determined the d-spacings and hkl values for the C_{III} phase based upon the reaction between synthesised chalcopyrite and lime. The X-ray diffraction analysis for natural chalcopyrite reacted with lime from the current study was at variance with those for synthesised chalcopyrite, therefore an attempt to re-define the d-spacings, assigned hkl values and lattice parameters was carried out for this phase. A proposed crystal structure for this compound is given in figure 6.8 (page 105). The C_{III} phase appears to be a solid solution of the FeO.CaS (C_{II}) phase with Cu^{+} ions replacing Fe^{2+} ions in the idealised C_{II} crystal lattice. The calculated lattice parameters, a and c, change with differing temperature and reaction condition due to the extent of replacement of iron by copper. The ionic radii for Fe^{2+} and Cu^{+} are 0.074nm and 0.096nm respectively. The determined data for this compound both analytically and experimentally agree with respect to the structure and d-spacings.

However, despite extensive investigations being carried out on the C_{III} phase, this study does not prove conclusively the crystallographic data for this phase. The C_{III} phase is a complex phase; therefore the determination of this phase is very difficult. Despite this difficulty a good attempt was made. For the purposes of the current study, assumptions of the structure are made based upon numerous evaluations, including X-ray diffraction analysis and electron microscopy. It is concluded that the analysis for the C_{III} phase in this study is an improvement on the initial analysis reported by Jha and Grieveson (1992b) from the reaction of synthetic chalcopyrite and lime. The determination for the

compound from synthetic chalcopyrite was based on fewer analyses. Where there have been reports of intermediary oxysulphides being observed, little or no work has been completed to investigate these phases.

From continued comparison to the work on synthesised chalcopyrite further differences in phase analysis were observed. Jha and Grieveson (1992b) observed the formation of a third oxysulphide phase, C_1, of the formula 4FeO.3CaS at 900°C and 1000°C. The C_1 phase was not detected from X-ray analysis of natural chalcopyrite reacted with lime. Instead the C_{11} phase was observed from this reaction which is in disagreement with the research on the synthesised compound. The authors reported no evidence for the C_{11} phase.

At 1100°C metallic copper is produced from the reaction between natural chalcopyrite and lime in agreement with the research on synthesised chalcopyrite although the metal was also detected at the lower temperatures of 900°C and 1000°C for synthesised chalcopyrite. The formation of metallic copper from the reaction between chalcopyrite and lime is given in equation 7.2.

$$CuFeS_{2\,(s)} + 2CaO_{\,(s)} = Cu_{\,(s)} + FeO.CaS_{\,(s)} + CaS_{\,(s)} + \tfrac{1}{2}\,O_{2\,(g)} \qquad (7.2)$$

Other metal sulphides also yield the metal from the reaction with lime: an example is lead, produced from its sulphide at 900°C and 1000°C (Igiehon 1992). Metallisation also occurs from the reaction of other complex metal sulphides, for example arsenopyrite (FeAsS), famatinite (Cu_3SbS_4) and tetrahedrite ($Cu_{12}Sb_4S_{13}$) (Igiehon 1994a, 1994b).

Although metallic copper forms from the reaction of chalcopyrite, considered to be a complex metal sulphide, and lime, metallic iron never forms. This observation is in agreement with the findings from synthesised chalcopyrite. Instead this component of chalcopyrite is found as either one or both of the two oxysulphide compounds, C_{111} and C_{11}. Vert and Kamenstev (1956) report the formation of calcium ferrites from the reaction between FeO and CaS. However, these phases were not detected in reacted chalcopyrite and lime.

7.2.2 Carbothermic Reduction of Chalcopyrite in the Presence of Lime

Metallic copper and iron are both formed from the reduction of chalcopyrite by carbon in the presence of lime. The other phases evolved are CaS, C_{111} and C_{11}. Calcium sulphide is the predominant phase produced from reduction, as expected from equation 7.3:

$$CuFeS_{2\,(s)} + 2CaO_{(s)} + 2C_{\,(s)} = Cu_{\,(s)} + Fe_{\,(s)} + 2CaS_{\,(s)} + 2CO_{\,(g)} \qquad (7.3)$$

At low temperatures, 850° and 900°C, residual lime was detected; above 900°C, this reactant phase disappears completely. Neither of the other reactants, $CuFeS_2$ and carbon were observed from phase analysis. The weight loss data for this temperature showed a low percentage yield: in the 120 minute reaction period only 40% reduction occurred.

Calcium sulphide was observed at the lowest temperature (850°C) and shortest reaction time (5 minutes). The CaS phase is the first product of the reduction reaction in the same way that it is the first product of the reaction between chalcopyrite and CaO. C_{111} appears in the temperature range 850°C to 900°C, whilst C_{11} is found from 900°C to 950°C. Similarly, these phases were also observed from the reaction of chalcopyrite and lime at these, and higher temperatures.

Initial observations of the percentage reduction curves as a function of time, of figures 6.9 and 6.11 on pages 108 and 110 respectively, suggest two different processes occur at each temperature. The initial fast rate of reaction is found in the first five minute period of reduction. This is subsequently followed by a slower reaction rate. Various kinetic equations were applied to the weight loss data obtained from TGA analysis to provide appropriate models for the reduction mechanism. Figure 7.1 is an example of the weight loss data at 900°C with the two kinetic equations that apply. Line 1 represents the first stage of the reduction with data plotted to the kinetic equation 7.4. Line 2 is data according to the kinetic equation 7.5. The modelling of data in this way provides evidence for the two stage reduction.

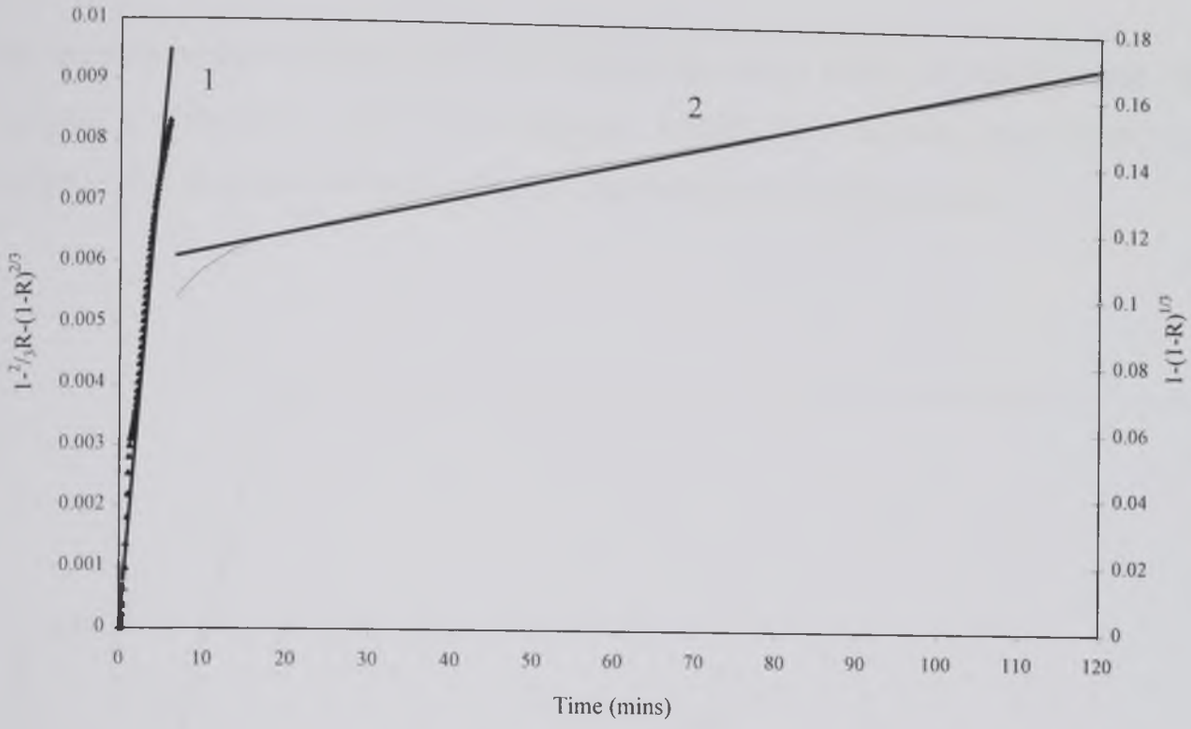

Figure 7.1 Data from weight loss at 900°C plotted according to two different applicable kinetic equations.

The first stage can be represented by a solid/ solid reaction, equation 7.4, where a reaction occurs between all initial starting powders. The products of this reaction are CaS and the intermediary oxysulphides, C_{111} and C_{11}. X-ray analysis and electron microscopy give evidence for the production of these phases during the first stage of reduction. The weight loss is due to carbon monoxide evolution; none of the reactant carbon powder was present in samples analysed by analysis of the reacted samples.

$$CuFeS_2 + CaO + C = C_{11}/C_{111} + CaS + CO \qquad (7.4)$$

$$S_1 + S_2 + S_3 = S_4 + S_5 + G_1$$

From preliminary modelling the kinetic equation representing the first stage of reduction is given as equation 7.5. Figure 7.2 is a plot of data according to this equation for each temperature as a function of time.

$$1 - {}^3/_3 R - (1-R)^{2/3} = kt \qquad (7.5)$$

The fraction reacted is given as R, the time of reaction, t and k the rate constant. This equation is obeyed for 900°C (0-6 minutes), 1000°C (0-4 minutes) and 1100°C (0-1 minute). This reaction is an example of a chemically controlled reaction.

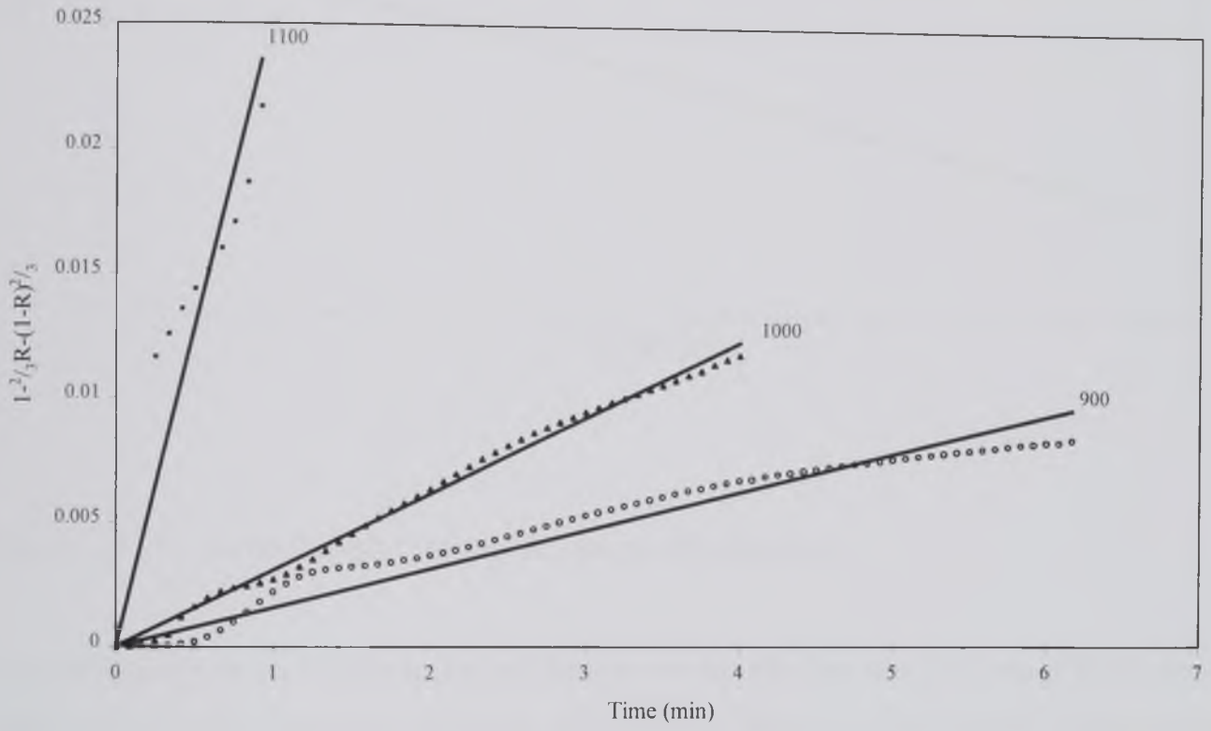

Figure 7.2 Data of fraction reduced plotted according to equation 7.5.

For each temperature the slope from figure 7.2 was determined, hence k was evaluated. These values are plotted as an Arrhenius plot in figure 7.3 to investigate the effect of temperature on the reaction. The plot of log k against 1/T gives a straight line from which the activation energy for the reaction was determined as 97.45 kJ mol^{-1} within the temperature range 900 to 1100°C. The plot shows a good fit at 900.C and 1100.C but less so at 1000°C.

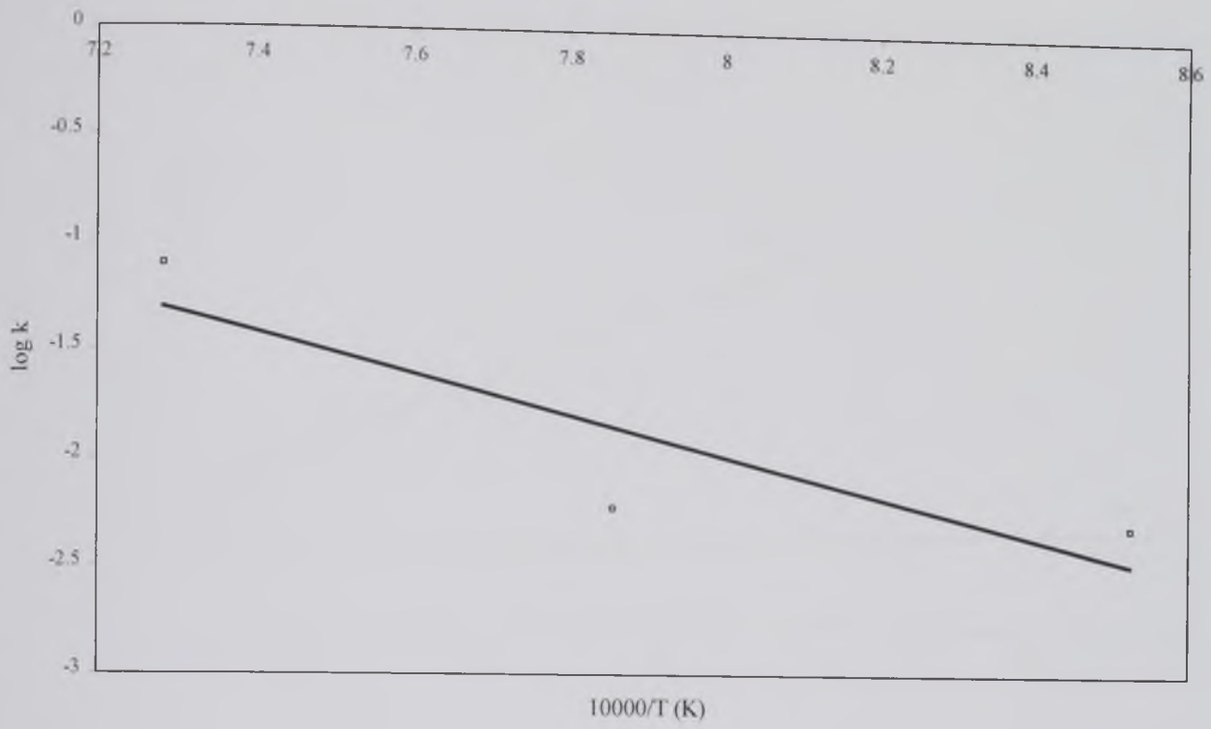

Figure 7.3 Arrhenius plot for the first stage of reduction.

From observations of the percentage reduction versus time curves, the rate of the second step is slower than that of the first step. As shown in figure 7.1, the kinetic equation that best applies to this stage of reduction is equation 7.6. The kinetic data is plotted against this equation in figure 7.4 for each temperature.

$$1-(1-R)^{1/3} = kt \qquad (7.6)$$

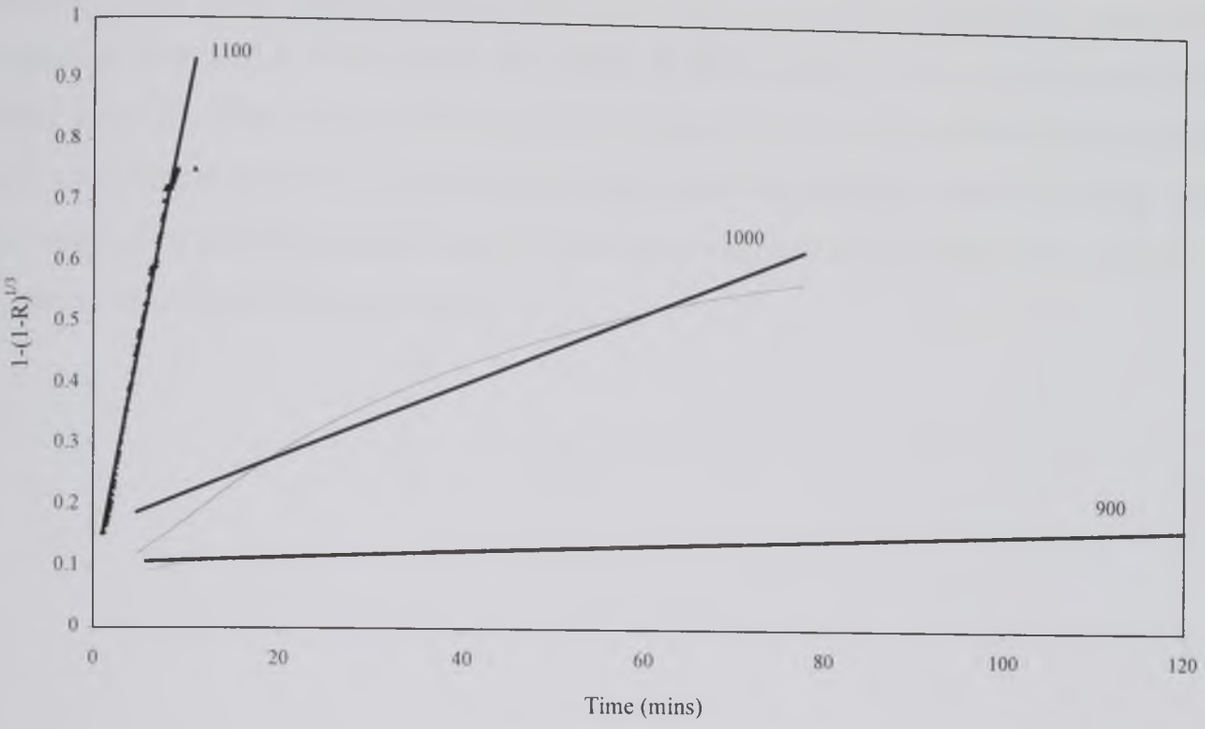

Figure 7.4 Plot of kinetic data for equation 7.6.

For the second stage of reduction the reaction can be represented by equation 7.7.

$$C_{11}/C_{111} + CO = Cu + Fe + CaS + CO_2 \qquad (7.7)$$

$$S_1 + G_1 = S_2 + S_2 + S_3 + G_2$$

The final products of this reaction are metallic copper and iron with further CaS. The weight loss during this stage is due to carbon dioxide evolution. This stage occurs over a longer period of time than the first step. The second step is indicative of diffusion control. Due to the time period over which the diffusion controlled reaction occurs several reaction products were observed. X-ray analysis and electron microscopy point to various reaction products. At lower temperatures and times, the products are generally CaS and the oxysulphide compounds. As the temperatures and times increase the metallic phases begin to be observed.

In figure 7.5 an Arrhenius plot for the second stage of reduction is given. From the slope of this plot in the temperature range 900 to 1100°C, the activation energy is 32.24

kJ mol^{-1}. This value agrees with the expected range of values for diffusion controlled reactions. The weight loss during this stage of the reaction is due to CO_2 evolution rather than CO. The microscopical analysis indicated the reacted mixtures being porous. This observation was true at all reaction times and temperatures further agreeing with the conclusion that the second stage of reduction is diffusion controlled. This control is characteristic of solid/ gas reactions.

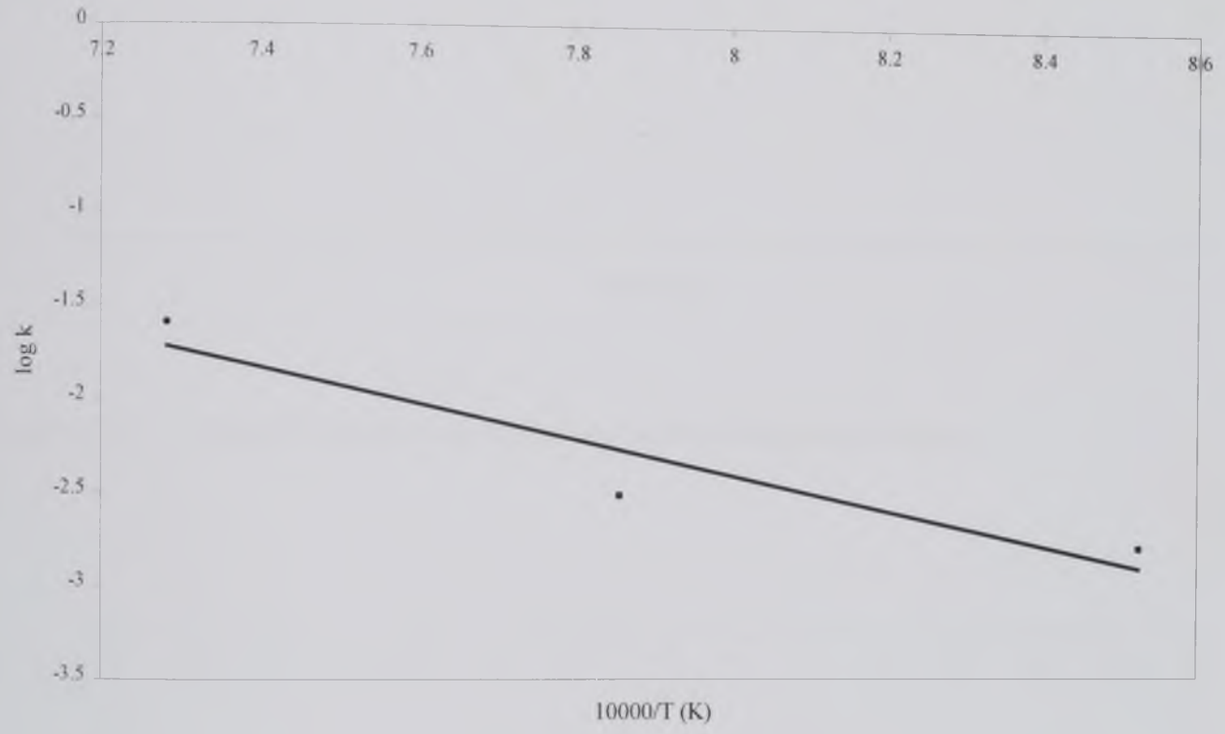

Figure 7.5 Arrhenius plot for the second stage of reduction.

Although two rates occur during the reduction reaction, it is still useful to know the overall activation energy for the process. Therefore, from measurements obtained at each temperature on the TGA furnace the rate constants were determined, the plot to determine the rate for reduction is given in figure 7.6. From this graph the values for k were determined at each temperature and hence an Arrhenius plot was constructed for the reduction reaction. The rate dependence on temperature fits well a straight line in the temperature range of 900°C to 1100°C. This plot is given as figure 7.7 from which the activation energy is derived as 106.05 kJ mol^{-}.

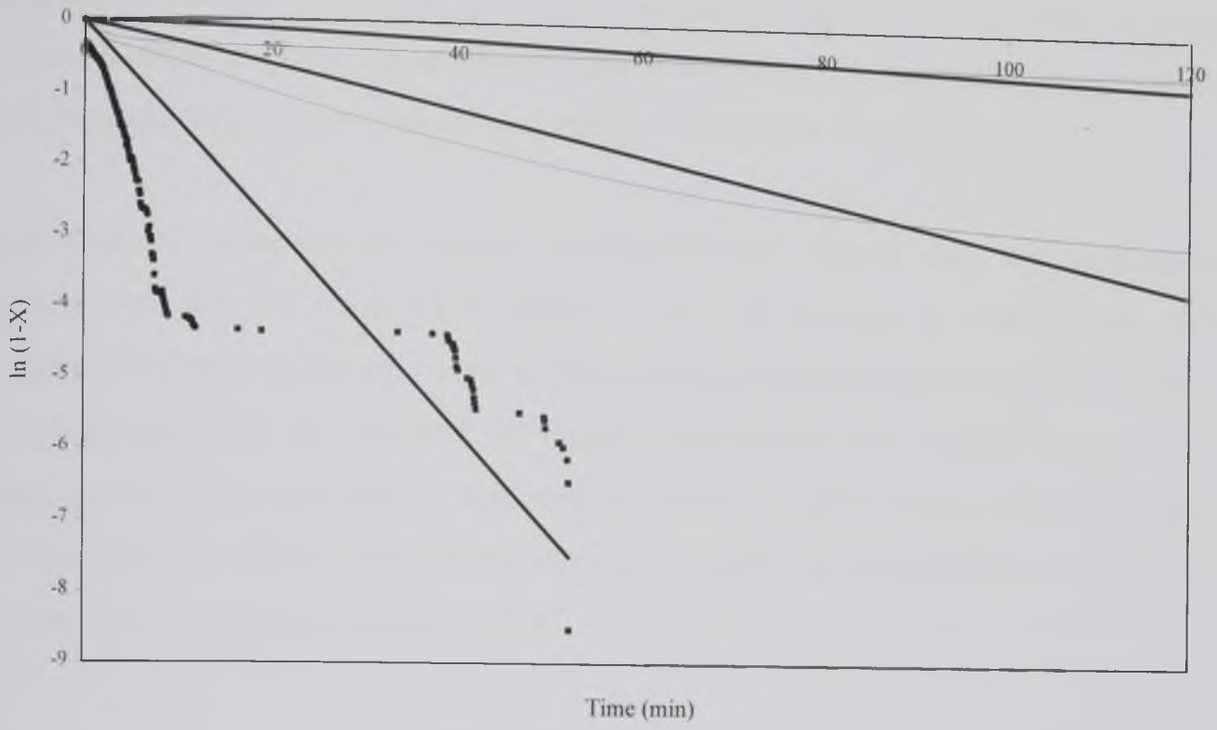

Figure 7.6 Plot of kinetic data for the complete reduction reaction.

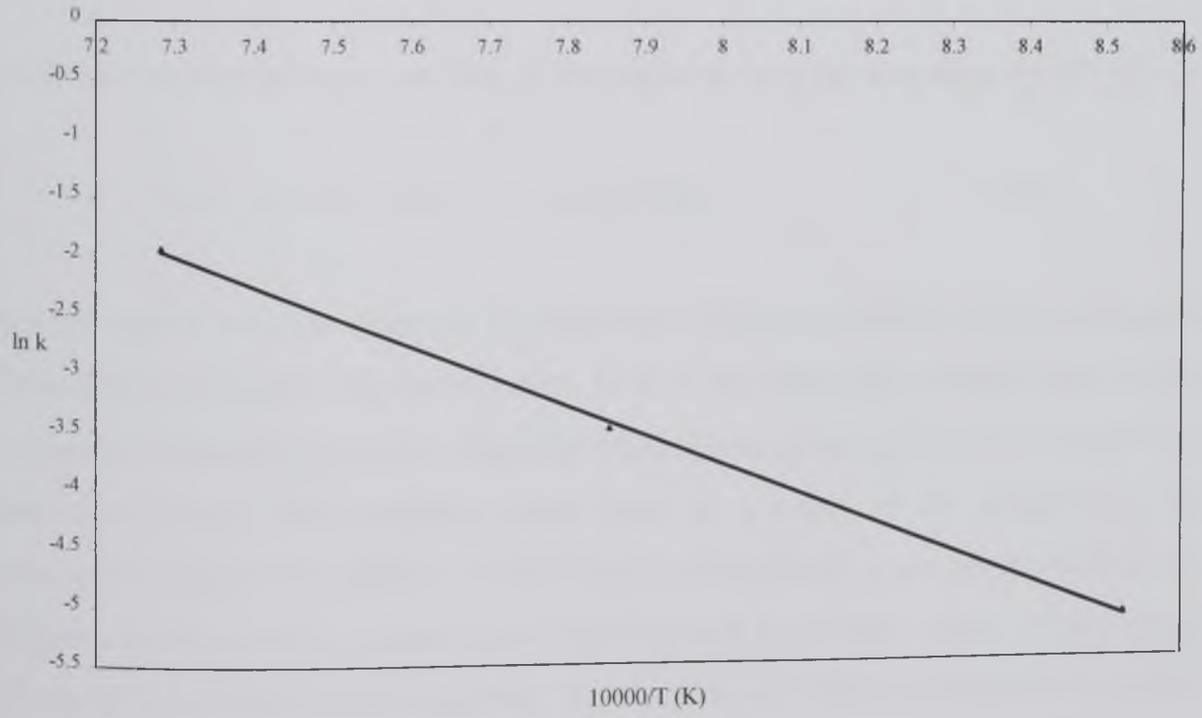

Figure 7.7 Arrhenius plot of the reduction of chalcopyrite from weight loss measurements carried out on the TGA furnace

Meaningful comparisons of the activation energies determined in this work to earlier studies is difficult. There is no kinetic data available in the literature concerning the carbothermic reduction of chalcopyrite, neither synthesised nor natural.

The rates of reduction for natural chalcopyrite are higher than for synthesised chalcopyrite. For the synthesised sulphide, after 120 minutes at 1000°C only 85% reduction occurs (Jha and Grieveson 1992b), whereas for the same temperature and time complete reduction is observed of natural chalcopyrite. At 900°C for synthetic chalcopyrite, 30% reduction is achieved compared to 40% for the natural mineral. Comparisons at higher temperatures are not available as the investigation into the synthetic mineral did not exceed 1000°C.

In general the reaction can be viewed as occurring in two reduction stages as proven by kinetic studies. The initial direct reduction of chalcopyrite by carbon, producing the intermediary phases (C_{II} and C_{III}) , CaS and CO:

$$CuFeS_2 + 2CaO + 2C = C_{III}/\ C_{II} + CaS + 2CO \qquad (7.8)$$

and the subsequent indirect reduction of the products from the first stage by CO gas:

$$C_{III}/\ C_{II} + CO = Cu + Fe + CaS + CO_2 \qquad (7.9)$$

Metallic copper was first observed to form from reduction at 900°C and was identified as present at all higher temperatures both from X-ray diffraction analysis and electron microscopy. Metallic iron is only detected when the temperature is raised to 950°C. As mentioned earlier, these metallic phases form as a result of the reduction of the oxysulphide phases by carbon. At 850°C only CaS and C_{III} are produced from the reduction reaction: the C_{II} phase is not observed as it forms only when metallic copper is formed. When iron is first observed, the C_{III} phase is little in evidence and finally disappears from X-ray analysis at 950°C. The general trend from X-ray analysis indicates that as the temperature increases the observation of metallic phases also increases with the amounts of oxysulphide phases observed decreasing.

The results for the metallisation of copper and iron from the reduction of natural chalcopyrite do not agree well with synthetic chalcopyrite metallisation. Both copper and iron metal form from synthetic chalcopyrite at 850°C and above. The percentage reduction for the natural chalcopyrite is higher than that for the reduction of the synthetic sulphide.

The microstructural evidence from the reduction of natural chalcopyrite points to a tendency for phase separation between copper and iron. At elevated temperatures, i.e. at 1100°C phase separation occurs. Copper metallisation occurs towards the top of the reacted mass. Only a small amount of copper is found at the bottom of the sample with metallic iron. However below this temperature both metallic phases are present together uniformly through the reacted samples.

From the results of the reduction reaction of natural chalcopyrite a reaction mechanism has been determined. Initially chalcopyrite reacts with lime to produce calcium sulphide and the C_{III} oxysulphide phase. The intermediary phase is reduced by carbon from which metallic copper is produced first. The depletion of copper from the intermediary phase in some areas of the sample results in the formation of the C_{II} phase. As the reaction is proceeding carbon monoxide is evolved and further calcium sulphide is formed. When metallic iron first forms the presence of intermediary phases is low, disappearing completely as more iron is produced. Complete reduction is achieved when both metallic species are observed with calcium sulphide without the presence of the oxysulphide phases. The data from weight loss analysis and X-ray diffraction analysis determine complete reduction to occur at 1000°C and above.

7.2.3 Oxygen Potential Measurements

In Chapter 4 a graph of log Pso_2 values as a function of temperature is given in figure 4.2, page 64. This figure was constructed to demonstrate the univariants relevant to the reduction reaction. It can be seen that at certain values of log Pso_2 metallic copper will form and metallic iron will not. From the experimental results for the reduction of chalcopyrite, 50°C separates the temperatures at which these two metals will form. Thus

indicating there is a difference in SO_2 partial pressure at which each metal will form. There is a large region of liquid immiscibility in the temperature range of relevance between copper and iron found on the Cu-Fe binary alloy diagram (Hultgren at al (1973)) given in figure 3.4, page 43. It is as a result of these observations that it is possible to manipulate the metallic copper production from the C_{111} phase by controlling the oxygen partial pressure in the system and so leaving the iron in solution.

Further investigation into the manipulation of the reduction reaction was carried out by the study of the oxygen potential during the reduction reaction as detailed in Appendix 2. Three sets of data were recorded for the oxygen partial pressure during reduction. Comparison between these sets of data gives good agreement. The determined oxygen potentials from measured emf values during the reduction of chalcopyrite were compared with theoretical values for the reaction. The experimental values compare well to the theoretical values.

From the determined oxygen potential values, log Pso_2 values were determined for the reduction reaction and compared against the calculated univariants in a plot of log Pso_2 against the reciprocal of temperature. This graph is given in figure 7.8

The measurements of oxygen potential during the reduction reaction indicates that for lower temperatures in the initial phase of reduction the equilibrium is represented by the Cu + CaO univariant. This phase of reduction occurs in the temperature range from 700°C to 950°C. With increased time the equilibrium shifts towards the Cu + CaS and Fe + SO_2 univariants. The shift in equilibrium occurs from 950°C to 1150°C. The two distinct regions of log Pso_2 values can be compared to the results from the reduction reaction. The first range of log Pso_2 values from –6 to –3 occurs in the temperature range of 600°C to 950°C. As the reaction proceeds the partial pressure of SO_2 increases with increased temperature to 950°C with respect to the formation of the oxysulphide phases. At 950°C a sharp reduction in partial pressure occurs to log Pso_2 values of –7. The decrease in partial pressure can be related to the metallisation of copper and subsequently iron from the oxysulphide phases.

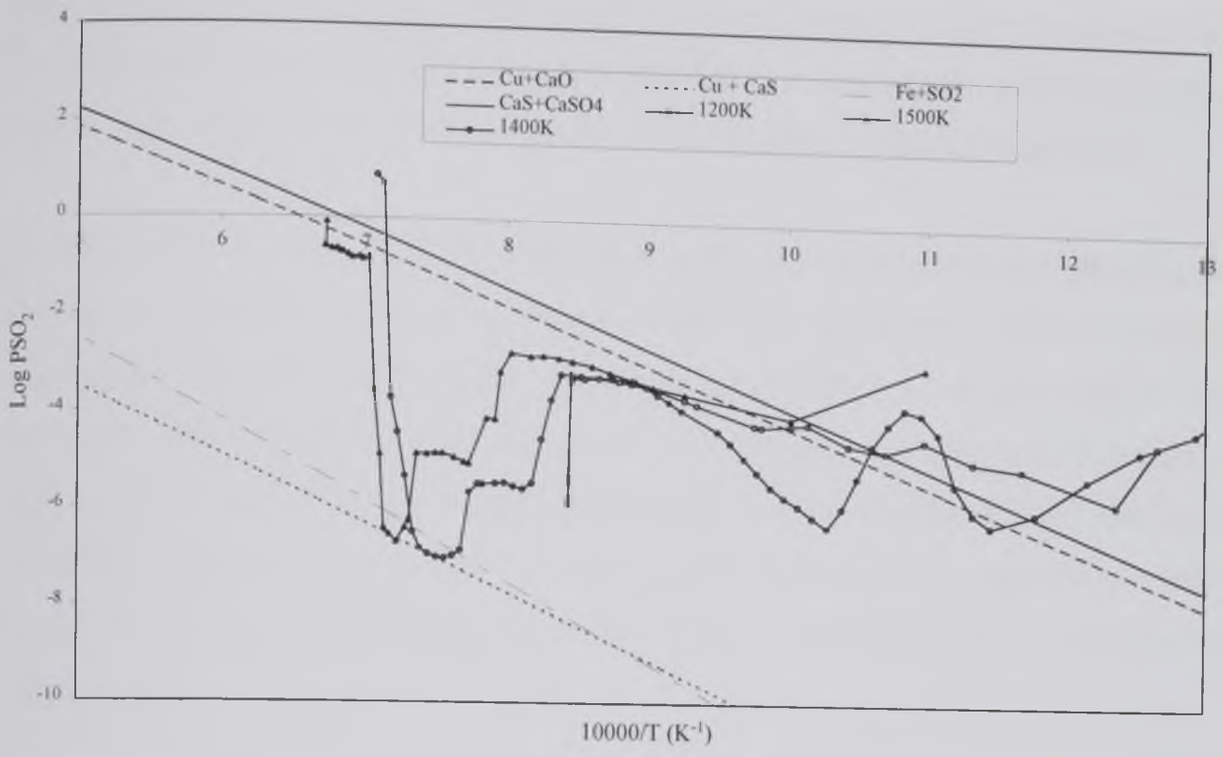

Figure 7.8 Comparison of experimental log P_{SO_2} values with calculated data for selected univaraints.

In figure 7.8 there exist two particular isochemical potential regions for the reduction reaction. One of these regions is observed near the log P_{SO_2} value of –3.0. The other is discerned when the log P_{SO_2} values are around –5.0. Both of these regions occur at temperatures above 1100K. For the temperature region 1100K-1250K the equilibrium for the metallisation of copper is maintained with respect to the Cu+CaO line. At temperatures around 1200K to 1250K the equilibrium shifts to the Cu+CaS and Fe+SO_2 equilibria before the end of the experiment.

7.2.4 Comparison of Graphite Powder and Activated Carbon as the Reducing Agent

The most obvious comparison made between the two carbon sources on the reduction of chalcopyrite is the appearance of reduced samples after reaction. Samples reduced by graphite powder were a dullish grey colour after reaction whereas those reduced by activated carbon showed a red colouration on the top surface. The red colouration is due to small layer of copper growth on the surface. The microstructure for chalcopyrite

reduced by activated carbon reveals metallic copper is produced fairly uniformly with the other products of reduction. Copper metallisation as seen on the surface of samples reduced by activated carbon was not observed for graphite reduced chalcopyrite.

Further analysis both by X-ray diffraction and electron microscopy indicated the formation of metallic copper at lower temperatures than with normal carbon. In samples reduced by activated carbon copper was observed at 850°C, lower than that for non-activated carbon. Metallic iron also forms at lower temperatures from reduction of chalcopyrite by activated carbon. Both copper and iron are metallised from chalcopyrite by activated carbon 50°C lower than for non-activated carbon. The oxysulphide phases are present at low temperatures but are not formed as the temperature is raised above 900°C.

Complete reduction occurs at 950°C for the reduction by activated carbon. The addition of activated carbon increases the rate of reduction to the extent that every stage during reduction happens at temperatures 50°C below those for non-activated carbon. As determined from the kinetic modeling of the reduction reaction the first stage of the reaction occurs from a solid/ solid reaction. Activated carbon has a higher surface area than non-activated carbon therefore increasing the area of contact for the solid/ solid reaction to occur. A higher weight loss is observed at lower temperatures with activated carbon suggesting a higher rate of carbon monoxide evolution, which further enhances the second stage of reduction. Due to the increased rate of the second stage of reduction less intermediate phases were observed at lower temperatures. Comparisons between different sources of carbon on the reduction of nickel sulphide (Machingawata 1989) and tennanite (Igiehon 1994b) have been made: both compared reduction by graphite powder and coal and both determined that the rate of reduction is improved with coal.

Phase separation of copper and iron is observed at 1100°C when chalcopyrite is reduced by non-activated carbon. The phase separation occurs at the lower temperatures of 950°C and 1000°C when activated carbon is the reducing agent as indicated by the growth of metallic copper on the surface of reduced chalcopyrite. Where this metallic copper growth is observed metallic iron is not in evidence and phase analysis through the rest of the reacted sample show copper depleted regions.

7.2.5 Effect of Increased Sample Size on Reduction

The results from this set of experiments suggest that there is a high degree of comparability between small scale (2g) and medium scale (50g) trials. X-ray analysis performed on reduced samples point out the formation of similar phases as identified in small scale experiments. Calcium sulphide forms in the temperature range 900°C to 1250°C. The metallic phases of copper and iron are also observed. Metallic copper was first observed at 1000°C for 120 minutes with iron detected in the sample reduced at 1000°C for 180 minutes. Copper was not observed at 900°C although was identified at that temperature in small samples. The oxysulphide phases, C_{111} and C_{11}, also form from the reduction reaction on a larger scale. These phases are produced at higher temperatures than in smaller samples, usually 50°C higher.

It appears from the X-ray analysis of reduced medium scale charges that although similar phases are produced to small scale samples the temperatures of formation are higher, indicating the degree of reduction is higher in smaller samples. This could be due to the evolution of gases during the reaction. The samples were reduced in clay crucibles with the sample filling only half of the crucible volume. During reduction carbon monoxide evolved from the reaction does not move freely and does not leave the mixture as quickly as from smaller samples. Despite this the degree of reduction is only slightly reduced at this scale therefore a good degree of reproducibility can be achieved in larger samples.

7.2.6 Effect of Additions of Metallic Silver and Silver Sulphide during Reduction

The behaviour of silver during the reduction reaction was the focus of the investigation of experiments with silver sulphide and silver metal additions. The temperatures for the reactions were kept the same to facilitate comparison between the two sets of experiments. The additions were of appreciable weights, 1 wt.% each.

7.2.6.1 Ag_2S Additions

Experimental results point out that when silver is added as a sulphide, the compound undergoes carbothermic reduction, in the same way that copper sulphide and iron sulphide do, the reaction for which is given as:

$$Ag_2S + CaO + C = 2Ag + CaS + CO \qquad (7.10)$$

Where the free energy for the reaction is: $\Delta G° = 66.31 - 0.128\ T\ kJ/mol^{-1}$

X-ray analysis of the reduction reaction in the presence of silver sulphide shows that the reaction proceeds in the same way as the reduction reaction without the addition. Both metallic copper and iron were produced from reduction: metallic silver was not observed, as was expected due to the limited concentration within the sample.

At 1150°C the silver sulphide is reduced to metallic silver which is observed at the grain boundaries between copper and iron, although preferentially with copper. It was also noticed that silver segregates into the copper phase, but will not do so with the iron.

Analysis on the electron probe microanalyser (EPMA) allowed the silver segregation into copper to be observed more clearly than with the scanning electron microscope employing BSE imaging. Figure 6.53, page 161, shows the BSE image of a typical area within the sample, figures 6.54, 6.65 and 6.66 are elemental dot maps of iron, copper and silver present in the region. Silver was not found to be present in the metallic iron phase but is seen to segregate into the copper phase. This analysis agreed with the observations determined from BSE imaging on the scanning electron microscope.

During the reduction reaction the Cu_2S-Ag_2S system would have existed as a liquid phase before being reduced to the metallic elements. From analysis of the reduction reaction the copper and iron are found as a quinary oxysulphide phase. As the partial pressure of oxygen decreases due to reduction by carbon the production of copper increases. It is assumed that the silver would exist as an intermediary compound similar to the C_{111} phase and that as the copper is produced from the solution the silver will also

be produced as the metallic phase. Iron is the last phase to be produced from the solid solution phase, there is an immiscibility between silver and iron, and therefore the silver will not stay in solution with iron.

7.2.6.2 Metallic Silver Additions

When silver metal was added to the carbothermic reduction mixture and reacted at 1150°C for three hours an eutectic was formed. The eutectic structure was composed of silver and copper, the BSE image of figure 6.62 shows these phases. The phase formed as a result of the solidification of the binary eutectic: in this case the minor phase is the copper phase. It appears from the micrograph images that it is the copper that is embedded in the silver.

The point at which the copper-silver eutectic forms is seen on the phase diagram in figure 3.8, page 50. From the phase diagram it can be noted that the eutectic observed in figure 6.62 has the compositional volume fraction of 0.399 copper and 0.601 silver. The temperature that the eutectic is formed is 1050 K, above this temperature there is liquid copper and liquid silver miscibility, allowing one metal to dissolve in the other.

From the reduction reaction metallic copper is produced, as has been discussed previously. The metallic copper is seen as the new phase whereas the added silver is the metastable parent phase in the reaction. Metallic copper dissolves in the liquid silver and the eutectic structure results on cooling.

X-ray analysis confirmed the presence of metallic copper in the reduced sample, metallic iron was also found to be present. The presence of these metallic phases together with calcium sulphide indicates reduction occurred. Despite these similarities the microstructure of the sample was different to the microstructure found from the reduction reactions and with the reactions with silver sulphide additions. In the samples where silver was added as the sulphide, the microstructure was similar in appearance to the reduction reactions as discussed previously. The eutectic between copper and silver, already discussed, is one marked difference in microstructures. Figure 6.66 (page 170) shows this eutectic, which appears to be present in the areas where the added silver

metal is found. Investigation into other areas of the sample showed very little evidence of copper in either metallic or oxysulphide form. In the reduction reactions of section 6.4 metallic copper is found with metallic iron throughout the sample. The addition of silver metal inhibits the formation of metallic copper elsewhere in the sample, the copper is produced from the reduction reaction as liquid metal. The liquid silver moves through the sample to the copper where the copper dissolves in the silver before undergoing the phase transformation to the silver-copper eutectic phase. In the regions away from these eutectics, metallic iron is observed, therefore the presence of metallic silver allows for the separation of metallic copper from iron. Iron is not observed in the regions with silver agreeing with the findings from the experiments with silver sulphide where no silver-iron miscibility was observed.

From the evidence of the copper-silver mixing it can be deduced that when separating the copper from iron it will allow the removal of silver within the copper phase extracted. The copper phase containing silver would provide a valuable metallic phase for the copper extraction process.

7.3 Reaction of Chalcopyrite with Calcium Sulphate and Silica

The reaction of chalcopyrite, calcium sulphate and silica was considered with respect to the possible control of the elimination of impurities during copper extraction. Initially reactions were carried out between chalcopyrite and calcium sulphate followed by experiments with silica added.

7.3.1 Reaction of Chalcopyrite with Calcium Sulphate

The experiments gave information of the phase analysis for this reaction in order to help determine the reaction with silica. In comparison with the reaction of chalcopyrite with lime calcium sulphide is observed. The CaS phase was present at each temperature and observed to be the most predominant phase in the X-ray diffraction analysis data. The oxysulphide phase, C_{111}, was observed at 850°C and 900°C. However the C_{11} phase was not detected. The phase is not expected to form from this reaction as its presence in

reactions between chalcopyrite really only occurs when metallisation of copper also forms. The metallisation of copper does not happen from the reaction between chalcopyrite and calcium sulphate as expected.

The other phases observed appear to be a mixture of calcium silicates and calcium ferrites, neither of these types of compounds are observed from the reaction between chalcopyrite and lime. Vert and Kamentev (1956) identified calcium ferrites forming from the reaction between iron sulphide and lime. However it would appear that the reaction of chalcopyrite and lime preferentially produce calcium sulphide. Although CaS is the predominant phase from the reaction of chalcopyrite with calcium sulphate calcium ferrites also form. The presence of the C_{111} phase is subdued in preference to the production of calcium ferrites and copper sulphide phases.

7.3.2 Reaction of Chalcopyrite with Calcium Sulphate and Silica

These experiments were carried out to investigate the initial stage for the control and elimination of deleterious impurities from chalcopyrite concentrates. The aim of these experiments was to produce a calcium silicate phase to entrap iron and these impurities.

Results from X-ray analysis and electron microscopy confirm the formation of a calcium iron silicate phase. In addition, calcium ferrites and copper sulphide were present. Metallisation does not occur from the reaction between chalcopyrite, calcium sulphate and silica. If a partially reducing atmosphere were maintained during the reaction, metallisation of copper would occur from chalcopyrite calcined with silica as given by equation 7.6. The copper sulphide produced as a result of the calcination of chalcopyrite would be reduced to metallic copper.

$$2CuFeS_2 + 3CaSO_4 + 4O_2 + 2SiO_2 + C = 2Cu + 2FeO.SiO_2.3CaO.SiO_2 + 7SO_2 + CO \qquad (7.11)$$

The phase analyses of these experiments show favourable results, i.e. the production of the calcium iron silicate phase with separate copper sulphide. However the X-ray diffraction analyses of the heat treated samples were very complicated with the presence

of different silicate and ferrite phases indicating that even under reducing conditions the reaction would not strictly proceed as given in equation 7.6. The research on this reaction given in this thesis can only be seen as a preliminary investigation.

The addition of copper metal to the reaction between chalcopyrite, calcium sulphate and silica facilitated the separation of copper from iron. The copper content naturally occurring in the chalcopyrite mineral was found either with the copper metal added or as a band of copper sulphide surrounding the copper regions. The observations from this experiment predict that additions of copper metal can facilitate the metallisation of copper from chalcopyrite under inert atmospheres whilst producing the calcium silicate phases.

CHAPTER EIGHT

Conclusions and Suggestions for Further Work

8.1 Conclusions

Metallic copper and iron are produced from direct reduction of the chalcopyrite mineral in the presence of lime. The metallisation of copper is preferential over the metallisation of iron. Metallic copper is first observed to form from reduction at 900°C whereas metallic iron is first noticed at 950°C. Complete reduction of chalcopyrite was observed at 1000°C as indicated by X-ray diffraction analysis and weight loss analysis. The reduction of chalcopyrite was enhanced when activated carbon was used as the reducing agent. The rate of reduction for any specified temperature was greater for activated carbon reduction as was the degree of metallisation. The phase analyses on reduction of medium scale samples revealed favourable results for the application of the reduction to a larger scale.

There are two stages to the reduction of chalcopyrite, the first as direct reduction by carbon resulting in the formation of the oxysulphide phases (C_{111} and C_{11}), and calcium sulphide. The second stage of the reaction occurs by indirect reduction of the oxysulphide phases by the carbon monoxide evolved from the first step of the reaction. This leads to the formation of the metallic phases and further CaS; the gas evolved is carbon dioxide. Complete reduction has occurred when only the metallic phases and calcium sulphide are present in the reduced samples. The reduction reaction was observed to be temperature dependant indeed increased temperature lead to increased reduction rates.

The tendency for phase separation between copper and iron can be achieved by maintaining an oxygen or SO_2 potential during the reduction reaction. By selecting a particular partial pressure metallic copper can be produced from the reduction of chalcopyrite whilst the iron stays in the oxysulphide matte phase. Further phase separation can be achieved by the addition of silver metal to the reduction mixture prior to the reaction. Silver dissolves preferentially in the copper matrix and thus enhances

the metallic phase separation. Silver and iron were never present together when silver metal was present in the initial reactant mixture. The preferential segregation of silver into copper produces a valuable metallic product from the reduction reaction.

The preliminary investigation into the control and elimination of impurities from chalcopyrite provided favourable results. A calcium iron silicate phase was produced indicating that it would be possible to entrain elements such as arsenic and antimony as a slag phase rather than as flue dusts from volatilisation. The copper sulphide produced can be reduced under partial oxidising conditions hence producing metallic copper.

8.2 Suggestions for Further Work

Several aspects of the reduction reaction could be investigated further to provide more analysis on the mechanism of this reaction. Although the determination of the structure for the oxysulphide phase has been attempted in this research further analysis needs to be completed to provide accurate crystallography data for such a complicated phase. The analysis of such a phase would provide interesting results, not just in relation to the work covered by this thesis but in addition to other researcher's work producing similar compounds.

Further work needs to be completed on the selective separation of metallic phases from chalcopyrite during reduction. From further analysis by oxygen potential measurements a detailed analysis of the oxygen or SO_2 potential is needed to determine the exact stages of copper metallisation. The size of the samples reduced should be increased to determine phase reproducibility with respect to adaptability for industrial sized scale processing. This aspect is of particular importance if the extraction process was to be of use for industrial purposes.

The investigation into precious metal recovery from chalcopyrite via reduction processing can also be furthered by investigating other precious metals during reduction to obtain a complete analysis for these constituents of the natural mineral.

As already mentioned the preliminary research carried out on the reactions between chalcopyrite, calcium sulphate and silica provided some interesting results with relation

to the control and elimination of impurities found naturally occurring in chalcopyrite. This work needs to be furthered with respect to the metallisation of copper to ascertain the reaction kinetics for this reaction.

REFERENCES

Abdollahy M. (1996): PhD Thesis: University of Leeds: chapter 1

Abramowitz, M.S. and Rao Y.K. (1978): Inst. Min. Metal: Sept: C: 180-188

Baier R. and Kushma M. (1954): in *Copper: The Science and Technology of the Metal, its Alloys and Compounds*: Ed. Butts A.: Reinhold Publishing Co., New York: p.p. 119-137

Bale C.W. and Toguri J.M. (1976): Can Met Quart: 15: 4: 305-318

Berry L.G. and Mason B. (1959): *Mineralogy*: W.H. Freeman and Company, U.S.: pp 218-228

Biswas A.K. and Davenport W.G. (1980): *The Extractive Metallurgy of Copper*, Pergamon Press, New York

Blythe F.G.H. and de Freitas M.H. (1979): *A Geology for Engineers*: 6th Ed: Edward Arnold, London: pp.164-167

Bodswoth C. (1983): *Physical Chemistry of Iron and Steel Manufacture*: Longmans, London.

Bogdanov Y.V. (1984): *Geology and Metallogeny of Copper Deposits*: in Proc. Copper Symp. 27th Int. Geol. Congress, Moscow: 492-503

Boggs W.B. (1954): in *Copper: The Science and Technology of the Metal, its Alloys and Compounds*: Ed. Butts A.: Reinhold Publishing Co., New York: p.p. 72-118

Bosqui F., Dyrenforth D., Marriott A. (1954): in *Copper: The Science and Technology of the Metal, its Alloys and Compounds*: Ed. Butts A.: Reinhold Publishing Co., New York: p.p. 63-71

Bronson M.C. and Sohn H.Y. (1983): Met Trans: 14B: 605-615

Byerley J.J., Rempel G.L., Takebe N. (1972): Met Trans: 3: 2133-2138

Byerley J.J., Rempel G.L., Takebe N., Teo W.K. (1973): Met Trans: 4: 1507-1511

Cailteux J. (1984): *Geology and Metallogeny of Copper Deposits*: in Proc. Copper Symp. 27th Int. Geol. Congress, Moscow: 398-411

Cech R.E. and Tiemann T.D. (1969): Trans AIME: 24B: 1727-1733

Chadwick J. (1998): Mining Magazine: October: 195

Chadwick J. (1999): Mining Magazine: March: 122-126

Chaubal P.C. and Nagamori M. (1988): Met Trans B: 19: 547-556

Chaubal P.C. (1989): Trans. Inst. Min. Metal: C: 83-85.

Chesti A.R. and Sircar S.C. (1971): Indian J. Technology: 9: 339-343

Clifford D. (1997a): Mining Magazine: August: 114-120

Clifford D. (1997b): Mining Magazine: August: 121-127

Cole E.R., Dressel W.M., Fine M.M. (1974):

Cullity B.D. (1959): *Elements of X-ray Diffraction*: 2nd Ed., Addison-Wesley Publishing Company, U.S.

Darken L. and Gurry R. (1953): *Physical Chemistry of Metals*: Maple Press Company, New York.

Deer W.A., Howie R.A., Zussman J. (1977): *An Introduction to the Rock-Forming Minerals*: Longman Group Ltd, London.

Dokken R.N. and Elliot J.F. (1965): Trans AIME: 233: 1351-1358

Dunn J.A. (1964): *Copper*: in Bulletins of the Geological Survey of India: Ed. Jhingran A.G., Nautiyal S.P., Chowdhury M.K.: Geological Survey of India.

Elliot J.F. (1976): Met Tans: 7B: 17-33

El-Rahaiby S.K and Rao Y.K. (1984): Met Trans: 15B: 19-22

Evans A.M. (1983): *An Introduction to Ore Geology*: 3rd Ed.: Blackwell Scientific Publications, Great Britain: p.p. 130-143

Flood H, Forland T, Grjotheim K. (1953): in *The Physical Chemistry of Melts*: Symp. Molten Slags and Salts, IMM, London. p.p. 46-59

Foose M. and Weiblen P. (1984): *Geology and Metallogeny of Copper Deposits*: in Proc. Copper Symp. 27th Int. Geol. Congress, Moscow: 8-24

Gablina I.F. (1984): *Geology and Metallogeny of Copper Deposits*: in Proc. Copper Symp. 27th Int. Geol. Congress, Moscow: 524-539

Gaskill D.R., Palacidous J., Samsin C.(1980): in Elliot Symp. Proc. P.p. 161-172.

Geological Survey of India (1974): *Geology and Mineral Resources of the States of India: Part V-Bihar*: Miscellaneous Publication No.30: pp.20-21.

Gilchrist J.D. (1989): *Extraction Metallurgy,* 3rd Ed. Pergamon Press, Exeter.

Habashi F. and Dugdale R. (1973): Met Trans: 4: 1865-1871

Habashi F. and Yostos B. (1977): J of Metals: July: 11-16

Habashi F. (1978): *Chalcopyrite and its Chemistry and Metallurgy*, McGraw-Hill, U.S.

Hang Goo Kim and Sohn H.Y. (1998): Inst. Min. Metall. (c) p.p.43-59.

Hino M. and Toguri J.M. (1987): Met Trans B: 18: 189-194

Holeczy J., Shmeidl J., Sehnalek. (1964): JOM: 16: p.p.416-420

Hultgren R, Desai P, Hawkins D, Gleiser M, Kelly K.K. (1973): *Selected Values of Thermodynamic Properties of Binary Alloys*, American Society for Metals, Ohio: 737-741

Hutchinson R.W. (1973): Econ Geol: 8: 1223-1243

Hyvarinen O. ? (1984): Met. Soc. AIME: 41: 537-548

Igiehon U.O., Terry B.S., Grieveson P. (1992a): Trans. Inst Min. Metal: C: 101: 144-154

Igiehon U.O., Terry B.S., Grieveson P. (1992b): Trans. Inst Min. Metal: C: 101: 155-158

Igiehon U.O., Terry B.S., Grieveson P. (1992c): Trans. Inst Min. Metal: C: 101: 159-164

Igiehon U.O., Terry B.S., Grieveson P. (1994a): Trans. Inst Min. Metal: C: 103: 41-47

Igiehon U.O., Terry B.S., Grieveson P. (1994b): Trans. Inst Min. Metal C: 103: 48-53

Igiehon U.O., Terry B.S., Grieveson P. (1994c): Trans. Inst Min. Metal: C: 103: 54-61

Itagaki K. and Yazawa A. (1985): in *Complex Sulphides Processing of Ores, Concentrates and By-Products*: Proc.Soc. AIME.

Jaireth S. (1986): J Geol Soc India: 27: April: 359-368

Jensen M.L. and Bateman A.M. (1979): *Economic Mineral Deposits*: 3rd Ed. John Wiley and Sons, U.S, p.p. 312-356

Jha A, Grievson P, Jeffes H.E. (1989): Scand J Metal: 18: 31-45

Jha A, Igiehon U.O, Grievson P. (1991): Scand J Metal: 20: 270-278

Jha A. and Grievson P. (1992a): Scand J Metal: 21: 50-62

Jha A. and Grievson P. (1992b): Scand J Metal: 21: 127-137

.Jimbo I., Goto S., Ogawa O. (1984): Met Trans B: 535-541

Johansen E-B., Rosenqvist T., Torgersen P. T. (1970): J of Metals: Sept: 39-46

Johnston C. and Pickles C.A. (1990): Inst. Min. Metal: C: 100-104

Kor G.J.W. (1974): Met Trans: 5: 339-343

Krendelev F.P., Narkelyun L.F., Trubachev A.I., Salikhov V.S., Volodin P.N., Kunitsin V.V., Chechetkin V.S., Bakun N.N. (1984): *Geology and Metallogeny of Copper Deposits*: in Proc. Copper Symp. 27th Int. Geol. Congress, Moscow: 513-523

Krivsky W.A. and Schumann R. Jr. (1957): Trans AIME: 209: 981

Lambert I.B., Knutson J., Donnelly T.H., Etminan H. (1984): *Geology and Metallogeny of Copper Deposits*: in Proc. Copper Symp. 27th Int. Geol. Congress, Moscow: 540-558

Lau K.H., Brittain R.D., Lamoreaux R.H., Hildebrand D.L. (1983): Met Trans B (14) p.p. 171-174.

Levin E.M., Robbins C.R., McMurdie H.F. (1969): *Phase Diagrams for Ceramists,* American Ceramic Society.

Machingawata N. and Broadbent C.P. (1994): Inst. Min. Metal: C: 1-8

Machingawuta N., Jha A., Grievson P. (1989): Scand J Metal: 18: 81-88

Mankhand T.R. and Prasad P.M. (1982): Met Trans: 13B: 275-282

Mendelevich A.Y., Krestovnikov A.N., Glaznov V.M. (1969): Russian Journal of Physical Chemistry: 43 (12): 1723-1724

Milliken C. (1970): *Copper Metallugy*: in Proc. Extractive Metallurgy Symp. on Copper Metallurgy, Denver: pp. 83-90

Minerals Yearbook (1993): US Bureau of Mines.

Mining Magazine: (1997): February: 100-101

Mohan M.K, Mankhand T.R, Prasad P.M. (1987): Met Trans: 18B: 719-725

Moinpour M. and Rao Y.K.(1985): Can. Inst. Min and Metal: Can. Met. Quarterly: 24 No. 1: 69-81

Moinpour M. and Rao Y.K.(1991): Inst. Min. Metal: C: 100: 97-104

Morrison B.H. (1985): in proc. Conf. Ext. Metal: Inst. Min. Metal: Sept: 249-69

Nagamori M. and Mackey P.J. (1978): Met Trans: 9B: 255-265

Padilla P., Ruiz M.C., Sohn H.Y. (1997): Met Trans: 28B: 265-274

Pennebaker E.N. (1954): in *Copper: The Science and Technology of the Metal, its Alloys and Compounds*: Ed. Butts A.: Reinhold Publishing Co., New York: p.p. 21-62

Radhakrishna B.P. (1979): J Geol Soc India: 20: Sept: 457-469

Raghavan V. (1988): *Phase Diagrams of Ternary Iron Alloys*, *Part 2*, Indian Inst. Metals, Calcutta.

Rajamani K and Sohn H.Y. (1983): Met Trans: 14B: 175-179

Rao S.K.L. (1971): Base Metals (Part 1): Miscellaneous Publication No. 16: Geological Survey of India: pp. 283-231

Rao Y.K. (1983): J of Metals: July: 46-50

Rao Y.K. and El-Rahaiby S.K. (1985): Met Trans: 16B: 465-475

Read H.H., Watson J (1973): *Introduction to Geology: Volume 1 Principles*, 2nd Ed: Macmillan Press, London and Basingstoke.pp.588-608

Robiette A.G.E. (1973): *Electric Smelting Processes*, Charles Griffin and Co. Ltd, London: 207-217

Roine A. (1987): Met Trans B: 18: 203-212

Roine A. and Jalkanen H. (1985): Met Trans B: 16: 129-141

Rosenqvist T. (1975): in Proceedings of 4th Nordic High Temperature Symposium: NORTEMPS: 75: p.p. 239-255

Rosenqvist T. (1951): Trans AIME: July: 535-540

Schwartz G.M. (1923): Econ Geol: 18: 270-277

Scloen J.M. and Elkin E.M. (1950): Trans AIME: 188: 764-77

Sengupta P.R. and Das M.K. (1968): Copper: Miscellaneous Publication No. 13: Geological Survey of India: pp.115-124

Sinha S. N., Sohn H. Y., Nagamori M. (1985): Met Trans: 16B: 53-59

Skinner B.J. (1969): *Earth Resources*, Prentice-Hall, Inc., Englewood Cliffs, New Jersey, 1st Ed.

Sohn H.Y. and Won S. (1985): Met Trans: 16B: 645-661

Sohn H.Y. and Won S. (1985a): Met Trans: 16B: 831-839

Sood M.K., Wagner R.J., Markazi H.D. (1984): *Geology and Metallogeny of Copper Deposits*: in Proc. Copper Symp. 27th Int. Geol. Congress, Moscow: 422-442

Sridhar R., Toguri J.M., Simeonov S. (1997a): Met Trans: 28B: 191-200

Sridhar R., Toguri J.M., Simeonov S. (1997b): J of Metals: April: 48-52

Strauss G.K. and Gray K.G. (1984): *Geology and Metallogeny of Copper Deposits*: in Proc. Copper Symp. 27th Int. Geol. Congress, Moscow: 304-324

Swalin R. (1972): *Thermodynamics of Solids*: John Wiley & Sons, Inc., U.S.

Taylor L.A. (1979): Met Trans: 1: 2523-2529

Thiam Chye Tan and Ford J.D. (1984): Met Trans: 15B: 719-723

Turkdogan E.T. (1961): Trans AIME: 221: 546-553

Turkdogan E.T. (1980): *Physical Chemistry of High Temperature Technology*, Academic Press, London: 5-24

Udupa A.R, Smith K.A, Moore J.J. (1984): Inst. Min. Metal: C: 93: 99-101

Udupa A.R, Smith K.A, Moore J.J. (1986): Met Trans: 185-196

Udupa A.R., Moore J.J., Smith F.A. (1987): Met Trans: 18B: 519-527

Vert Z.L. and Kamenstev M.V. (1956): Journal of Inorganic Chemistry: Vol 11, No.3: 489-498

Wadia D.N. (1953): *Geology of India*: 3rd Ed.: Macmillan and Co. Limited, London.

West E.G. (1982): *Copper and its Alloys*, John Wiley and Sons, U.S.

Wreidt H. A., Morrison W. B., Cole W.E. (1973): Met Trans: 4: 1453-1456

Yazawa A., (1974): Can. Metal. Quart: 13: No. 3: 443-453

APPENDIX

APPENDIX 1

X-RAY DIFFRACTION PHASE ANALYSIS DATA

JCPDS Files

CaO Card File No. 4- 777

d-spacing Å	Relative Intensity %
2.41	100
1.70	50
2.78	30
1.45	10
1.39	10
0.98	10

CaS Card File No. 8- 464

d-spacing Å	Relative Intensity %
2.85	100
2.01	70
1.64	20
1.27	20
1.16	10
1.42	10
0.95	10
0.90	10

Cu Card File No. 4- 836

d-spacing Å	Relative Intensity %
2.09	100
1.81	50
1.28	20
1.09	20
0.83	10
0.81	10
1.04	10
0.90	10

Fe Card File No. 6- 696

d-spacing Å	Relative Intensity %
2.03	100
1.17	30
1.43	20
0.91	10
1.01	10
0.83	10

$Cu_{1.96}S$ Card File No. 29- 578

d-spacing Å	Relative Intensity %
2.74	100
2.30	80
1.99	40
1.88	40
2.26	30
2.00	30
1.97	30
1.76	30

Cu-S Card File No. 23- 958

d-spacing Å	Relative Intensity %
1.94	100
2.37	90
1.86	90
2.86	80
2.63	70
3.35	60
3.00	50
1.68	40

CuS Card File No. 6- 464

d-spacing Å	Relative Intensity %
2.81	100
1.90	80
3.05	70
2.72	60
1.74	40
1.56	40
3.22	30
1.57	20

Ca_2Cu Card File No. 22- 524

d-spacing Å	Relative Intensity %
2.81	80
7.24	100
2.33	60
5.63	60
2.99	60
2.59	60
3.11	60
2.62	60

Ca_2SiO_4 Card File No. 20- 237

d-spacing Å	Relative Intensity %
2.75	100
2.69	80
2.19	50
4.65	30
3.81	30
3.37	30
2.87	30
2.37	30

Ca_3SiO_5 Card File No. 31- 301

d-spacing Å	Relative Intensity %
2.79	100
2.61	90
2.19	80
2.77	70
3.02	70
2.75	70
1.78	70
3.06	60

$Ca_3Si_2O_7$ Card File No. 22- 539

d-spacing Å	Relative Intensity %
2.72	100
3.18	80
4.48	70
3.84	70
3.03	60
1.82	60
3.20	50
2.90	50

$Ca_3Fe_2(SiO_4)_3$ Card File No. 10- 288

d-spacing Å	Relative Intensity %
3.02	100
2.70	90
1.61	90
2.46	80
1.96	50
1.67	40
1.12	40
1.32	20

$Ca_2Fe_2O_5$ Card File No. 19- 222

d-spacing Å	Relative Intensity %
2.69	100
2.80	70
2.72	70
1.95	70
7.37	40
2.08	40
2.06	40
1.85	40

Fe_2SiO_4 Card File No. 31- 649

d-spacing Å	Relative Intensity %
2.50	100
2.83	90
3.56	90
3.55	80
2.57	70
1.52	70
1.52	70
2.31	60

C_{11} Oxysulphide Compound – Data reported by Jha et al. (1992b)

d-spacing Å	Relative Intensity
5.70	W
3.25	W
3.10	S
2.82	M
2.46	VS
2.09	VW
1.94	WM
1.88	S
1.82	VW
1.74	VW
1.63	S
1.55	S
1.49	VW
1.48	VW
1.46	VW

APPENDIX 2

MEASUREMENT OF OXYGEN POTENTIAL DURING THE CARBOTHERMIC REDUCTION OF CHALCOPYRITE IN THE PRESENCE OF LIME

Introduction

The research detailed in this appendix is the result of work carried out in conjunction with a visiting research fellow, S Srikandth, from National Metallurgical Laboratory in Jamshedphur, India. For this work facilities in the Mining and Mineral Engineering department were utilised. The aim of this work was to discover if the measurements of O_2 partial pressures and hence the determination of SO_2 partial pressures could help understand the reduction reaction.

The assessment of oxygen chemical potential was undertaken by carrying out measurements of the electromotive force (EMF) cell voltage by using an oxygen sensor. Oxygen sensors can give direct information about the oxygen partial pressure in a given situation as an electrical signal. The cell is given as:

$$Po_2' \text{ (reference)/ solid electrolyte/ } Po_2'' \text{ (sample)} \qquad (1)$$

For the above cell the EMF can be represented by the Nernst equation:

$$E = {}^{RT}/_{ZF} \ln (Po_2''/ Po_2') \qquad (2)$$

For the reduction of chalcopyrite the EMF cell was based on Cu/Cu_2O in equilibrium with $CuFeS_2 + 2CaO + 2C$. Yittria stabilised zirconia was used as an oxygen ion conductor and the reference electrode is Cu/ Cu_2O. The cell description is therefore:

cell (+) Pt, $\{Cu_{(s)} + Cu_2O_{(s)}\}$ // $(Y_2O_3)\ ZrO_2$ // $\{CuFeS_2 + 2CaO + 2C\}$, Pt (-)

The oxygen potential of the reduction reaction can be expressed as equation 3.

$$\text{Log } Po_2 \text{ (atm)} = -\frac{(10.0785E)}{T} - \frac{17590.7}{T} + 7.443 \qquad (3)$$

From each measured EMF (E) value, the oxygen potential was determined. This data allowed the chemical potential of SO_2 to be determined from equation 4.

$$\log Pso_2 \text{ (atm)} = 1.5 \log Po_2 + \frac{23672.1}{T} - 3.9814 \qquad (4)$$

Experimental Procedure

Oxygen potential experiments were conducted in the Mining and Mineral Engineering department at the University of Leeds on equipment provided by this department. The experimental apparatus for these experiments in shown figure 1.

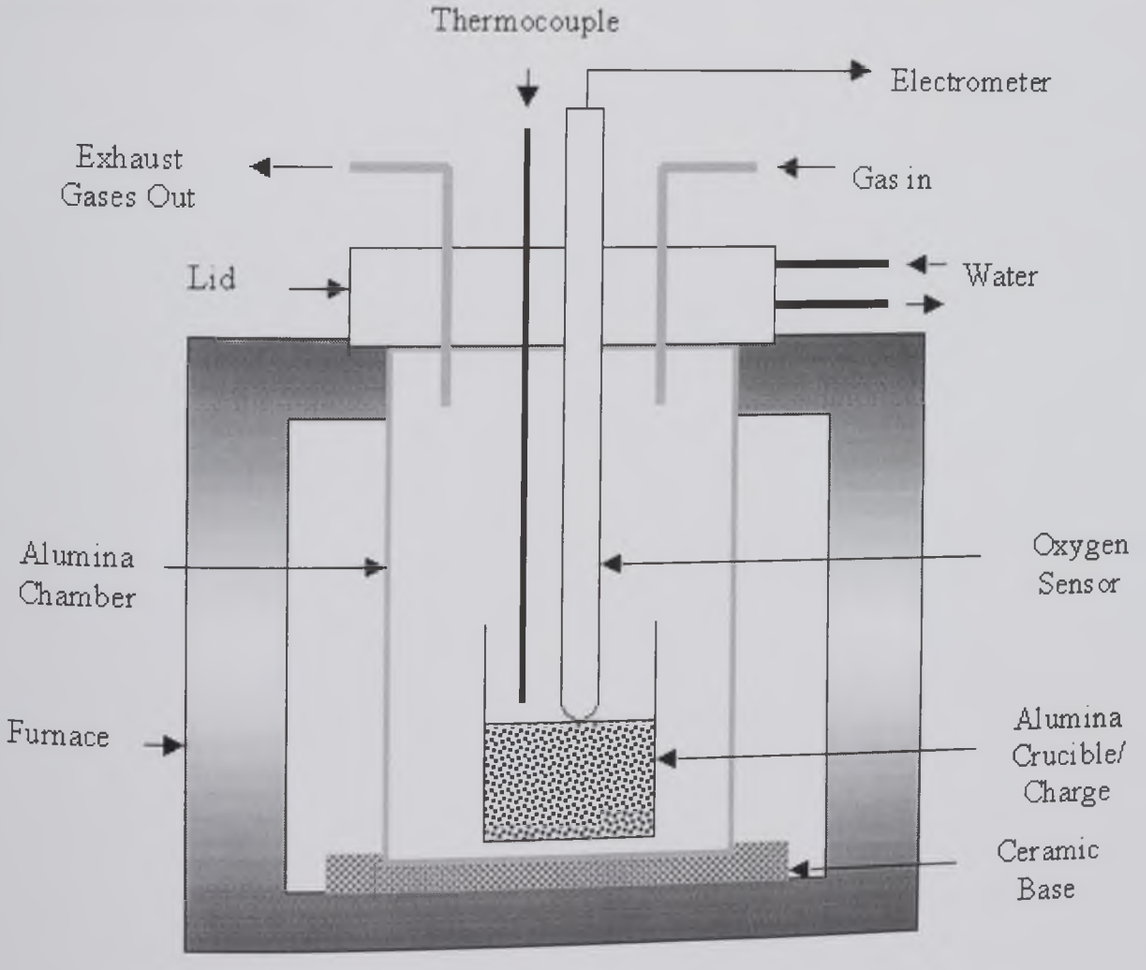

Figure 1 Schematic diagram of the experimental set-up for oxygen potential measurements.

Three sets of EMF measurements were taken each at different temperatures, 950°C, 1200°C, 1320°C. For each set of measurements 100g of a 1:2:2 mixture of $CuFeS_2$, CaO and graphite were mixed and packed into an alumina crucible. Each sample was reacted in an inert atmosphere controlled furnace and held at the selected isotherm for 30 minutes. With the sensor in place, readings from the electrometer of electromotive force (mV) were recorded every 30 seconds during the 30 minute period. After the reaction the sample was allowed to cool before being prepared for X-ray diffraction analysis.

Results

A graph of measured EMF values, during the experiments, as a function of temperature is given in figure 2. The three sets of data plotted agree fairly well with distinct changes in voltage occurring at similar points. A steady rise in EMF occurred from 550K to 1150K where a sharp rise to 1350K appears before completely dropping back down to the initial EMF values.

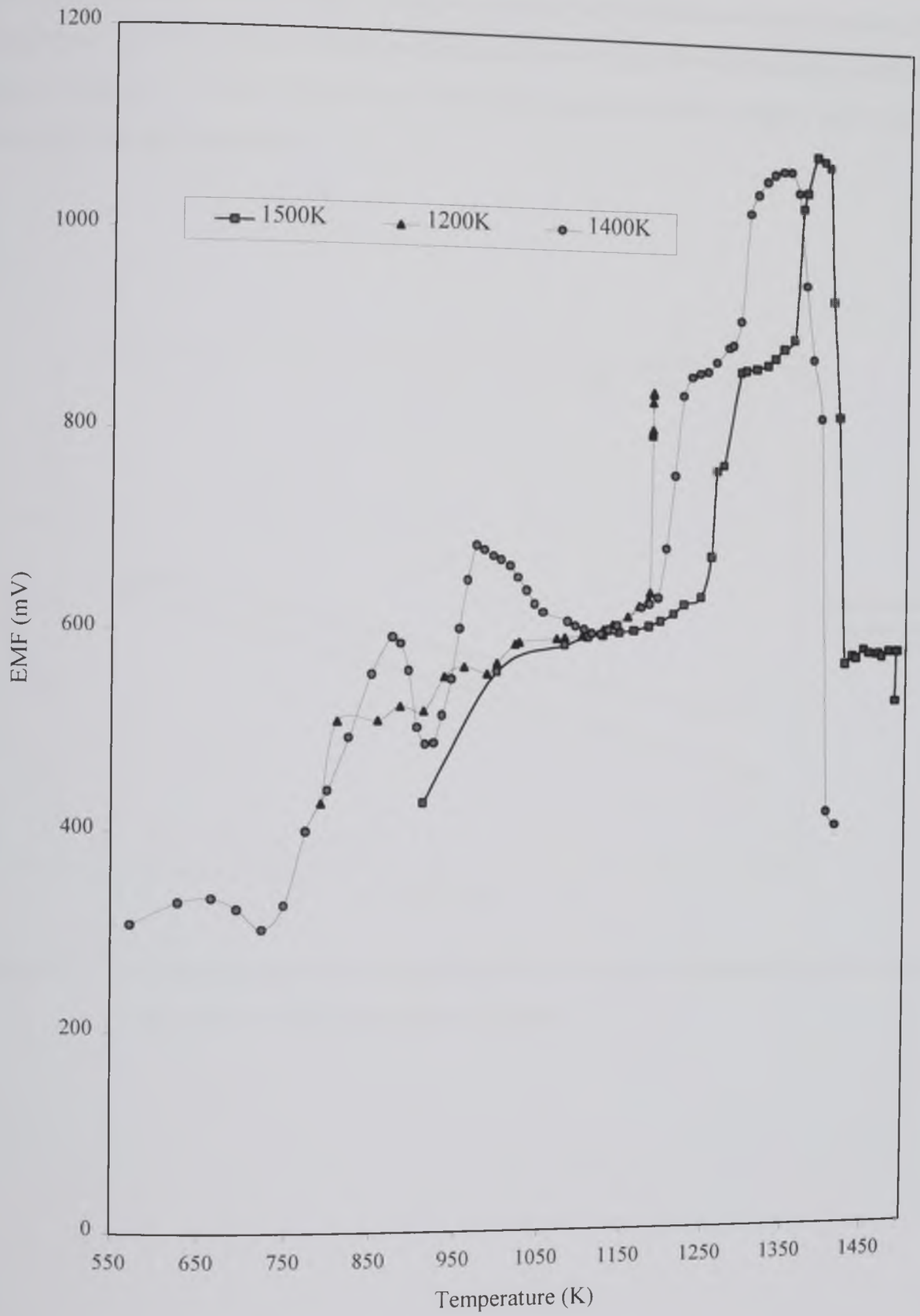

Figure 2 Measured EMF values from the reduction of chalcopyrite, using oxygen sensors, taken to three different set isotherms 1200K, 1400K and 1500K.

For each measured value of EMF the log Po_2 values were determined from equation 3. A comparison of these values with theoretical calculated values for the reduction reaction is given in figures 3, 4 and 5. The values from experimental analysis compare well with the theoretical oxygen potentials.

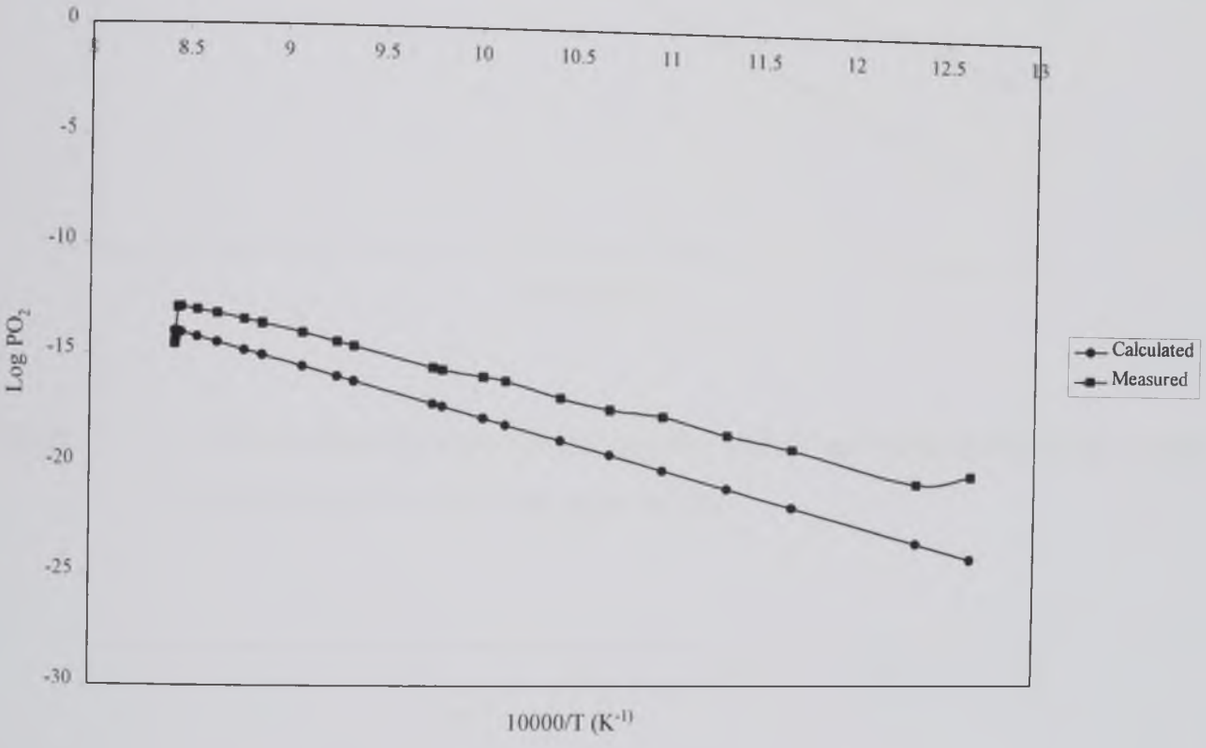

Figure 3 Comparison of experimental log Po_2 values and calculated log Po_2 values for $CuFeS_2$:2CaO:2C taken to 1200K.

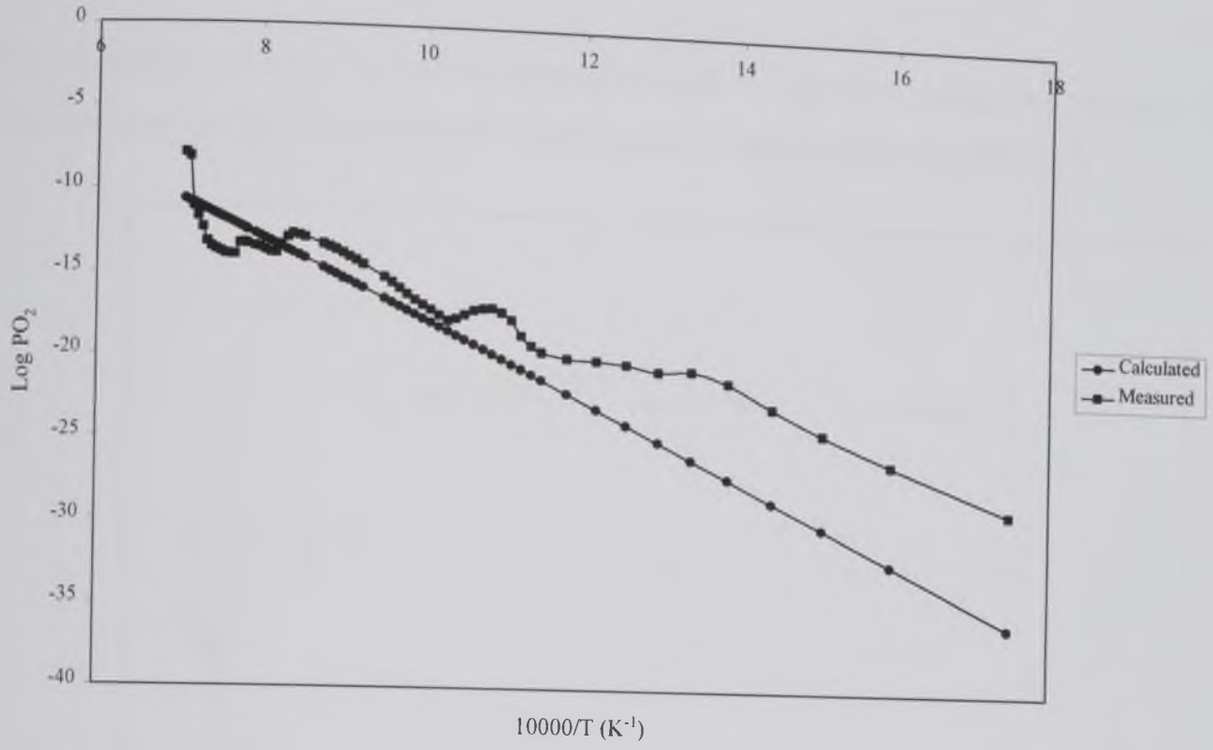

Figure 4 Comparison of experimental log Po_2 values and calculated log Po_2 values for $CuFeS_2$:2CaO:2C taken to 1400K.

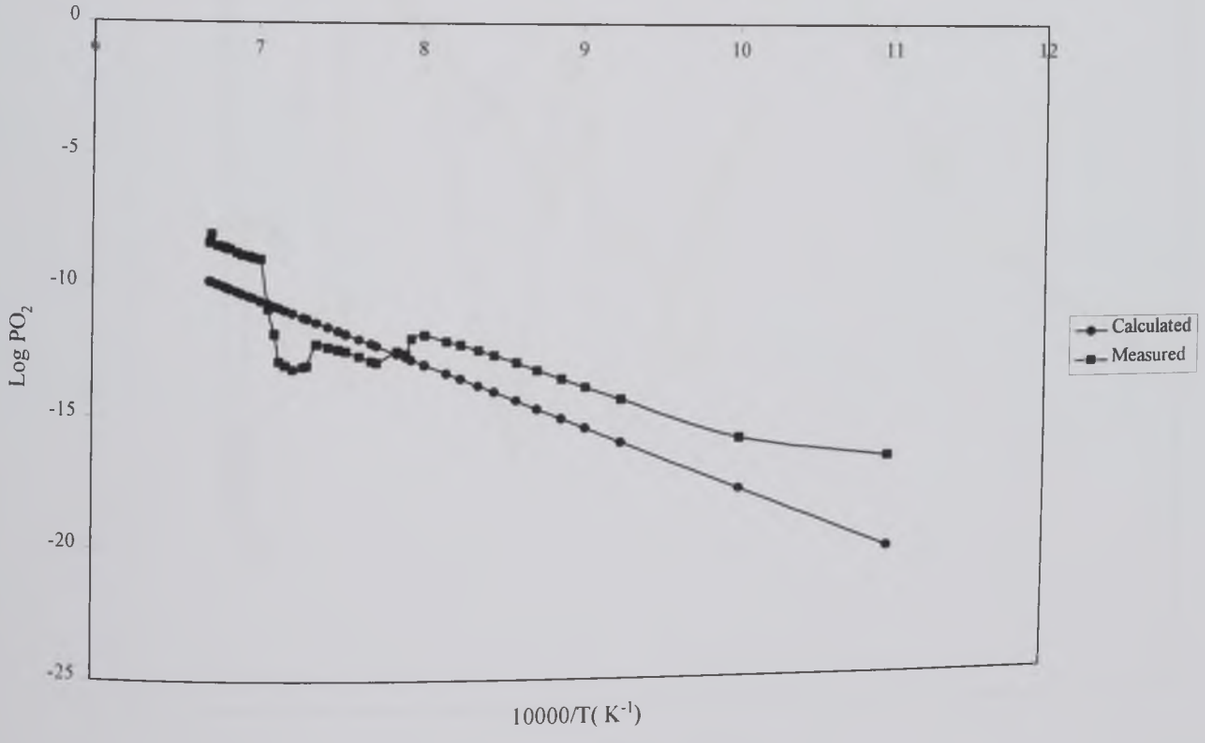

Figure 5 Comparison of experimental log Po_2 values and calculated log Po_2 values for $CuFeS_2$:2CaO:2C taken to 1500K.

The experimental log Po_2 values were converted to log Pso_2 values via equation 4. These values are plotted in figure 6 as a function of temperature (10000/T K^{-1}).

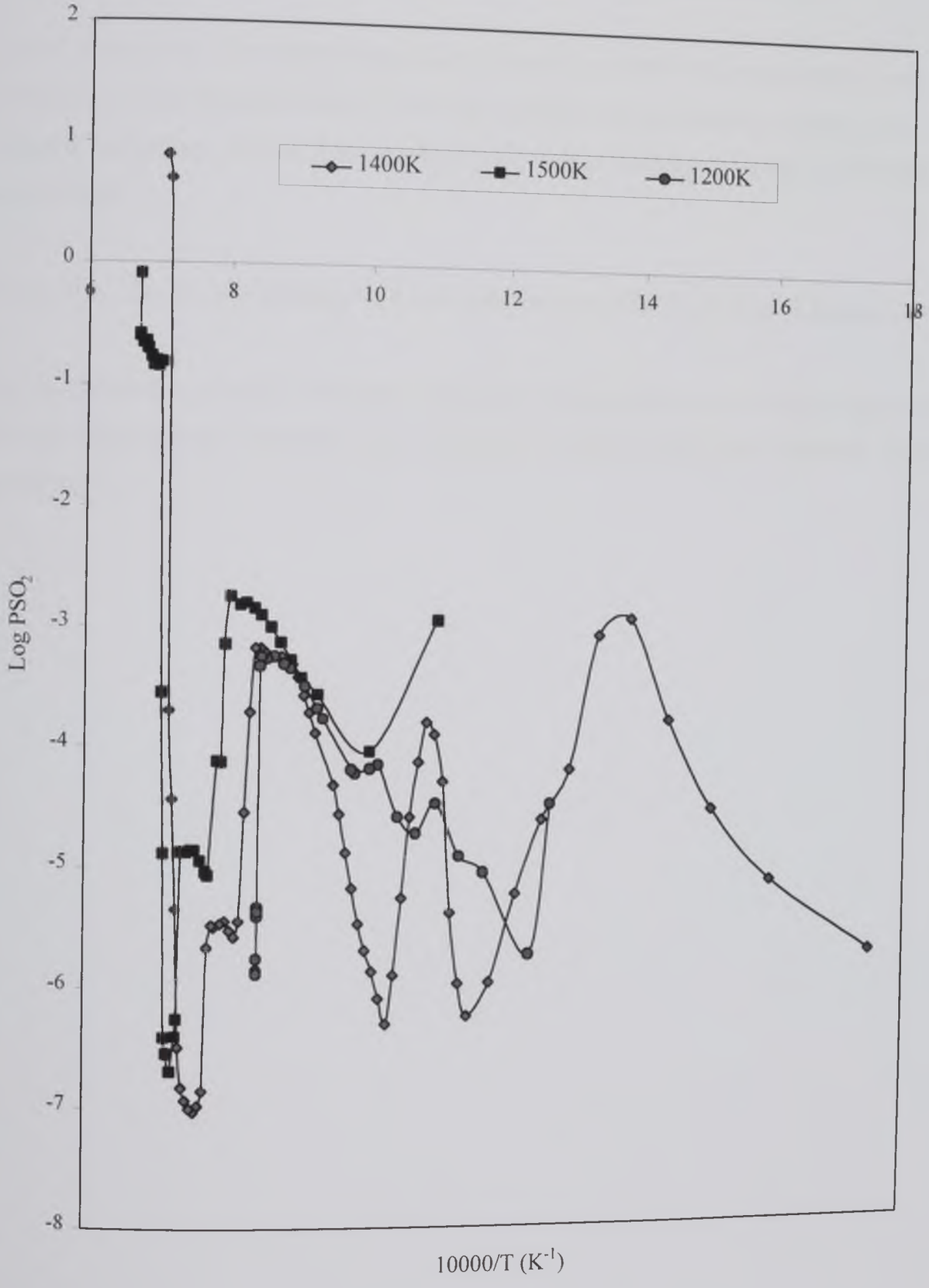

Figure 6 Calculated log Pso_2 values during the reduction of chalcopyrite.

APPENDIX 3

PRESENTATIONS AND PUBLICATIONS

Jha A., Srikanth S., Kale G.M., Payne N.S., Clowe S.J. (1998): Phase Equilibria in the Extraction of Non-ferrous metals", Proc. Environment and Innovation in Mining and Mineral Technology, Ed. M. Sanchez et al, Univ. Chile, Concepcion, May 12-16th 1998, pp.677-689

Payne N.S., Jha A. and Srikanth S.: Poster presentation at REWAS, San Sebastian 1999

Jha A., Srikanth S., and N. S. Payne: "Aspects of Physical Chemistry of Phase Separation during Chalcopyrite Reduction and Smelting", Metallurgical and Materials Trans (submitted).

APPENDIX 3

PRESENTATIONS AND PUBLICATIONS

Jha A., Srikanth S., Kale G.M., Payne N.S., Clowe S.J. (1998): Phase Equilibria in the Extraction of Non-ferrous metals", Proc. Environment and Innovation in Mining and Mineral Technology, Ed. M. Sanchez et al, Univ. Chile, Concepcion, May 12-16th 1998, pp.677-689

Payne N.S., Jha A. and Srikanth S.: Poster presentation at REWAS, San Sebastian 1999

Jha A., Srikanth S., and N. S. Payne: "Aspects of Physical Chemistry of Phase Separation during Chalcopyrite Reduction and Smelting", Metallurgical and Materials Trans (submitted).